THE UNIVERSITY *of* EDINBURGH

An Investigation into the potential of Energy Storage to tackle Intermittency in Renewable Energy Generation

Edward Barbour

Doctor of Philosophy

THE UNIVERSITY OF EDINBURGH

2013

Abstract

Renewable Energy is by nature intermittent and matching the supply of energy to specific time dependent demand poses huge challenges. Energy storage is a useful tool in handling this temporal disparity, although except for regions very suitable for pumped hydroelectric storage schemes, it suffers from being technically difficult to implement and costly as a result.

This study investigates the potential benefits offered by various scales of energy storage to different types of renewable energy generation. It also explores the economic drivers behind energy storage operating as part of an electricity spot market. A stochastic optimisation algorithm for determining the maximum possible arbitrage revenue available to energy storage devices is presented and schedule of operation of storage acting in this manner is analysed. The schedule of operation for maximising the revenue is compared to the schedule of operation for minimising the fuel cost to the network and it is demonstrated that because prices are more volatile than the demand which drives them, storage devices do not always act to decrease the fuel cost to the network. It is shown that storage behaving in the right manner can offer significant benefits to electricity systems, and increases the usage of base-load generation, reducing peak electricity demands and the need for expensive peaking plants. The value of storage also increases as the penetration of renewable energy generation increases, although the current electricity market framework is perhaps not the best way to encourage this behaviour.

Advanced Adiabatic Compressed Air Energy Storage (AA-CAES) is also identified as a theoretical storage option which deserves further scrutiny. Using thermodynamic modelling the efficiency of this type of system is estimated in the range of 63-67%, and we suggest that this may be increased closer to 73% by using direct contact heat exchangers rather than indirect contact heat exchangers (and a separate thermal fluid), as described in the currently available literature. However, dealing with large pressure ranges (leading to large variations in pressure ratios) encountered in the expansion process is a problematic area which will have to be resolved before this type of system can be constructed with “off-the-shelf” components. Some small scale experiments are used to gain valuable insights into a AA-CAES system. While these suffer from a very low overall efficiency, they highlight the effect of variable pressure ratio on expander efficiency. We conclude that AA-CAES is thermodynamically sound and will be achieved one of two ways: either through the construction of expanders that can work with high efficiency over large pressure ratios, or by resolving the engineering issues with maintaining a constant storage pressure.

Acknowledgements

I would like to express my gratitude to everyone who has in some way played a part in this project for their help, advice, support, good humour, persistence, patience, tolerance and many other qualities which I'm sure I have tested to near-breaking but completely forgotten about. A special mention of thanks should be extended to the following people:

to my supervisor, Professor Ian Bryden.
to my office mates, especially Dr David Forehand and Dr Scott Couch.
to my fellow PhD students Sam Harding, Richard Ferrier and Atul Agarwal for their insights and good humour.
to my colleagues at the Universities of Sheffield and Strathclyde with whom I collaborated, Grant Wilson and Simon Gill
to Dr. Andrew Firth for invaluable help with labwork.
to Prof. Gareth Harrison, Dr. Dimitri Mignard and Dr. Colin Pritchard for sharing their wisdom.
to several anonymous reviewers.
to Peter Fraenkel at Marine Current Turbines Ltd.
to my arch-nemesis Alex Barrows.
to my flatmate Andrew Latham.
to Mum, Dad and Tara, for their belief, encouragement and (financial) support.
to all the people, especially my fellow PhD students, at the University of Edinburgh's Institute for Energy Systems for making my time working on this project so enjoyable.

This work was funded by the Engineering and Physical Sciences Research Council (EPSRC) under grant number DTG J74909.

Declaration

I declare that this thesis was composed by myself, that the work contained herein is my own except where explicitly stated otherwise in the text, and that this work has not been submitted for any other degree or professional qualification except as specified.

Significant parts of the work outlined in this thesis have been published in academic journals.

Chapter 3 is based on: “Energy storage in association with tidal current generation systems”, E Barbour and I G Bryden, Proceedings of the Institution of Mechanical Engineers, Part A: Journal of Power and Energy 2011 225:443 and Chapter 4 on: “Towards an objective method to compare energy storage technologies: development and validation of a model to determine the upper boundary of revenue available from electrical price arbitrage”, Edward Barbour, I. A. Grant Wilson, Ian G. Bryden, Peter G. McGregor, Paul A. Mulheran and Peter J. Hall. Energy Environ. Sci., 2012, 5, 5425-5436.

While not explicitly a part of this thesis, the work in Chapters 3 and 4 provided the basis for and led directly to: “Maximising revenue for non-firm distributed wind generation with energy storage in an active management scheme”, Simon Gill, Edward Barbour, I. A. G. Wilson and David Infield, IET Renewable Power Generation, 2013, doi: 10.1049/iet-rpg.2012.0036.

Contents

Figures and Tables

Figures

Tables

Nomenclature

The main notation used throughout this paper is stated as follows:

Letters

A	area [m^2]
Bi	Biot Number [-]
C_p	power coefficient [-]
CS	size of the connection to the grid [kW]
$\dot{C}$	heat capacity flow rate [WK^{-1}]
$\dot{C}_c$	cold fluid heat capacity flow rate [WK^{-1}]
$\dot{C}_h$	hot fluid heat capacity flow rate [WK^{-1}]
$\dot{C}_{max}$	maximum heat capacity flow rate [WK^{-1}]
$\dot{C}_{min}$	minimum heat capacity flow rate [WK^{-1}]
C^*	ratio of heat cap. flow rates ($= \frac{C_{min}}{C_{max}}$) [-]
D_h	hydraulic diameter [m]
E	energy [J]
E_{stored}	energy contained within the store [J]
G	core mass velocity [$kgm^{-2}s^{-1}$]
I	current [A]
K_c	contraction loss coefficient [-]
K_e	expansion loss coefficient [-]
L	length [m]
NN_{bias}	nearest neighbour bias parameter when choosing two time periods [s^2]
Nu	Nusselt number [-]
NTU	Number of Transfer Units [-]
O_1	actual power output from the coupled storage TCEC system [W]
$O_{storage}$	energy output with storage [W]
$O_{without}$	energy output without storage [W]
OTG	the output to the grid from the storage device [W]
P	power [W]
ΔP_f	frictional power losses [W]
P_T	power of tidal current energy converter [W]
PLI	Power Limit Into the store [W]
PLO	Power Limit Out of the store [W]
Pr	Prandtl number [-]
Q	heat [J]

R	specific molar gas constant [$\mathrm{Jkg^{-1}K^{-1}}$]
$\bar{R}$	universal molar gas constant [$\mathrm{Jmol^{-1}K^{-1}}$]
$\tilde{R}$	load resistance [Ω]
R_{th}	thermal resistance [$\mathrm{KW^{-1}}$]
Re	Reynolds number [-]
SOC_{max}	maximum storage capacity [J]
$SOC(t)$	the state of charge of the store at time t [J]
T	temperature [K]
T_a	ambient temperature [K]
T_{TES}	thermal energy store temperature [K]
$T_{h,i}$	hot fluid inlet temperature [K]
$T_{h,o}$	hot fluid outlet temperature [K]
$T_{c,i}$	cold fluid inlet temperature [K]
$T_{c,o}$	cold fluid outlet temperature [K]
U	interal energy [J]
V	volume [$\mathrm{m^3}$]
V_i	initial volume [$\mathrm{m^3}$]
V_f	final volume [$\mathrm{m^3}$]
V_s	storage volume [$\mathrm{m^3}$]
$\tilde{V}$	voltage [V]
W	work [J]

$a_{spring(ns)}$	mean peak spring velocity along the north-south direction [$\mathrm{ms^{-2}}$]
$a_{neap(ns)}$	mean peak neap velocity along the north-south direction [$\mathrm{ms^{-2}}$]
$a_{spring(ew)}$	mean peak spring velocity in the east-west direction [$\mathrm{ms^{-2}}$]
$a_{neap(ew)}$	mean peak neap velocity in the east-west direction [$\mathrm{ms^{-2}}$]
c_f	fluid specific heat capacity [$\mathrm{Jkg^{-1}K^{-1}}$]
c_p	specific heat capacity at constant pressure [$\mathrm{Jkg^{-1}K^{-1}}$]
c_v	specific heat capacity at constant volume [$\mathrm{Jkg^{-1}K^{-1}}$]
c_s	solid specific heat capacity [$\mathrm{Jkg^{-1}K^{-1}}$]
d_p	average particle diamter [m]
f	fanning friction factor [-]
h	specific enthalpy [$\mathrm{Jkg^{-1}}$]
$\hat{h}$	heat transfer coefficient [$\mathrm{Wm^{-2}K^{-1}}$]
$\hat{h}_{vol}$	volumetric heat transfer coefficient [$\mathrm{Wm^{-3}K^{-1}}$]
k	polytropic exponent [-]
m	mass [kg]
p	pressure [Pa]
p_0	ambient pressure [Pa]

p_s	storage pressure [Pa]
$p_{c,int,1}$	intermediate compression pressure 1 [Pa]
$p_{e,int,2}$	intermediate expansion pressure 2 [Pa]
$\tilde{r}$	motor internal resistance [Ω]
r_i	inner radius [m]
r_o	outer radius [m]
s	specific entropy [$JK^{-1}kg^{-1}$]
t	time [s]
t_w	wall thickness [m]
u_0	superficial velocity [ms^{-1}]
$\bar{u}$	specific interal energy [Jkg^{-1}]
v	velocity [ms^{-1}]
v_{ns}	north-south velocity [ms^{-1}]
v_{ew}	east-west velocity [ms^{-1}]
$\bar{u}$	specific volume [m^3kg^{-1}]

Greek characters

χ	hoop stress [Pa]
ε	heat exchanger effectiveness [-]
ϕ	void fraction [-]
γ	adiabatic exponent [-]
η_{in}	charging efficiency [-]
η_{out}	charging efficiency [-]
$\eta_{pol,c}$	polytropic compressor efficiency [-]
$\eta_{pol,t}$	polytropic turbine efficiency [-]
η_s	round trip efficiency of the storage system [-]
λ	thermal conductivity [$Wm^{-1}K^{-1}$]
μ	dynamic viscosity [Pas]
ρ	density [kgm^{-3}]
ρ_f	fluid density [kgm^{-3}]
ρ_i	inlet density [kgm^{-3}]
ρ_o	outlet density [kgm^{-3}]
ρ_s	solid density [kgm^{-3}]
σ	exchanger free-flow to front area ratio [-]
τ_1	period of the semidiurnal tide ($\sim$12.4 hours) [s]
τ_2	period of the spring-neap cycle ($\sim$354 hours) [s]
τ_s	storage time constant [s]
ξ	electromotive force [V]
ψ	particle shape factor [-]

Abbreviations

AA-CAES	Advanced Adiabatic Compressed Air Energy Storage
BETTA	British Electricity Trading and Transmission Arrangements
CAES	Compressed Air Energy Storage
CCGT	Closed Cycle Gas Turbine
DECC	Department of Energy and Climate Change
LMTD	Log Mean Temperature Difference
MCT	Marine Current Turbines
OCGT	Open Cycle Gas Turbines
OFGEM	Office of gas and Electricity Markets
PBHE	Packed Bed Heat Exchanger
PHS	Pumped Hydroelectric Storage
PRC	Percentage Rated Capacity
REC	Renewable Energy Converter
SMES	Superconducting Magnetic Energy Storage
TES	Thermal Energy Store
TCEC	Tidal Current Energy Converter/Conversion
TSO	Transmission Systems Operator
WEC	Wave Energy Converter

Chapter 1

Introduction

1.1 Background

Sustainable energy is at the forefront of humanity's issues. In 1956 American geophysicist M King Hubbert presented a paper (Hubbert, 1956) to the American Petroleum Institute predicting that oil production in the U.S. would peak in the late 1960's or early 70's, and that world oil production would peak in the mid nineties. When U.S. production did in fact peak in 1970, the fact that fossil fuels could not be used to power the world forever began to be increasingly accepted in the public mind. Another issue that has come to be of paramount importance is Climate Change. While the details of this issue are still hotly debated, it seems prudent to assume that our usage of immense amounts of fossil fuel has a de-stabilising effect on the present, relatively benign environment. One obvious pathway to a sustainable energy future and the mitigation of Climate Change seems to lie with renewable energy sources, such as wind, tidal, solar and wave energy and globally the energy flux from these soures is several times the total current energy use of humanity. Indeed, the last 30 years has seen a considerable increase in the installation of renewable energy converters and some of the world's biggest energy economies now have sizeable capacities of renewable energy generation. However, one huge hurdle along this path is the issue of intermittency. That is, there is continuous variation with time in the magnitude of these energy sources, most of which is unpredictable, so that guaranteeing that sufficient energy will be available for conversion at a certain time is not always possible. Effective energy storage is an obvious tool for mitigating this issue.

There are other ways of dealing with the intermittency associated with renewable energy, and perhaps the favoured approach in recent times has been that of interconnectivity. The principle of this approach is that by introducing a very large geographical spread of renewable energy converting devices, it becomes more and more likely that favourable conditions for producing electricity will be found somewhere. This approach depends on a very strong infrastructure to connect the geographically spread renewable energy generation but in general renewable resources are most abundant in sparsely populated areas which tend to have low energy transmission capability.

Recent approaches to renewable generation are also focussing on smaller-scale generation

embedded within the distribution network, which is inherently a weaker infrastructure than the transmission network. This allows for renewable energy to be generated closer to the point of usage. A large part of the justification for this work comes from speculation that small-to-medium scale energy storage could provide benefits for embedded renewable generation in distributed networks, and while the prospect of large scale (GW days) energy storage seems daunting and impractical (except by way of stockpiling of fossil fuel), small - medium scale (10^2kWh - 10^2MWh) energy storage devices seem feasible and much of the engineering is already in place. It is expected that these small - medium scale energy storage units could provide benefits in terms of greater utilisation of renewable energy, lower emissions and reducing the need for network upgrades.

In the UK, the current government has set out to reach a target of 15% of energy generated to come from renewable sources by 2020 (DECC, c), compared to a value of 3% in 2009. The scale of this increase is considered a huge challenge due to the issues surrounding intermittency. However, the UK's indigenous renewable resource is itself huge, with the potential for 13GW of onshore wind and 18GW of offshore wind to be installed by 2020 (DECC, d), the extractable wave resource estimated at around 6GW (DECC, b) and the extractable tidal resource estimated as 2-7GW (L S Blunden and A S Bahaj, 2007). Given that the UK's peak electricity demand is roughly 80GW these resources have the potential to power a large proportion of our energy needs.

1.2 Project Objectives and Scope

This project has a number of distinct objectives:

- To gather information on the "state-of-the-art" of energy storage devices.
- To build on previous work carried out by Bryden and Macfarlane (2000) assessing the potential benefits of energy storage working in conjunction with tidal current energy conversion.
- To assess the economic drivers behind the implementation of energy storage, and examine the value of energy storage to electricity networks.
- To scrutinize Advanced Adiabatic Compressed Air Energy Storage as a small - medium scale storage mechanism and appraise its ability to assist with the grid-integration of marine renewable energy.

1.3 Thesis Contribution

This thesis will test the hypothesis that

> "With careful selection and sizing of an appropriate energy storage medium, energy storage is a useful tool for electricity systems which include a significant proportion of electricity generation from renewable energy conversion."

The research should provide valuable insights into the nature of energy storage and how an energy storage system can be carefully matched to its required task. It should develop an understanding of how a storage system would operate within the current UK spot market framework and explain why and where potential changes in market management may be useful. Identifying a gap in current energy storage technologies, the work goes on to speculate that Advanced Adiabatic Compressed Air Energy Storage (AA-CAES) is a process worth further investigation and that it may offer some advantages over other current storage technologies.

1.4 Outline

This thesis is divided into 7 chapters and an appendix. Chapter 1 provides a brief introduction to the project, states the project objectives and outlines the structure of the report.

Chapter 2 is essentially a literature review, starting by detailing a brief introduction to the main types of renewable energy generation. Energy storage is then discussed, starting with some reasons outlining the need for energy storage, after which a summary of the characteristics of various energy storage devices is presented and the current role played by energy storage in an electricity network is explained.

Chapter 3 examines the specific case of energy storage and tidal power, building on the previous work done by Bryden and Macfarlane (2000). A model for creating a generator time series for a Tidal Energy Converter is presented, which is then used to assess the benefits of introducing an energy storage device. It is shown that an energy storage device can reduce losses if there are transmission constraints present. The storage requirements for both firm and demand-matching supply from Tidal Current Energy Conversion are deduced and it is shown that a 1.2MW tidal current energy generator associated with a 1MWh storage system of modest efficiency can offer significant advantages over the generator working alone.

In Chapter 4, the economics of energy storage operating on electricity spot market are explored. Firstly, to give context, the structure of the UK electricity market is explained and then secondly, an algorithm with the capability to determine the maximum revenue available to a given storage device operating on an electricity spot market is described. Some results are presented and it is concluded that, although price differentials exist through which it is possible for energy storage to generate revenue, these are unlikely to be enough to encourage the participation of storage on the UK spot market. However, it is concluded that not only is

storage participation positive for the operation of the market in general but it should also reduce network carbon emissions. Thus it is suggested that there should be some consideration given to providing additional rewards for storage devices operating in this manner.

Chapter 5 investigates the value of energy storage to electricity networks. It is demonstrated that storage is useful to electricity networks because it can both reduce the variability of the power that has to be provided by thermal generation and reduce the overall network fuel cost. It also has the effect of increasing the usage of base-load generation, while reducing peak demands and thus removing some of the need for expensive peaking plants. It is concluded that the value of storage is exaggerated in networks with higher proportions of intermittent renewable energy generation (such as wind) as it acts to mitigate the temporal disparity between intermittent energy supply and energy demand.

Chapter 6 proposes Advanced Adiabatic Compressed Air Energy Storage as a potential energy storage medium. An understanding of how this type of system may function is developed by explaining the background thermodynamics involved. Some models of an AA-CAES plant are constructed and used to predict plant performance. The sensitivity of plant performance to the various model assumptions is assessed and it is found that this type of system is not only very sensitive to isentropic compressor and turbine efficiency, but also to heat exchanger performance (effectiveness and pressure drop).

Chapter 7 leads directly on from Chapter 6, and develops a model of an Advanced Adiabatic Compressed Air Energy Storage system with packed bed heat exchangers acting as both the heat exchanging mechanisms and the thermal energy stores. It is concluded that direct contact heat exchangers may offer benefits both in terms of performance and simplicity over more the commonly cited indirect contact exchangers.

Experiments aimed to test some of the more crucial elements of the AA-CAES model are outlined in Chapter 8. The experimental setup and methods are explained, and the results from the experiments are presented. Although using a simple reciprocating expander gives a very low efficiency, the experiments illustrate how a variable storage pressure during the expansion stages is potentially problematic.

Chapter 9 provides a summary of the work and emphasises some of the key conclusions. It also provides direction for future work.

Finally, the Appendix A explains the detailed operation of the MonteCarlo maximisation algorithm used in Chapter 4. Appendices B and C provide details of some of the loss calculations in Chapter 6 and 7. Appendix D details the calibration of the DC electric motor and generator used in the experiments described in Chapter 8.

Chapter 2

A brief overview of renewable energy and energy storage

2.1 Renewable Energy

Twidell and Weir (2006) defines renewable energy as

> "energy obtained from natural and persistent flows of energy occurring in the immediate environment".

This requires that the flow of energy is passing through the environment irrespective of whether or not some of it is extracted for use. To reiterate, the flow of energy is not manufactured; it is simply tapped (or altered). As stated in Chapter 1, renewable energy is one pathway to a sustainable energy future. In this sense perhaps the most informative way of describing what renewable energy is to list some examples of the types of energy flows that are present in the immediate environment and can be tapped. These are wind energy, solar energy, wave energy, tidal current energy, biomass, hydro and geothermal energy.

The following contains a brief qualitative section about the major forms of renewable energy.

2.1.1 Hydroelectric Power

Hydroelectricity is the worlds most extensively used form of renewable energy, accounting for 16% of the worlds total electricity generation. Indeed (as of 2012), the 3 biggest electricity generating plants in the world are all hydroelectric, the biggest being the Three Gorges Dam in China with a capacity of 21,000MW and an annual generation of 84.4TWh, followed by the Itaipu Dam on the border between Brazil and Paraguay (shown in Figure 2.1b), with a capacity of 14000MW and an annual electricity generation of 94.7TWh. It is one of the most mature renewable energy technologies - the first hydroelectric plant was built in 1878 at Cragside, Northumberland by William George Armstrong, to power a single light bulb in his house.

The principle behind hydroelectricity is straightforward. The kinetic energy and pressure of water as it flows is used to turn a turbine, which is used to drive a generator. Figure 2.1a shows a schematic of a conventional hydroelectric generation scheme. In order to create a fast

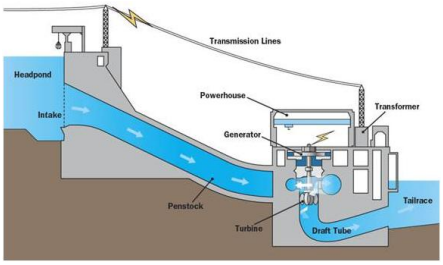

(a) Hydro Schematic

(b) Itaipu Dam

Figure 2.1: (a) a schematic of a conventional pumped hydro scheme, (b) the itaipu dam, on the border between Brazil and Paraguay.

flow of water, a dam is usually constructed which not only funnels the water but creates a large controllable flow, which can be changed from the natural flow rate that the river would otherwise have. In this manner, hydroelectricity has intermittent aspects but at the same time is largely dispatchable (the output can often be manipulated as required), as there may be natural variations in rainfall levels that affect water available but flow can usually be stopped and turned on when power is required.

Hydroelectricity is not without its problems as damming rivers can result in the flooding of fertile river valleys. For example, the Three-Gorges-Dam in China flooded an area of 10000sq miles of arable land and displaced over 1 million people. The potential social and environmental problems with hydroelectricity are discussed in Rosenberg *et al.* (1997).

Furthermore, worldwide, and especially in the UK, hydroelectricity has been largely exploited in those places where it is easy to implement without causing large environmental impacts, and as a result there is a limited potential for further large-scale hydroelectric generating capacity.

2.1.2 Solar Power

The idea of using energy from the suns rays to create electricity is another old idea. The first Solar Engine was invented by French mathematician and engineer Augustin Mouchot in 1866, using parabolic mirrors to boil water and drive a steam engine (Mouchot was also one of the earliest pioneers to speak out about the need for renewable energy to replace finite fossil fuels). Around the same time John Ericsson, a Swedish-American mechanical engineer who was instrumental in thermodynamics, built a similar solar powered engine using parabolic mirrors. The first practical solar or photovoltaic cells were built in the 1950's, at Bell Laboratories.

Solar generated electricity has two main principles of operation; using the light from the sun to super-heat water and drive a steam turbine, or generating electricity directly via the photoelectric effect. Figures 2.2 and 2.3 show examples of plants utilising these two principles

Figure 2.2: Seville's solar power tower, Spain. Light is focussed on the central tower and used to create super-heated steam.

of operation, with Figure 2.2 showing the former and Figure 2.3 the latter. In the former, rays from the sun over a large area are reflected and focussed onto a very small area, yielding a very high temperature, which is used to create super-heated steam. This highly energetic steam is then used to drive a turbine which in turn drives a generator. The latter principle utilises solar cells. Solar cells consist of p-n junctions, which are the boundary between two types of semiconductor material, p-type and n-type. The p-type and n-type regions are created by doping the semi-conductor with impurities and creating regions with electron 'holes' and regions with surplus electrons. Thus there is a built in potential difference at the interface between these two regions (at equilibrium). A solar cell works as when light falls on a semiconducting material such as silicon, a photon with enough energy can be absorbed by an electron in the material's valence band. It is then promoted into the conduction band, leaving behind a hole. This process is called photogeneration. The oppositely charged carriers (the conduction band electron and the hole) drift to opposite sides of the p-n junction due to the built in potential difference, and electric current flows.

Figure 2.3: Solar panels on the roof of a house which turn light directly into electricity.

Solar power is a very promising form of renewable energy, with the solar flux at the earth's surface being approximately 200 Wm^{-2}. This is more than enough to power all of our energy needs; however, the best of this resource is concentrated at lower latitudes, and is therefore somewhat impractical as an option for large population centres located at high latitudes. There are also issues with intermittency - as the sun doesn't always shine and often the strongest

resource occurs in the summer when the demand for energy and electricity are lowest (although in warmer climates the intermittency issue is slightly less, as there is often large demand for cooling when the sun is shining brightly). Currently the cost of solar cells is high and they are impractical for large scale energy generation. However, recent research on organic-based solar cells seems to have the potential to reduce costs (Shaheen *et al.*, 2005).

In the UK the solar resource is strongest in the summer but demand is highest in the winter, so seasonal energy storage would be particularly aided by seasonal energy storage. Solar energy use in the UK is increasing, at the end of 2012 totalling 1.8GW of PV capacity with 925MW installed in 2012 (European Photovoltiac Industry Association, 2013).

2.1.3 Wind Power

The idea of using wind power to do useful work dates back to the middle ages, when the earliest windmills were constructed, using the energy in the wind to turn a large stone mill which was used to grind corn. Due to worries over climate change and high fossil fuel prices wind power has recently has experienced a renaissance. Converting wind power to electricity involves using the kinetic energy associated with a moving air flow to turn a turbine which in turn drives a generator. As the flow of air is unconstrained there is a limit to the amount of energy that can be extracted by the turbine. This lies at 59% of the kinetic energy in the air flow and is known as the Betz limit. Wind power is intermittent and forecasts more than a few days in advance are very unreliable. Modern wind power can also be separated into two key divisions- onshore and offshore wind- referring to whether the wind turbine is located on land or in the sea. Figure 2.4 shows Vattenfalls spectacular Lillgrind site. Each of the Siemens 2.3MW turbines is 115 m tall and has a rotor diameter of 93 m.

Figure 2.4: Offshore wind turbines at Vattenfalls Lillgrund site.

Although wind power is fairly well established, the intermittent nature of the wind resource reduces the usefulness of large amounts of wind generation (Oswald *et al.*, 2008; Gross and Heptonstall, 2008). Additionally, the exact environmental impacts of onshore and offshore wind farms are still a source of ongoing debate and research (for example, Fox *et al.* (2006)).

(a) Pelamis device

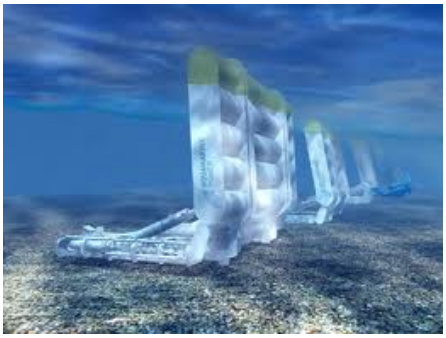

(b) Oyster device

Figure 2.5: Two very different looking WECs: (a) the Pelamis snake and (b) the Aquamarine Oyster device.

The UK has a very large wind energy resource and there is the potential to have 31GW of installed wind capacity by 2020, of which 18GW is offshore and 13GW onshore (DECC, d).

2.1.4 Wave Energy Conversion

Wave power involves converting the orbital motion of water waves in the ocean to electricity. This in itself poses some technical challenges, as it is neither straightforward to convert this orbital motion into the circulator motion required to drive a conventional generator, nor is it straightforward to design an effective linear generator. Wave power interest experienced a boom in the 70's, possibly driven by the oil crisis of 1973; however, despite promising research, funds were cut as fossil fuel prices reduced and nuclear energy experienced a boom in popularity. More favourable recent attitudes towards sustainable energy have meant that wave power is once again an area of significant research. The Salter Duck is an early example of a Wave Energy Converter (WEC), invented by Stephen Salter at the University of Edinburgh (Salter, 1974).

There are several types of WEC's in the design phase, with ideas ranging from the snake-like Pelamis (as shown in Figure 2.5a), to the Oyster device made by Aquamarine (shown in Figure 2.5b), to onshore devices resembling World War 2 bunkers which use the impact of waves to drive and suck air through Wells turbines. Wave power depends fundamentally on the wind and is thus both intermittent and difficult to predict accurately more than a few days in advance.

The extractable UK wave resource is estimated at around 6GW (DECC, b).

2.1.5 Tidal Current Energy Conversion

Tidal Current Energy Conversion involves extracting the kinetic energy from the fluid flow of water moving in tidal currents, very much analogous to wind energy. Tidal turbines are placed in the fluid stream, and are turned by the flow of the tides, in turn driving generators. The main difficulties involved with TCEC lie with the hostile nature of the marine environment and with the intermittency inherent in tidal cycles. Often in the places where the resource is strongest (like the Pentland Firth North of Mainland Scotland), the currents are very fast and energetic, and the slack-water period is very short, making device installation technically very challenging.

Like wave energy there are a handful of operational devices in the latter stages of the design phase. Figure 2.6 depicts one of these devices, the 1.2MW MCT Seagen device.

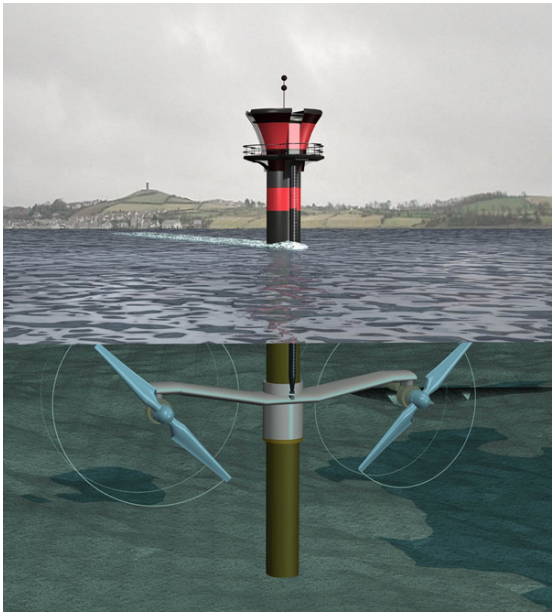

Figure 2.6: An artists impression of the new MCT turbine operating in Stranford lough, Northern Ireland.

The UK has a considerable potential tidal current energy resource. Current estimates of the total power dissipated by tidal currents in the waters around the UK are of the order of 200GW (Cartwright *et al.*, 1980; Ray and Egbert, 2001). However the extractable resource is smaller. L S Blunden and A S Bahaj (2007) estimates the extractable resource at 2 to 7 GW and Black & Veatch (2011) estimates that 20.6 TWh per year (∼2.4 GW) could be practically extracted from 30 key tidal stream sites in the UK. Black & Veatch (2011) also suggests that this could be increased up to 29 TWh through a shift in priorities from other sea uses (i.e. shipping, fishing and designated conservation areas) to energy generation from tidal streams. There is considerable uncertainty in all the resource estimates as, despite a growing understanding of tidal dissipation processes, there is not yet a fully robust data set which could be used to inform

the assessment process. However, even with this uncertainty, one must conclude that there is indeed a sizable tidal resource which could contribute a significant proportion of the UK's energy requirement.

2.1.6 Geothermal Power

Geothermal energy generation is the process of using heat sources from within the earth to create electricity. There are three main types of geothermal plant; dry steam plants, flash steam plants and binary cycle plants. Although they use differing methods to generate steam, they all use heat from the earth to create steam and electricity is generated in the same manner as in a conventional thermal power station. Where available, it is a very good source of electric power as it is generally regarded as sustainable and reliable (no associated intermittency). The geothermal temperature gradient between the very hot core of the planet and its surface drives a continuous heat flow from the center of the earth to the surface. This temperature gradient is usually very gradual through the earths outer crust, but there are some places where high temperature geothermal resources are available near the earths surface. These are generally located near tectonic plate boundaries. Until recently geothermal plants have been built exclusively in these regions but the development of binary cycle plants and advances in drilling technology are allowing lower temperature geothermal resources to be more widely exploited. The Chena Hot Springs plant in Alaska came online in 2006 with a record-low hot fluid temperature of 57^{o}C (Erkan *et al.*, 2008). However, even with these recent advances geothermal power is still not as widely applicable as most other renewable sources of energy.

2.1.7 Biomass

Biomass is biological material that has come from living or recently living organisms. As a renewable energy source biomass refers to the conversion of this biological material into energy. The natural history of biomass is microbial decay of organic material, releasing energy very diffusely into the environment. By gathering up biomass and substituting microbial decay for combustion, the potential for a thermal plant to generate industrial power can be realised. Microbial processes can also be used to produce combustible gases, i.e. production of methane from landfill sites.

It is a useful and versatile source of energy as biomass can also be converted into biofuels, which can be used in the same way as fossil fuels (i.e. in the transport industry). One very satisfactory method of energy production from biomass is the production of combustible gases from food waste, waste from food crops, and human and animal waste. However biomass has several outstanding issues; burning biomass produces CO_2 and other air pollution (in some cases this is more so than traditional fossil fuels), and to use it extensively would require huge areas of arable land which would otherwise be available for food production.

One potentially promising area in biomass is the production of biofuels from algae. Gouveia and Cristina (2009) describe recent research on microalgae which have potential to permit the use of non-arable land and non-potable water for biofuel production.

2.1.8 General Remarks

Of all the types of renewable energy listed, some are inherently easier to exploit than others. The fluid flows associated with hydroelectric and wind energy are easily utilised to drive a generator, with fewer engineering issues than are involved in installing and maintaining tidal current energy converters. The heating effect from focussing the suns rays can simply be used to boil water, and solar cells are becoming more efficient and longer-lasting. Geothermal can provide a very easy to exploit source of heat if the source is located very near or on the surface of the earth. Some forms of renewable energy do not have problems with intermittency. Geothermal and Biomass can essentially be conventional thermal power plants without the dependence on fossil fuels, hence are no more intermittent than conventional thermal generation (although biomass is also largely seasonal in temperate climates), and geothermal also essentially removes all the CO_2 production from the electricity generating process.

Each form of renewable energy conversion also suffers from its own set of problems. Wind, wave, tidal and solar are all intermittent, although tidal currents are cyclic and thus largely predictable. Hydroelectricity suffers from intermittency but not to the same degree; however this is still an issue, especially in regions where large seasonal variations in rainfall exist. Hydroelectricity and geothermal power require favourable geography, and due to this fact many of the most suitable sites for these types of systems have already been used up. Hydroelectricity and Biomass both have issues in terms of the arable land use (which could be used to grow food), and biomass involves carbon emissions, and so doesn't address the issue of climate change as directly as other renewables.

The UK has a vast indigenous wind, wave and tidal energy resource, so these appear to be the renewable resources most suitable for widespread exploitation in the UK. However, all of these resources are intermittent in nature.

If this huge renewable potential is to play a significant part in the UK's future energy generation, many technical challenges will have to be overcome, and it will be crucial to devise ways of coping with the intermittent output of these resources.

2.2 Energy Storage

Energy storage refers to the process of storing energy that can then be released to perform a useful operation at a later stage. In the present context of electricity grids and networks, the phrase energy storage is used to describe the process of removing electricity (or energy that would have otherwise been converted to electricity) from an electricity grid and returning it to the grid at some later point in time. Therefore an energy storage device is one which can take or withhold energy from an energy network (in times of surplus), and return it to the network at a later time (of high demand). Low-cost large-scale efficient energy storage would contribute to a platform on which to base a 100% renewable energy network.

2.2.1 General Reasons for Energy Storage

Effective energy storage would contribute significantly to achieving the following goals:

1. Decarbonisation: A low carbon energy future
2. Energy security and reliability
3. Energy price stability

Decarbonisation here refers to the removal of carbon (in any form, i.e. CO_2, CO etc..) from the exhaust of thermal generation plants. In its 2010 energy mission statement (DECC, a) the UK government states that it seeks to deliver "secure energy on the way to a low carbon energy future". In this context, "low carbon energy future" means a drastic reduction in the CO_2 emissions from electricity generation, transport and heating systems.

Energy Security deals with our ability to guarantee energy supply. The UK is currently hugely reliant on fossil fuels for our energy needs. Approximately 8% (net) of oil, 32% of gas and 70% of coal is imported (DECC, a). With the oil and gas output from the North Sea in decline, projections for 2020 suggest that oil will be in the region 45-60% imported and gas could be more than 70% imported (DECC, a). This begs the question of where these supplies will come from. Globally, 48.1% of oil reserves are located in the Middle East, and 49.3% of the world's gas is located in Russia, Qatar and Iran (BP statistical Review 2012). Lots of the oil and gas rich countries here are in states of civil unrest or in the process of major political upheaval, and the wisdom of relying on them for something as crucial as energy needs must be questioned. 2012 has seen significant growth in unconventional gas resource estimates- particularly shale gas in the U.S. and this has the potential to change global energy mixes. There is keen interest in what the prospects for the UK may be, though the resource is still relatively unexplored, and there are significant concerns over its economic viability and safety. Also, with the energy needs of developing countries such as India and China (amongst others) hugely increasing, the demand for fossil fuels can only be expected to increase, sending prices soaring.

Matching renewable energy supply and demand, and avoiding renewable curtailment. Energy supply and demand are constantly varying. The supply must have some flexibility to

cope with fluctuations in demand. Intermittent energy however may or may not be available at peak demand periods, and so introduces different effects to the network. At any point in time the network will have some demand to be met at a certain physical location. This location will have a certain size of connection to the rest of the network allowing for the maximum demand at that location to be met. If renewable energy supply is added in this region, then there will be some times when the renewable generation is effectively reducing the demand at that point in the network. If enough renewable generation is added then it may exceed all the local demand at certain times, and either it must be curtailed or it must export power into the rest of the network. This will require some export capacity of the local network. Hence the constraint imposed by the network on renewable energy generation at that point in the network will be the export capacity plus the local demand, and as local demand will vary with time, this constraint will too. This is especially relevant to renewable energy generation embedded in the distribution network. Energy storage could help ease this constraint on renewable energy generation by essentially providing increased demand at times when renewable energy would otherwise be constrained. This stored energy would then be used to either meet local demand at a later time or be exported from the local network when transmission constraints eased. Figure 2.7 illustrates this case.

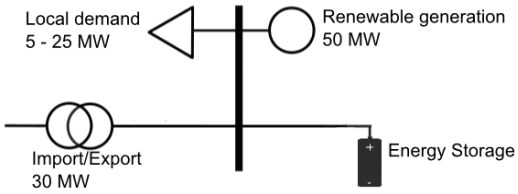

Figure 2.7: Illustrating a network section with local demand, distributed renewable generation and energy storage.

In Figure 2.7, the local demand varies between 5 and 25 MW. There is 50 MW of renewable generation. Therefore, when the demand is at the maximum of 25 MW, there is 25 MW of renewable power which can be exported to the rest of the grid via the 30 MW Import/Export link. At minimum demand however, only 5 MW of renewable energy can be used locally, and 30 MW can be exported. Therefore the network imposes a constraint of 35 MW on the renewable generation. By adding 15 MW of storage with sufficient capacity any curtailment could be avoided and the stored energy either used to meet local demand when the intermittent renewable generation was not sufficient or exported to the rest of the grid if the prices were favourable. In this manner local energy storage could offer benefits in terms of increasing the amount of renewable energy exported from renewable sources, allowing more renewable energy to meet local demand and avoiding the need for transmission upgrades in these regions.

Reliability refers to the ability to cope with unpredictable variations in supply and demand. A reliable energy network is one in which energy must be provided at all times when it is

necessary- there must be minimal "loss-of-load" probability. This issue is magnified when intermittent (renewable) energy sources are incorporated into the supply portfolio. When this is the case unpredictable supply-side variations are increased. Any increase in unpredictable supply-side fluctuations resulting from renewable energy generation must be covered by the grid reserves, i.e. the short term reserve capacity- this could be provided by pumped storage or part-loaded steam plant. In the UK, the reserve requirements of the grid are to cover 3 standard deviations (more than 99%) of the potential unpredicted fluctuations (in both supply and demand), as implied by Equation 2.1 (Gross *et al.*, 2007). σ_d and σ_s are the standard deviations of the potential uncertain fluctuations in demand and supply respectively. Hence, any increase in the supply side fluctuations will increase the reserve requirements.

$$Reserves = \pm\sqrt{\sigma_d^2 + \sigma_s^2} \tag{2.1}$$

Controlling Frequency Response. Energy storage is also particularly suitable for controlling the frequency response of the grid to ensure that system frequency can be maintained within statutory and operational limits. When a large load is connected to the grid the frequency falls, as generators slow down, and when a large load is removed, frequency rises. The primary response to a change in load is the slowing down or speeding up of the generators as they encounter more or less resistance. Energy storage can provide secondary response, being very quickly dispatched in order to counter this change in frequency, by either increasing its output to increase the frequency or by absorbing power to decrease the frequency. This is often referred to as "spinning reserve". It can also be provided by thermal generators working at part-load that can quickly change their output.

Energy Price Stability is a direct consequence of variation in supply and demand. The price of energy is fundamentally linked to the economy (indeed the current UK recession is in part being blamed on high oil prices), and affects the price of virtually every traded commodity. Oil prices in 2011 exceeded $100 a barrel for the first time (BP statistical Review 2012). The 2009 UK electricity spot market price ranged from 5.27 £/MWh to 517.46 £/MWh and the 2010 spot market price ranged from 18.6 £/MWh to 326.09 £/MWh (Elexon). While most consumers do not participate directly in markets showing these levels of volatility, Regnier (2007) concludes that

> "price fluctuations are nevertheless painful for household consumers".

Decarbonisation can occur through the replacement of conventional fossil fuel power plants with renewable energy generators. These renewable energy generators have much lower carbon emissions, as they have no fuel associated carbon footprint. However, renewable energy sources cannot simply provide continuous power without energy storage, and energy storage appears to offer significant opportunities for effective supply-demand matching. With storage, some of the energy generated during times of high power output can be used to cover periods of

low output, giving a continuous power output and thus allowing for the complete removal of fossil fuel generating capacity. Even with storage over relatively small timescales or using small amounts of storage in weak grid networks, storage can facilitate a significant increase in the usage of renewable energy (Barton and Infield, 2004). Indeed, Barton and Infield (2004) conclude that

> "Energy management incorporating energy storage over 24 h and energy curtailment can allow up to three times the amount of wind energy to be absorbed by a weak grid compared to conventional grid connection of wind farms"

Capacity credit is a term describing the ability of intermittent generation to displace thermal plants (without compromising reliability). Energy storage theoretically allows for renewable generation with 100% capacity credit. As a consequence of Equation 2.1 an increase in renewable generation leading to an increase in supply side fluctuations will increase the reserve requirements of the grid and so, indirectly, increase the price of electricity. The presence of energy storage should mitigate this increase in supply side fluctuations.

Effective energy storage would provide an important increase in flexibility to future energy systems with high proportions of renewable energy, which is crucial to sustainable development. Connolly et al. conclude that in order to facilitate the widespread implementation of renewable energy, future energy systems will need a mix of energy storage, demand-side management and interconnectivity (Connolly *et al.*, 2011).

Storage increases the level of energy security by allowing wider integration of renewable energy generation into the Grid. There have been several articles written examining the suitability of various energy storage technologies for the grid integration of intermittent energy generation (Carrasco *et al.*, 2006; Barton and Infield, 2004). Indeed, flexibility within future energy systems is often regarded as crucial to sustainable development and there is growing opinion that in order to facilitate the widespread implementation of renewable energy, future energy systems will need a mix of energy storage, demand-side management and interconnectivity (Lund, 2011; Connolly *et al.*, 2011). The UK has a large indigenous renewable resource, while the indigenous fossil fuel resource is in constant decline. As previously stated storage facilitates the replacement of fossil fuel generating capacity with renewable sources. Hence the ability to generate electricity becomes independent of the volatile price and availability of fossil fuels (not only is petrol volatile in its chemistry but in its worth!). Stockpiling of fossil fuels is currently the most important means of providing some degree of energy security (Wilson *et al.*, 2010).

Storage also offers resolution to the problem of maintaining energy price stability in electricity markets. It is expected that any energy storage device acting on the electricity market would buy at times of low-cost and sell at times of high. The effect of this should be a general smoothing of electricity prices, as market players anticipate that storage will act to increase demand when it is low and to increase supply when demand is high. This is further discussed in Chapter 4.

2.3 Energy Storage: the state-of-the-art

The next section provides a brief description of most of the relevant methods of energy storage and the current state-of-the-art.

2.3.1 Pumped Hydro Storage (PHS)

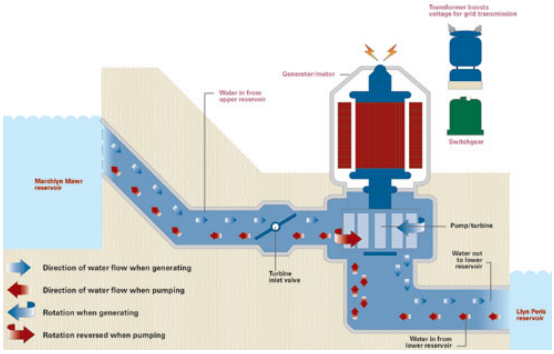

Figure 2.8: A Schematic diagram of a pumped hydro storage system.

This is by far the most satisfactory method for storing large amounts of electrical energy (MWhrs). With relatively simple engineering involved yielding round trip efficiencies in the range 70-85% (utilizing high efficiency Francis/Kaplan/Pelton type turbines) for PHS (Ibrahim *et al.*, 2008; Schoenung *et al.*, 1996; Kaldellis, J and Zafirakis, 2007) this is a commercially available and economically attractive way of storing energy. PHS systems are reasonably common worldwide in areas with favourable geography. Figure 2.8 is a schematic diagram of a typical pumped hydro scheme.

However, the storage capacity and discharge rate of conventional PHS is fundamentally limited by the geography of a region, and as a result the best sites in the UK have been implemented. To increase the potential for PHS this limitation must be relaxed. Investigations into Underground PHS (U-PHS) (Uddin *et al.*, 2003) and seawater PHS schemes are underway, and if they prove commercially viable widespread implementation can be expected.

2.3.2 Secondary Batteries (electrochemical)

Secondary batteries are rechargeable batteries which are designed to be used multiple times, as opposed to primary batteries which are disposable batteries designed to be used once and then discarded. Battery storage technology provides the most widespread and satisfactory method of storing relatively small amounts of energy which can be used to power portable electrical devices. Energy is stored in electrochemical form; during charging the positive active species is oxidised, while the negative is reduced. There are a wide range of battery technologies available (see Hadjipaschalis *et al.*, 2009; Divya and Ø stergaard, 2009). Lead Acid batteries are most

common, and are commercially used for utility applications as well as smaller scale applications. For larger applications, modular systems can be used, although these must be complex in construction to meet high voltage and current requirements. Lithium based technologies have the best energy densities (up to 2000Wh/kg) (Ibrahim *et al.*, 2008).

Due to limitations on cycle life, depth of discharge, and the complexity required to meet high voltage and current requirements, secondary batteries are not especially suitable for applications that require rapid cycling. The chemical species involved also mean that secondary batteries are not suitable for use in environmentally sensitive sites and remote locations with harsh environments. At present the technology seems most suited for small-medium scale capacity requirements where rapid recharge is not required, maintenance can be easily performed and there are no environmental concerns - i.e. not generally applicable in hostile environments where leakage could be an issue.

Modern battery research is focussing on achieving higher energy densities- by using silicon nanowires the energy density of a lithium based battery can be increased by a factor of 10 (Chan *et al.*, 2008). However, the fundamental hurdle for batteries is a relatively short cycle life (especially for large amplitude cycling) and current high costs (Ibrahim *et al.*, 2008).

Another promising variant for larger scale non-mobile applications are the Sodium Sulphur batteries (Tamyurek *et al.*, 2003), which have relatively high efficiencies (in excess of 85%) and long cycle life. Although often quoted as having no self-discharge, they must be constantly heated to keep them at temperatures around 300^{o}C, which can effectively be converted into a time-dependent loss depending on the level of insulation. This type of technology has been demonstrated outside of laboratory conditions but current costs are too high for it to be commercially attractive at present- currently cost estimates lie at about £2-3 million for a 10 MWh unit (Wen *et al.*, 2008).

2.3.3 Batteries (flow batteries)

A flow battery is essentially a rechargeable fuel cell that functions by passing electrolytes through an electrochemical power cell which converts chemical energy to electricity and vice versa. Figure 2.9 shows the main characteristics of a typical flow battery system.

The basic principle involves storing two active species (electrolytes) in different oxidation states. These species then flow through the electrochemical cell where there is an ion exchange through an ion selective membrane (Bartolozzi, 1989).

The major potential advantages of flow batteries are the ability to independently manipulate the power and energy capabilities (power can be varied by the sizes of the electrodes while energy capacity can be varied with ion concentrations and size of electrolyte tank) and that they can also be fully charged and discharged without significantly affecting longevity (Ponce De Leóna *et al.*, 2006). However, the technology is still in its infancy and there are few products

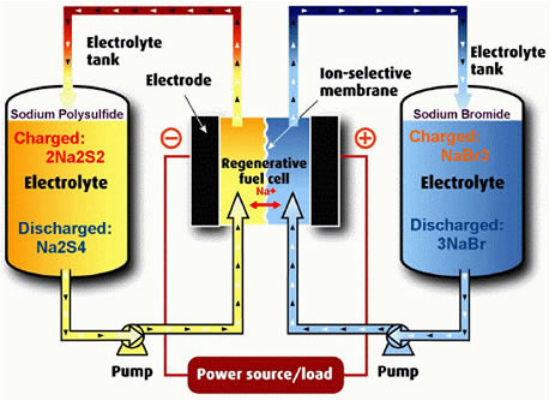

Figure 2.9: A depiction of a PSB flow battery (source Ibrahim *et al.* (2008)).

available on a commercial basis. There has been some UK interest in flow batteries, like the Regenesys flow battery project at Little Barford in 2002 that had a design of 120 MWh with 12 MW power, but this has since been discontinued. The exact reasons for this are unclear, with statements from the parent company RWE power blaming a combination of financial and engineering problems.

Variants like Vanadium cells (V/V), Polysulphide Bromide Batteries (PSB) and zinc bromine (ZnBr) offer promise and recent work has been carried out investigating the potential for wind energy integration (Holzman, 2007).

2.3.4 Flywheels

The principle behind flywheel energy storage is to store energy in the form of rotational kinetic energy. The amount of energy stored depends upon the moment of inertia, I, of the rotating mass and its angular velocity, ω, as described by Equation 2.2.

$$E = \frac{1}{2} I \omega^2 \tag{2.2}$$

To charge the flywheel useful energy (usually electrical, although direct mechanical drive systems are being explored) is used to increase the rotational speed of the flywheel- thus increasing its energy content. To discharge, kinetic energy is extracted from the flywheel (the flywheel is slowed) and converted into electricity via a generator (driven by the flywheel). Flywheels have long lifetimes (and require very little maintenance), can be very rapidly cycled and have good efficiency over short timescales.

They can generally be separated into two categories. Low speed systems (up to around 6000rpm) and high speed systems (up to around 50,000 rpm). Low speed systems are a reasonably mature technology, are commercially available and indeed are extensively used in power quality applications. High speed systems are a technology more in research and development, and

must be constructed of composite materials (to tolerate very high tensile stresses). They usually require low friction magnetic bearing setups and spin in a vacuum enclosure (Hebner and Beno, 2002).

Flywheels are really only suitable for applications which require high cycling, high power and small response times. Crucially, they suffer from very high self discharge rates making them unsuitable for storage over timescales much longer than a few tens of minutes. Currently, there is interest in flywheel systems for regenerative braking in buses and trains, and several prototype systems exist.

2.3.5 Super-Capacitors

A Super capacitor (also called an Electric double-layer capacitor) is a capacitor with a relatively high energy density. The energy is stored via an electrostatic field. The energy stored by a capacitor, E (Joules), is given by Equation 2.3:

$$E = \frac{1}{2}CV^2 \tag{2.3}$$

Where E is the electrostatic energy stored, C is the capacitance and V is the voltage difference across the capacitor plates. The capacitance C is given by Equation 2.4:

$$C = \frac{\varepsilon_r \varepsilon_0 A}{d} \tag{2.4}$$

Here ε_r is the relative static permittivity, ε_0 is the electric constant (also sometimes called permittivity of free space) ($= 8.854 \times 10^{-12}$ Fm^{-1}), A is the area of overlap of the plates and d is the seperation distance between the plates.

Whereas a conventional capacitor uses a dielectric to separate the capacitor plates, a super capacitor consists of virtual plates that are actually two layers of the same substrate. The super capacitor then stores energy between a solid porous electrode and oppositely charged electrode ions. The very large surface area of the porous electrode allows for much higher capacitance than conventional capacitors.

The energy density of super capacitors is generally an order of magnitude less than that of conventional batteries, but the power density is generally 1-2 orders of magnitude greater. They can also be cycled much more effectively, generally showing very little degradation over thousands of charge/discharge cycles (Mufti *et al.*, 2009).

They suffer from relatively high self-discharge rates compared to conventional batteries and require more complex electronic control as the voltage of capacitors falls significantly as they are discharged. Current applications rely on combining super capacitor and battery technology, in order to combine the power performance of the former with the energy storage capability of

the latter. Commercially super capacitors are available with energy densities of 6Wh/kg (see Maxwell Technologies), although experimental variants exist based on graphene materials with 28.5Wh/kg and a power density of 10kW/kg (Wang *et al.*, 2009).

2.3.6 SMES

Superconducting Magnetic Energy Storage (SMES) is a method of energy storage based upon the fact that a current will continue to flow in a superconductor even after the voltage across it has been removed. When the superconductor coil is cooled below its superconducting critical temperature it has negligible resistance, hence current will continue to flow (even after a voltage source is disconnected).

The SMES concept started with the idea of very large plants with capacities of GWdays, that were intended for diurnal load levelling (Buckles and Hassenzahl, 2000). However, with the advance of superconductor technology, notably the increase in T_c (the critical temperature of the superconducting transition), recent research has mostly been on smaller scale applications. However, costs are the fundamental hurdle, with estimates of $40 - $50 million for a 1MWh plant (Lieurance *et al.*, 1995).

2.3.7 Hydrogen Energy Storage

Hydrogen energy storage usually involves the electrolysis of water to form Hydrogen gas, which is then compressed and stored, then recombined into water to release electrical energy using a fuel cell. In terms of energy storage potential, hydrogen has the huge advantage that it is a portable fuel and can be used in portable applications, like fuel for the automotive industry. Honda and Nissan have developed cars which run on compressed hydrogen stored at a pressure upwards of 350bar (see Honda).

The main issues involved with Hydrogen energy storage are low efficiency and storage of the hydrogen which usually requires very high pressures. The best round trip efficiencies currently lie around 35-40% (Ibrahim *et al.*, 2008) due to the combination of losses in the electrolyser (about 70% efficient) and the fuel cell (about 50% efficient). Figure 2.10 shows the fuel cell part.

However, there is ongoing research on combining hydrogen storage with wind turbines (and solar power) so that at times of potential curtailment the electricity generated by the wind turbines is used to drive the electrolyser rather than simply be curtailed. The prospect of using hydrogen as fuel for vehicles is one possible way in which the transport sector could be decarbonised, which would be necessary in a 100% renewable energy system (Lund, 2007; Turner, 1999).

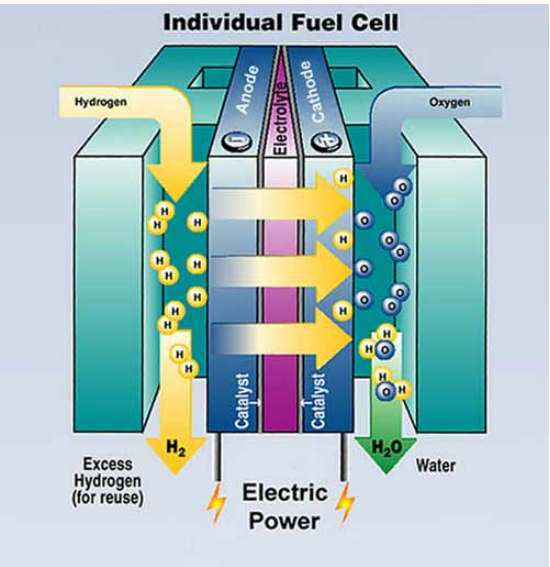

Figure 2.10: An individual fuel cell (source US D.O.E., office of energy efficiency and renewable energy).

2.3.8 The special case of Compressed Air Energy Storage (CAES)

Currently there are two commercial CAES plants world wide; the Huntorf plant in Germany and the McIntosh plant in Alabama. Both of these run a ***diabatic*** system in which off-peak grid electricity is used to compress air into large underground caverns, as illustrated in Figure 2.11. Diabatic means that the temperature (of the air) is independent of the temperature change caused by adiabatic processes, in this case the air is heated externally by combustion. The compression is done in several stages coupled with inter-cooling to dump the heat of compression. During peak times, compressed air is then mixed with natural gas and combusted in a gas turbine. By using low-cost electricity to pre-compress the air, the efficiency is raised significantly above that which could be expected from a single cycle gas turbine (a typical peaking plant). SCGT's usually have an efficiency of between 35-40%.

The Huntorf plant, commissioned in 1978 to become the world's first CAES plant, uses 0.8kWh of electricity and 1.6kWh of gas to produce 1kWh of electricity. This yields an overall efficiency of 41.7% (B.I.N.E. Informationsdienst, 2007). The McIntosh plant does rather better as it incorporates a recuperator. It uses 0.69kWh of electricity and 1.17kWh of gas to produce 1kWh of electricity(B.I.N.E. Informationsdienst, 2007). Calculating efficiency is problematic- as either one can take the approach that the 0.69 kWh of electricity input required $\sim$1.725 kWh of gas (assuming a gas turbine efficiency of 40%), implying an overall efficiency of $\frac{1}{1.17+1.725}$ = 34.5%, or equally it could be suggested that 1.17 kWh of gas would have produced 0.468 kWh of electricity, and the efficiency should be $\frac{1}{0.69+0.468}$ = 86.4%! Nevertheless both plants find it commercially viable to buy the respective quantities of off-peak electricity and gas required to produce peak electricity.

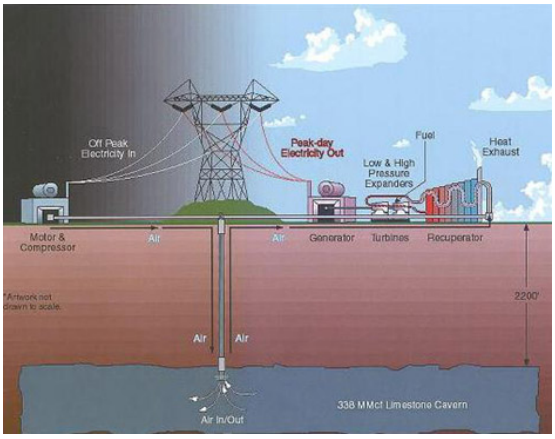

Figure 2.11: A schematic diagram of a conventional diabatic CAES system.

There is also recent interest in the possibility of running a CAES system without the need for natural gas. This would run an adiabatic system rather than a diabatic system, and is usually refered to as Advanced Adiabatic Compressed Air Energy Storage (AA-CAES). At present there is no such plant in existence. This is the subject of Chapter 4 and is very extensively discussed.

2.3.9 Pumped Heat Energy Storage (PHES)

Pumped Heat Energy Storage (PHES) is a new idea for a method to store energy, exploiting the high energy density of sensible heat contained in solids. The process stores energy as sensible heat and cold in both a high temperature and low temperature vessel. The principle idea is to take electrical energy from the grid, using it to pump heat from the cold vessel to the hot vessel, propagating a cold thermal front through the low temperature storage vessel and a hot thermal front through the high temperature storage vessel. The charging process is analogous to a heat pump, and can achieve coefficients of performance (COP) many times unity — by pumping heat from cold to hot it is possible to move more heat energy than the electrical energy input that is inputted. The discharging process is then a heat engine, using the difference in temperature between the hot and cold storage tanks to generate work. This allows a warm front to propagate through the cold storage and a cool front through the hot storage, bringing the system temperatures closer together. Even though the conversion of heat to electrical energy is relatively inefficient in absolute terms, the fact that the heat pump can have a high COP means that preliminary calculations suggest an efficiency in excess of 70% is achievable. Figure 2.12 shows a schematic diagram of a PHES system.

The PHES idea has several advantageous aspects. It should have a favourable energy density compared with many other types of energy storage (with bricks at 1000^{o}C the energy density is about 600 kWh/m^3 (water at 360 m height has 1 kWh/tonne, Li-Ion batteries have about 200 kWh/tonne)), it doesn't require any favourable geography and percentage energy losses from

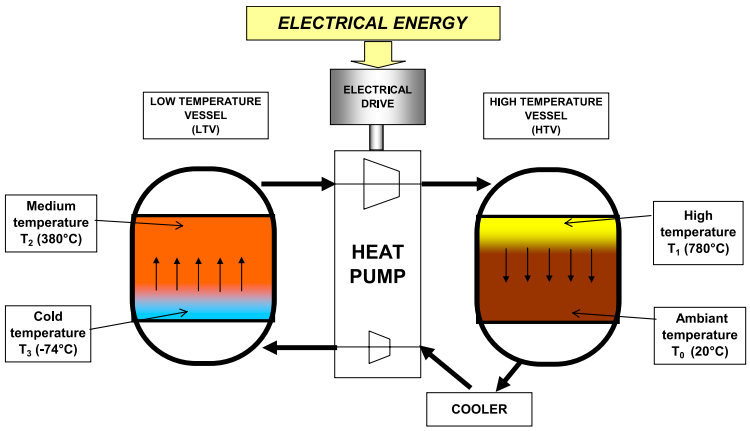

Figure 2.12: The charging cycle for a PHES system. Medium temperature gas is compressed to a high temperature in a compressor. This pushes out ambient temperature gas of the high temperature vessel which is expanded to a low temperature in an expander. The cycle is reversed to discharge. Taken from Ruer *et al.*

heat losses are reduced as the system size gets bigger (this is because heat losses depend on surface area whereas capacity depends on volume). However, it is a new technology in research and development, and currently only prototype devices exist. Several companies are currently investigating this as a technology that could be used to solve the energy storage problem on a large-scale, including Isentropic Ltd and Saipem (Ruer *et al.*). Isentropic claim that they can achieve a levelised cost of storage of $35/MWh (Isentropic Ltd).

2.3.10 Thermal Energy Storage

Thermal energy storage refers to the storage of thermal energy in storage reservoirs for later use. The temperature of the storage reservoir may be hotter (hot storage) or colder (cold storage) than the ambient environment. There are three types of thermal energy storage: These are sensible heat storage, latent heat storage and thermo-chemical storage. Sensible heat storage exploits the specific heat capacity and refers to the case in which energy is stored by raising or lowering the temperature of the medium in the thermal storage reservoir, without any phase change occurring. For example, the storage of heat in water or rock with no phase change (boiling or melting) encountered. Latent heat storage refers to the case in which the heat transfer induces a phase change, and as such a significant amount of energy is stored in the latent heat of the phase change. The energy is stored in Phase Change Materials (PCM's), which offer particular advantages over sensible heat storage in terms of high energy-density storage and the isothermal nature of the phase change transition. However the material (and the temperature of its phase transition) must be carefully matched to the exact application, they often suffer from poor thermal conductivity and can have problems with segregation and chemical stability. Thermo-chemical storage relies on the energy absorbed and released in the breaking and reforming of molecular bonds in a completely reversible chemical reaction.

Thermal energy storage is very useful tool and has a large potential for further expansion when the end form of the energy required is heat. Most commonly thermal energy is stored from Combined Heat and Power (CHP) plants, though heat from solar collectors is also often stored. This is used in district heating systems. Water is often used as a storage medium, due to its relatively high heat capacity (4.19 $kJkg^{-1}K^{-1}$), however, rocks or concrete (which has a heat capacity of 0.88 $kJkg^{-1}K^{-1}$) can be heated to a much higher temperature without melting, so the chosen medium in which to store the heat needs to be matched to the application. There is also significant research and several pilot schemes underway into inter-seasonal thermal energy storage, for example the Drake Landing Solar Community in Alberta, Canada and the Passive House in Galway, Ireland.

While the author regards thermal energy storage as a useful and significant contribution to energy systems, due to it only being applicable when the end requirement for energy is heat, it is not discussed further in this thesis, except as a constituent part of other storage systems.

2.3.11 General Remarks

Some of the information from section 2.3 is summarised in Table 2.1. It allows the comparison of the following attributes for the various storage methods; capacity, available power, efficiency, cycling capacity and rough costs per kWh. PHES has not been included as it is in such an early developmental stage. For bulk energy storage, the properties that matter are the cost, the scalability and the time dependent loss (self-discharge). High roundtrip efficiency will also be important if the storage is to be used for energy arbitrage (profiting by buying and selling electricity), although this may be less important if there is a very cheap source of low cost energy that would otherwise be wasted- i.e. curtailed energy from a wind farm.

In general most of the forms of energy storage discussed are not yet suitable for large-scale grid energy storage, with the obvious exception of pumped hydro, which where suitable has been widely implemented, but its further use is fundamentally limited by the need for suitable geography to keep costs to a reasonable level. CAES is also suitable for large-scale use in an electricity network, but doesn't allow for the complete removal of fossil fuels, as conventional CAES depends on burning natural gas. Hydrogen also has potential on a large scale, and would be a very attractive method due to its portable nature; however costs need to be hugely reduced in order for this to be the case. Pumped heat energy storage (PHES) has the potential to be very effective on a large scale, however it is still in development and currently only small-scale prototype systems exist.

There also seems to be potential for energy storage devices on a small-medium scale as well as for large centralised energy storage plants. This scale of energy storage is likely to be applicable to the integration of small-scale renewable generation into regions of the grid with weak infrastructures, as generation shifts away from large centralised units towards smaller renewable generation installed at distribution level. Batteries already seem to have the capability

to operate suitably at this level, but current costs are very high and environmental issues are often restrictive. It is anticipated that an AA-CAES plant would be best equipped to operate in this range.

2.4 The Current Role of Energy Storage

Energy Storage is currently used in a wide variety of roles to help manage power flows in energy networks. Pumped hydro schemes are used extensively to try and balance electricity networks on a large scale, and often operate on the reserve markets. They are used to provide a secondary response as output can be quickly increased to boost the network frequency when a large load is suddenly added to the network or they can very quickly start pumping (to provide load) when a large load is removed. In the UK the pumped hydro schemes are heavily used by the grid to balance the network. That is, they are one of the first ports of call for the TSO to balance the network after the bidding on the spot market closes (1 hour ahead of real time in the UK) at gate closure.

Batteries are used to provide short term back-up power to electricity grids on a small to medium scale, although many of these systems still constitute the latter stages of research rather than being today commercial ventures. Batteries and flywheel systems (and more recently super-capacitors) are often used for uninterruptible power supply (UPS) - very short term energy storage systems and power quality applications - due to their high cycling capacity and rapid rates of charge and discharge. For example, using a battery or flywheel to provide emergency power when mains power fails or there is an unacceptable transient condition on the line, so as not to damage electrical/computing/communication equipment. SMES systems are also currently used for power quality applications where very clean power is needed, for example, in microchip manufacturing plants.

Table 2.2 lists some of the largest Energy storage schemes of each type currently in existence, taken from Gill *et al.* (2013).

2.5 Chapter Summary

This chapter has presented a very brief introduction to all of the main types of renewable energy generation, outlining the features that make each form of renewable energy conversion suitable for implementation in particular locations.

Energy storage has been suggested as a way to combat the intermittency of renewable energy, to add flexibility to energy networks, and to decrease their reserve requirements.

Attribute	PHS	CAES	Hydrogen Storage	Super Capacitors	Secondary Batteries	Flywheels	SMES	Flow Batteries
Storage Capacity (Whr)	0.5-20GWhr[1]	1.15-5MWh[1]	—	up to 3kWh[1,2]	0.5-50MWh[2]	Single rotors from 0.25-6kWh Composites to 5MWh[2]	LS : Up to 1.5GWh[3] SS:1-140kWh	Up to 120MWh[4] —
Available Power (W)	Up to 3GW	currently up to 290MW[5]	up to 2.2MW[6]	1-10MW[2]	Up to 140MW	1-10MW[2]	LS: up to 1GW SS: 1-30MW[2]	Up to 12MW[4]
Efficiency (%)	70-85[2,7,8]	—	35-45[7,8]	90[2]	75[2]	80-95[1]	95[1]	60-70[8]
Cycling Capacity	High	High	High	High	Low	High	High	High
Energy Cost (per kWh)	$15[2], € 10-20[8]	$10[2], € 5[8]	€ 1000-6000[6,8]	€ 13000[2]	$50-200[2], € 210-270[8]	$100-800[2]	SS:$1100 LS:$3000[2]	€ 125-150[8]
Comments	Limited by geography	Limited by geography, requires fuel	High cost	Low Capacity, high self-discharge	Commercially available, high cost for large capacity	Commercially available, high self-discharge	Very high costs	Available but largely unproven yet

[1] Guerrero *et al.* (2009)
[2] Schoenung *et al.* (1996)
[4] Ter-Gazarian (2011)
[4] Sandia National Laboratories
[5] B.I.N.E. Informationsdienst (2007)
[6] INVESTIRE-NETWORK
[7] Ibrahim *et al.* (2008)
[8] Kaldellis, J and Zafirakis (2007)

Table 2.1: Table summarising the properties of the storage systems.

Finally, the main types of energy storage methods in existence have been discussed and information has been gathered on the current state of the art, with the current role of energy storage subject to a brief discussion.

Type of system	Name of system	Peak Power	Energy Stored	Date of use	Footnote
Pumped Storage	Bath County Pumped Storage Station, USA	3000MW	33GWh	1985 -	[1]
Battery - NiCad	GVEA BESS, Fairbanks, USA	27MW	14.6MWh	2003 -	[2]
Battery - $LiFePO_4$	Zhangbei, China	140MW	36MWh	2011 -	[3]
Battery - Lead Acid	Chino, CA, USA	14MW	40MWh	1998-1997	[4]
Vanadium Redox Flow	Gills Onions, Oxnard, CA, USA	600kW	6MWh	2010-	[5]
Zinc Bromide Flow Battery	ZBB Energy	250kW	500kWh	Unknown	[6]
Supercapacitor	SITRAS Stationary Energy Storage (SES)	0.7MW	2.5kWh	2008 -	[7]
Flywheel	Stephentown, USA	20MW	5MWh	2011 -	[8]
CAES	Huntorf	290MW	5MWh	1978 -	[9]
SMES	Florida State University (test bed)	100MW	28kWh	Unknown	[10]
Hydrogen Fuel Cell	Areva Myrte platform, Corsica	200kW	440kWh	2012 -	[11]

[1] Dominiom Corporate
[2] DeVries *et al.* (2004)
[3] BYD Battery Energy Storage
[4] Doughty *et al.* (2010)
[5] Prudent Energy
[6] ZBB Energy Corporation
[7] Siemens
[8] Beacon Power
[9] Crotogino *et al.* (2001)
[10] Luongo *et al.* (2003)
[11] AREVA Group and the University of Corsica

Table 2.2: Existing energy storage technologies with an example of their largest implementation, taken from Gill *et al.* (2013).

Chapter 3

Energy storage in association with tidal current generation systems

In Chapter 2 it was recognised that the intermittency involved with tidal energy conversion is largely due to the cyclic nature of the tides. This cyclic nature makes the intermittency associated with tidal energy different from more unpredictable renewables- such as wind or wave- and may make it particularly suitable for use with energy storage. In this chapter we assess the benefits of combing tidal energy conversion with energy storage. The purpose of this work is two-fold: Firstly, to show that storage can decrease the loss of output from tidal current energy conversion when there are transmission constraints present. Secondly, to specify the properties of the storage system (efficiency, capacity, input/output power limit and self discharge rate) required in order to produce either demand-matching or base-load output from tidal current energy conversion. This is achieved by building a numerical model of a tidal energy converter and an energy storage device, and imposing various constraints on the system output. The model is then run over several spring/neap cycles with each of the constraints, to determine the time dependence of the whole system. It is shown that a 1.2MW tidal current energy generator associated with a 1MWh storage system of modest efficiency can offer significant advantages over the generator working alone.

3.1 Introduction

As has been previously discussed in Chapter 2, capacity credit is the ability of intermittent generation to displace thermal plants (without compromising reliability). At present, findings suggest that capacity credit from renewable supply is in the range 20-30% (Gross *et al.*, 2007) of installed intermittent capacity. This is due to the inability of renewable energy generation to match demand, i.e. the output of the renewable source will not necessarily coincide with times when demand for electricity is high. Energy storage is one way of mitigating the unpredictable fluctuations involved with renewable energy supply, thus increasing its capacity credit. This has the potential to reduce the costs associated with renewable energy technologies through easing

any grid constraints, decreasing system reserve requirements and replacing expensive thermal peaking plants with sustainable and renewable energy generation technologies.

As has been discussed in Chapter 2 (see section 2.2.1), localised renewable energy generation could result in sections of the distribution network reaching their limit to export energy, if the renewable generation exceeds the output transmission capacity and the local demand. Energy storage could be used with intermittent energy supply is to avoid loss of output due to transmission constraint occurring when the output of the Renewable Energy Converter (REC) is larger than the size of the connection (the export capacity) to the grid. Otherwise, energy must be spilled (curtailed/wasted) and loss of energy and hence a loss in potential revenue occurs. This can obviously be circumnavigated by increasing the size of the connection to the grid. This, however, is also costly, especially when the energy generator is remotely located, like an offshore wind farm or a Tidal Current Energy Converter (TCEC), and the local demand is small and only requires a small connection to the grid. Local energy storage (located near the point of generation) could be utilised when the output exceeds the grid capacity, and discharged when the REC output falls below the grid capability. If the costs associated with the on-site storage device were less than the cost of increasing the size of the connection, then this approach should increase the revenue of the renewable energy converter more than increasing the connection size.

Unlike most other sources of renewable energy, the tidal resource is largely cyclic and thus easily forecast to a very high degree of accuracy. While it is still a 'soft' (intermittent) energy source, this predictability allows exact specification of the storage system to which a given tidal plant must be coupled to give a desired output. The coupled output of the REC plus energy storage could be purely baseload, or could be configured to provide more power during times of peak demand. Each of the desired output forms (baseload, demand matching etc.) will specify a different set of requirements of the storage system.

This chapter explores to what extent energy storage in association with tidal current energy generation systems can be used to limit energy losses due to transmission constraints and to provide various different forms of output from TCEC's.

3.2 Energy Storage for Tidal Power

In this section two different approaches to using energy storage with tidal power are developed. Firstly, storage is used as a way to reduce energy curtailment as a result of transmission constraints, increasing the amount of useful energy exported from the REC and potentially reducing the size of the required grid connection. Although this constraint will be variable in time (due to both intermittent energy supply and varying local demand), this chapter illustrates the effect of having a limited 'connection' (capacity for exporting the REC output) by using

a fixed connection size to a REC whose peak output is larger than the size of the connection. Secondly, energy storage is realised as a way to manipulate the form of the output produced by the REC, allowing an output that matches demand, or is purely base-load. In this way, the properties of a storage system required to produce a desired output may be specified.

Note that these approaches are not specific to tidal current energy conversion but the largely cyclic nature of the tidal energy resource, and thus the much higher degree of predictability (than other renewable resources, like wind or wave), allows the requirements of the storage system to be specified with much greater confidence.

3.2.1 Modelling the output from a Tidal Current Energy Converter (TCEC)

In order to estimate the properties of the storage system (i.e. capacity (kWh), input and output efficiency, decay constant (self-discharge rate) (hrs), maximum input rate (kW) and maximum extraction rate (kW)) that are required to produce a desired output from a TCEC; the output from the TCEC must be modelled.

The case of a single 15 m diameter tidal turbine in a tidal stream is considered; based on the MCT device currently in the water in Strangford Lough, Northern Ireland (MCT). Assuming that the form of the tidal diamond is known (which can be measured); a relatively robust and satisfactory model can be made. Many tidal diamonds have an approximately elliptical form, with varying degrees of eccentricity. If the form of the tidal diamond is not well described by the equation of an ellipse, then the underlying steps to simulate the flow in the tidal stream must be changed. Otherwise the velocity of the tidal stream can be readily described as shown in Equation 3.1.

$$\begin{aligned} v_{ns}(t) &= \frac{1}{2}((a_{spring(ns)}+a_{neap(ns)})+((a_{spring(ns)} \\ &\quad -a_{neap(ns)})cos(\frac{2\pi t}{\tau_2}))) \times cos(\frac{2\pi t}{\tau_1}) \\ v_{ew}(t) &= \frac{1}{2}((a_{spring(ew)}+a_{neap(ew)})+((a_{spring(ew)} \\ &\quad -a_{neap(ew)})cos(\frac{2\pi t}{\tau_2}))) \times cos(\frac{2\pi t}{\tau_1}+\Theta) \end{aligned} \tag{3.1}$$

The time-evolution of the resulting tidal diamond will depend on the ratio of the north to south and east to west velocities and the phase difference (Θ) between them. The instantaneous resultant speed of the tidal flow can be calculated using Pythagoras theorem, as shown in Equation 3.2.

$$v^2(t) = v_{ns}^2(t) + v_{ew}^2(t). \tag{3.2}$$

The power per unit area from the kinetic energy flux in the fluid stream is given by Equation 3.3

$$P = \frac{1}{2}\rho v^3. \tag{3.3}$$

In this work, it is assumed that the energy extracted by a stand alone tidal turbine is proportional to this. If we were to place more than one turbine in series then a more sophisticated interpretation is required, as we would have to deal with turbulence, loss of head and frictional dissipation of energy (Bryden and Couch, 2006). This requires a more complex treatment and the effect of large numbers of devices on the resource itself is a scope of much debate. Consequently, here a single turbine is considered.

By analogy with a wind turbine, the output from an axial flow design underwater turbine can be described by Equation 3.4 (taken from Kirke (2006)).

$$P = \frac{1}{2}C_p A \rho v^3 \tag{3.4}$$

Here C_p is the power coefficient, simply the fraction of the total kinetic energy in the fluid stream that is extracted by the turbine. This has a theoretical maximum of ~59%, and is commonly known as the Betz limit.

The Output of the Turbine

Here, the following approach is adopted to simulate the output from a tidal turbine: The power curve of the present simulated tidal turbine (shown in Figure 3.1a) has been designed to closely follow the form of the power curve of the Seagen device as published by MCT in MCT and shown in Figure 3.1a. A cut-in speed at 1 ms^{-1} is used, as suggested is appropriate by the MCT power curve. One can work out the maximum power coefficient from the power curve (Figure 3.1b), $C_{p(max)}$ = 0.42. It is assumed that a cut-out speed is not required. The model is conservative when compared to Seagen output (MCT state that on average C_p = 0.48 (MCT)).

The performance of most real turbines is likely to be constrained (as shown in Figure 3.1a), so that there is a maximum power that can be converted. In the context of tidal streams, where fluid velocities that are high enough to damage the turbine are highly unlikely, the reason for rating the turbine is to specify the generator and the drive train required.

The output of the generator in this chapter has been simulated using Equations 3.1, 3.2 and 3.4, and the power curve shown in Figure 3.1b. The power has been constrained at 1200 kW, the same as the MCT turbine used at the Strangford narrows, Northern Ireland (MCT) (the MCT device consists of two 600kW turbines so has a total generating capacity of 1200kW).

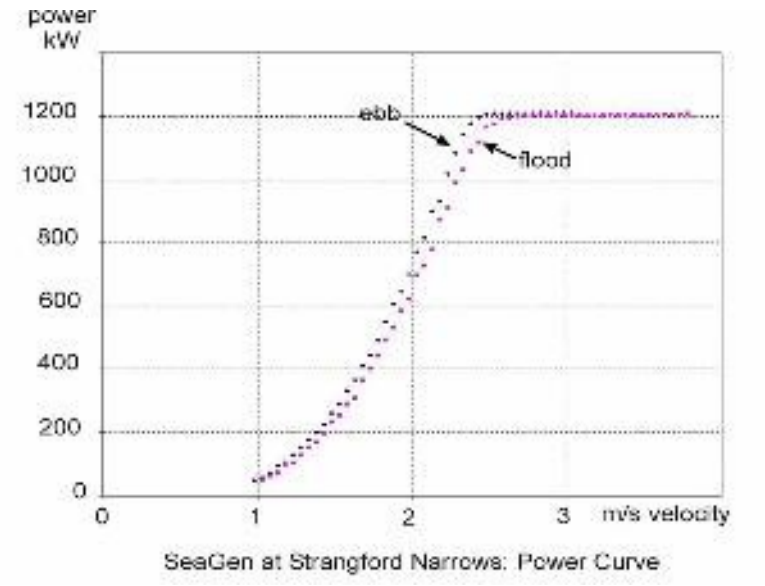

(a)

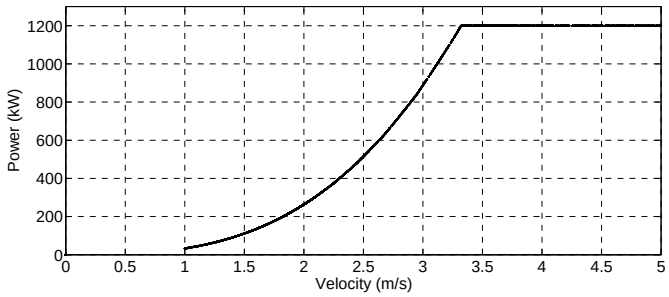

(b)

Figure 3.1: Power curves for (a) Seagen device MCT (graph reproduced from MCT, courtesy of MCT), and (b) the present simulated tidal turbine.

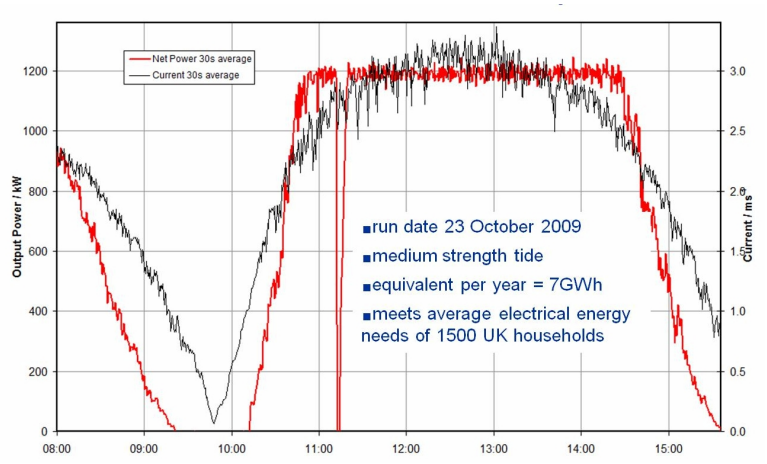

(a)

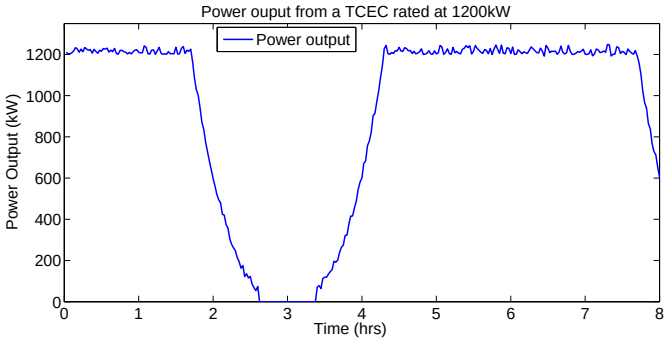

(b)

Figure 3.2: Comparing (a) the output Trace for the Seagen Device (graph reproduced from MCT courtesy or MCT) to (b) the output trace for the simulation.

The output of the SeaGen MCT turbine is shown in Figure 3.2a. The noise (small timescale fluctuations) seen in the output of the real turbine are simulated using a biased random number generator. These are included for completeness, but as the effect of storage is essentially to integrate the output, they will have little overall effect. Figure 3.2b shows the output trace for the simulation.

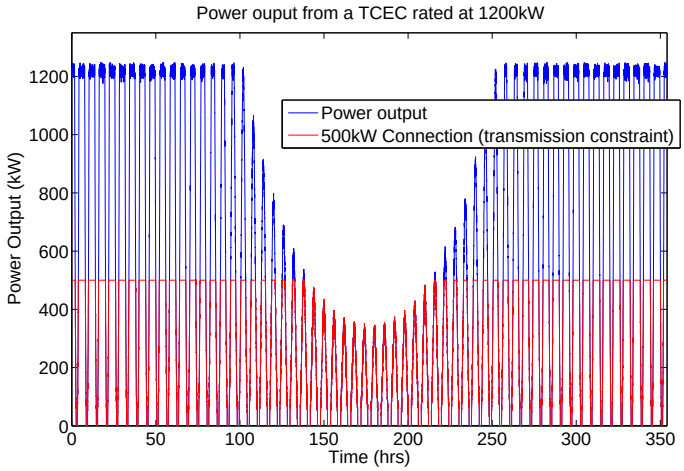

Figure 3.3: Outputs generated using the procedure outlined. Note that the turbine is rated at 1200kW.

Table 3.1 shows some of the Mean Spring Peak (v_{msp}) and Mean Neap Peak (v_{mnp}) velocities for some UK sites with the largest tidal resources, which together, are thought to represent 54.4% of the UK tidal resource (Black & Veatch).

Site	$v_{msp}(ms^{-1})$	$v_{nsp}(ms^{-1})$
Pentland Skerries	6.18	2.64
Stroma p. Firth	5.15	2.20
Duncansby Head	5.15	2.20
Casquets	2.57	1.39
S. Ronaldsay P. Firth	4.89	2.05

Table 3.1: Velocities of UK tidal sites, taken from appendix 1 of Black & Veatch.

As such, it seems reasonable to use the following parameters (table 3.2) for the simulation.

As the perpendicular (east-west) components are equal to zero, the simulation describes a purely bi-directional site. The blue line in Figure 3.3 shows the simulated output for the turbine using the parameters shown in Table 3.2.

Mean spring peak velocity (ns) (ms^{-1})	5
Mean neap peak velocity (ns) (ms^{-1})	2
Mean spring peak velocity (ew) (ms^{-1})	0
Mean neap peak velocity (ew) (ms^{-1})	0
Phase difference (rad)	0

Table 3.2: Table 2: Simulation parameters.

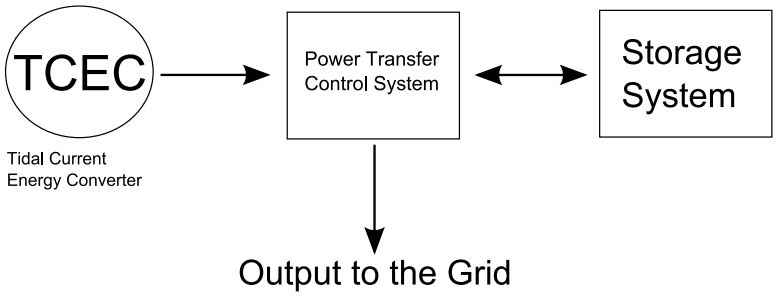

Figure 3.4: Schematic of a tidal current energy converter coupled with a storage system.

3.2.2 Energy Storage when Transmission Constraints limit Peak Output

If the TCEC is connected to the grid using a connection that is smaller than the rated power of the turbine (i.e. Connection size $<$ 1200kW), then only some of the actual energy converted will be sent to the grid.

If a storage system is coupled with the TCEC (using a power transfer control system between the storage and the TCEC), then, when the output from the TCEC is greater than the size of the connection, the difference between the output and the connection is transferred into the storage system. When the output is less than the size of the connection, energy is output from the storage system. In this way, much less of the output from the TCEC is wasted. Figure 3.4 shows a schematic of the system. There will still, of course, be some losses from the storage. These have been modelled as follows:

- There is a round trip efficiency of η_s associated with storing and recovering energy. It has been assumed that the storage and recovery aspects of the process have equal efficiencies of $\eta_s^{1/2}$.
- The energy in the storage system decays with a time constant τ_s, so that after a time t, without any input or output of energy, an energy store of E, will have fallen to $Ee^{\frac{-t}{\tau_s}}$.

The power at which the energy storage system is charged/discharged is governed by Equations 3.5, 3.6, 3.7, 3.8 and 3.9:

$$\begin{aligned} \text{IF } P_T &> CS \\ P_{charge} &= \sqrt{\eta_s} \times (P_T - CS) \qquad (3.5) \\ \text{IF } P_T &< CS \text{ AND } E_{stored} > 0 \\ P_{charge} &= \frac{1}{\sqrt{\eta_s}} \times (P_T - CS) \qquad (3.6) \\ \text{IF } P_T &< CS \text{ AND } E_{stored} = 0 \\ P_{charge} &= 0 \qquad (3.7) \\ \frac{dE_{stored}}{dt} &= P_{charge} - \frac{E_{stored}}{\tau_s} \qquad (3.8) \\ 0 &\leq E_{stored} \leq SOC_{max} \qquad (3.9) \end{aligned}$$

The model then allows the choice of the SOC_{max}, τ_s, η_s and CS (SOC_{max} is the maximum storage capacity). The percentage increase (PI) of the usable energy output from the system with storage ($O_{storage}$) compared to the case without storage ($O_{without}$) can then be calculated by integrating the respective outputs, with and without storage, divided by the integrated power from the turbine (P_T), Equation 3.10.

$$PI = \frac{\int_0^t O_{storage} dt - \int_0^t O_{without} dt}{\int_0^t P_T dt} \times 100 \qquad (3.10)$$

As discussed, the device modelled is a 15m diameter turbine rated at 1.2 MW (velocities as in Table 3.2). Figure 3.3 shows the output over a spring/neap cycle. To illustrate how a significant proportion of the energy generated may be curtailed, the red line in Figure 3.3 shows the energy exported to the grid when the TCEC output is constrained at 500kW. The figure shows that there is a large amount of potential energy wasted and, in fact, upon integration Figure 3.3 it is calculated that with a 500 kW constraint only 56.1% of the total output of the TCEC is usefully exported to the grid. The 500 kW constraint is used throughout this section as it represents the case where the majority of the energy is still exported, but a large fraction is wasted, and hence it is expected that storage will yield a significant increase in the useful energy export.

A 1MWh capacity storage system coupled to the TCEC before the connection to the grid (500kW) is then added to the model. The storage system is assumed to have a transfer efficiency of 80% each way, giving a maximum round trip efficiency $\eta_s = 64\%$, and a decay time constant $\tau_s = 24$hours, hence after 24 hours 23.5% of the energy originally transferred to the store can be extracted. Figure 3.5a shows the output from the coupled system (red line) and the power output of the turbine (blue line). Comparing this to Figure 3.3 we can see that much more useful energy is outputted. In fact, the useful output as a percentage of the total output of the TCEC has been raised to 70.4%. Figure 3.5b shows how the energy in the store will vary across the spring-neap cycle. Figure 3.5b shows us the rate of energy input (P_{charge}) to the storage system.

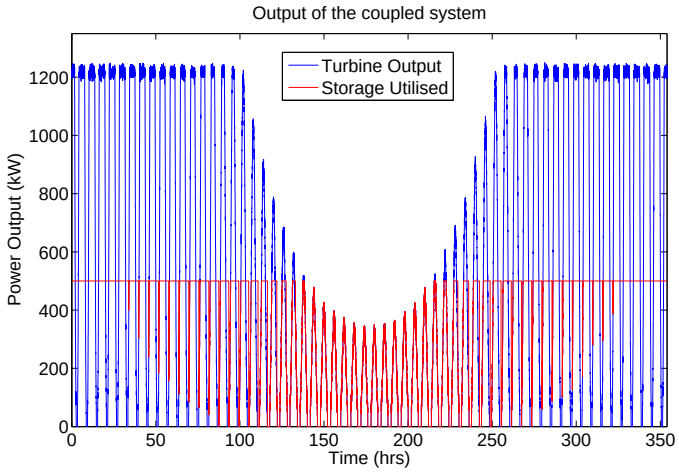

(a)

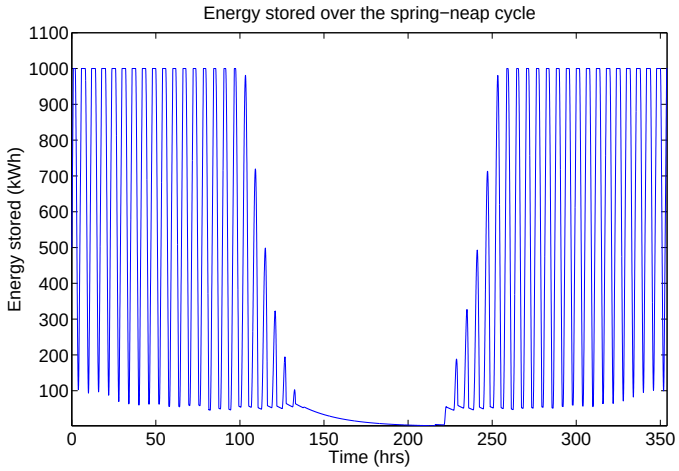

(b)

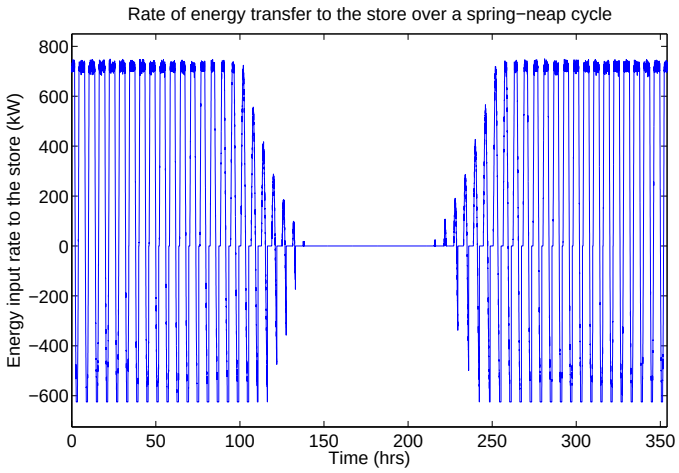

(c)

Figure 3.5: (a) The output of the TCEC coupled to a 1MWh storage system is shown along with the total power output from the TCEC over a spring-neap cycle. (b) The energy level in the store as a function of time over a spring-neap cycle. Only once the energy in the store falls to zero does the output reduce from the size of the connection. (c) The input rate to the store over a spring-neap cycle.

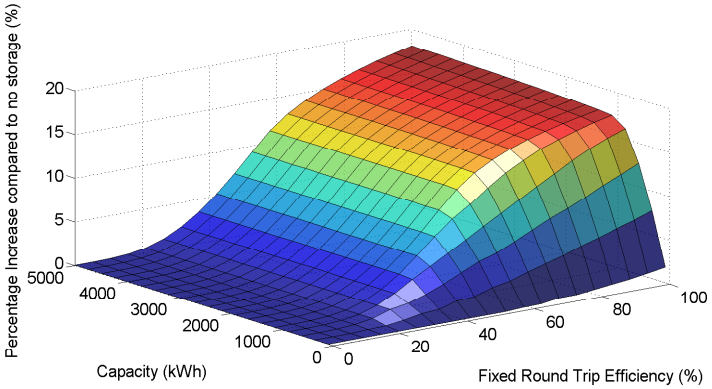

Figure 3.6: The Percentage Increase compared to the no storage case with transfer efficiency and capacity, when the connection size is 500kW and the decay time constant is 24hours.

We can see that the maximum input rate (charging) is 750 kW and the maximum output rate (discharging) is 625 kW.

This is the equivalent energy increase that would be associated with increasing the size of the connection from 500 kW to ∼696 kW.

For a connection size of 500 kW and a storage decay time constant of $\tau_s = 24$hours, the effect of changing the round trip storage efficiency and the storage capacity on percentage increase (using storage compared to without) is shown in Figure 3.6. It is interesting to note that percentage increase is not directly proportional to efficiency, but seems to fall off sharply below about 60%. This illustrates that with this connection size, there isn't much benefit to having a storage capacity above 1MWh, and that the returns on increasing the storage efficiency are reduced after the efficiency exceeds 60%. Figure 3.7 shows that initially percentage increase grows as the size of the connection is increased, and then falls, reaching zero when connection size = rating of the TCEC. Again there is very little benefit in a storage device larger than 1MWh if the tidal output is from just one turbine. The percentage increase grows as decay time constant, storage capacity and storage efficiency are increased, the amount by which depending on which one of these three parameters is the largest limiting factor.

3.2.3 Using Energy Storage to meet demand

As stated earlier, the predictability of the tidal resource exactly specifies the requirements of the storage system to which it must be coupled to provide a desired output. Obviously these requirements will be different for plants with differing outputs, but the method of determining these requirements will be the same.

Consider a TCEC coupled to a storage system, as shown in Figure 3.4. The output, P_T, of the tidal energy generation system is inputted to the power transfer control system. This then decides whether energy is inputted or extracted from the storage system. The net energy gain

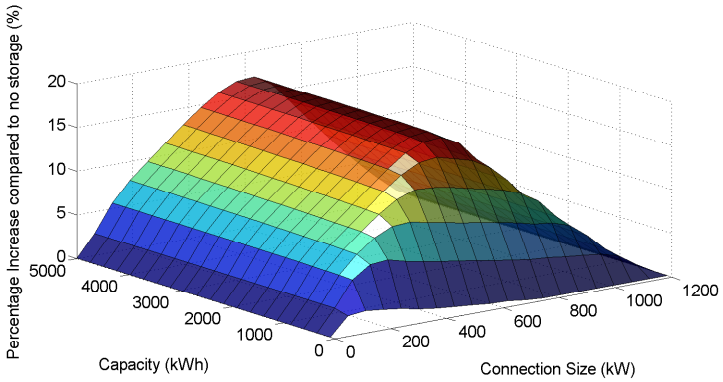

Figure 3.7: The Percentage Increase compared to the no storage case with connection size and capacity, when the maximum round trip transfer efficiency is 64% and the decay time constant is 24hours.

of the storage system at any given point in time depends on the desired state of the output to the grid, O_1, and the input (from the TCEC), P_T.

Conservation of energy requires that the total energy outputted is equal to the total energy inputted, as shown in Equation 3.11.

$$\int_0^T P_T\,dt = \int_0^T O_1 + Losses, dt \tag{3.11}$$

In the model that follows, we define the useful output of the whole system as O_1, and it is expressed using Percentage Rated Capacity (PRC), which is defined as the total useful energy outputted over the total energy inputted, as described in equation 3.12.

$$PRC = \frac{\int_0^T O_1\,dt}{\int_0^T P_T\,dt}. \tag{3.12}$$

$PRC = 1$ then corresponds to a lossless system, while a $PRC = 0.6$ would correspond to a situation where 60% of the energy inputted was outputted as useful energy.

The losses are modelled the same way as for the previous section.

So in the case of $PRC = 0.6$ these losses would sum to 40% of the total inputted energy. Note that the form of the useful output, O_1, has not yet been specified, so that this is true for any form of output, be it purely baseload (a constant output) or any other form.

Again, the tidal input used is the same as that described in Section 3.2.1.

The model is now run to determine the storage requirements (Capacity SOC_{max} (MWh), decay time constant τ_s (hours), round trip transfer efficiency η_s and the maximum input/extraction rates (which will specify the connection size to the grid) (kW)) for a given input to provide a desired output. The governing Equations 3.13 and 3.14 are now slightly different:

$$\begin{aligned} \text{IF } P_T &\geq O_1 \\ Rate &= \sqrt{\eta_s} \times (P_T - O_1) \end{aligned} \tag{3.13}$$

$$\begin{aligned} \text{IF } P_T &\leq O_1 \\ Rate &= (P_T - O_1) \times \frac{1}{\sqrt{\eta_s}} \end{aligned} \tag{3.14}$$

At this stage the form of the output is defined. It is specified by choosing a form (i.e. a flat output, an output that is flat over a 24 hour period, a spiked output that only contributes at times of peak demand etc, shown in Figure 3.8) and assigning the chosen output weight in terms of the *PRC*. So for an output of any form, $PRC = 0.5$ would mean that the useful output from the coupled system corresponded to half of the total output from the TCEC (see Equation 3.12).

In order to estimate the storage requirements the model is run from a set of initial conditions (large τ_s and large initial E_{stored}) which lead to a situation in which the minimum energy stored throughout several spring-neap cycles is greater than zero. The time constant τ_s is then reduced until the minimum stored energy is equal to zero. The initial energy stored $E_{stored}(t = 0)$ is then reduced until it is equal to the energy stored at the corresponding points in the next spring-neap cycles, and any correction to the time constant made. In this way a steady state with the desired output is achieved. The required capacity is then given by the maximum stored energy, and the connection size is given by the maximum output to the grid.

This will lead to one solution for providing the specified output. By increasing the time constant of this solution and decreasing the capacity until the minimum stored energy once again is equal to zero a series of solutions with different storage system properties (time constants and capacities) can be attained.

As examples, the storage requirements to produce the three aforementioned forms of output (flat, constant for each 24 hour period, and a 2 hour spike every day), all at *PRC*=60%, are determined.

- Output 1, the purely base-load (flat) output is shown in Figure 3.8a.
- Output 2, an output constant over each 24 hour period is shown in Figure 3.8b.
- Output 3, that releases all the energy from 1 day in a 2 hour spike is shown in Figure 3.8c.

As in the previous section, the storage system is assumed to have a maximum round trip of efficiency of η_s = 64%. The model results are as follows: Figures 3.8a and 3.9a show model results for output 1. The required storage capacity is 34.8 MWh, the maximum rate of energy inputted to the store is 929 kW, the maximum extraction rate is 401 kW, and the decay time constant is 142 hours. Figures 3.8b and 3.9b show the model results for output 2. Here the

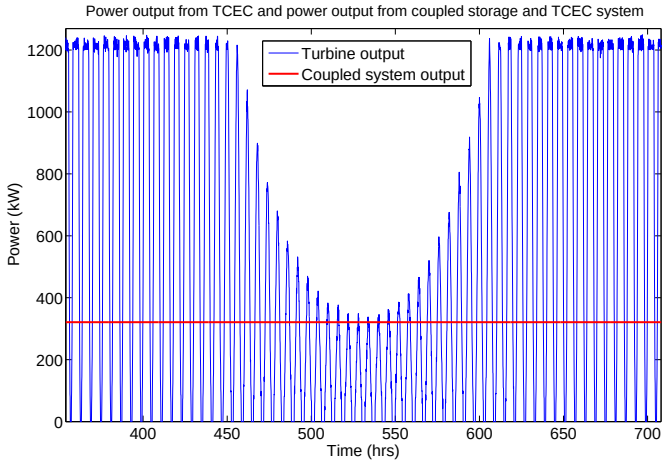

(a)

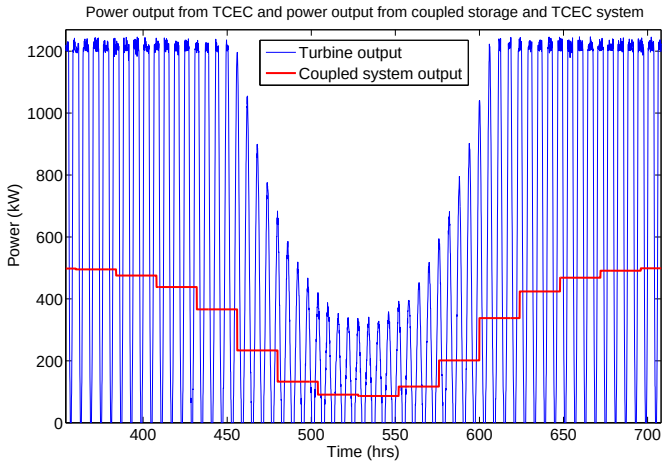

(b)

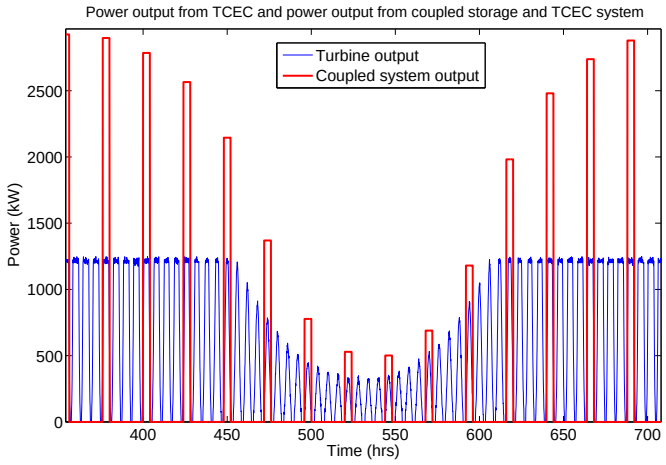

(c)

Figure 3.8: Model results for a 1200 kW turbine and storage system in a bidirectional flow with spring-peak v = $5ms^{-1}$ and neap-peak = $2ms^{-1}$, with the following outputs at PRC=60%:
(a) Output 1- baseload (flat).
(b) Output 2- a constant output each day.
(c) Output 3- all the energy from one day released during a 2 hour period corresponding to peak demand.

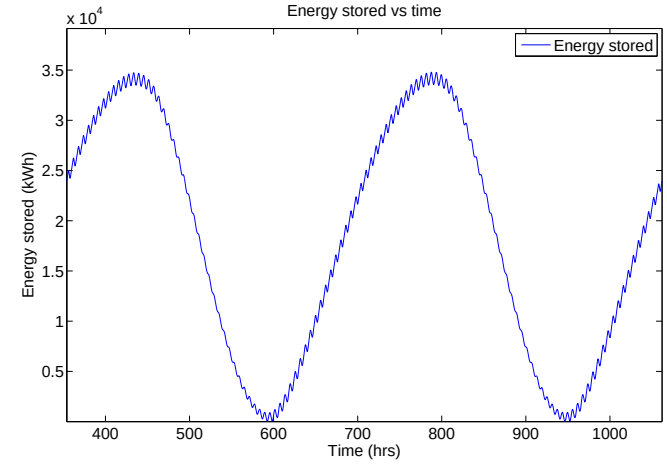

(a)

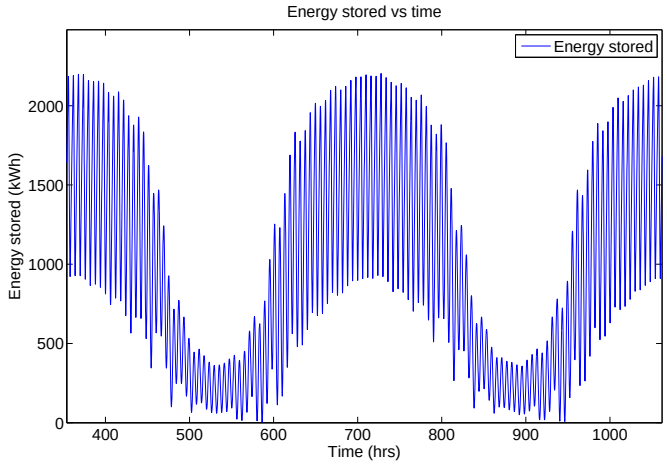

(b)

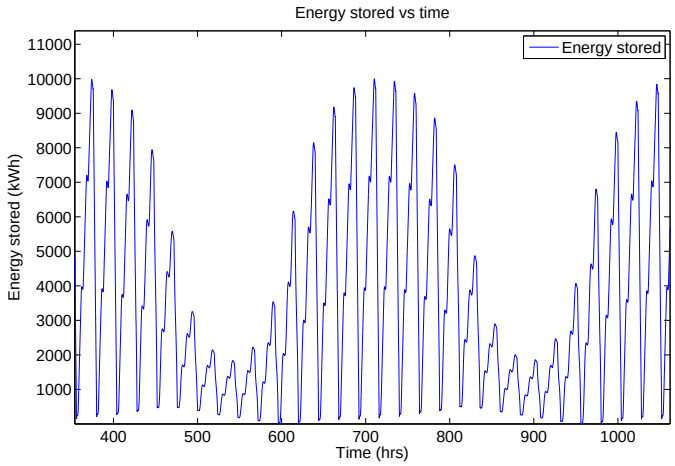

(c)

Figure 3.9: The corresponding stored energy against time for each of the outputs shown in Figure 3.8.
(a) Energy stored for output 1.
(b) Energy stored for output 2.
(c) Energy stored for output 3.

required storage capacity is 2.2 MWh, the maximum rate of energy inputted to the store is 979 kW, the maximum extraction rate is 624 kW, and the decay time constant is 7.1 hours. Finally figures 3.8c and 3.9c show model results for output 3. The required storage capacity is 10.1 MWh, the maximum rate of energy inputted to the store is 1250 kW, the maximum extraction rate is 2990 kW, and the decay time constant is 40.9 hours.

As would be expected for output 1 the time constant and the required capacity are the largest. The outputs that are constant over a smaller section of the spring-neap cycle (outputs 2 and 3) have much smaller requirements for capacity and time constant. Output 2 has by far the smallest required time constant and capacity, while those for output 3 lie between the requirements of 2 and 1. The input/extraction rates show the opposite trend, with the maximum input and extraction rate required to produce output 3, and the smallest for output 1. The same is true for the required connection size to the grid, it being largest for output 3, which actually requires a greater connection size than the rating of the turbine. Outputs 1 and 2 require connections significantly lower than the size of the grid connection.

By increasing the time constants for all the outputs the required capacity can be decreased. This would likely equate to a reduction in the physical size of the storage system, essentially meaning that a smaller more effective store (more effective meaning the same fixed efficiency but less loss of energy per unit time) could do the job of a larger less effective one. The results are plotted in Figure 3.10.

The results show that as the time constant is increased, initially there is a sharp decrease in the required capacity, corresponding to the reduction in losses over the respective time period, however the minimum capacity is fundamentally limited by the need to store at least enough energy to produce the desired output over the time during which there is no/small output from the TCEC. For example, if a constant output of 2 MW was required over 1 hour in which there was no output from the TCEC, and one way transfer efficiency of the storage system was 50%, then the minimum storage required would be 4 MWh.

It is also interesting to note that in the case of output 2, that requires the least storage, the required capacity shown in Figure 3.10b is not as large as the capacity predicted earlier. This can be explained due to the fact that the energy in the store is only ever close to zero near the neap part of the cycle. Therefore with a decay time constant of $\sim$7 hours, limiting the energy stored during the spring part of the cycle has very little effect on the neap part, as any energy left over from this period has already decayed (leaked from the store due to its self-discharge). This is not the case for the other two outputs, as they require much larger time constants.

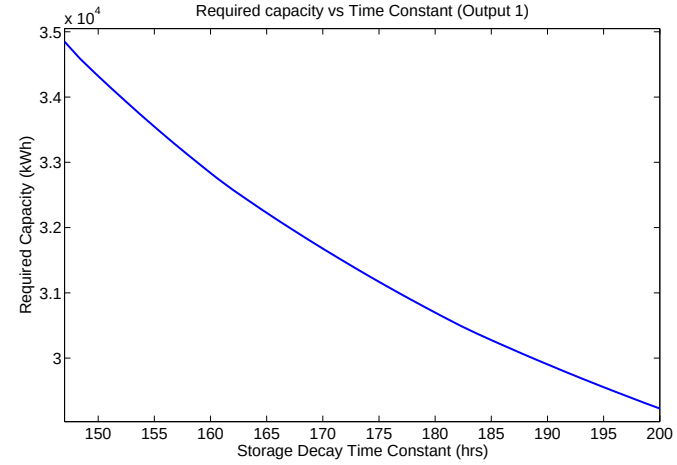

(a)

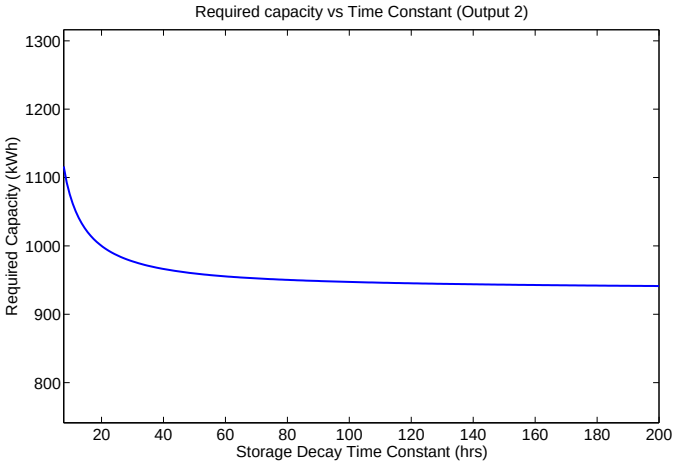

(b)

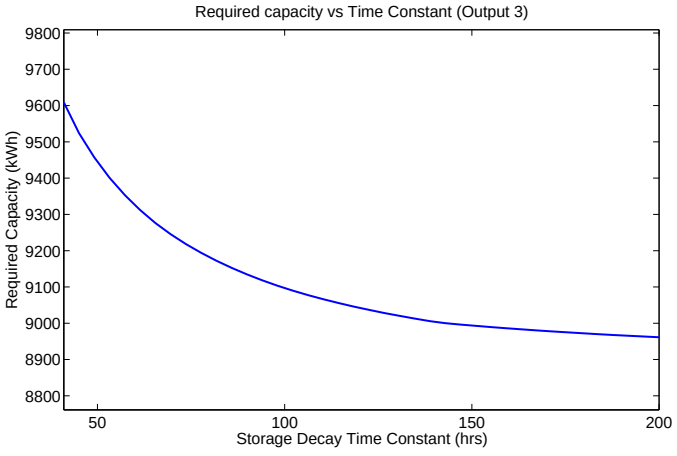

(c)

Figure 3.10: The required storage capacity against storage decay time constant for each of the three outputs described. (a) Output 1, (b) Output 2, and (c) Output 3.

3.3 Discussion

This Chapter is intended to highlight the advantages involved with coupling energy storage devices to REC's, especially to TCEC's. It builds on the ideas illustrated in Bryden and Macfarlane (2000), providing a more general analysis. What the previous sections have shown is how energy storage can be used as a way to reduce peak shaving, and potentially it can be used as a way to generate 'firm' energy supply from Tidal Current Applications. The impact of this could be significant: If baseload (or demand matching) energy supply can be achieved with TCEC's, then it offers the possibility of a renewable source with 100% Capacity Credit, i.e. renewable generation that can fully replace fossil fuel capacity.

The modelling described in this Chapter suggests that even a storage system of modest efficiency would offer some sizable benefits in the context of reducing the losses associated with transmission constraints, or would allow manipulation of the output profile from a TCEC into potentially much more useful forms. It also suggests that a system with quite small capacity could provide some benefit. In terms of transmission constraints, looking at Figure 3.6, a storage system with 0.5 MWh capacity (with modest efficiency) could yield an increase of up to $\sim$12% in useful output. While in terms of output manipulation, Figure 3.10b shows that an output of the form shown in Figure 3.8b can be achieved with a capacity of $\sim$ 1 MWh (provided the time constant is greater than 20 hours). This output has a minimum of 85 kW, and thus provides 85 kW of firm generating capacity. This corresponds to 7.1% of the rated power (1200 MW) of the turbine.

The costs of intermittent penetration have been estimated in Gross *et al.* (2007) at £5-£8/MWh, provided that the total penetration of renewable energy is relatively small (below 20%). These costs are due to the need for increased reserve requirements and increased system margin (due to increases in supply side fluctuations) to maintain system reliability. As the proportion of renewable generation increases (in the UK) the costs of coping with intermittency will increase. Storage then provides a way of mitigating these extra costs associated with intermittency. Therefore, as the amount of installed renewable generating capacity is increased there will be more and more incentive to utilise storage.

It is also suggested here that storage may even at present be a way to increase revenue from TCEC's. This could be achieved by increasing the amount of energy outputted if there are transmission constraints present, or by using storage to shift the outputs of TCEC's to times of peak demand, when the cost of electricity is highest. On inspection of output 3 in Section 3.2.3, it is evident that implementing this type of output would increase the transmission requirements, so an on-site storage unit is unlikely to provide any benefit, rather a central storage system, located near the demand could be used. As such it is suggested that the next logical step is to carry out a thorough cost analysis of TCEC's with storage included. This should aim to provide levelised costs for systems coupled with storage of various sizes and grid connection sizes, and compare these to the respective revenues, with the various storage

systems providing differing outputs sold at different prices (by comparing the outputs to the expected demand curves). In this way net present values could be compared, quantifying the advantages of energy storage to marine developers.

3.4 Conclusions

It has been shown that energy storage can be used both as a way to increase the output of a TCEC when there are transmission constraints present and to increase the value of the energy outputted from tidal current generation by time shifting the output into a more useful form of output.

The form of the output available using tidal current energy generation combined with energy storage is dependent on the properties (capacity, power, charging and discharging efficiency and self-discharge) of the energy storage system, but with even with relatively modest efficiency and capacity devices, some element of 'firm' energy generation can be provided.

Accordingly, energy storage used with tidal current energy conversion has the potential to replace conventional thermal generating plant without comprising reliability, and therefore doesn't increase the reserve requirements of the grid as much as standalone renewable energy conversion.

Chapter 4

Assessing the economic drivers for and the benefits of energy storage in an electricity market structure

In Chapter 2, reasons for energy storage were outlined and some approximate costs of different energy storage technologies were mentioned in Table 2.1. Tidal energy was shown to be particularly suited for use with energy storage in Chapter 3. Ultimately, if there is to be investment in energy storage technologies there has to be the potential for energy storage to be profitable. This chapter begins to explore the economics of energy storage. Firstly, an introduction to the UK electricity market structure is given followed by some brief speculation on how energy storage may operate in each of the market segments. Then secondly, a method to objectively compare the revenue that a storage device is able to produce is presented. This is applicable to an energy storage device operating on a spot market, based on the UK electricity spot market. The method enables the upper boundary of the revenue that would have been available over a historical period with known spot market prices to be compared for different energy storage devices. The schedule of operation that produces this revenue is also an output of the method and it is shown that in order to generate the maximum possible revenue the devices tend to mimic the underlying price pattern. This is a useful tool both for comparing energy storage devices and for understanding how they would operate on the market in order to maximise the revenue they generate. It is also concluded that while the operation of the device is beneficial to the market in terms of smoothing prices, and should also be beneficial in terms of carbon savings and increasing reliability, at present the revenue generated from arbitrage alone is unlikely to be sufficient to warrant investment in bulk energy storage. Hence the model here is also useful in terms of informing policy makers what incentives would need to be offered in order to benefit from the presence of energy storage on the electricity market.

4.1 UK Electricity market structure

Most modern electricity networks can be split into four segments; generation, transmission, distribution and supply. Generation deals with the conversion of energy (in many forms) to electrical energy. Transmission involves moving electrical energy in very high voltage wires- usually over relatively long distances. Distribution involves taking electricity from the transmission network and moving it to homes and businesses. Supply then deals with the financial organisation of the electricity network: The suppliers buy electricity in bulk, and sell the electricity to the consumers, paying fees to the transmission and distribution systems for their use. Figure 4.1 shows a schematic diagram illustrating the electricity network.

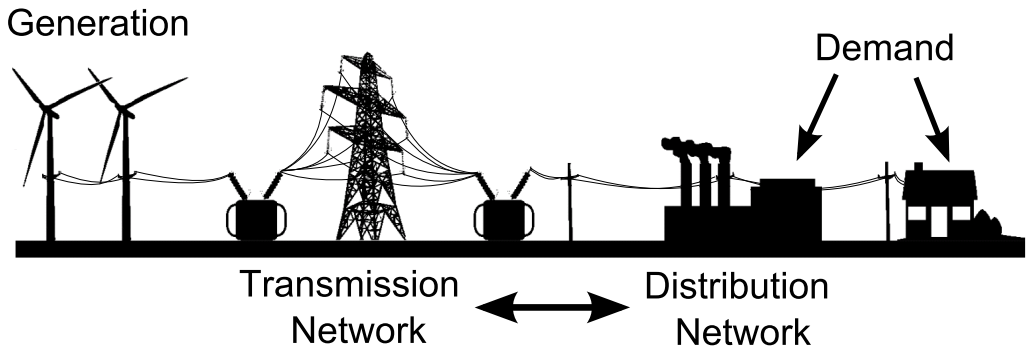

Figure 4.1: A schematic diagram showing the four components of the electricity network.

In the UK's deregulated electricity market there are many different generators which sell the electricity they generate to the suppliers. There are also many suppliers who can buy electricity from the many different generators and sell it on to the consumers. The idea behind the deregulated market is to encourage competition between the various generators and suppliers, and thus to provide the best service to society for the lowest price. Whether the market has succeeded in this respect is a source of ongoing debate (Defeuilley, 2009; Kwoka and Madjarov, 2007; Littlechild, 2009; Price, 2005). The transmission and distribution networks are monopolies, but are regulated by the Office of Gas and Electricity Markets (OFGEM). Matching supply and demand is handled by and large through the operation of the market, although this is overseen by the Transmission System Operator (TSO) who has the responsibility of ensuring that supply and demand are balanced in the short-term, in Britain this is the national grid (National Grid). BETTA — the British Electricity Trading and Transmission Arrangements — provide the market rules under which generators and suppliers must operate.

The relationship between the market and the actual operation of the electricity system is complex. In the UK, what is known as the electricity market really consists of four distinct markets which facilitate the trading of electricity: the forward market, the power exchanges, the balancing market, and the ancillary services market (the reserve market). The Association of Electricity Producers give the volume of electricity traded through the first three of these as over 90% through the forward market, 3% through the power exchanges and 2-3% through

the Balancing market (Association of Electricity Producers). Other countries with similar electricity market structures have different statistics, such as Nord Pool Spot (the Nordic region electricity market) where the volume of electricity traded through the power exchange is much larger, 74% (Nord Pool Spot Market).

Each day in the UK market is split into 48 1/2 hour periods, with one long day (50 periods) and one short day (46 periods) to account for daylight saving.

In the forward market, suppliers and generators enter into bilateral agreements. These contracts can often be made months and years ahead of real-time and generally have no specific format — they may include clauses for the delivery of electricity during certain periods of the day if the generator in question is dispatchable (dispatchable generation refers to generation whose output can be changed on a human defined schedule). Suppliers usually have a portfolio of these agreements with many different types of generation, allowing them to mitigate the risks involved with intermittent generation, such as wind energy conversion, or add flexibility to traditionally base-load generation, such as nuclear. For example, a supplier might hold a contract with a wind-farm to take all of its output in the next 20 years at a certain price, and may also have a contract with an open cycle gas turbine plant to provide power everyday between the hours of 17.00 and 20.00 in the evening (the usual time of peak electricity prices in the UK winter profile).

The power exchanges or ‘spot market’ allows market players to anonymously trade volumes of electricity for the rolling half hour market periods. It operates from a couple of days ahead of real time until one hour before real time. The power exchanges allow market players to correct for any period in which they may anticipate an imbalance between their output and their contractual obligation. This market of last resort then allows market players to escape the potential penalties applied for falling short of their stated quota in a bilateral contract, or allows them to sell any anticipated surplus generation.

At one hour before real-time, all trading between market players ceases and the TSO is notified of the volume of all the energy trades. This point (1-hour ahead of real-time) is known as ‘Gate Closure’ and the volume of energy notified is known as the Final Physical Notification (FPN). It is physical in the sense that it provides information on the physical properties of the contracts, but not the price information. The balancing market then operates to allow the TSO to accommodate any anticipated shortfalls or excesses (possibly due to a fault or maintenance at a generator or an expected increase in the demand of a large consumer). The TSO compares its projected system demand to the FPN and accepts bids or offers from market players in order to balance the system. This is done through direct trades between the TSO and large generators and consumers of electricity. The payments for these trades are made after the period in question and are known as ‘settlements’. Physical limits on the system such as network constraints (like thermal line capacity) and generator ramp-rates are also considered when evaluating the bids and offers.

Finally, the TSO has at their disposal the ability to instruct plants with which it has contracts for balancing the system to increase or decrease output. These contracts are arranged on the ancillary services market. The TSO is likely to have at their disposal a large range of plant operating on this ancillary services market, in order to cope with unexpected circumstances and keep the network within its frequency and voltage limits.

After the 30-minute period, the settlement code company (ELEXON) uses metered data to work out any discrepancies between the FPN's (accounting for any transactions on the balancing market) and actual volumes of electricity traded. Some degree of over-supply or under-supply relative to contractual positions is inevitable. System Buy Prices and System Sell Prices are calculated 'post-hoc' and form a basis to eventually pass on the cost of the imbalances to the parties that caused them.

Similarly, the spot market prices are also calculated 'post-hoc', and are a weighted average of all the transactions that occurred through the power exchanges for the 30-minute period in question. They are important as the spot market prices are generally used as a reflection of the market prices and are thus referred to in the arrangement of the bilateral contracts both on the forward and ancillary markets.

4.1.1 How might grid energy storage operate?

Grid energy storage with a sufficiently low self-discharge rate could operate on any of the four markets; however, it is unlikely that it would plan to operate solely on the balancing market, rather than opportunistic use by a device also operating on another market. In the forward market the value of storage would likely be to off-set peaking plant, by arranging to buy a quantity of energy each day at the usual times of low price and sell this energy during times of higher price in the evening. In order for the device to make a gain in revenue, the price difference between buying in the early morning hours and selling during the evening peak times would have to be great enough to cover the energy losses associated with the charging and discharging of the storage device, and the energy leakage from the store over the time period in question. Indeed to make a profit, the revenue gain over the lifetime of the device would have to be greater than the lifetime costs (including O&M, installation, etc...).

On the spot market (the power exchanges), it seems likely that storage would act such as to buy at times with low prices and sell at times with high prices. The storage operator would then have to place bids to buy electricity at times for which they anticipate low prices and place offers to sell electricity at times for which they anticipate high prices. Again the bids and offers would have to be such as to cover the round trip losses of the storage device, with consideration to the lifetime costs of the device. Acting in this manner on the spot market, the effect of storage should be such as to reduce the overall volatility in the spot market price, as at times when market players expect high prices, they will anticipate offers from the storage device, and thus revise their bids down accordingly. The consequence of this is speculated

as follows: the more storage that is present in the market, the less the price will vary and as such the less profitable storage will become. If it is assumed that price broadly reflects demand and system reliability, then storage acting on the spot market should level demand and thus increase reliability. Therefore storage acting in the power exchange would be socially beneficial in terms of reducing price volatility and offsetting carbon intensive and expensive peaking plant. Of course, to evaluate any carbon saving one would have to consider from what source the storage was originally charged. It does not seem unreasonable to expect that in a market with a high proportion of renewable generation, storage would be very likely to charge using energy from renewable generation such as wind, wave or tidal plant if it was available at times of low demand, due to the marginal fuel costs of these devices. This would presumably be further enhanced were renewable subsides present, the existence of which meaning that the renewable plant would receive significant payments even if the energy generated was sold in the power exchanges for zero price. This begs the question of whether or not there should be extra incentives offered to storage devices who act on the spot market.

Storage with very small time dependent losses also seems likely to be well suited to the ancillary market. The reasons for this are due to the inherently large ramp rates of storage devices (Eyer, 2010; Schainker, 2004a) and the expectation that storage devices would be used less on this market, thus lessening the problems with cycling- which is a problem for many types of storage system. However, as soon as the time dependent losses become significant, the storage device will be constantly 'leaking' energy, which will have to constantly be replaced in order to keep the energy stored at a constant level while the device is not in use. Hence, in the case of a storage device with significant time dependent losses, a generator based on fossil fuel may be more efficient and less carbon intensive — unless the 'leaky' storage device could constantly be charged with low carbon energy, which seems unlikely given the intrinsic intermittency of most low-carbon methods of generation.

It is anticipated that the market on which a given energy storage technology will operate is likely to depend largely on the self-discharge of the device. Devices with high self-discharge rates, like current flywheel technologies (Ibrahim *et al.*, 2008; Ryddell) are only suitable for power quality applications. Medium to low self-discharge rates will be suitable for spot market operation if the losses associated with charging and discharging are small enough to exploit the market price differentials available and devices with very low self-discharge rates will be suitable both for spot market (with the same restrictions on charging and discharging losses) and ancillary market operations.

4.2 Towards an objective method to compare energy storage technologies

The rest of this chapter proposes a methodology to calculate the upper boundary of the revenue available from the storage and time-shifting of electrical energy. The inputs to the mathematical model are a discrete time-series of the market index prices over a particular period of interest, and also specific energy storage device parameters. By using a Monte Carlo based optimisation method, the upper boundary of the revenue available from time-shifting energy is determined. The method is explained and validated by showing that it finds the optimum solution that is the upper boundary for time-shifting revenue. In other words, a storage operator could never derive more revenue than this value from time-shifting alone and calculating this upper-boundary gives a reference value to compare the efficacy of other methods of estimation. The user defined storage device parameters include fixed efficiencies for charging and discharging (%), the maximum capacity of the storage device (kWh), the charging and discharging power limits (kW), and the inclusion of an additional time-dependent efficiency that models the self-discharge of storage devices (% loss per hour). The combination of these parameters enables this method to give an objective comparison between different storage devices in terms of maximum arbitrage revenue. The output of the model provides not only a single value of the upper boundary revenue, but also the corresponding charging/discharging schedule.

4.2.1 Introduction

Recently there has been greater global interest towards energy storage in order to reduce the perceived risks associated with greater penetration of non-dispatchable renewable generation (e.g. not available on demand) within electrical networks at both the distribution and transmission level. Although storage at many scales is an internationally important active area of research and development on a technical level, there is a need for greater understanding of the economic and market drivers for widespread energy storage deployment.

The methodology presented in this chapter is able to compare energy storage devices with access to spot market prices. The data used in testing the model is the historical UK market index price for electricity (the electrical spot price data).

Table 4.1 shows the characteristics of the four pumped storage schemes in the UK, with currently (2012) an additional ∼60 GWh (600 MW power) of pumped storage development in the Scottish planning system (Lannan, 2010).

Figure 4.2 shows the historical level of electrical energy output from pumped storage facilities in the UK from 1970 - 2009, from a built capacity of 2788 MW. During this time Foyers and Dinorwig pumped storage schemes were comissioned, and there was also an incremental increase in Dinorwig's energy storage capacity in 2007 from ∼9.4GWh to ∼10.1 GWh (1728 MW power). The contribution from pumped storage has only recently climbed above 1% of the

Site	Storage (GWh)	Output (MW)	Location	Year
Ffestiniog	∼1.3	360	Wales	1963
Ben Cruachan	∼10	440	Scotland	1966
Foyers	∼6.3	300	Scotland	1974
Dinorwig	∼10.1	1728	Wales	1983

Table 4.1: Hydro Pumped Storage Schemes in UK.

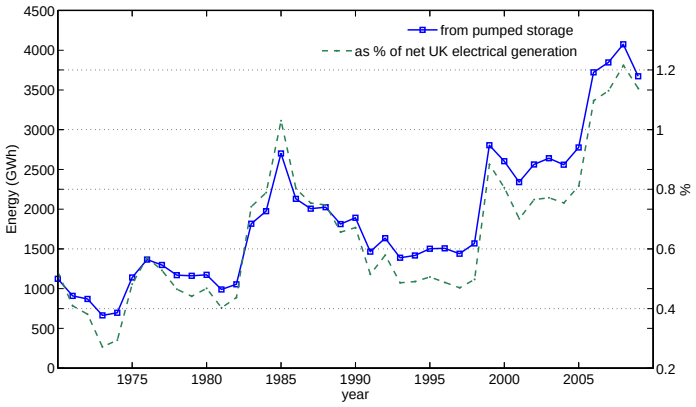

Figure 4.2: GWh of electrical energy from UK pumped storage schemes 1970 - 2009, and expressed as a % of the net electricity supplied by major power producers (DUKES, 2010).

total net electricity supplied from the major UK power producers and this is thought to be partly due to the increase in the capacity of Dinorwig mentioned previously, coupled with a more favourable price environment for electrical energy arbitrage from 2006 -2008. Other recent interest in bulk electrical energy storage includes the discontinued Regenesys flow battery project at Little Barford in 2002 that had a design of 120 MWh with 12 MW power.

It is not known with a high degree of certainty how the expected increase in renewable energy generation (large scale > microgen scale) will impact the price volatility of electricity markets, but in terms of long-term price forecasting of UK electrical energy prices there is a view that they will become more volatile in the future, as the contribution from renewable energy sources increases (Cox, 2010; Gross *et al.*, 2007; Green and Vasilakos, 2010). The economic argument for storage should improve if the revenues derived from daily arbitrage of energy were to increase. It is notable that in the United Kingdom the level of energy traded through the power exchanges is currently less than 3% of all electrical energy traded (Association of Electricity Producers), as over 90% of electrical energy is traded through the forward market in confidential bilateral contracts between generators and suppliers (Wilson *et al.*, 2011). Although the power exchange market may seem small, it is crucial not only as a market of last resort but also as the market where the spot price of electricity is discovered, which then influences the prices in the forward and ancillary markets.

Bulk electrical energy storage is seen by the author as providing a service to address the mismatch between supply and demand of electricity, and is viewed as a complementary technology to greater market interconnectivity and also demand side management. Specifically, it is a useful tool to match the temporal disparity between supply and demand. This function has historically been undertaken by using the "store" of electrical energy contained within fuels i.e. by increasing or decreasing dispatchable generation, and thus matching supply to demand. The overwhelming choice for these "stores" of electrical energy in the UK continues to be fossil fuels (Wilson *et al.*, 2010).

Although it is erroneous to directly compare electrical energy prices to other types of commodity prices, due to the unique nature of electrical energy (it has generally been used when it is produced as it has been uneconomic to store in bulk), it is interesting to note that the price volatility of electrical energy is much greater than that of other types of traded goods or services, with daily price swings of greater than 100% being commonplace (see Figure 4.4). Papers by Weron and Misiorek (2007) and Madaleno (2008) give a comprehensive overview of the stylised facts of energy prices, which include inter alia; high volatility, seasonality of prices, the inclusion of price spikes and also mean reversion to a daily pattern. (Weron, 2006) (pp25) captures this when he states,

> "One of the most pronounced features of electricity markets are the abrupt and generally unanticipated extreme changes in the spot prices known as jumps or spikes. Within a very short period of time, the system price can increase substantially and then drop back to the previous level."

Several studies have looked at quantifying the revenues available from time-shifting energy, including Mokrian (2006) that looked at the optimisation of storage over a 24-hour period, by comparing a linear, a multi-stage stochastic and a dynamic method of optimisation. Crampes and Moreaux (2010) model an electricity market in which an operator manages both a pumped hydro station and a thermal plant, providing the optimal dispatch for each, but only considered this using an off-peak and peak price. Figueiredo and Flynn (2006) looked at the costs as well as the revenue element of arbitrage, but used a fixed round trip efficiency of 80%. The previous chapter (published in Barbour and Bryden (2011)) illustrated how the required properties (capacity, self-discharge, fixed input/output efficiencies and charging and discharging power limits) of a storage system change depending on the form of the time-shifted output required, and although the focus is mainly on tidal current energy conversion, this approach is applicable to any form of energy conversion.

It is acknowledged that this problem (calculating the upper boundary of the revenue that a storage device could derive using price differentials within electrical spot market data) can be approached with other programming methods e.g. Connolly *et al.* (2011). The method presented in this chapter is a novel approach that not only calculates the maximum revenue for long user defined periods of interest (from days to years), but also includes a time dependent efficiency loss that aims to model self-discharge. The introduction of a time-dependent variable

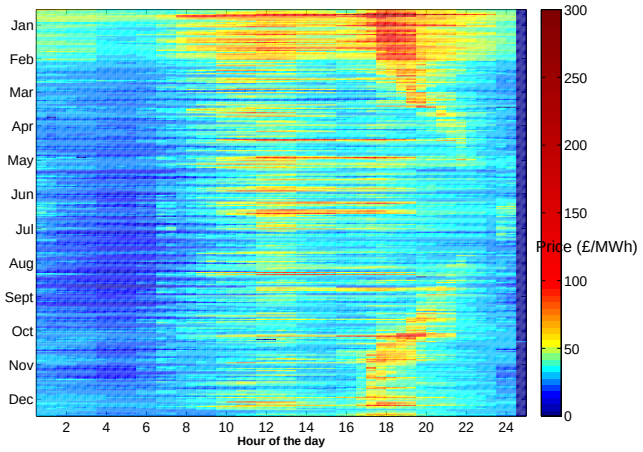

Figure 4.3: 'Heat map' illustrating the pattern of daily price variations throughout 2009. The figure is corrected for daylight savings, with day 88 being 23 hours long and day 298 being 25 hours long.

provides another layer of complexity that then requires a non-trivial solution.

4.2.2 UK market index price data analysis

In the UK, the market index price is a discrete time-series of price data, which is a post-hoc weighted average of the trades through the power exchanges for a specific 30 minute period. Historical market index price data from the UK power exchanges are used as the price input to the model for the purposes of this chapter, in order to remove the errors associated with price forecasting and due to the availability and robustness of the price data set. The data is freely available for the UK, is robust after 2005 (Elexon) and can therefore be used by other groups to compare or contrast different methods of determining the revenue available from the storage and time-shifting of electrical energy. Historical price data is the equivalent of perfect forecasting and by this reasoning, using historical price data provides the upper boundary of the arbitrage revenue available to a given storage device for that particular timeframe i.e. a storage operator will never be able to gain more than the upper boundary revenue deduced here via arbitrage alone. This is independent of forecasting ability, but better forecasting should allow an ever closer approach to this upper boundary revenue figure.

Figure 4.3 illustrates the 2009 prices as a 'heat map'. The different colours illustrate how the price changes throughout the day over the year 2009; it is interesting to note that the time of the highest daily price does seem to vary significantly from season to season, with the winter peak prices in the early evening 17:00 to 20:00 timeframe and the summer peak prices scattered throughout the daytime. The lowest prices do not show this seasonal variation to the same degree, and are likely to happen between the hours of 03:00 and 06:00 throughout the year (also see Figure 4.5). It is this variation in the price of electrical energy that provides opportunities

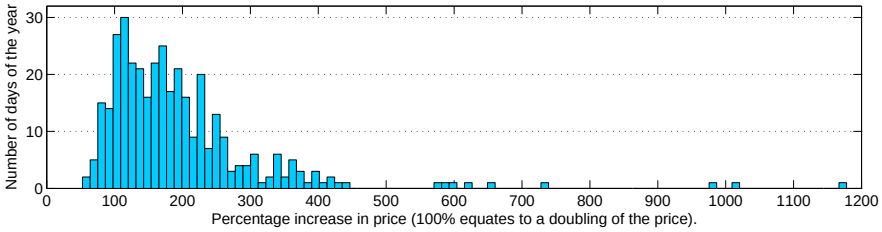

Figure 4.4: 2009 UK market index price data - percentage price increase between the lowest daily spot price and the highest daily spot price. The % price increase is calculated relative to the buy price, therefore 0% in this graph would be: sell price = buy price = no change in price.

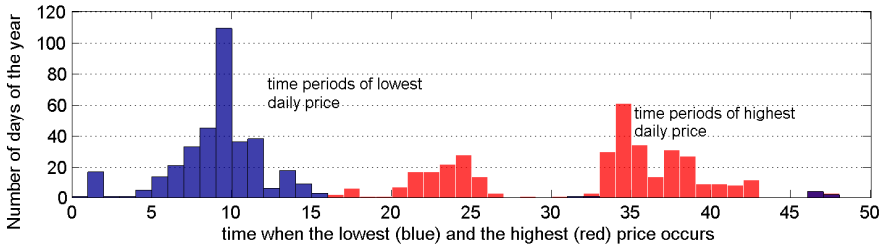

Figure 4.5: 2009 UK market index price data - 30-minute time-period within the day when the lowest and highest price happened. Red correponds to the highest daily price and blue the lowest, with the overlap being marked by a mixture of the two colours.

for energy storage device operators to exploit price differentials. The percentage figures used throughout this chapter for sale prices are expressed in terms of a percentage increase of the initial buy price, i.e. if the sale price is twice the buy price, it is expressed as a 100% increase relative to the buy price.

Figure 4.4 is a histogram of the number of days plotted against the percentage increase in price within that day for 2009. The percentage increase is calculated by determining the greatest possible change in price in each day (starting at 00:00 and finishing at 24:00). This may not, however, be the same as the difference between the absolute highest and lowest prices in a given day if the highest price occurs before the lowest price.

The period starting point was investigated to determine whether starting at 00:30, 01:00 etc. would cause a difference in the calculated percentage price increases. By changing the start period incrementally from 00:00 to 24:00 it was found that the average change in price for the year was $\sim 1\%$ between time period starts from 00:00 and 05:00, and that the 00:00 start time gave the highest yearly average change in price, throughout a range of differing years. In contrast, using a start time between 05:00 - 21:00 gave a significantly reduced average figure for the price increase. The price histograms presented here use a 24-hour period that begins at 00:00 and ends at 24:00 (Figures 4.4 and 4.5). The model algorithm, however, can be based on longer timeframes and is unaffected by a daily start point.

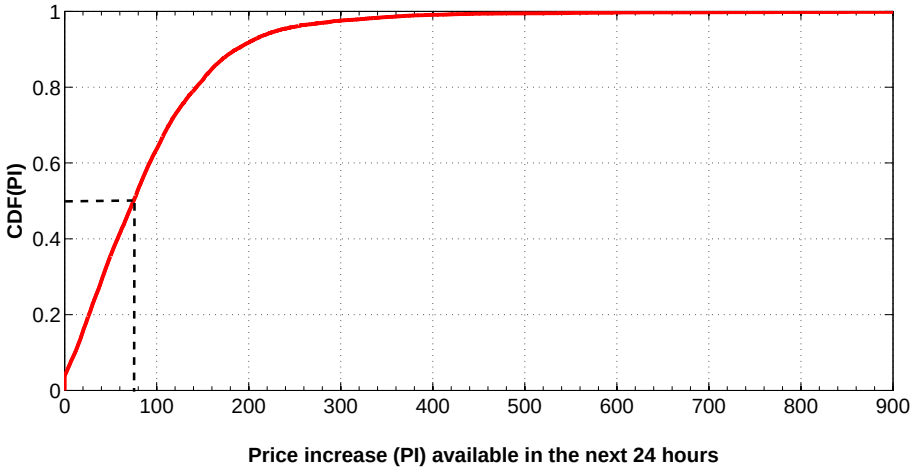

Figure 4.6: A cumulative distribution function (CDF) to show the price increase (PI) available for every period in the year. The value of 0% means there is no price higher than the current price over the next 24 hours.

It should be noted that the percentage price increase (as a measure of the ability to cover the costs of the efficiency losses in the system) is a relative rather than an absolute measure. A higher absolute price differential will afford a storage operator a greater absolute revenue e.g. buying at £25/MWh and selling at £50/MWh has the same percentage price change as buying at £100/MWh and selling at £200/MWh, but the latter will yield the storage operator greater increased revenue than the former.

The minimum percentage increase in price within any day of 2009 was 52%. This means that each and every day there was the opportunity to sell energy for at least 52% more than the buying price, i.e. there was a daily opportunity for a storage system that is more than 66% efficient (= 100/(1+0.52)%) to cover the cost of the round trip energy efficiency losses. Figure 4.5 shows the time periods within a day when the lowest and the highest prices occur.

Figure 4.6 shows the cumulative distribution function for the price increase available in the next 24 hours, for every period of 2009. It can be seen from the figure, that the median price increase is 75%, meaning that for a $\frac{1}{2}$ hour period of the year picked at random, there will be a 50% chance that the price increase available in the next 24hours is greater than 75%.

Having established that in the UK market there exists the daily opportunity for a storage system of greater than 66% efficiency to cover the financial penalty from the round trip losses; a model to determine the maximum revenue available to storage systems (with user defined properties) is introduced.

4.2.3 Model Assumptions

In calculating the upper boundary of the revenue available to the storage system the following assumptions are made:

The storage device is a price taker and does not influence the overall spot market price. This is likely to be a good approximation for any individual grid-connected small storage device. However, as the overall level of storage increases on a network, it is likely to have a smoothing effect on market index prices, as bulk storage generally acts to create extra demand when prices are low, and provide supply when prices are higher. It is expected that greater levels of dispatchable bulk storage will begin to influence the price spread behind the time-shifting revenue stream. However, this is not thought likely to be an issue in the UK market in the short to medium term.

The time taken to change the charging or discharging rate within the power limits of the storage device is negligible compared to the spot price period. The validity of this assumption depends on the device in question, but storage devices generally have much higher ramp rates than conventional generators. Even Pumped Hydro which is usually regarded as having a slow response for a storage medium can often increase its ramp rate by several hundreds of MW per min.

The storage device is not subject to network capacity constraints. Any network constraint would reduce the ability of the storage device to operate - therefore reducing the potential revenue. The revenue would therefore be expected to be less than the upper boundary figure calculated for zero network constraints.

The device parameters are assumed to have constant values. The charging/discharging efficiencies do not change with the charging rate, and the time constant describing the self-discharge remains constant in this model. An interesting approach outlined in Darling *et al.* (2011) regarding the evaluation of levelised costs based on distributions of assumed values may be a feasible approach for future work in order to get confidence intervals on the upper boundary estimation associated with uncertainty in device parameters.

Price forecasting This work makes no attempt to deal with the area of price forecasting, which is a large, complex and heavily researched field of work in its own right in both the public and private sphere. One potential advantage of this is that the maximum revenue deduced here is independent of forecasting ability.

The aims of this work are two-fold; to add to the debate around the level of revenue achievable from the storage and time-shifting of energy by calculating the upper boundary of revenue a device could expect to generate using spot markets, and to stimulate thought in other groups and researchers interested in the financial value of energy storage.

The use of historical price data and the methodology proposed here calculates the maximum

possible revenue that could have been attained with historical market conditions. If this information is combined with lifetime costs of the storage devices (O&M, installation cost, connection costs etc...), this should allow for a more informed decision of whether or not a given storage device is likely to provide a desired level of profitability.

4.2.4 Principles of the model

The model is based on the price differentials that are required to cover the round trip energy losses, which are a factor for any storage device. For example, if an energy storage device has a total round trip efficiency of 33% then the sale price would need to be at least treble the purchase (buy) price just to cover the efficiency losses, an increase of 300%.

The ability of any storage system to produce a positive revenue stream from the time-shifting of energy will depend on the relative price variation of bought and sold electrical energy and the round trip efficiency of the system (composed of both fixed and time dependent efficiencies). This is true irrespective of the separation in time between buying and selling.

The model is able to consider two different forms of efficiency losses: those that are time dependent, and those that are not. It is assumed that there will be a fixed penalty for transferring energy into and out of the store, and once the energy has been transferred 'in store' there will be a loss rate dependent on the amount of stored energy, as described by the exponential term in Equation 4.1. This time dependent loss of energy models the self-discharge of the storage device. As such, the energy output ΔE_2 from the store (at time period t_2), after an amount ΔE_1 has been input (at time period t_1) will be given by Equation 4.1 below.

$$\Delta E_2 = \Delta E_1 \eta_s(\Delta t) = \Delta E_1 \times \eta_{in}\eta_{out} \times exp(\frac{t_1 - t_2}{\tau_s}) \tag{4.1}$$

In Equation 4.1, η_{in} is the fixed efficiency of the transfer into the store (charging efficiency), η_{out} is the fixed efficiency of the transfer out of the store (discharging efficiency), and the time dependent self-discharge rate from the store is: $\frac{d(SOC)}{dt} = \frac{SOC(t)}{\tau_s}$. The combination of all three of these losses yields the round trip efficiency of the storage process between t_1 and t_2, $\eta_s(\Delta t)$, where $\Delta t = t_1 - t_2$.

Similarly, the change in energy contained in the store ΔE_3, at an intermediate period t_3, where $t_1 < t_3 < t_2$, will be given by Equation 4.2.

$$\Delta E_3 = \eta_{in} \times exp(\frac{t_1 - t_3}{\tau_s}) \tag{4.2}$$

Therefore, if the price of electricity at t_2 is more than a factor of $\frac{1}{\eta_s}$ than the price at t_1, then buying energy at t_1 (to store) and selling at t_2 will give a positive addition to the overall revenue available to the storage operator. This is the governing driver of the model; to establish whether

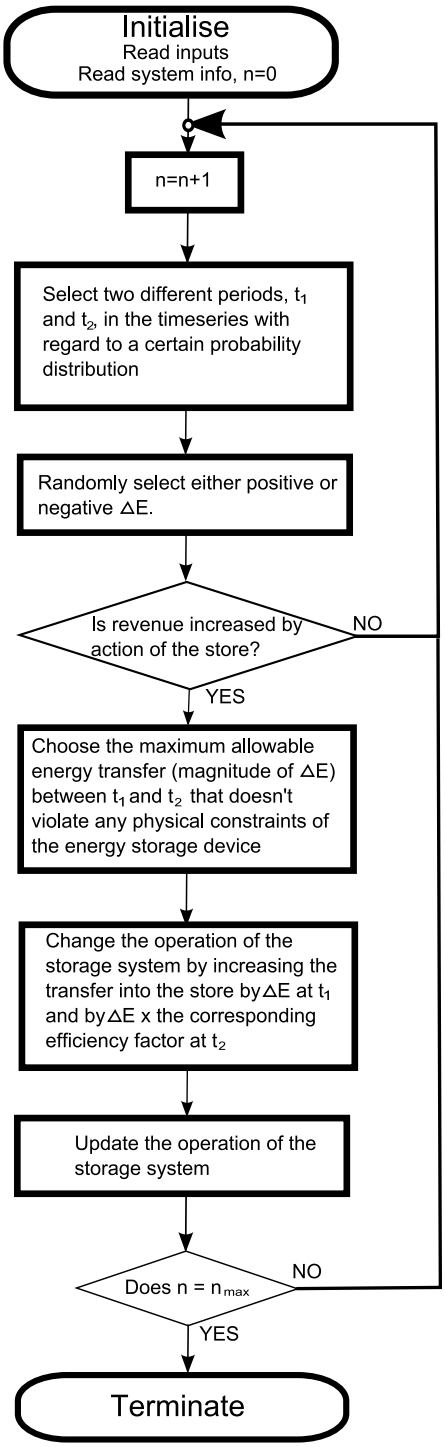

Figure 4.7: A flowchart depicting the action of the optimisation algorithm.

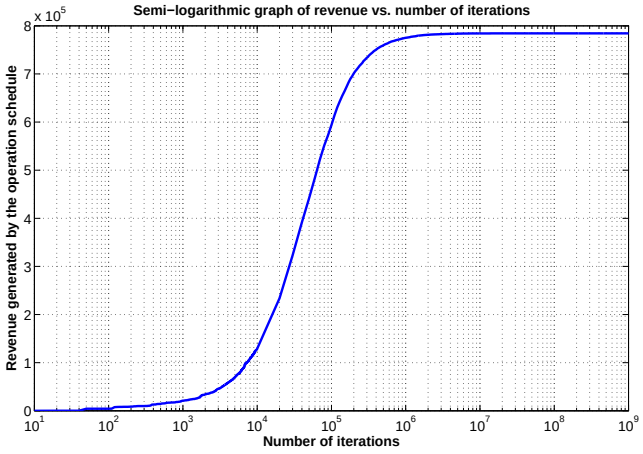

Figure 4.8: A graph illustrating the approach of the algorithm to the optimal solution (for a PHS system with 20 MW rated power for 2009 - Table 4.2). The time window is a year (17520 $\frac{1}{2}$ hour periods) and the maximum number of iterations is 10^9. The graph plots revenue achieved by the operation of the system vs. Log_{10}(iteration number).

a potential time-shifting of energy will indeed increase the overall revenue, after the fixed and time dependent losses have been taken into account.

The Monte Carlo optimisation algorithm searches the space of feasible solutions finding the solution which corresponds to the global maximum in the revenue. The detailed operation of the method is outlined in the Appendix A. A flowchart illustrating the operation can be seen in Figure 4.7. A feasible solution is defined as a schedule of operation of the storage system, which could in principle be implemented - i.e. a solution that is physically realisable and does not violate any of the constraints.

Once the solution reaches a point where the revenue has stopped increasing, the solution is considered to be optimal. As a non-deterministic algorithm, the path to get to the optimal solution will differ from one run to the next, but (with enough iterations) the same final optimal solution will be attained. Figure 4.8 shows the convergence of the algorithm on the upper boundary of arbitrage revenue.

The code for the model was initially written and tested in MATLAB, and was ported to FORTRAN95 for speed. Implemented in FORTRAN95, the algorithm takes around 5 minutes to run 108 iterations on a 2.99GHz processor (Dell Optiplex 760, Intel Core Duo CPU E8400, 2.99GHz). Using the High Performance Computing facilities at Strathclyde and Edinburgh Universities allows access to far greater computing power, giving the potential to run the algorithm for different types of storage devices with different fixed and time dependent loss characteristics over much longer timeframes e.g. from pumped hydro systems having significant fixed losses and very little time dependent losses (Schoenung *et al.*, 1996; Ibrahim *et al.*, 2008), to flywheels with higher self discharge rates but relatively small fixed losses

(Ryddell). The maximum feasible revenue (the upper boundary that the storage system could have generated over the time period in question) is attained by following the optimal schedule of operation for the storage system (also an output of the algorithm).

4.2.5 Model Validation

In order to validate the model, some test scenarios that have intuitive solutions for the optimum schedule of operation of the storage system are considered. To simplify the situation, an artificial input price regime is used (referred to as the test price). The scenarios and model results are as follows:

Figure 4.9a — Scenario 1: The time-series test price is a square wave varying between £50/MWh and £100/MWh. This is run with an infinite capacity 100% efficient storage system, with charging and discharging limits of 20 MW (PLI, PLO = 20 MW). Therefore, we would expect the optimised result to output a schedule that charged at 20 MW for the first 12 hours, then discharged at 20 MW for the following 12 hours, and then repeated. The Figure 4.9a of the model results is an excellent fit with the expected schedule.

Figure 4.9b — Scenario 2: shows the model's output schedule for charging or discharging the store when the time constant of the store is 12 hours (i.e. the store loses 50% of its energy every 8.3 hrs). The charging/discharging limits, infinite capacity and input test price are the same as the previous scenario. The output is as expected; a square wave which aims to minimise the time over which energy is stored.

Figure 4.9c - Scenario 3: The test price used is a sine wave with a period of 24 hours and amplitude of £50/MWh, centred on £50/MWh (varying from £0 to £100/MWh). The storage system has a fixed round trip efficiency of 10%, a charging limit of 20MW, a discharging limit of 60 MW, and an infinite storage capacity that has no time dependent losses. The figure shows the model's output schedule for charging or discharging the store, along with the corresponding electricity test price. As would be expected, the model only stores and releases energy when energy can be bought for less than 10% of the selling price.

Figure 4.9d - Scenario 4: The test price is a decaying sine wave test price, with a period of 18 hours centred on £50/MWh ($price(t) = 50 + (50 - \frac{t}{2})sin(\frac{\pi t}{9})$). The storage system has infinite capacity, no losses, a charging limit of 5 MW, and an unconstrained discharging limit. The algorithm finds the optimum result where the storage operator charges at the maximum rate until the highest price, at which point all of the accumulated energy is sold. When a further price increase becomes available, the storage operator begins charging again, selling all the accumulated energy at the next highest peak price. This sequence continues until the last period in question.

Figure 4.9e - Scenario 5: The test price used is the actual spot price from the 7th January 2009. The storage system is similar to scenario 4, an infinite loss-less storage system except

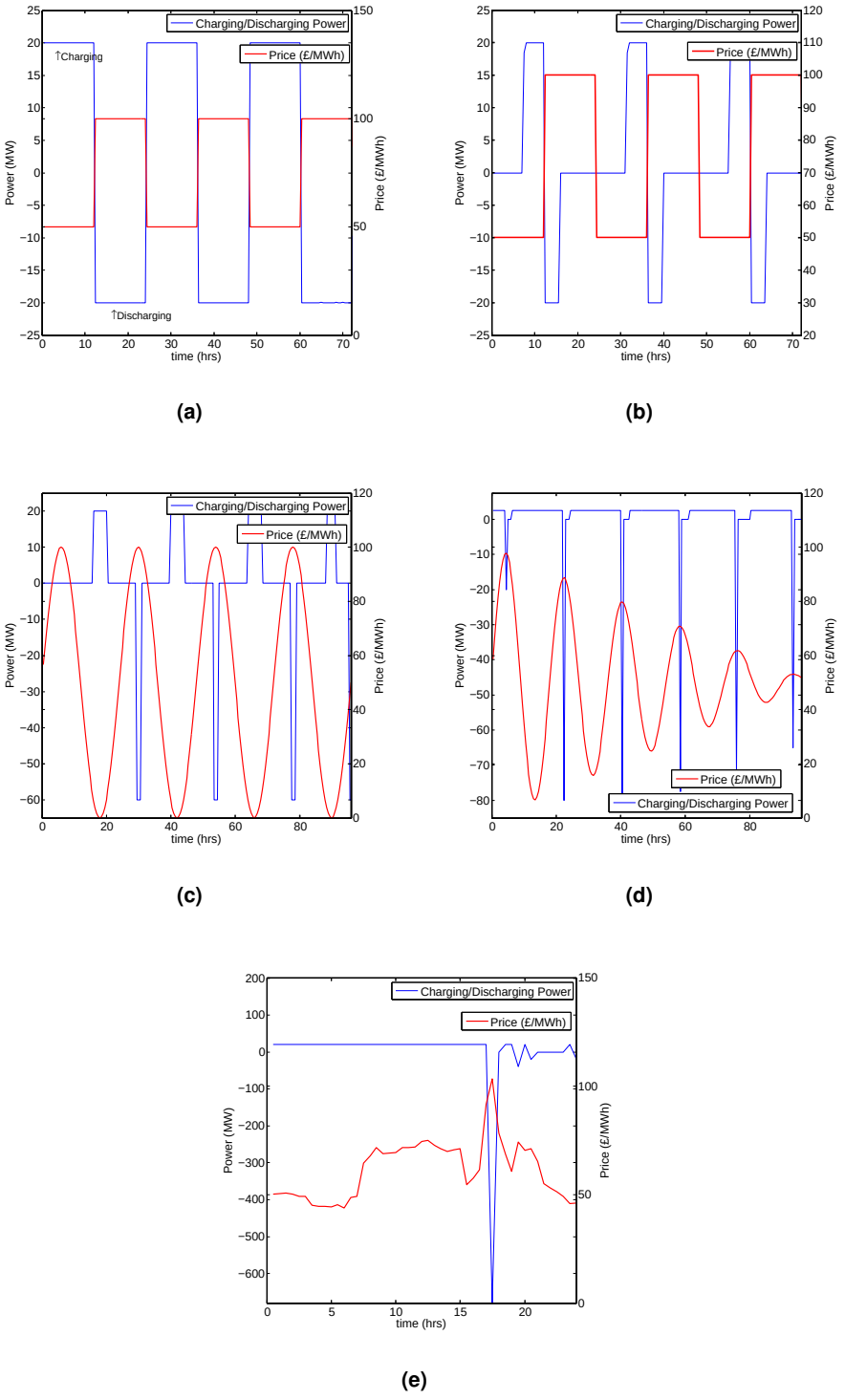

Figure 4.9: Results for optimisation of each of the 5 test cases described in the model validation section. (a) Scenario 1, (b) Scenario 2, (c) Scenario 3, (d) Scenario 4 and (e) Scenario 5. The figures all show the models output schedule for energy transfer to and from the store with the given price input and constraints specified for each case.

that the charging limit is now 20 MW. The Figure 4.9e shows that in this case, the model again finds the optimum solution, storing all the energy until the price spike at 17.30, at which point it sells all the previously stored energy. It then waits for the next highest price and repeats this process.

The figures all show the model's output schedule for energy transfer to and from the store with the given price input and constraints specified for each case. The blue line is charging/discharging power, with a positive value indicating charging, and a negative value indicating discharging.

4.2.6 Preliminary Results

To further demonstrate the capability of the algorithm, it is used to find the upper boundary in revenue for five theoretical Pumped Hydro Storage, Hydrogen Storage, and Battery Storage systems for the years 2005-2010. All the devices have the same capacity (200 MWh) but have varying charge/discharge limits of 20 MW, 50 MW, 100 MW, 200 MW, and 400 MW. The fixed efficiencies of the Pumped Hydro, Hydrogen and Battery systems are 75%, 50% and 85% respectively. The battery system is based loosely on a Sodium Sulphur (NaS) system, with a typical efficiency of around 85% (Tamyurek *et al.*, 2003), however the focus is to demonstrate the capability of the model rather than on the specific efficiency values. The time constant for the Pumped Hydro and Hydrogen storage is set at 10 years whereas the time constant for the battery storage system is set at 830 hours. This means the battery will have lost 63.2% of the stored energy after 830 hours; hence the round trip efficiency for energy stored over this period will be 85% Œ 36.8% = 31.3%. Table 4.2 shows the additional characteristics of the systems, as well as the calculated upper boundary values, which are then displayed graphically in Figure 4.10. As an example of the schedule output of the model, Figure 4.11a shows the operating schedule for the first 700 hours of 2009 for the 20 MW PHS case, along with the corresponding spot market prices.

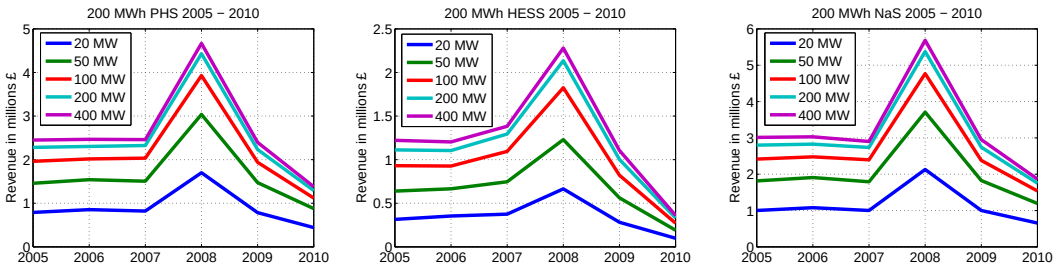

(a) PHS **(b)** HESS **(c)** NaS

Figure 4.10: Graphs showing the relationship between the charging/discharging power and revenue generated for the systems modelled in Table 4.2. All the systems have a capacity of 200Mwh.

Table 4.2: Storage characteristics and model output.

System	Capacity (MWh)	Charge/Discharge Power (MW)	Overall Fixed Efficiency (%)	τ_s, storage time constant	Annual upper boundary revenue using UK Market Index Prices					
					2005	2006	2007	2008	2009	2010
					Millions of £					
PHS	200	20	75	10 years	0.7896	0.8543	0.8213	1.7006	1.7843	0.4423
PHS	200	50	75	10 years	1.4578	1.5407	1.5059	3.0372	1.4726	0.8765
PHS	200	100	75	10 years	1.9625	2.1066	2.0352	3.929	1.9387	1.1198
PHS	200	200	75	10 years	2.281	2.3028	2.3249	4.4306	2.2326	1.2925
PHS	200	400	75	10 years	2.4502	2.4658	2.4601	4.667	2.3947	1.3797
HESS	200	20	50	10 years	0.3151	0.3533	0.3748	0.665	0.2819	0.0988
HESS	200	50	50	10 years	0.6397	0.6657	0.7468	1.22973	0.5623	0.1909
HESS	200	100	50	10 years	0.9306	0.927	1.0948	1.825	0.8211	0.2713
HESS	200	200	50	10 years	1.11193	1.1045	1.2938	2.1346	1.0027	0.3308
HESS	200	400	50	10 years	1.2216	1.2035	1.3828	2.2801	1.1054	0.3604
NaS	200	20	85	830 hours	1.0005	1.0783	1.0007	2.1287	1.0018	0.6558
NaS	200	50	85	830 hours	1.8144	1.9082	1.7919	3.7088	1.825	1.1952
NaS	200	100	85	830 hours	2.4167	2.4778	2.3957	4.7672	2.3778	1.5378
NaS	200	200	85	830 hours	2.8003	2.8261	2.7356	5.3759	2.7414	1.7511
NaS	200	400	85	830 hours	3.0121	3.0284	2.8995	5.6843	2.952	1.8644

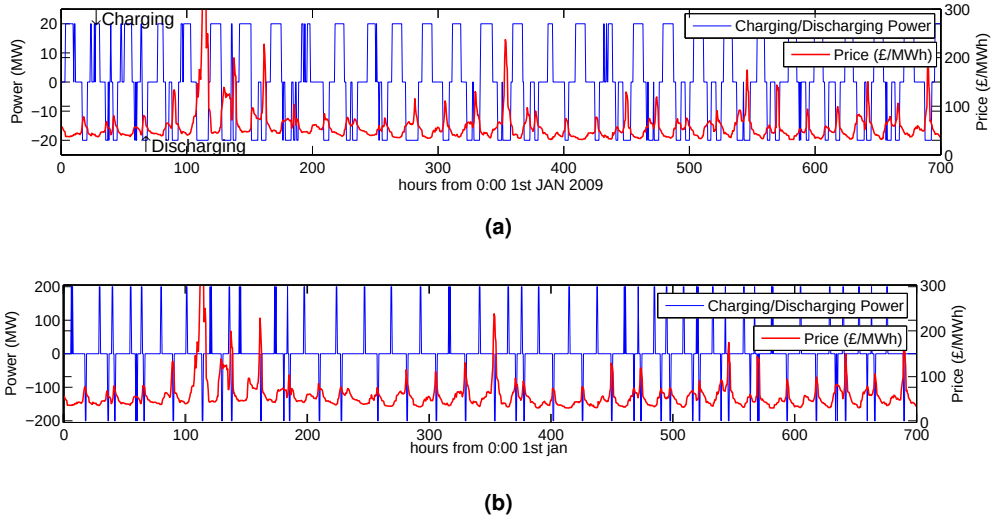

Figure 4.11: Graphs of the optimal schedule of operation for the 20 MW PHS and 200 MW PHS storage systems specified in Table 4.2 during the first 700 hours of 2009, along with the corresponding UK spot market price.

4.2.7 Discussion

The output schedules of the devices simulated in Table 4.2 (of which those shown in Figure 4.11 are typical) seem to favour arbitrage cycles of at least a diurnal nature in order to maximise the revenue from time-shifting. In essence, the model seems to favour a dispatch schedule that tends to mimic the period of the underlying price, and if this happens to be diurnal in nature, the schedule will tend to be diurnal in nature too. This is an important consideration for policy makers to be aware of regarding the promotion of bulk energy storage; if the payment mechanism for stimulating investment in bulk storage is through the spot market then storage operators will tend to follow the period of the underlying price structure, and this may or may not be a desirable timeframe for storage. Policy makers should also take account of the other markets from which energy storage devices can derive revenue streams, e.g. balancing and black start markets, as provision of one service may preclude or disrupt the provision of a similar service to a differing market. Table 4.2 shows that more revenue is generated with an increased power rating and as each data point in the spot price input file has a timeframe of 30 minutes, increasing the discharging/charging power beyond that which can entirely empty/fill the storage system in 30 minutes will not generate any additional revenue. With regard to the scenarios in Table 4.2, increasing the charging/discharging power beyond 400 MW will generate no additional revenue.

As initially expected, the outputs in Figure 4.11 show that in order to maximise the revenue generated, the storage schedule buys at times of lower prices and sells at times of higher prices. The spot market price is influenced by a multitude of variables, but a major factor is the marginal cost of the next generating plant that offers to sell energy into the market. Therefore

it is expected that a storage device operating on the spot market will act such as to smooth the variability between demand and supply and by doing so increase the overall reliability of the system. While this may be of a wider social benefit to the system, there is no mechanism by which the storage operator is paid for these benefits through the spot market. Furthermore, a situation is forseeable in which a large amount of wind energy becomes available at a time of low demand. A storage operator is likely to buy large amounts of this cheap electrical energy, and then sell it at times of higher demand and corresponding higher prices. This could reduce the need for higher marginal cost and carbon intensive peaking plant such as diesel or fuel oil generators.

The model results also clearly show that storage devices that have higher round trip efficiencies over the typical market time period will have greater upper boundary revenues than less efficient storage devices. In addition to this obvious conclusion, it is interesting to note that the variability of spot prices from year to year gives a greater risk to a storage operator in terms of upper boundary revenues than the efficiency of the device alone would suggest e.g. in the space of two years (from 2008 - 2010) the upper boundary of revenue dropped by approximately 75% — a high degree of revenue variability to account for in assessing the viability of a storage investment.

In terms of the amount of “storage” available to provide security of supply to any network - it is important to make a distinction between storage that works on a cycling timeframe of less than 48 hours (less than hundreds of GWhours of storage), and storage that is at a strategic level (TWhours of storage) that may be hoped never to be used at all. The latter will have a cost - but the benefit could be argued to be a social benefit to the system as a whole and should therefore be funded through differing mechanisms than the revenues derived from the market based time-shifting of energy - indeed it could be considered as an insurance against the occasions when the network requires stores of energy that are large enough to last into the weeks - months range. These “stores” of energy are currently and historically in the form of coal, gas and nuclear fuel stocks, which may well continue to be used if low carbon abatement technologies allow. However, it would be shrewd to consider the role for large-scale strategic storage that is not dependent on these fossil or nuclear fuels e.g. hydrogen or some other low carbon “fuel”.

If a long term goal is to be independent of fossil fuels — then the storage role currently carried out by fossil fuels will require replacement. It is likely that the size of future energy stores will be driven by future needs and markets, rather than the energy equivalents of historical fossil fuel stockpiles, which are driven by price variability and the perceived risks associated with long supply chains.

4.2.8 Conclusions

A model for determining the maximum possible revenue available to storage operators, operating on a market with a single valued price for a discrete time series has been presented. The model provides the optimal solution for the schedule of operation for a storage device that yields the upper boundary of revenue available from energy arbitrage. The model has the ability to simulate systems of various types, through the parameters of discharging and charging power limits, input efficiency, output efficiency, a self-discharge rate and maximum storage capacity. The input to the model is a time-series for the market index price in which the storage system operates.

As demonstrated by the preliminary results, the model can be used to calculate the upper boundary of revenue on a per MW or a per MWh basis, for any given storage device. Thus far, the model has been used with historical electrical spot prices, whereas of course, any real world system would not be able to forecast prices perfectly. However, knowing the maximum revenue available to storage devices in previous markets should be a useful addition to the general knowledge base on storage. Therefore, a potential use of the model is to inform policy makers as to the type of incentives they may need to offer storage operators if they wish to encourage the inherent network reliability and potential carbon savings that come with bulk electrical energy storage devices.

Overall, the model is sufficiently robust and flexible enough to consider various types of storage devices in different markets.

A logical extension of the work carried out using the model would be to compare various storage technologies in different markets, in order to gain an idea of their comparative attractiveness as an investment. Also, if used in conjunction with the carbon intensity for differing generators, the overall CO_2 production in electrical networks with and without storage could be estimated. If feasible, this could then be used to calculate any net CO_2 savings resulting from the use of energy storage in an electricity network, e.g. when wind energy at a time of low demand is used to offset more CO_2 intensive peaking plant at a later time. The algorithm has already been extended in order to compare the increased revenues available from using storage with renewable energy generation suffering from different levels of curtailment, although this is particularly network dependent. Further development of the model in this direction is a rich area of interest.

The method presented provides an objective tool with which to compare storage systems through the provision of a single value for the maximum achievable revenue for the time-shifting of electrical energy in historical markets. A storage operator would not have been able to derive a greater revenue than the upper boundary figure from arbitrage alone. For a full economic assessment, other costs would need to be included, e.g. the capital and operation/maintenance costs of the storage systems, as well as analysis of other potential sources of

revenue such as the ancillary services markets.

The development and deployment of energy storage is essential as part of a sustainable and low carbon energy future. This itself is crucially dependent on a more detailed techno-economic analysis for both policy makers and potential investors alike, and the time-shifting model presented here provides valuable insights.

Chapter 5

What is the value of energy storage to the electricity network?

While chapter 4 investigated the revenue that could be generated by energy storage technologies, this chapter addresses the questions of what benefits energy storage can provide to electricity systems, how this depends on different amounts of renewable electricity generation and whether the market will encourage energy storage to participate in this manner. A similar optimisation technique to that described in chapter 4 (and published in Barbour *et al.* (2012)) is used along with a hypothetical fuel cost supply curve to estimate the value of electrical energy storage to electricity systems in terms of minimising the overall system fuel cost. We also examine the effect that the optimum schedule of operation has on demand profiles. By using historical data for the GB electricity demand and assuming a simple fuel cost curve for different plants, the action of energy storage in a simulated electricity system can be optimised in order to minimise the overall fuel cost to the system. This is done in a system based on the existing GB network in 4 different energy storage scenarios; UK current (3GW, 30GWh), low (6GW, 30GWh), medium (12GW, 60GWh) and high (20GW, 100GWh), and each with 10GW of installed wind capacity in a no wind, low wind (23TWh), medium wind (28TWh) and high wind (31TWh) simulation. All the storage is based on Pumped Hydro Electric storage. The demand data is taken from the national grid half hourly metered data (National Grid, 2012) and the wind data is extracted from an existing data set from a hindcast from a mesoscale weather forecasting model at 3km resolution and assuming 10GW of wind generation capacity spread across the UK (Hawkins, 2012). It is demonstrated that the value of storage is increased in systems with high wind generation, storage allows for a higher level of base-load generation and that a storage device acting to maximise its profits does not necessarily act to reduce the system fuel cost.

5.1 Introduction

The purpose of any electrical network is to provide electrical power reliably where ever it is needed, avoiding any loss-of-load. In order to do this effectively electricity networks usually consist of various different types of plant, giving a generation portfolio. Different types of plant are suitable for generating electricity at different times and in different contexts. For example, coal and nuclear power are very capable of providing a constant base-load power relatively cheaply. Nuclear power is especially inflexible, and although coal plants are flexible, there are efficiency penalties for running them at part load. Gas turbines however, are generally more expensive to run (especially Open Cycle Gas Turbines (OCGT)), but their output can be easily manipulated and they can be switched on or off very quickly, so can be used to cover temporary spikes in demand. Renewable (intermittent) energy generation, like wind generation, has no associated fuel cost, but the supply is often only weakly correlated with demand (Sinden (2007) demonstrates that in the UK wind has a small positive correlation with demand), and it is because of this very weak correlation that it cannot simply displace the conventional thermal generators. The costs of this intermittency in UK terms are considered in Gross (2006).

Energy storage allows for supply and demand matching, and is unaffected by the type of supply plant. Therefore, instead of using gas plants to provide peak electricity, it may be possible to use storage and a cheaper (but maybe more inflexible plant), or indeed an intermittent renewable supply. However, as any charge, storage, and subsequent discharge of energy will have losses associated with it, this process will only result in a reduction in the system fuel cost if the electricity used to charge the storage is a factor of $(1/\eta_s)$ less than the fuel cost of generating the required energy at the storage discharge time (η_s is the round trip efficiency of the storage process and other costs, i.e. initial costs and O&M, are not considered at this stage). If this is the case, then the action of energy storage should allow for a reduction of the overall system fuel cost (while still meeting the total demand). This may also be the case for CO_2 emissions (or other emissions), as energy storage could also be used to displace plants with higher emissions. In this chapter, we concentrate on a minimisation in terms of fuel cost, although the method presented could be used to minimise in terms of emissions, using emission data from each type of power plant.

There has been much previous work speculating on how energy storage may work with wind power. Green *et al.* (2011) considers a UK based system with a very high capacity of wind and hydrogen electrolysers. Korpaas *et al.* (2003) considered the economic benefits of using energy storage to smooth variations in wind power, noting that variations in actual power production compared to forecast production generally lead to a loss in revenue when generation is sold on an electricity spot market. Bathurst and Strbac (2003) look at the added value of wind energy provided by energy storage, taking an economic approach, concluding that energy storage offers significant added value to wind even when the rated power of the storage is much less than that of the wind. Benitez *et al.* (2008) also present a model with the capability to optimise

the schedule of an energy storage device to minimise total system costs considering a system based on the Alberta electricity system with different levels of wind, conventional hydro and a single large pumped hydro storage. They conclude that the system copes better with high wind when there is more hydro and pumped hydro, however they do not analyse how the storage behaves in any detail. Barbour *et al.* (2012) provides an optimisation technique which is used to determine the maximum historical revenue available to a given storage device. It has a greater capability of simulating different types of storage device as the algorithm can account for both time dependent and time independent efficiency components. This model is adapted in the present work to minimise in terms of fuel cost, rather than maximise in terms of revenue. Although we focus on pumped hydro (as the only currently effective method of grid energy storage, apart from stockpiling fuel), this method has the potential to simulate different energy storage devices. We also present and analyse the schedule of operation of the storage device, and compare the schedule required to minimise the total system fuel cost to that required to generate the maximum revenue.

The present analysis considers a hypothetical system, which is loosely based on the existing GB network. In this hypothetical system there is an installed capacity of 10GW of wind, representing a significant proportion of the total UK capacity as wind generation, whose output is simulated using a Weather Research and Forecast model (WRF) as described in Section 5.3. The UK currently has around 6.5GW of installed wind capacity (National Grid, 2011), though could have more than 10GW by 2015 (National Grid). The low, medium and high wind scenarios are created using the WRF model, by simulating historical wind speeds for years with low, medium and high average wind speeds; 2010, 2006 and 2008 respectively. Archived half hourly demand data from 2010 (National Grid, 2012) gives the demand profile used throughout all the simulations, in order to allow direct comparison between the various scenarios. We construct a simple aggregate fuel cost function in order to estimate the fuel costs in each scenario (outlined in Section 5.2). We consider four different energy storage scenarios and in all the simulations the energy storage considered is based on Pumped Hydroelectric Storage. This is simulated with charging efficiency times discharging efficiency = 75% (i.e. $\eta_{charge} \times \eta_{discharge} = 75\%$) and a nominal time constant of 100 years, so that the round trip efficiency is effectively always 75% (for further information on the model algorithm and definitions see Chapter 4 Section 4.2 and Appendix A). The four storage scenarios modelled are UK current (3GW 30GWh), low (6GW 30GWh), medium (12GW 60GWh) and high (20GW 100GWh). The UK currently has $\sim$28.2GWh of Pumped Hydro with a total rated power of 2744MW, see Tables 4.1 and 5.1.

Table 5.1: Capacity by plant type of all existing plants (National Grid). The offshore and onshore wind capacities shown here only represent plants connected to the transmission network, i.e. not including any generation connected in the distribution network.

Plant Type	2010/2011	2011/2012	2012/2013	2013/2014	2014/2015	2015/2016	2016/2017	2017/2018
Biomass	45	45	45	45	45	45	45	45
CCGT	29022	29022	29022	29022	29022	29022	29022	29022
CHP	2069	2069	2069	2069	2069	2069	2069	2069
Hydro	1113	1113	1113	1113	1113	1113	1113	1113
Large Unit Coal	4342	4342	4342	4342	4342	4342	2284	2284
Large Unit Coal + AGT	21440	21440	21440	21440	21440	21440	17517	17517
Medium Unit Coal	1102	1102	1102	1102	1102	1102	0	0
Medium Unit Coal + AGT	1131	1131	1131	1131	1131	1131	0	0
Nuclear AGR	8246	8246	8246	8246	8246	8246	8246	8246
Nuclear Magnox	1390	960	0	0	0	0	0	0
Nuclear PWR	1207	1207	1207	1207	1207	1207	1207	1207
OCGT	578	578	578	578	578	578	478	478
Oil + AGT	3636	3636	3636	3636	3636	3636	0	0
Pumped Storage	2744	2744	2744	2744	2744	2744	2744	2744
Small Unit Coal	783	783	783	783	783	783	783	783
Wind Offshore	997	997	997	997	997	997	997	997
Wind Onshore	2093	2128	2128	2135	2135	2135	2135	2135
Total Capacity(MW)	81938	81543	80583	80590	80590	80590	68640	68640

5.2 Building a simple fuel cost curve

Table 5.1 (taken from National Electricity Transmission System (NETS) Seven Year Statement (National Grid)) shows the GB installed plant capacities for the next 7 years.

The values shown Table 5.1 are simplified and collated into the values shown in Table 5.2, which are used to create a simple fuel cost curve for the simulation. The wind simulations are explained in Section 5.3.

Table 5.2: Simplified and collated by type plant capacities used in the simulation (approximated from Table 5.1).

	Installed Capacity (MW)
Nuclear	10413
Coal	28798
CCGT	29022
OCGT+Oil	4214
Onshore Wind[1]	8000
Offshore Wind[1]	2000
Others not included	
Biomass	45
CHP	2069
Hydro	1113

[1] These are the assumed values used in the simulation.

Table 5.3 then shows the estimated fuel costs for the types of generation included in the simulation. It should be noted that these are fuel cost estimates, rather than short run marginal costs (the cost of producing a small amount of additional units of electricity). The costs have been taken from Department of Energy and Climate Change (2011), and have also been used in reports by Mott MacDonald (2010) and Parsons Brinkerhoff (2011). The costs have been estimated by assuming that the fuel cost is the dominant factor in the levelised cost, and using plant efficiencies as shown in Table 5.3.

Assuming that plant availability for each type of generation is 80% (that is to say that on average 80% of the total generating capacity will be available to meet the demand); Figure 5.1 shows the stepped aggregate fuel cost function. Table 5.4 shows the fuel cost (taken from the central fuel cost scenario) and the plant capacities available at 100% and 80% plant availability.

Table 5.3: Estimated fuel costs (£'s per MWh electricity generated) by generation technology in 2030 (Department of Energy and Climate Change, 2011; Mott MacDonald, 2010; Parsons Brinkerhoff, 2011).

Plant Type	Low (£/MWh)	Central (£/MWh)	High (£/MWh)	Assumed Plant Efficiency (%)
Nuclear	5.0[1]	5.0[1]	5.0[1]	-
Coal	17.2	23.7	33.4	45.0
CCGT	26.0	40.5	57.8	59.0
OCGT	37.4	58.3	83.2	41.0

[1] This is the levelised fuel cost over the lifetime of a new plant (built in 2011) estimated by Mott MacDonald (2010).

Table 5.4: Generating capacities by plant type. The simulation assumes 80% plant availability.

Plant Type	Installed Capacity	Generating capacity 80% available	Central Fuel Cost
Nuclear	10413	8330	5.0
Coal	28798	23038	25.9
CCGT	29022	23218	40.5
OCGT	4214	3371	58.3

In order to make the costing function more realistic, a piecewise polynomial is fitted to the stepped function shown in Figure 5.1, as shown in Figure 5.2. This should be a better representation of the actual GB merit order, as it doesn't assume that all generators of the same technology have exactly the same cost. In reality, those generators which are used to meet higher demand values will have a higher associated cost to the network, as they are run less often, and so will charge a higher price for the times that they are used. This will in part be justified by the fact that generators used less often will spend a higher fraction of time ramping up and down, so will have a higher fuel cost than generators of the same type which are used more frequently. Note: The fuel costs remain constant throughout modelled scenarios.

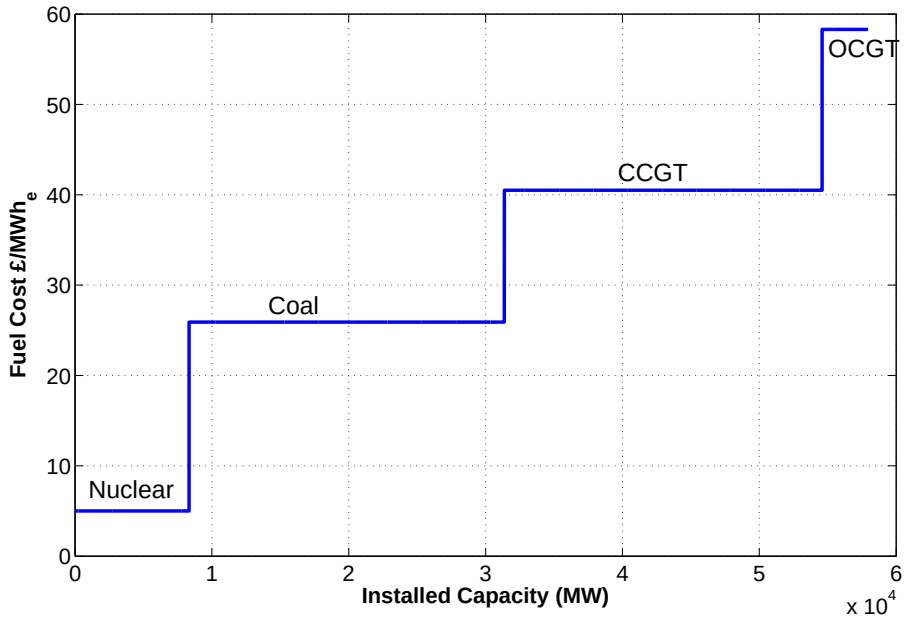

Figure 5.1: An estimate of the UK aggregate fuel cost curve. The different tiers mark the estimated prices of Nuclear, Coal, CCGT and OCGT accordingly.

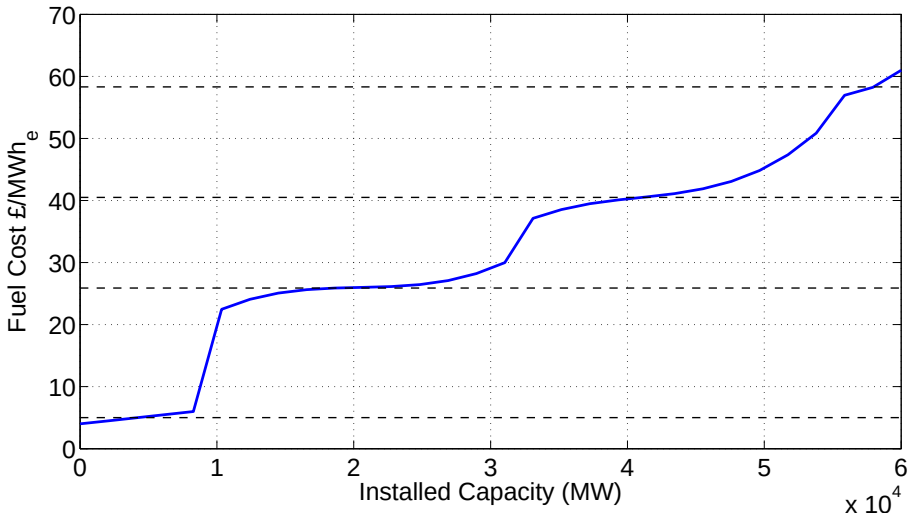

Figure 5.2: The cost function used in the simulations: The dotted lines mark the prices of Nuclear, Coal, CCGT and OGCT as shown. The curve is a piecewise polynominal fitted to function in Figure 5.1. Note that there are still price jumps between generators of different types, but there is also some variation in the price of generators of the same type.

5.3 The Wind Resource Model

The Weather Research and Forecast (WRF) model (Joseph B. Klemp, 2008) was used to simulate hourly wind speeds over a ten year period using the high performance computing platform HECToR to form a wind speed data set for the UK. It was run with three nested domains down to a final resolution of 3km, taking boundary conditions from the Global Forecast System (GFS) final analysis at 0.5 degree resolution. The data set of simulated wind speeds was then compared to previous observations from networks of meteorological stations, wind-farm monitoring masts, offshore buoys and offshore platforms. Simulations agree well with observations, and have thus validated this approach to providing a realistic and representative wind speed data set. It is this data set which is used to create the various wind scenarios.

The wind scenario presented in the simulation represents a significant growth of onshore wind as well as the development of shallow water and near-shore offshore sites. The offshore sites leased by the Crown Estate are outlined in RenewableUK (2010), with more than 30GW of offshore capacity under consideration. Wind speeds are converted to power outputs using representative power curves typical of onshore and offshore farms, following the methodology presented in Norgaard and Holttinen (2004). Simulated monthly capacity factors for existing sites are compared to published data, which confirm this approach produces realistic power estimates for both onshore and offshore wind farms.

The simulation assumes 10GW of installed wind capacity (as outlined in Table 5.2). This is similar in magnitude to the wind capacity expected in 2014/15 (see Table 2 of National Grid (2011)). The distribution of wind generating capacity is shown in Figure 5.3. The regions have been divided according to GB's distribution network operator boundaries.

The assumed installed wind capacity in each region is shown in Tables 5.5 and 5.6.

Using the spread of generation illustrated in Figure 5.3 and detailed in Table 5.6, the data set created by the WRF was then used to provide a time series for the total wind power production at all of these locations in a high wind (2008), a medium wind (2006) and low wind year (2010).

The creation of this data set using the WRF is described in detail in Hawkins (2012).

5.4 Methodology

In a similar manner to the model outlined in Chapter 4, the model described here works on the principle that if the cost of generating electricity at an earlier time to meet the demand at a later period is less than the cost of generating the electricity at the later period (accounting for storage system losses), then the action of energy storage will introduce an overall fuel cost saving to the network.

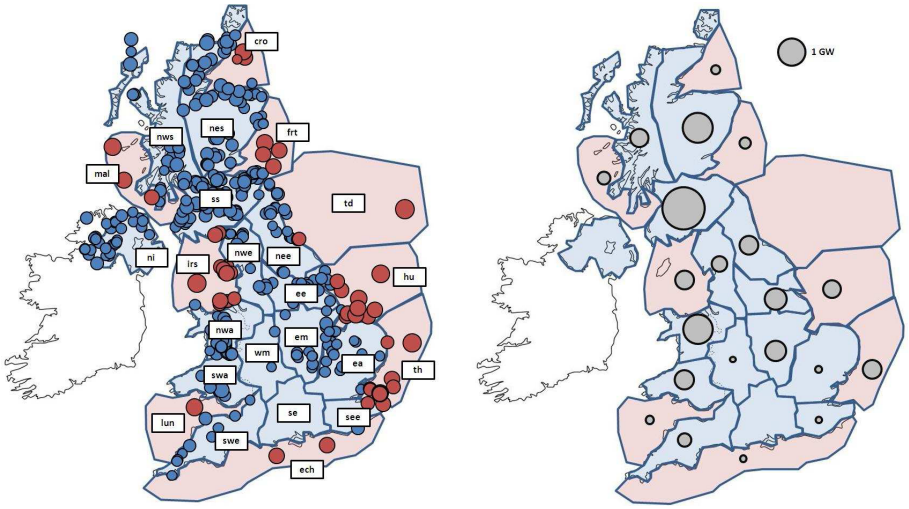

Figure 5.3: (left) 337 onshore and 49 offshore wind sites by region. Regions were divided up according to GB's distribution network operator boundaries. (right) 10 GW of installed wind capacity by region.

The following example aims to illustrate this concept: Consider a demand of 35GW in the 30 minute period 19 (9 am) of a given day. Upon inspection of Table 5.4 we see that this demand can be met by using 8330MW of Nuclear at a cost of £5/MWh, 23038MW of Coal at a cost of £25.9/MWh, and 3632MW of CCGT at a cost of £40.5/MWh. The total cost of generation is £392,715.10. Now consider that the demand at period 10 (4.30 am) was only 25GW. This can be generated by using 8330MW of Nuclear at a cost of £5/MWh and 16670MW of coal at a cost of £25.9/MWh, yielding a total cost of £236701.50.

If a storage device which has a round trip efficiency of 75% between the two time periods in question is used to increase the demand at period 10 by 4843MW, and decrease the demand at period 16 by 3632 MW (25% of the 4843 MW is lost) then the new cost of generation is at period 10 is increased to £299,418.35, an increase of £62,716.85. The cost of generation at period 19 is however now reduced to £319,167.10, yielding a saving of £73,549. Therefore the total fuel cost of the network has been reduced by £10,831 and there is no longer any CCGT required to generate electricity at period 19. This is illustrated in Figure 5.4. In this manner it is possible that storage devices can reduce the total fuel cost of an electricity network, and can decrease the maximum required generating capacity available.

In the example, there is no benefit to reducing the demand at period 19 by more than 3632MW, as it is only this amount of electricity that will be generated by CCGT. Further reduction would lead to a decrease in the coal generation at period 19, which could only come from an increase in coal generation at period 10, therefore the losses involved with the storage process would lead to a loss in any cost savings when reducing the demand by more than 3632MW (and would

Table 5.5: UK wind regions considered in model.

Onshore		Offshore	
ea	East Anglia	cro	Cromarty
ee	East England	ech	English Channel
em	East Midlands	frt	Forth
nee	North East England	hu	Humber
nes	North East Scotland	irs	Irish Sea
ni	Northern Ireland	lun	Lundy
nwa	North Wales	mal	Malin
nwe	North West England	td	Tyne and Dogger
nws	North West Scotland	th	Thames
se	South England		
see	South East England		
ss	South Scotland		
swa	South Wales		
swe	South West England		
wm	West Midlands		

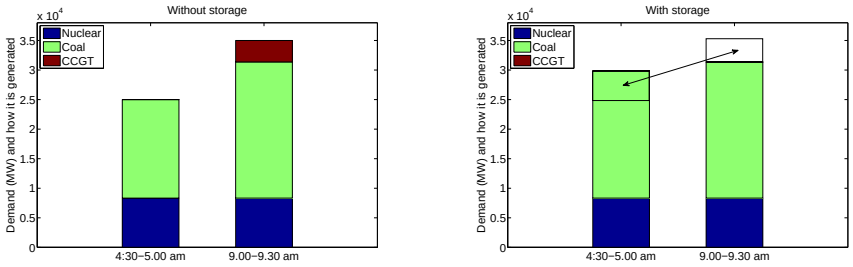

Figure 5.4: An illustration of the example described. (left) without the storage and (right) with storage.

eventually lead to an increase in the total fuel cost).

The minimisation algorithm is very similar to the revenue maximisation algorithm outlined in Chapter 4 (and described in detail Appendix A), but instead of a move of energy being accepted between the two randomly selected time periods if it leads to a higher revenue, a move of energy is accepted if and only if it leads to a reduction in total fuel cost, i.e. the total fuel cost of meeting the new demand at each period must be less than the total cost of meeting the old demand. If the fuel cost of meeting the new demand is lower then the move is accepted, providing it is physically realisable (which is checked by the other constraints as outlined in

Table 5.6: Installed wind capacities by region.

	Onshore		Offshore	
	Region	Capacity (MW)	Region	Capacity (MW)
Scotland	nes	1207.6	cro	110.5
	nws	437.6	frt	168.5
	ss	2354.8	mal	221.0
		4000.0		500.0
England/Wales	ea	66.9	ech	58.2
	ee	622.5	hu	421.4
	em	562.9	irs	460.0
	nee	465.9	lun	87.3
	nwa	1135.1	td	0.0
	nwe	324.6	th	473.0
	see	56.9		
	se	0.0		
	swa	487.3		
	swe	231.9		
	wm	45.9		
		4000.0		1500.0
Total		8000.0		2000.0

Appendix A).

5.4.1 Simulation Assumptions

- The simulations are run using the 2010 demand data, with 3 different years simulated wind data- 2008 as a high wind year, 2006 as a medium wind year and 2010 as a low wind year. It is recognised that demand and wind are not entirely uncorrelated, but the purpose of this exercise is to illustrate how the value of storage changes dependent on the amount of wind energy present, and so this approach is used to provide a first approximation
- It is also assumed that there are no network capacity constraints present, so that the storage can charge or discharge at its full rated power at any period during the simulation.
- Storage Ramp rates are not considered, i.e. it takes negligible time to change the charging/discharging rate of the storage device, and it is assumed that the storage device parameters do not depend on the rate of charge or discharge.
- Demand and wind forecasting are also neglected; as with price forecasting in Chapter 5. Again these are exceedingly complex areas in their own right. Uncertainty in these

areas will lead to a reduction in the benefit provided by energy storage; this is further discussed in the chapter conclusions.

- There is no curtailment of any wind energy- it is assumed that wind will always displace thermal generation when it is available. The validity of this assumption will depend on the exact mix of thermal generation available, and its ability to vary its output. With very high penetrations of wind generation, curtailment becomes very likely as wind becomes likely to encroach on baseload/inflexible-plants. With significant curtailment then the value of storage is increased dramatically.

5.5 Results

5.5.1 Total Cost Savings

Simulations for the no, low, medium and high wind scenarios were run for the current, low, medium and high energy storage scenarios. Table 5.7 shows the results of simulations in terms of fuel cost saving (the total system fuel cost in each wind scenarios with no storage is also shown). This information is displayed graphically in Figure 5.5.

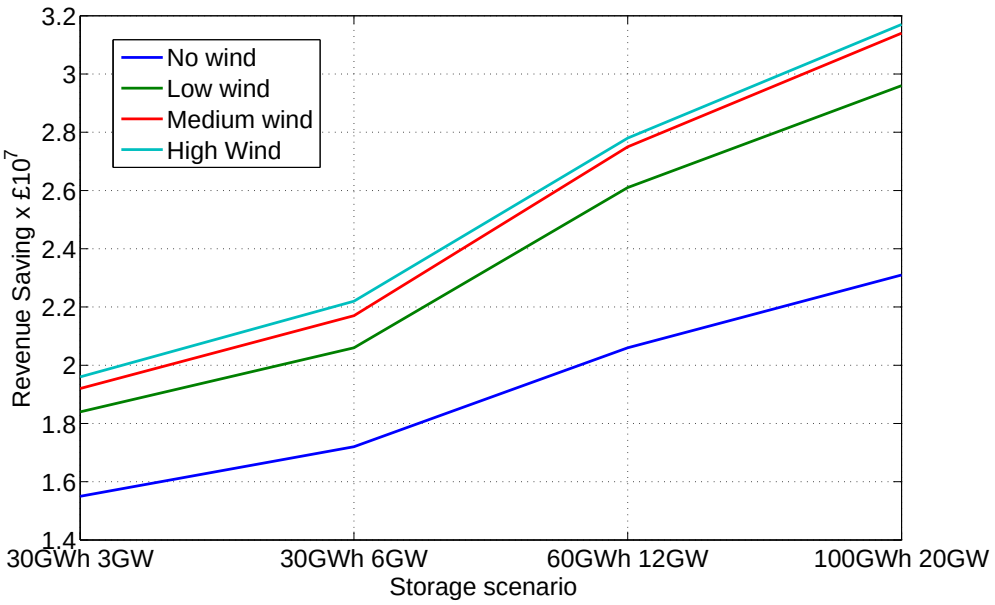

Figure 5.5: Total network fuel cost saving for the different storage/wind scenarios.

The first thing to note is that the variation between wind scenarios is much larger (roughly an order of magnitude) than the difference between the storage scenarios: With 10GW of installed wind on the network, the High wind year (2008) scenario provides 3109GWh of electricity into the network, accounting for 9.72% of the total yearly electricity demand, while the low wind year provides 2304GWh, accounting for 7.2% (the total yearly demand is 31999GWh). This

Table 5.7: Total fuel cost saving to the system in different storage and wind scenarios with 2010 demand. The no storage system total fuel cost is also shown.

2010 Wind Profile		2006 Wind profile	
Scenario	Fuel Cost Saving (£$\times 10^7$)	Scenario	Fuel Cost Saving (£$\times 10^7$)
30GWh 3GW	1.84	30GWh 3GW	1.92
30GWh 6GW	2.06	30GWh 6GW	2.17
60GWh 12GW	2.61	60GWh 12GW	2.75
100GWh 20GW	3.00	100GWh 20GW	3.12
No storage cost	664.02	No storage cost	645.18
2008 Wind Profile		No Wind	
Scenario	Fuel Cost Saving (£$\times 10^7$)	Scenario	Fuel Cost Saving (£$\times 10^7$)
30GWh 3GW	1.96	30GWh 3GW	1.55
30GWh 6GW	2.22	30GWh 6GW	1.72
60GWh 12GW	2.78	60GWh 12GW	2.05
100GWh 20GW	3.17	100GWh 20GW	2.31
No storage cost	634.84	No storage cost	746.71

equates to a difference in fuel cost between the wind scenarios of £2.92 $\times 10^8$. The difference due to storage is much less, with the highest cost saving provided by the High wind High storage scenario, equating to £3.17 $\times 10^7$ per year.

The High Wind High Storage scenario offers the biggest cost saving to the network, even though the initial total fuel cost is the lowest. There are two reasons for this; firstly because despite the higher wind scenario having less total demand which has to be met by thermal generation, this demand has a higher variability, so there are more opportunities for storage to replace a higher cost generation method with a lower cost one. Secondly the general reduction of the required thermal generation by wind means that there are more occurrences of coal having to reduce its output, which the storage avoids and uses to displace gas plants at peak times. This trend of more wind leading to higher cost savings from storage holds for all the simulations; the higher the amount of wind energy present on the network the larger the fuel cost saving available.

5.5.2 Storage operational schedule

Figure 5.6 shows the first 4 weeks of the result for the No Wind Current Storage simulation. Figure 5.6a shows the power that must be met via thermal generation with and without storage (the storage is used to minimise the network fuel cost) and Figure 5.6b shows the corresponding storage charging and discharging schedule along with the energy contained. The area under the blue (Energy transfer) line corresponds to the change in the storage level (green line, Energy contained). Figure 5.7 shows the same for the High Wind High Storage scenario.

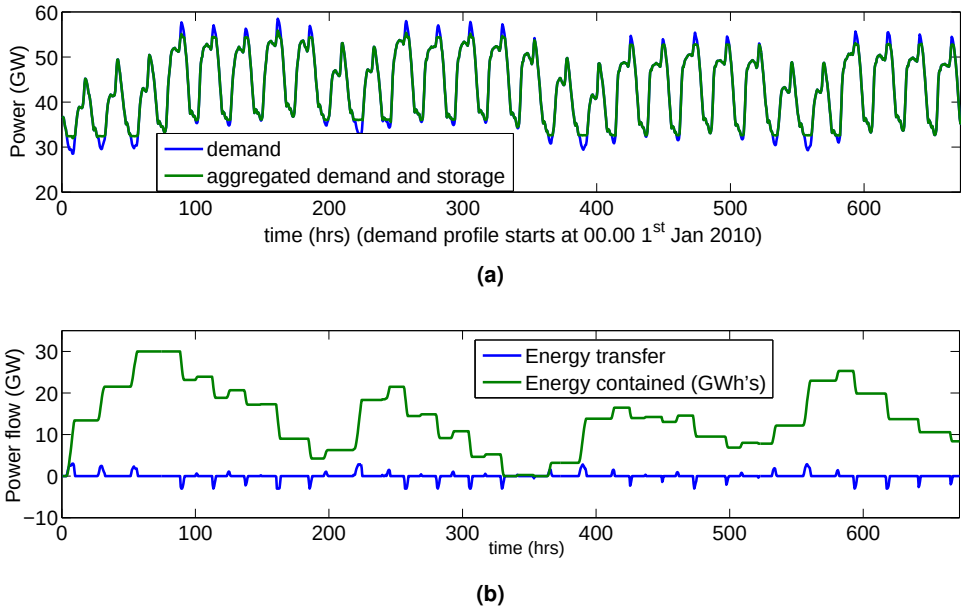

Figure 5.6: Simulation results for the first 4 weeks of the No Wind Current Storage scenario. Figure 5.6a shows the demand that has to be met with thermal generation (nuclear, coal gas etc) in both the storage and no storage case. Figure 5.6b shows the storage charging and discharging schedule, as well as the energy contained within the storage. With no time dependent loss the area under the blue line equals the change in the green line over the same period.

The results suggest that storage operates in a peak shaving and valley filling manner, and acts such as to decrease the variability of the demand that has to be met by thermal generation. It is notable that in the High Wind High Storage scenario a large amount of the rated power of the storage (20MW) isn't used (whereas the whole energy capacity is used). This can be explained by the form of cost curve in Figure 5.2, which is such that generators of the same type have similar fuel costs. Hence unless there is a very large difference in demand it is unlikely to be optimal to increase the demand to the extent that it requires generation by a different technology, as this is very likely to be the technology that would otherwise be used for generation at the later period anyway, i.e. there is no point in storing energy from CCGT

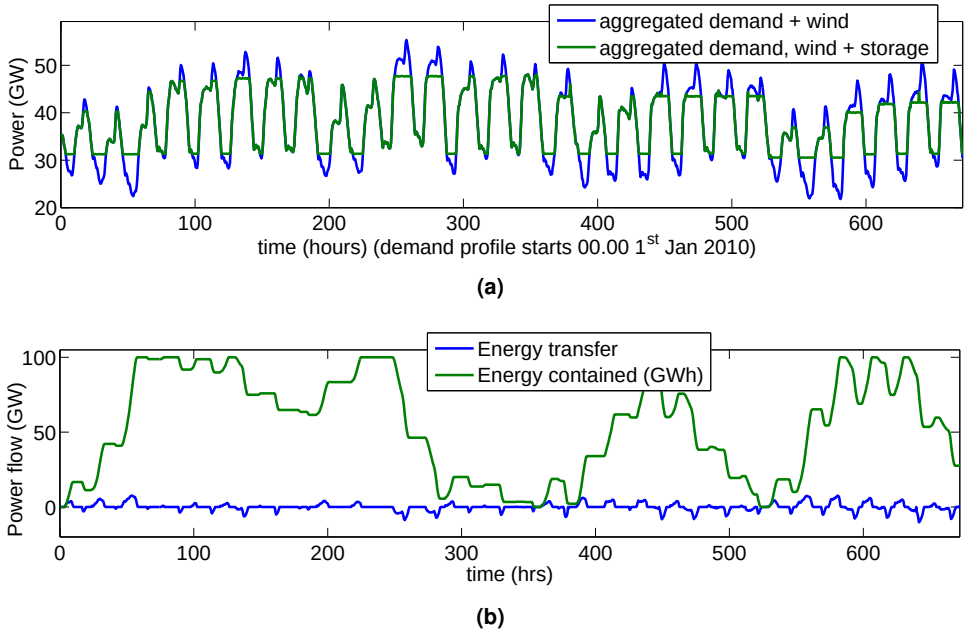

Figure 5.7: Simulation results for the first 4 weeks of the High Wind High Storage scenario. Figure 5.7a shows the demand that has to be met with thermal generation (nuclear, coal gas etc) in both the aggregated just storage and wind and no storage cases. Figure 5.7b the corresponding storage charging and discharging schedule, as well as the energy contained within the storage device.

generation at an earlier period to replace CCGT generation at a later period, due to the round trip losses in the storage process.

They also (Figure 5.6 and 5.7) seem to suggest that in order to minimise the network fuel cost the storage is likely to operate at least partially on a daily cycle (charging in the early morning hours using coal and displacing peak CCGT or OCGT at peak times), with aspects of a weekly cycle overlaid (there is generally more charging at weekends) but this is strongly affected by the wind generation. The year 2010 started on a Friday (and was a UK public holiday) and it can be seen that for the first 3 days of each of the simulation the storage is mostly charging. The energy stored is then released at peak times during the following week to displace more expensive peaking plants. The High wind scenario also significantly lowers the average demand that has to be met with fossil fuels. This means that the valleys in the demand profile are often deep into coal generation, allowing the storage more opportunities to reduce the network fuel cost by continuously running base-load plants (like coal or nuclear) and storing the energy rather than using CCGT for the spikes in demand.

The effect of the wind generation also has some interesting features. Figure 5.8 shows a 4 week sample of the storage output, energy stored (scaled by a factor of 4 for clarity) and wind production for each of the wind profiles in the high storage case. Figure 5.8a shows the High

wind (2008) profile, Figure 5.8b the medium wind (2006) profile and Figure 5.8c the Low wind (2010) profile. It can be seen that the presence of wind generation has a pronounced effect of the storage schedule, and when there is significant wind generation the storage operates much more. When there is a period of low wind (between 950 - 1200 hours of the high wind case, 600 - 850 hours of the medium wind case and 850 - 1250 of the low wind case) the storage has a tendency to release energy much more slowly, and only when demand is highest.

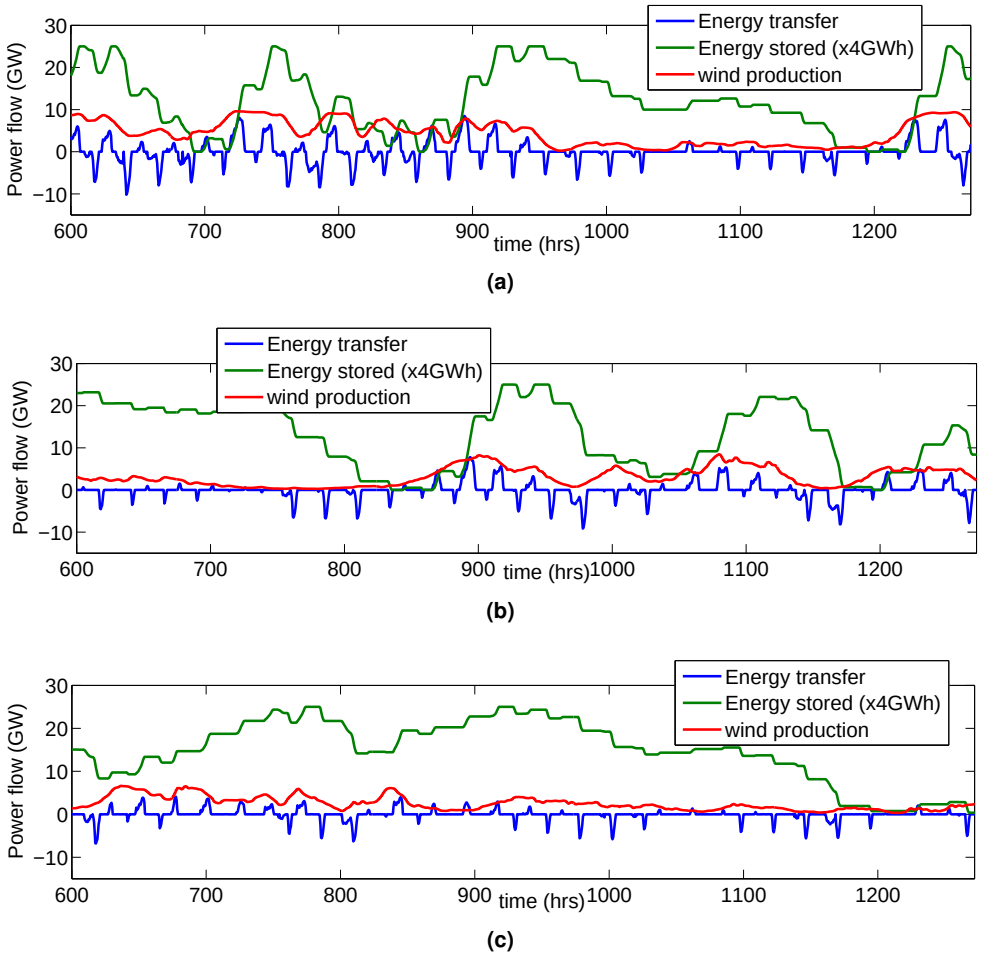

Figure 5.8: Illustrating how the optimum storage schedule for minimising system fuel cost depends on the amount of wind production.

5.5.3 The effect of the storage schedule on net demand

Figure 5.9 shows the duration curves for the original demand net of wind, and the demand net of wind and storage for the High Wind Current Storage and High Wind High Storage schedules. It illustrates that storage smoothes the curve. Storage increases the base-load generation of the system, and indeed a large amount of storage would likely make a larger base-load capacity favourable. The storage also reduces the peak demand to a lesser extent, largely due to the round trip losses in the storage. The point at which the curves intersect is the boundary between Coal and CCGT (at 31368MW), and is a result of the form of the aggregate cost function assumed. Storage also makes it less likely that wind will have to be curtailed, as the minimum demand (right hand edge of the curve) is much higher.

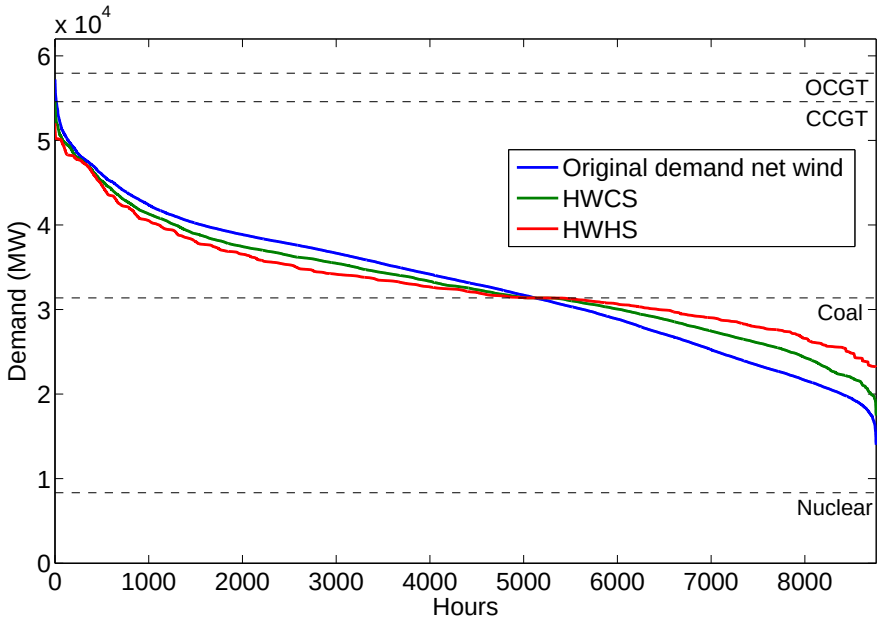

Figure 5.9: Duration curve for demand net wind and demand net wind and storage in the HWHS and HWCS scenarios.

5.5.4 Comparison to storage revenue maximisation

Using the revenue maximisation procedure described in Chapter 4 and the 2010 electricity spot market prices (Elexon), the optimum schedule of operation of the storage device in terms of network fuel cost can be compared to the optimum schedule of operation in terms of revenue for a single storage operator. Figure 5.10a shows the first four weeks (of January 2010) of the optimum storage schedule for the UK current storage (30GWh 3GW) no wind scenario and the schedule of operation of a single 10GWh 1GW pumped storage station that would generate the maximum revenue given the 2010 UK electricity spot market prices. The station generates £22 million. Figure 5.10b shows the same for the first four weeks of July 2010. It

must be stressed that for the revenue maximisation the storage plant is assumed to be a price taker, and thus its action does not affect the market spot price. The No Wind case has been used for the fuel cost minimisation, as assuming 10GW of wind generation would very likely significantly alter the spot market prices (In 2010 there was around 3GW of installed wind in the UK). It is clear that in maximising the revenue the device tends to operate on a diurnal cycle, which is sometimes similar to the fuel cost minimisation but often more frequent, as electricity spot market prices are much more volatile than the electricity demand. Figure 5.10a shows that the storage revenue maximisation schedule works more often than the system fuel cost minimisation during January. This is due to the January demand being generally higher, so that the majority of both the high demand and low demand periods require CCGT generation, and hence there is less opportunity to replace one type of generation with a cheaper type (due to the form of the fuel cost curve). Although the two schedules never work in opposition (one charging and the other discharging) the action of the 10GWh 1GW pumped storage station only yields a small fraction of the potential decrease in the total system fuel cost; the 10 GWh 1 GW pumped storage station working to maximise its revenue reduces the network fuel cost by £1.5 million, compared to by £15.5 million when the 30 GWh 3 GW station works to minimise network fuel cost.

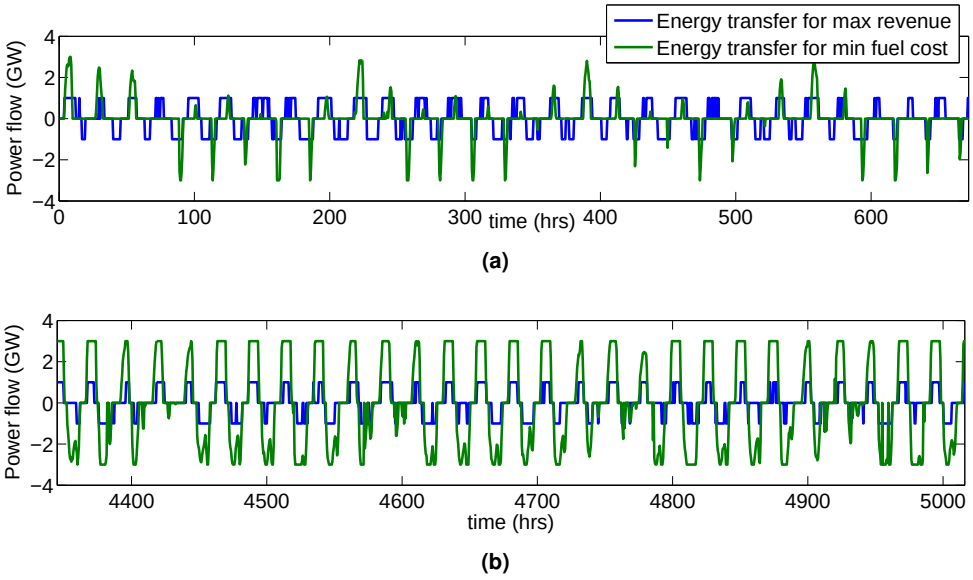

Figure 5.10: A comparison between the optimum storage schedule for minimising system fuel cost and that for maximising revenue to the storage operator.

Figure 5.11a shows the corresponding demand, demand net storage minimising system fuel cost, and demand net storage maximising its own revenue (scaled up to 30GWh 3GW) and acting as a price taker for Figure 5.10a (the first four weeks of January 2010), and Figure 5.11b shows the same for Figure 5.10b (the first four weeks of July 2010).

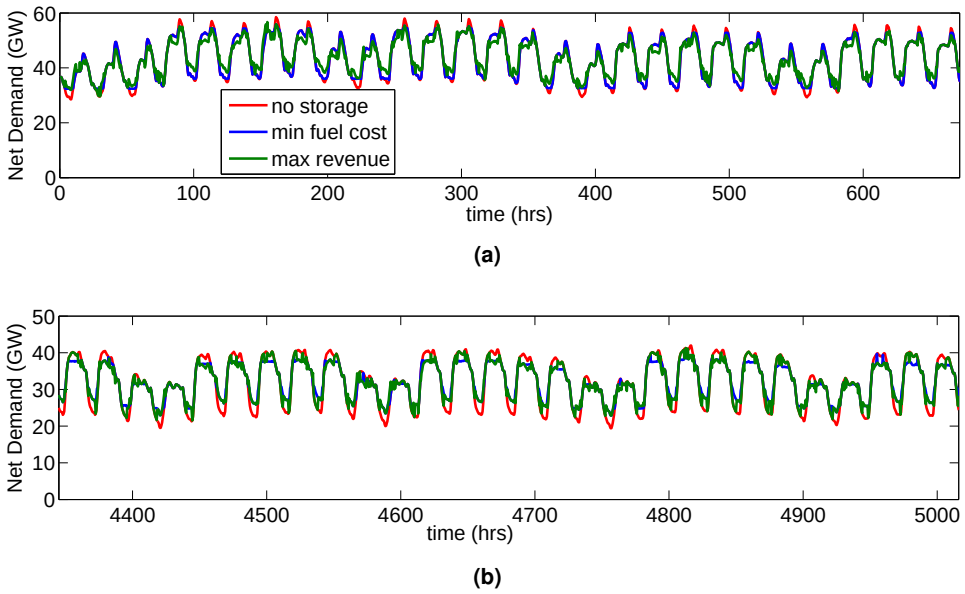

Figure 5.11: Comparisons between the corresponding net demand for the storage schedules shown in Figure 5.10. The green line shows the maximum revenue schedule, the blue the minimum fuel cost and the red is the no storage case.

5.5.5 Discussion on costs

Energy storage can be used to reduce the fuel cost to the network. In terms of costs, the fuel cost saving from the current level of storage (30 GWh 3 GW) in a high wind year with 10 GW of installed wind was ∼£20 million. When acting to maximise its own revenue the 10 GWh 1 GW pumped storage station made £22 million, however its action yielded only approximately 10% of the potential fuel cost saving to the network. Table 2.1 suggested that the cost of PHS (generally regarded as currently the cheapest form of energy storage) may be around €20/kWh (although recent informal estimates are around $55/kWh). Assuming the lower cost, 30 GWh of PHS would cost €600 million. In terms of fuel cost alone this equates to roughly a 30 year payback, which is unlikely to justify investment and with recent informal cost estimates the payback period would be more than double this. The revenue maximisation does better- with a 10 GWh PHS station generating £22 million, giving a payback of more like 10 years (using the lower cost estimate). However, given that PHS costs may be higher than this estimate it is still unlikely that this would justify private investment.

With the current price of energy storage, the financial argument for energy storage is not convincing. However, all of these estimates have assumed that there is no wind energy curtailment. Should significant wind energy curtailment become present then the fuel cost savings from storage will rapidly approach the difference in fuel cost between the wind scenarios (£292 million). With further increases in wind generation leading to further curtailment this can only be expected to increase. This financial argument is strengthened again by avoiding current

practices of paying wind to curtail.

As has been seen in the comparison in Section 5.5.4, without any wind curtailment energy storage acting to maximise its revenue on the spot market can generate larger revenues than network fuel cost savings, and the schedule to maximise revenue provides only a small fraction of the fuel cost saving. Therefore, at present the incentives to invest in energy storage come from the market (although they are too small to justify large investments in bulk energy storage), whereas in a future with large capacities of renewables and significant curtailment the fuel cost savings available are likely to far exceed any market incentives. It is up to policy makers to devise further market incentives for storage devices if they wish for significant levels energy storage to be present in future energy systems.

5.6 Conclusions

Firstly it should be stressed that the form of the aggregate fuel cost curve is very important, as it is the form of this curve that governs the way in which storage acts in these simulations. However, anticipating that the real merit order is broadly similar to Figures 5.1 and 5.2, the simulations outline the value of storage in electricity networks, especially those with high penetrations of wind energy generation. The results also show that the value of storage increases as the amount of wind energy generation increases. This is true despite the fact that in the higher wind scenarios the total required thermal generation is lower. Although the difference between the cost savings of the different storage scenarios is much less than the difference between the wind scenarios, it must be stressed that in this simulation only fuel costs have been considered, and in the simulation wind has no associated fuel cost and does not suffer any curtailment.

When storage is used to minimise the network fuel cost, it has a smoothing effect on the required thermal generating capacity, reducing its variability. The storage tends to fill in valleys in low cost generation (nuclear and coal), shaving peaks and displacing more flexible plant like CCGT. This behaviour significantly increases the amount of base-load generation that can be incorporated into an electricity system (as shown by the duration curves in Figure 5.9). The extent of this is exaggerated by larger penetrations of wind. This is in agreement with the conclusions of Green *et al.* (2011), who conclude that if large capacities of hydrogen storage were introduced it would be favourable to have a much higher level of nuclear generation.

It is also clear that storage helps to add value to wind energy generation, even without the threat of any wind curtailment, as in the networks with higher wind generation the average maximum daily demand to be met by thermal generation was reduced more than those networks with lower contributions from wind energy. Should curtailment be present then the value of storage will rise dramatically. Changes in the amount of wind production also alter the optimum schedule of the energy storage device and when wind production is low the storage has a

tendency to release energy only at the times of very highest demand, depleting the storage much more slowly.

Comparing the schedule that minimises system fuel costs to that which maximises revenue for the individual storage device shows that an individual storage operator doesn't always act to reduce the network fuel cost, as system prices are more volatile than demand. If we wish for storage operators to act in a way that most benefits the system as a whole then operating solely on spot market price differentials is unlikely to provide the necessary environment.

The simulation presented is very much a simplification and has assumed perfect demand forecasting and wind forecasting in order to estimate the maximum value of storage. Uncertainties will lead to reduction in the available savings, but the tendency for a significant proportion of the storage capacity to be utilised over a daily cycle (and the vast majority over a weekly cycle) means that effective day ahead forecasting should allow for a significant proportion of the fuel saving to be realised.

The main purpose of this work has been to demonstrate the potential value of bulk energy storage in electricity networks and the effect of different levels of renewable energy generation. The value of bulk storage lies in its ability to shift renewable energy to peak times, yielding savings in fossil fuels, and reducing volatility of electricity markets. With relatively small penetrations of renewables and lots of gas generation, the value in bulk storage is modest. However, should renewable penetrations increase to the point at which significant curtailment occurs, then the value of storage would increase hugely, and even at current costs could become a very attractive investment option. This method of network fuel minimisation should also be applicable to CO_2 emissions, given the CO_2 emission level per MWh of electricity generated for each type of generation.

Chapter 6

Advanced Adiabatic Compressed Air Energy Storage (AA-CAES)

This thesis has discussed using energy storage to manipulate the output from renewable energy converters (chapter 3) and looked at energy storage from an economic and systems perspective (chapters 4 and 5). As has been identified in chapter 2, while there are many promising current energy storage technologies available, with the exception of pumped hydro schemes (which require specific geography), these are all too expensive or too early on in developmental stages to be generally deployed. Hence this chapter investigates the potential for Advanced Adiabatic Compressed Air Energy Storage (AA-CAES) to provide useful energy storage. AA-CAES is a method of storing useful energy, allowing for energy generated at an earlier time to be used at a later time. This is particularly significant to renewable energy generation. It has been previously considered as a storage mechanism and its overall efficiency has been estimated as 75% (Bullough *et al.*, 2004), 72% (Grazzini and Milazzo, 2008) and 50% (Pickard *et al.*, 2009). However, there are at present no AA-CAES plants in existence, and the estimated efficiency is strongly dependent on the assumed values for the thermodynamic efficiencies of the constituent components. We undertake a sensitivity analysis in order to gain an understanding of the most crucial design elements of such a plant, and suggest that this type of storage plant offers efficiencies in the region of 64-67%. In this chapter it is found that efficiency depends very strongly on not only the polytropic compressor and turbine efficiencies, but also on heat exchanger effectiveness and pressure drop. Accordingly it is suggested that a viable design will be a trade-off between the efficiency gains accrued from more compressions and expansions against the pressure drops introduced by these stages. Over the timescale modelled (12 hours), the estimated losses from the Thermal Energy Stores (TES's) have much less of an impact than the other aforementioned parameters. If the heat of compression could be stored and returned to the air satisfactorily pre-expansion then this type of system has the potential to offer effective energy supply and demand matching without dependence on fossil fuels.

6.1 Introduction

Two commercial CAES plants have been in existence for more than 20 years; Huntorf, Germany (1978) and McIntosh, Alabama (1991) (Crotogino *et al.*, 2001; Nakhamkin and Chiruvolu, 2007). These plants are hybrid air-storage/gas-combustion plants, essentially using low-cost electricity to run the compressor in an open cycle gas turbine. A typical single cycle gas turbine (used as a peaking plant) is about 35-40% efficient, so uses 2.5-2.86 kWh of gas for each kWh of peak electricity produced, compared to the McIntosh CAES plant which uses 0.69 kWh of off-peak electricity and 1.17 kWh of gas to produce 1 kWh of peak electricity (B.I.N.E. Informationsdienst, 2007)). These plants successfully profit by using (low-cost) off-peak electricity to compress air, storing it and then discharging it when the price of electricity is higher. Some recent research has also suggested that conventional CAES working in conjunction with wind energy could provide affordable dispatchable energy generation (Greenblatt *et al.*, 2007; Cavallo, 2007), although Lund and Salgi (2009) suggest that other storage technologies may be better suited to this task in future energy systems due to high costs and conventional CAES's reliance on natural gas.

The AA-CAES concept is different from conventional CAES in that it functions without the combustion of natural gas and as such does not require the availability and storage of this fossil fuel. Fossil fuels have historically been regarded as storage and the vast majority of energy stores in the UK continue to be in this form (Wilson *et al.*, 2010). In AA-CAES, surplus energy is used to power compressors which drive air into a pressurised air store. The heat generated by the compression is stored in Thermal Energy Stores (TES's), and then used to reheat the air before it is expanded again. When there is a shortfall of electricity, the air is reheated and expanded through turbines driving generators. Although, to the best of the authors' knowledge, no AA-CAES plant has ever been built, it is often cited as a potential storage option in articles comparing energy storage technologies (Schoenung *et al.*, 1996; Ibrahim *et al.*, 2008; Schainker, 2004b), usually with an expected efficiency of 70-75% (Schoenung *et al.*, 1996; Ibrahim *et al.*, 2008).

There is some current interest in AA-CAES, with an EU based project called "Project ADELE" being undertaken by RWE Power, General Electric, Züblin and DLR, which again quotes the expected efficiency at 70% (RWE). Garrison and Webber (2011) describe recent research on a novel design for a CAES system which uses solar energy rather than natural gas for re-heating the compressed air before expansion, calculating an overall efficiency of 46% for the coupled solar-CAES system. Pimm *et al.* (2011) describes a novel approach in which bags of compressed air are stored in deep water, meaning that the pressure of the store will be the pressure at the depth of location, essentially giving isobaric storage. This approach is also being investigated by Cheung *et al.* (2012) in partnership with the company Hydrostor. Other companies (Lightsail Energy and SustainX smarter energy storage) are also investigating isothermal compressed air energy storage, but their technologies are yet to reach the market and

as a result details on the exact processes are scarce.

Several articles have also estimated the efficiency of AA-CAES, with ranging conclusions. Bullough *et al.* (2004) states an efficiency of approximately 75%, Grazzini and Milazzo (2008) model a 16,500 MJ (∼4.6 MWh) system and suggest an efficiency of 72%, while Pickard *et al.* (2009) concludes that, in practice, an efficiency of greater than 50% for a bulk storage AA-CAES facility (1 GWd) may be hard to achieve. This discrepancy is not easily explained, but seems at least in part to come from Pickard et al. modelling the cooling stages as isochoric rather than isobaric. We suggest that this is perhaps inappropriate, as heat exchangers are flow devices, and hence the isobaric heat capacity should be used in calculations. It should also be noted that the scale of the systems analysed are vastly different. Grazzini and Milazzo (2012) discuss the design criteria for an AA-CAES system, emphasizing the importance of using an appropriately designed heat exchanger (they size a shell and tube exchanger and calculate exchanger pressure drops between 200 — 15000 Pa).

This chapter aims to further inform the debate over what is achievable with AA-CAES. The sources of irreversibility in an AA-CAES system are explained and, unlike previous articles on the subject, the sensitivity of the model AA-CAES systems to these losses is explored. The background thermodynamics are presented and care is taken to account for the effect of the variable storage pressure when charging and discharging the store. The reasons for assessing small-scale AA-CAES as a storage mechanism is that there may be significant benefits of small-scale storage devices in distributed generation networks (Dell, 2001), to tidal current energy (Barbour and Bryden, 2011), and for applications in isolated island grids (Duić and da Graça Carvalho, 2004; Kaldellis, J and Zafirakis, 2007).

6.2 Background Thermodynamics

6.2.1 Compression and Expansion

Compressing a gas increases the kinetic energy of the individual gas molecules which results in an increase in the temperature of the gas. The problem facing AA-CAES is that in order to obtain any reasonable round trip efficiency the temperature of the gas during the expansion must be raised to temperatures close to that which it achieved in the compression. There are three fundamental types of compression which, using the ideal gas model may be described by;

$$pV^k = constant \tag{6.1}$$

These are; ***Isothermal Compression***, which occurs at a constant temperature and has $k = 1$; ***Adiabatic Compression***, which occurs when there is no net exchange of thermal energy with the ambient environment and has $k = \gamma = c_p/c_v$ ($= 1.4$ for air); and ***Polytropic Compression***,

which corrects the index so that there may be some heat transfer and some of the work applied can appear as temperature rise above adiabatic conditions as well as increased pressure.

Using the ideal gas law ($PV = n\bar{R}T$) to rearrange Equation 6.1 in terms of temperature and pressure rather than volume and pressure, and adding in the polytropic compression efficiency, the temperature of the gas after the pressure has been increased from p_i to p_f is given by;

$$T_f = T_i \left(\frac{p_f}{p_i} \right)^{\frac{k-1}{\eta_{pol} k}} \tag{6.2}$$

Reversible isothermal compression and expansion would provide the ideal case for a compressed air energy storage system as heat could theoretically be exchanged with the surroundings at ambient temperature. Hence a separate thermal energy store would not be required. However, although there is significant current research into isothermal compression for CAES (by companies like Lightsail and SustainX), it is not yet commercially available and any compression that approaches purely isothermal compression is, at present, too slow for industrial use (Grazzini and Milazzo, 2008; Pickard *et al.*, 2009) due to the impractically small temperature differences required.

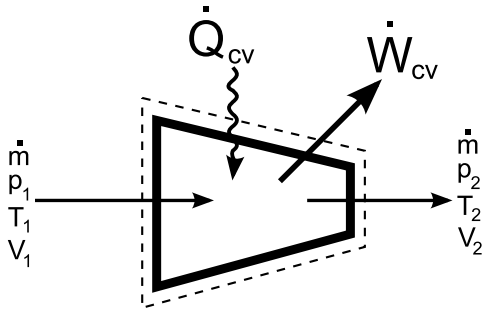

Figure 6.1: A control volume enclosing a compressor.

Consider a control volume enclosing a compressor, as shown in Figure 6.1. The energy balance can be described by;

$$\frac{dE_{cv}}{dt} = \dot{Q}_{cv} - \dot{W}_{cv} + \dot{m}(\bar{u}_1 + p_1\bar{v}_1 + KE_1 + PE_1) - \dot{m}(\bar{u}_2 + p_2\bar{v}_2 + KE_2 + PE_2) \tag{6.3}$$

where $\dot{W}_{cv}$ is the work flow rate out of the control volume, $\dot{Q}_{cv}$ is the rate of heat input, $\bar{u}_1$ is the specific internal energy of the gas at the inlet ($\bar{u}_2$ at the exit), p and $\bar{v}$ represent the pressure and specific volume of the states, $\dot{m}$ is the mass flow rate, KE_1 is the kinetic energy at the inlet and PE_1 is the potential energy at the inlet.

Assuming there is no net gain or loss of energy within the control volume, and neglecting the changes in potential energy and kinetic energy between the inlet and the outlet this reduces to

$$\frac{\dot{W}_{cv}}{\dot{m}} - \frac{\dot{Q}_{cv}}{\dot{m}} = h_1 - h_2 \tag{6.4}$$

In Equation 6.4, h is the specific enthalpy of the gas, and is equal to the sum of u and pv. If the compressor is well insulated then the compression can be considered adiabatic, and the heat term can also be neglected. In this case the work input (to the control volume) required is equal to the difference between the enthalpy of the gas at the inlet and the exit of the compressor. Noting that $dh = Tds + vdp$, then the work available along an infinitesimal fraction of an isentropic path (constant entropy, $ds = 0$) is $dW = Vdp$. Integrating this along an isentropic adiabatic path (for which $pV^k = constant$) we find the work available per unit mass between the inlet and the outlet of the compressor can be expressed using;

$$\frac{\dot{W}_{cv}}{\dot{m}} = c_p T_i \left[\left(\frac{p_f}{p_i} \right)^{\frac{\gamma-1}{\gamma}} - 1 \right] \tag{6.5}$$

where γ is the ratio of specific heats ($= \frac{c_p}{c_v}$).

Equation 6.5 can be modified to account for inefficiencies in the compressor by using either the isentropic or polytropic efficiency. We opt for the polytropic (or infinitesimal stage) efficiency, as it doesn't depend on the compression ratio, and thus allows for a more consistent comparison between different compressions, whereas the isentropic efficiency is dependent on compression ratio. For example, consider 2 compressions in series with compression ratio 4 (to get to a state with final pressure ratio 16), each with isentropic efficiency 90%. With no inter-cooling the total work required for both these compressions is the equivalent of that required for a single compression with an isentropic efficiency of 88%. Hence we use the following expressions to calculate the work required to compress a flow of air from an initial pressure p_i to a final pressure p_f and the work available from an expansion of a flow of air from an initial pressure p_i to a final pressure p_f.

For a compression:

$$\frac{\dot{W}_{cv}}{\dot{m}} = c_p T_i \left[\left(\frac{p_f}{p_i} \right)^{\frac{\gamma-1}{\eta_{pol}\gamma}} - 1 \right] \tag{6.6}$$

And for an expansion:

$$\frac{\dot{W}_{cv}}{\dot{m}} = c_p T_i \left[\left(\frac{p_f}{p_i} \right)^{\frac{\eta_{pol}(\gamma-1)}{\gamma}} - 1 \right] \tag{6.7}$$

However, unless the storage pressure can be kept constant (isobaric storage), the states described in the Equations 6.6 and 6.7 will be constantly changing. This is because each increment

of air, δm, passing through the system will only have to be compressed to just above the store pressure for air to flow into the compressed air store. Therefore, during the compression phase, the final pressure p_f will be constantly increasing as the pressure in the storage vessel increases from the ambient pressure p_0 to the maximum pressure $p_{s,max}$, and during the expansion phase the initial pressure p_i will be constantly changing as the pressure inside the storage vessel decreases from the maximum storage pressure back down to the ambient pressure.

In order to obtain the work required to compress a volume of gas from an initial pressure p_i to an increasing final pressure p_f (with a maximum value $p_{f,max}$), which depends on the mass (or number of moles) contained within the storage volume V_s, Equation 6.6 can be integrated to obtain (the details of the integration can be found in Appendix B):

$$W = \frac{p_{f,max} V_s c_p}{R} \left[\frac{p_i}{p_{f,max}} - 1 + \frac{\eta_{pol,c}\gamma}{\gamma - 1 + \eta_{pol,c}\gamma} \left(\frac{p_{f,max}}{p_i} \right)^{\frac{\gamma-1}{\eta_{pol,c}\gamma}} - \frac{\eta_{pol,c}\gamma}{\gamma - 1 + \eta_{pol,c}\gamma} \left(\frac{p_i}{p_{f,max}} \right) \right] \tag{6.8}$$

where $p_{f,max}$ is the maximum pressure in the storage volume. Similarly the expression for the work available upon expanding the air from an ever-decreasing initial pressure p_i (which depends on the amount of gas contained within the store), with a maximum value $p_{i,max}$ to a constant final pressure p_f is given by:

$$W = \frac{p_{i,max} V_s c_p}{R} \left[\frac{p_f}{p_{i,max}} - 1 + \frac{\gamma}{\eta_{pol,t}(\gamma - 1) - \gamma} \left(\frac{p_f}{p_{i,max}} \right) - \frac{\gamma}{\eta_{pol,t}(\gamma - 1) - \gamma} \left(\frac{p_f}{p_{i,max}} \right)^{\frac{\eta_{pol,t}(\gamma-1)}{\gamma}} \right] \tag{6.9}$$

which is acquired by integrating Equation 6.7.

6.2.2 Heat Exchanging

In order to avoid very high air temperatures the compression is staged, with inter-cooling between each compression and after-cooling before the air enters the store. In the present analysis, the heat exchanging phases are modelled as ***isobaric*** — that is except for frictional and turbulent losses, air pressure is constant as it passes through a heat exchanger — so a cooling stage will result in a reduction in volumetric flowrate and a heating stage will result in an increase.

A counterflow arrangement is the best heat exchanger configuration to bring the cold fluid as

close as possible to the inlet temperature of the hot fluid, as heat can only flow from hot to cold. Heat capacity flow rates should also be equal in order to ensure that the exit temperature of one fluid is as close as possible to the inlet temperature of the other. The heat transfer rate $\dot{Q}$ provided by an exchanger of effectiveness ε is described by (neglecting any heat losses to the environment):

$$\dot{Q} = \varepsilon \dot{C}_{min} \Delta T_{max} = \varepsilon \dot{C}_{min} (T_{h,i} - T_{c,i}) \tag{6.10}$$

Effectiveness ε is the ratio of the actual heat transfer to the theoretical maximum, and is thus a measure of heat exchanger performance (the second law of thermodynamics is implicitly involved in the definition as it determines the theoretical maximum heat transfer). $\dot{C}_{min}$ is the minimum heat capacity flow rate, given by the *mass flow rate* $\times$ *the heat capacity of the fluid.* As the heat capacity flow rates are equal $\dot{C}_{min} = \dot{C}_{max} = \dot{C}_h = c_h(dm/dt)_h = \dot{C}_c = c_c(dm/dt)_c$.

Using conservation of energy arguments, the outlet temperature of the hot and cold fluids ($T_{h,o}$ and $T_{c,o}$) can be calculated using:

$$\dot{Q} = \dot{C}_h (T_{h,i} - T_{h,o}) = -\dot{C}_c (T_{c,i} - T_{c,o}) \tag{6.11}$$

6.3 The AA-CAES system

The AA-CAES system usually cited in reports on energy storage has a design similar to that shown in Figure 6.2, although the number of compression and expansion stages and the physical form of the air store may vary. To minimise the work required to reach a given storage pressure, each compression stage usually has an equal pressure ratio (Lewins, 2003). Similarly the expansion is usually staged (with the same number of stages as the compression) with pre-heating before the first expansion and inter-heating before each subsequent expansion. This reduces the range of pressures that each turbine encounters as the storage pressure reduces from the maximum to the ambient. The number of expansion stages is the same as the number of compression stages to theoretically allow all the heat of compression to be returned without the addition of extra work (or a violation of the 2^{nd} law of thermodynamics). To illustrate this, consider a three stage compression with three cooling stages during the compression (two inter and one after). During each stage, one third of the total heat of compression is removed. Now consider that there are only two reheat stages during each of which half the total heat of compression is returned. The maximum temperature of the TES will be the maximum temperature of the air during the compression. Returning half the total heat in a single stage would necessarily imply heating the air to a temperature higher than that of the TES- thus violating the 2^{nd} law or requiring the addition of extra work (as is the case in existing CAES plants).

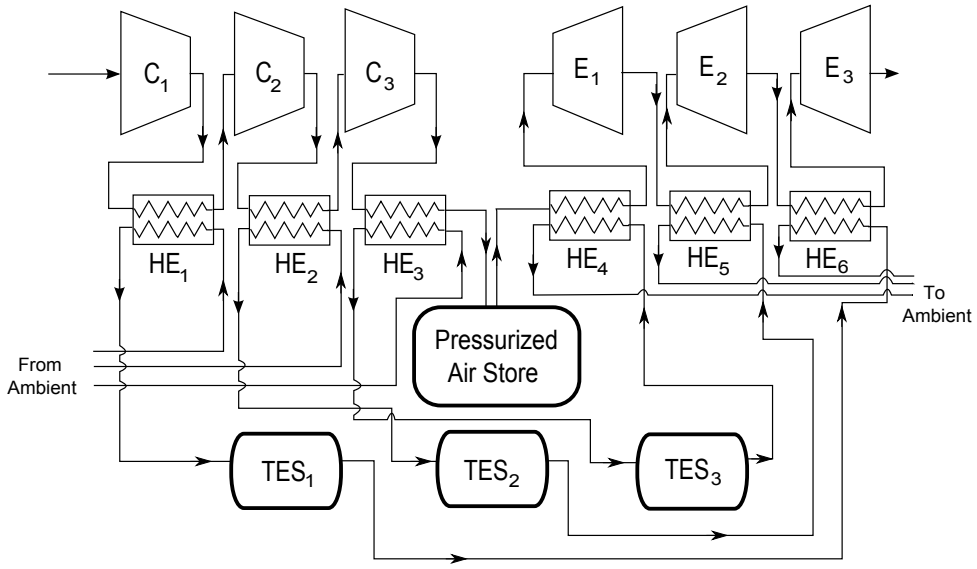

Figure 6.2: The standard AA-CAES system. $C_{1\text{-}3}$ represent the compressor units, $E_{1\text{-}3}$ the expanders and $HE_{1\text{-}6}$ the heat exchangers.

While the system in Figure 6.2 aims for isothermal compressed air storage, it is dubbed as "Advanced-Adiabatic" as the compressions are close to adiabatic, and in the ideal (lossless) case the whole system would be adiabatic- keeping heat from escaping to the ambient environment.

6.3.1 Sources of Irreversibility

The individual efficiencies of the real individual components in the AA-CAES system shown in Figure 2 is not 100% and will degradate the overall system performance; however the combined effect is not a straightforward multiplication. The losses in each of the components and their effects are discussed below:

1. A reduction in polytropic turbine efficiency ($\eta_{pol,t}$) decreases the work extracted between two pressures, as expected. Some of this loss manifests itself as a temperature rise of the exhaust air, so any subsequent expansion will start at a higher temperature.
2. The effect of the polytropic compressor efficiency ($\eta_{pol,c}$) is as follows: On the one-hand it increases the amount of work that needs to be done to compress the air by a given compression ratio. However, this extra work appears as increased air temperature, so the subsequent inter-cooling heat exchanger stores more heat for the same effectiveness.
3. There will be a loss of exergy associated with exhaust air exiting the system above or below the ambient temperature.
4. The heat exchanger effectiveness also simply reduces the amount of heat that can be extracted and returned to the air during the inter-cooling/heating stages. But it is only the

heat that cannot be returned in the inter-heating stages that is immediately lost. The heat that isn't extracted during inter-cooling remains with the air, and appears as a temperature rise in the stored air. This will have its own associated loss rate. Lower heat exchanger effectiveness will also result in a higher temperature in subsequent compression stages, and will increase the temperature of the subsequent TES's, increasing their loss rates.

5. As a result of the third observation, there is a TES for each compression stage in Figure 6.2. This is desirable because if the heat exchanger effectiveness isn't unity, then these different thermal stores will be at different temperatures, and combining them into one would result in extra entropy generation.
6. Each TES will suffer thermal losses depending on the degree of insulation and there will also be losses due to the loss of stratification. This is because air flowing through the compressor before the store will only be compressed to (just above) the storage pressure. Thus, as the storage pressure increases, the air exiting the compressor will be at an ever higher temperature, and thus so will the thermal fluid exiting the subsequent heat exchanger. Mixing of this fluid will result in a loss of exergy.
7. Frictional and turbulent losses associated with fluid flow through pipes and heat exchangers will result in lower pressures than would be otherwise expected at the outlets of the exchangers. Although pressure drops through the heat exchangers are under the designers control to some extent (by decreasing the fluid velocities lower losses can be achieved, with a larger exchanger area for the given effectiveness) they cannot be removed completely and designing for very small pressure drops could lead to very costly exchangers.
8. Any heat loss from the compressed air store will reduce the energy available during the expansion of the air, and could limit the post expansion pressure if the result was an unacceptably low final temperature.
9. Any leakages of coolant or working fluid in the system will result in losses.

6.4 Modelling AA-CAES

In order to ascertain the effect of the various losses on the overall system performance, three numerical models of a 2MWh 500kW AA-CAES system are constructed, one with 3 compression and expansion stages (as the design in Bullough *et al.* (2004))), one with 4 and the other with 5 (as suggested in Grazzini and Milazzo (2008)). Each has a storage volume which is initially at some minimum storage pressure and temperature (assumed 290K). To charge, air is driven into the store by the compressors, and the pressure in the store increases from some minimum to some maximum value. To discharge, air is extracted through a series of turbines, and the pressure in the store reduces back down to the minimum pressure. It is assumed that the air store maintains a constant temperature; it is well thermally connected to the ambient environment. Requirements for this to be the case are discussed in the results section. This

avoids cooling in the store leading to a reduction in the extractable air. Estimations are made for compressor/turbine polytropic efficiencies, heat exchanger effectiveness, thermal losses from the TES's and pressure drops in the heat exchangers. Then firstly, how the efficiency, the physical size of the store and the temperatures encountered vary with the maximum storage pressure is studied, and secondly the effect of varying each of these parameters on the overall system efficiency is analysed for each of the models.

As the compression is staged, not all the air must pass through every compressor. If reaching the final storage pressure requires multiple compression stages in series, then until the pressure in the store reaches the pressure at the end of the first stage, $p_{c,int,1}$ (the outlet pressure of the heat exchanger after the first compression), air must only pass through the first compressor and heat exchanger. After this, it must pass through the subsequent compressor and heat exchanger until the store pressure reaches the pressure at the end of the second stage, $p_{c,int,2}$. To minimise the pressure ratio encountered by each compressor and the temperatures achieved, $p_{c,int,1} = (\frac{p_{s,max}}{p_0})^{1/3}$ and $p_{c,int,2} = (\frac{p_{s,max}}{p_0})^{2/3}$. In this way, all the air added to the store must pass through the low pressure compression stage, but less will have to pass through each subsequent compression stage. This is illustrated for the 3-stage system in Table 6.1. In this table, T is the temperature of the air store and R is the specific gas constant.

Table 6.1: Compression for 3 stage AA-CAES system.

Compressor	Pressure at the end of each compression stage	Mass passing through each compression stage
Low pressure	$p_{c,int,1}$	$m_{s,max} - m_0$
Med. pressure	$p_{c,int,2}$	$m_{s,max} - \frac{p_{c,int,1}V_s}{RT}$
High pressure	$p_{s,max}$	$m_{s,max} - \frac{p_{c,int,2}V_s}{RT}$

The expansion phase is split in a similar manner. Before each expansion the air is heated in a heat exchanger using the heat extracted during the compression (stored in the thermal fluid). The high pressure expander works from the pressure $(p_s - p_{loss})$ down to some intermediate pressure $p_{e,int,1}$. Here p_s is the pressure in the store, which is reduced by the pressure drop associated with the heat exchanger before the first expansion. While the store pressure, p_s, is above $(p_{e,int,1} + p_{loss})$, air passes through all of the expanders. Table 6.2 illustrates how much air passes through each expander for the 3-stage system. The actual values of the intermediate pressures are the same as those used in the compression $(p_{e,int,1} = p_{c,int,2})$ to mimic the ideal lossless system, however there may be some small scope for optimisation by introducing slight variations. Figure 6.3 shows how the pressure through the components of the 3-stage system varies with the storage pressure during the expansion process. The positions of the intermediate pressures are marked.

The models have been constructed in MATLAB and adopt a numerical integration style ap-

Table 6.2: Expansion for 3 stage AA-CAES system.

Expander	Store pressure at the end of each expansion stage	Mass passing through each stage
High pressure	$p_{e,int,1} + p_{loss}$	$m_{s,max} - \frac{(p_{e,int,1}+p_{loss})V_s}{RT}$
Med. pressure	$p_{e,int,2} + p_{loss}$	$m_{s,max} - \frac{(p_{e,int,2}+p_{loss})V_s}{RT}$
Low pressure	$p_0 + p_{loss}$	$m_{s,max} - m_0 - \frac{p_{loss}V_s}{RT}$

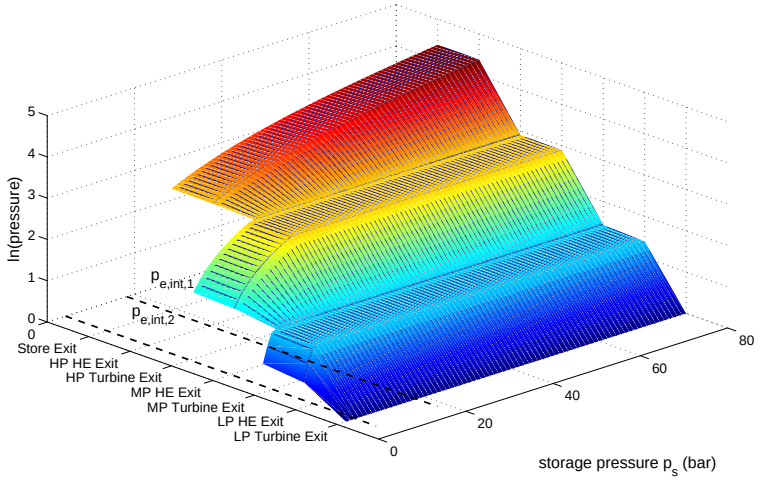

Figure 6.3: Illustrating how the pressure in the 3-stage AA-CAES system is expected to vary through the expansion phase. The dotted lines mark the position of the intermediate pressures. It can be seen from the figure that when store pressure is below $p_{e,int,1}$, air only flows through the Medium and Low Pressure stages.

proach. The model considers a finite increment of air, Δm, which is passed through the compression train and compressed from the ambient pressure to a pressure $\bar{p_f}$. The work required to compress this amount of air, Δm, depends on how many compressions it must undergo, with the work through the last compressor given by:

$$W = \Delta m c_p T_i \left[\left(\frac{\bar{p_f} + p_{loss}}{p_i} \right)^{\frac{\gamma-1}{\eta_{pol,c}\gamma}} - 1 \right] \tag{6.12}$$

Here, p_i and T_i are the respective inlet pressure and temperature of the last compression, p_{loss} is the pressure loss through the last heat exchanger and $\bar{p_f}$ is defined as,

$$\bar{p_f} = \frac{p_s(m) + p_s(m+\Delta m)}{2} \tag{6.13}$$

where p_s is the store pressure and is a function of the mass of air contained within the store.

If Δm passes through more than one compression, then the work required for any previous compressions is given by Equation 6.6.

Similarly during the expansion process an amount of air, Δm, is expanded from the store pressure to the ambient pressure. The work available depends on the number of expansions undergone; with the work available from the first expansion given by:

$$W = \Delta m \times mc_p T_i \left[\left(\frac{p_f}{\bar{p}_i - p_{loss}} \right)^{\frac{\eta_{pol,t}(\gamma-1)}{\gamma}} - 1 \right] \tag{6.14}$$

Now, T_i is temperature before the expansion, p_f is the pressure after the expansion, p_{loss} is the pressure loss through the previous heat exchanger and $\bar{p}_i$ is defined as:

$$\bar{p}_i = \frac{p_s(m) - p_s(m - \Delta m)}{2} \tag{6.15}$$

The work available from any subsequent expansions is given by Equation 6.7. The model results are supported by noting that the work calculated iteratively by Equations 6.12 and 6.14 tends towards the results given by Equations 6.8 and 6.9 as Δm tends towards zero.

6.4.1 Losses

To set up the initial models, the polytropic efficiencies of the turbine and compressor are assumed at 85%, while each heat exchanger is assigned an effectiveness of 90%. The turbines at the McIntosh CAES have isentropic efficiencies of 87.4-89.1% (Garrison and Webber, 2011), which given that the plant has 4 stages, and a high pressure between 60 and 80 bar, suggests a polytropic efficiency of ~86%.

There are several types of heat exchanger which could be used, offering ranging effectiveness and pressure drop. The most common heat exchangers are shell and tube exchangers, however to obtain a high thermal performance it is likely that a shell and tube exchanger will be very large. Plate heat exchangers offer better thermal performance for smaller size, and Packinox plate, brazed plate-fin and diffusion bonded plate-fin all have high enough pressure tolerances (see table 10.1 of Shah and Sekulic (2007)). Printed Circuit type Heat Exchangers (PCHE's) may also be appropriate and these are frequently used as compressor after-coolers in the oil and gas industry. They have high pressure tolerance and very high effectiveness, while being much more compact than a shell and tube exchanger of equivalent effectiveness (Shah and Sekulic, 2007). However due to their small hydraulic diameters fouling may become an issue without filtration, which would itself cause a significant pressure drop. Heatric manufacture PCHE units ranging from 6 kg to 60 tonnes with effectiveness in excess of 95%. It may also be that a direct-contact heat exchanger system offers a better thermal performance — i.e. a packed

bed of gravel — as these systems generally have very high heat transfer rates, good pressure tolerances and are often inexpensive.

In this analysis to gain a first estimate of the associated heat exchanger pressure drops a hypothetical shell and tube heat exchanger is sized with an effectiveness of 90% and the pressure drop estimated. The methods for estimating the thermal losses from the TES's and pressure losses in the heat exchangers are outlined in the following sections.

The Thermal Losses

An estimation of these is formulated as follows: It is assumed that each TES is at a uniform temperature T_{TES} (the fluid in the TES's is well mixed and any stratification is lost) and wholly contained within an insulated cylinder of inner radius r_i and outer radius r_o ($r_o - r_i$ is the insulation thickness). Applying Fourier's heat law allows the thermal resistance to be calculated, as shown in Equation 6.16, where L is the cylinder length and λ is the thermal conductivity of the insulation material. The derivation for the thermal resistance of a cylinder is shown in Appendix C.

$$R_{th} = \frac{ln\left(\frac{r_o}{r_i}\right)}{2\pi L\lambda} \tag{6.16}$$

The thermal resistance of the cylinder ends are also approximated. The total thermal power loss is the sum of the losses through the cylinder walls and the cylinder ends. A thermal conductivity of 0.25 $\mathrm{Wm^{-1}K^{-1}}$ is assumed, as insulation materials with this thermal conductivity are easily available (fibreglass typically has a thermal conductivity of about 0.05 $\mathrm{Wm^{-1}K^{-1}}$), and the insulation layer around the TES is assigned a thickness of 0.3 m. The amount of thermal fluid required can be estimated by the *mass flow rate of the thermal fluid* $\times$ *the total charging time*. The mass flow rate of the thermal fluid can be calculated as its heat capacity flow rate should match the heat capacity flow rate of the air (Equation 6.10). This will depend on the exact configuration (i.e. the number of stages and the final storage pressure) of the AA-CAES system. Given the volume of the thermal fluid, its temperature, and the time over which the thermal fluid is stored, a temperature drop is estimated. The dimensions of the TES can then be adjusted (for constant volume) to minimise this loss.

Using the 3-stage 2MWh AA-CAES system with a maximum storage pressure of 80 bar and assuming a thermal fluid heat capacity of 2.5 $\mathrm{kJkg^{-1}K^{-1}}$ requires a mass of $\sim$9 tonnes of thermal fluid at a maximum temperature of 480 K. This can be contained within a cylinder of length 3 m and radius of 1 m. A storage time of 12 hours yields a temperature drop of $\sim$8 K. The thermal fluid is based on Duratherm 600 which has a boiling point in excess of 570 K and a heat capacity of $\sim$2.5 $\mathrm{kJkg^{-1}K^{-1}}$ in the temperature range encountered (Duratherm heat transfer fluids).

This is the temperature drop assumed in the all the base models and should be conservative for the 4-stage and 5-stage systems, as their thermal stores will be at lower temperatures, and therefore will suffer from lower thermal loss rates.

It should also be noted that under the assumption that the store maintains a constant temperature throughout the entire storage cycle, any heat stored above the ambient temperature in the air entering the pressurised store is lost to the surroundings.

The Pressure Losses

The major contribution to the system pressure losses will be the frictional loss in the core of the heat exchangers, and there will also be smaller contributions from heat exchanger entrance and exit effects and friction losses through pipes. These are estimated for a hypothetical shell and tube exchanger with an effectiveness of 90%.

Using the ε-NTU method (Shah and Sekulic, 2007) of defining heat exchanger performance, the required transfer area on the air-side of the exchanger can be calculated, which combined with estimates for the width, height, free-flow to frontal area ratio and hydraulic diameter can be used to estimate the exchanger pressure drop (for a rigorous description of the ε-NTU method see Chapter 3 of Shah and Sekulic (2007)). This process can be iterated in order to achieve the desired effectiveness and pressure drop. The required transfer area on the air-side of the exchanger can be calculated using Equation 6.17, in which $\hat{h}$ is the heat transfer coefficient and NTU is a property known as the Number of Transfer Units, which is directly related to the exchanger effectiveness as shown in Equation 6.17 (for a counter-flow exchanger with heat capacity flow rate ratio $C^* = 1$).

$$NTU = \frac{\hat{h}A}{C_{min}} = \frac{\varepsilon}{1-\varepsilon} \tag{6.17}$$

The heat transfer coefficient, $\hat{h}$, will depend on the Prandtl number (Equation 6.18) and the Reynolds number (Equation 6.19), which will in turn depend on the exact geometry of the heat exchanger, thus calculating the required transfer area requires some assumed geometry and is itself an iterative procedure.

$$Pr = \frac{c_p \mu}{\lambda} \tag{6.18}$$

$$Re = \frac{GD_h}{\mu} \tag{6.19}$$

In Equation 6.19 G is the core mass velocity, which is the air mass flow rate per unit area of the minimum cross sectional exchanger area, D_h is the hydraulic diameter and μ is the

dynamic viscosity of air. Exactly how the heat transfer coefficient depends on Reynolds number and Prandtl number depends on the specific hydraulic regime, but for cooling in the regime $2500 < Re < 1.24 \times 10^5$ and $0.7 < Pr < 120$ the Dittus-Boelter correlation is likely to provide a good approximation. This relates the Reynolds and Prandtl numbers to the Nusselt number (the ratio of convective to conductive heat transfer rates) and is given by Equation 6.20 (see Chapter 7 of Shah and Sekulic (2007) for discussion on the working range), as taken from Shah and Sekulic (2007).

$$Nu = 0.026 Re^{0.8} Pr^{0.3} \tag{6.20}$$

Equation 6.21 shows how the Nusselt number is related to the heat transfer coefficient $\hat{h}$. Here λ is the thermal conductivity of air.

$$Nu = \frac{\hat{h} D_h}{\lambda} \tag{6.21}$$

In this way it is found that an effectiveness of 90% could be achieved with a shell and tube exchanger with $\frac{1}{2}$ inch tubes (hydraulic diameter of ~13 mm), 0.5 m height, 0.5 m width and 6.6 m length. It is also worth noting that $NTU = 9$ for this exchanger, which is typical for a regenerator used in an industrial gas turbine engine. For the 3-stage system this corresponds to a Log Mean Temperature Difference (LMTD) of ~18 K and for the 5-stage system this corresponds to a LMTD of ~10 K (the LMTD is lower in the 5-stage system as the exchanger inlet temperatures are much lower).

Equation 6.22 can then be used to estimate the airside pressure drop of this heat exchanger. As pressure drop is proportional to G^2 (the square of the core mass velocity), the pressure drops are calculated for the 5-stage system, as for the same final storage pressure the 5-stage system requires a larger mass of air, and thus a larger mass flow rate, to store the same amount of work as the 4-stage or 3-stage systems (less compression work is required to reach the same final pressure with more stages). The pressure drops in the 4-stage systems will be lower than those in the 5-stage system and lowest in the 3-stage system.

$$\frac{\Delta p}{p_i} = \frac{G^2}{2\rho_i p_i}\left[1 - \sigma^2 + K_c + 2\left(\frac{\rho_i}{\rho_o} - 1\right) + \frac{4fL\rho_i}{D_h}\left(\frac{1}{\rho}\right)_m - (1 - \sigma^2 + K_e)\frac{\rho_i}{\rho_o}\right] \tag{6.22}$$

In Equation 6.22, σ is the free-flow to frontal area ratio, and K_c and K_e are the contraction and expansion loss coefficients, which are empirically estimated depending on the Reynolds number and σ. Their dependence on Reynolds number is illustrated graphically on page 386

of Shah and Sekulic (2007). f is the Fanning friction factor which can be estimated using the Moody chart, and depends on the Reynolds number and relative pipe roughness. A typical Moody chart is shown in Figure 6.4. Upon inspection of the Moody chart we see that the Darcy-Weisbach friction factor should be around 0.05, given that a steel pipe of diameter $\frac{1}{2}$ inch would have a relative roughness of approximately 0.01. This corresponds to a Fanning friction factor of 0.0125. For conservative estimates the models use a Fanning friction factor of 0.025.

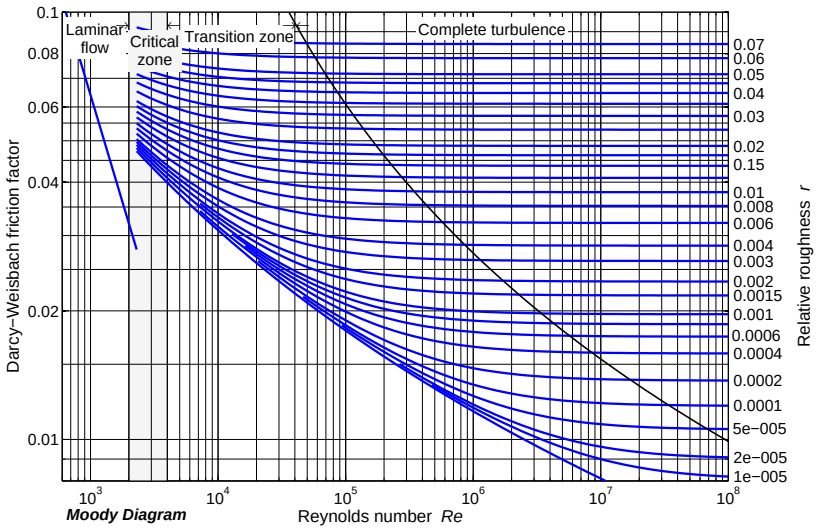

Figure 6.4: The Moody diagram for estimating friction factors in pipes, generated in MATLAB using code adapted from Metzger & Willard. NOTE the friction factor shown is the Darcy-Weisbach friction factor which is 4× the Fanning friction factor.

Table 6.3 shows the estimated area requirement and associated pressure drop for the hypothetical shell and tube heat exchanger.

Table 6.3: Properties of the hypothetical shell and tube heat exchanger.

Exchanger	Flow *Re*	Surface area	Transfer Area to Vol. ratio	Pressure drop
Shell and Tube	14700	158 m^2	95 m^2/m^3	11.8 kPa

Given that the losses associated with pipe friction, bends and valves have been neglected, the pressure loss introduced by each exchanger is rounded up to 0.2 bar (=20 kPa). This also seems reasonable considering the pressure losses at the McIntosh CAES plant; with a maximum storage pressure of 80 bar the loss of 0.2 bar introduces an overall pressure loss of 5.8% for a 3-stage compression, 9.6% for a 4-stage compression and 13.5% for a 5-stage compression. The McIntosh CAES plant (which has four compression stages) heat exchanger pressure losses are 12.7% and the maximum storage pressure at the existing McIntosh CAES facility is 79.3 bar (Nakhamkin *et al.*, 1992).

Summary of the Losses

Table 6.4 summarises the loss parameters used to set up the initial models.

Table 6.4: Loss parameter assumptions in the base models.

Parameter	Value	Unit
Polytropic turbine efficiency	85	%
Polytropic compressor efficiency	85	%
Heat exchanger effectiveness	90	%
TES temperature drop	8	K
Pressure drop through each exchanger	0.2	bar

6.5 Results

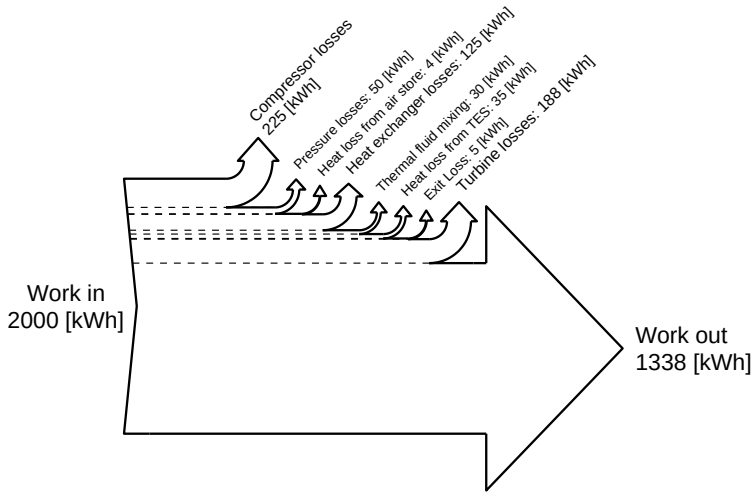

Figure 6.5: An availability diagram showing how the input energy is distributed for the 3-stage AA-CAES system throughout the storage process. The exit loss represents the loss of energy because air doesn't necessarily exit the system at the ambient temperature. Heat exchanger losses include exergy carried out in coolant.

Using the parameters outlined in Table 6.4, the efficiency of the simulated 3-stage system is 66.9%, the efficiency of the 4-stage system is 65.7% and the efficiency of the 5-stage system is 64.3%. To help visualise the results, Figure 6.5 shows an availability/exergy diagram illustrating how the losses for the 3-stage system are distributed. The heat loss during the compression represents the heat that is lost from the pressurised air store. The pressurised air store has a volume of 166.3 m^2.

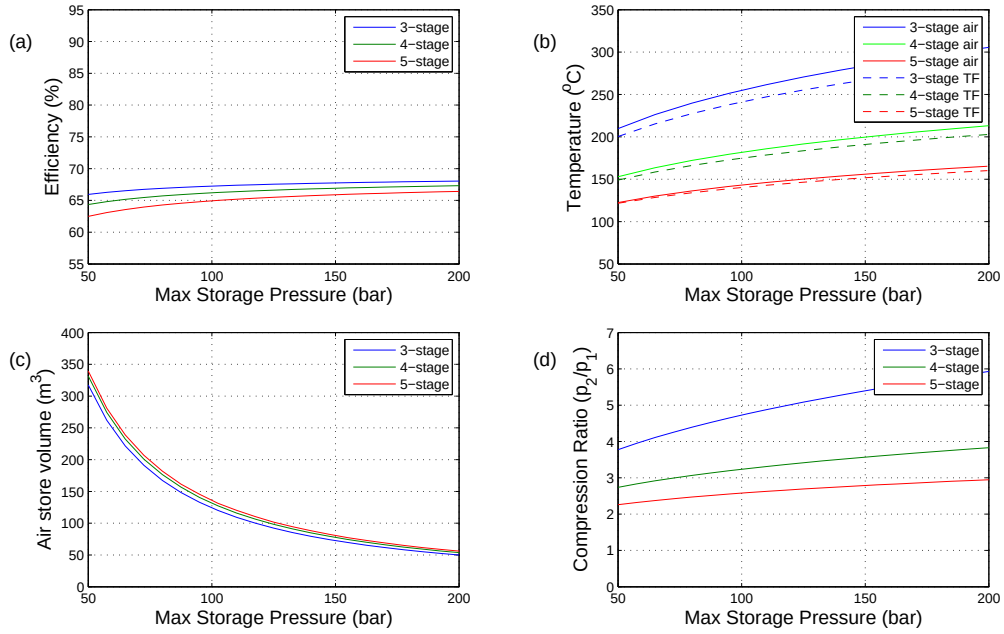

Figure 6.6: Graphs of (a) efficiency against pressure, (b) maximum air and thermal fluid temperatures against pressure, (c) required storage volume against pressure for 2000kWh of storage and (d) compression ratios against pressure for the 3-stage, 4-stage and 5-stage AA-CAES models

For the 3-stage system, there is 2 MWh of work input during the compression phase, leading to 1.94 MWh of thermal energy stored in the thermal fluid [1]. Of this, 1.44MWh is returned during the expansion, generating a useful work output of 1.34 MWh.

During the charge a total of 60 kWh of heat enters the air store above the ambient temperature. In order to maximise the mass of air that can be added during the charge and prevent excessive cooling in the air store during discharge, we aim to keep the store at the ambient temperature. Therefore during charging it should lose heat at a rate of 15kW. If the air store is a sphere of radius 3.42 m, a heat transfer coefficient around of 20 $\mathrm{Wm^{-2}K^{-1}}$ would be required which is probably higher than typical free convection values for air. However, by choosing a store geometry with a higher surface to volume ratio, this heat loss rate should be easily achievable, i.e. using 10 interconnected cylinders with radius 1 m and length 5.35 m would give a surface area nearly 3 times that of the sphere of equivalent volume, and thus the heat transfer coefficient required would be closer to 7 $\mathrm{Wm^{-2}K^{-1}}$ which would be readily achievable via free convection.

1. This is slightly counterintuitive as there is also potential energy stored in the cool compressed air. It is explained as the charging process is analogous to a heat pump, with coefficient of performance greater than 1. Only by the recombination of all the heat with the cool compressed air, and using perfectly reversible compressors and expanders, could all the compression work be returned on expansion

6.5.1 Effect of maximum storage pressure

Figure 6.6a shows how the efficiency of a 2 MWh AA-CAES plant varies as the maximum storage pressure is increased for systems with three, four and five compression and expansion stages. Figure 6.6b shows the maximum air and coolant temperatures for each of the systems while Figure 6.6c shows how the volume of the air store varies with the maximum pressure. Figure 6.6d shows the compression ratio (p_2/p_1) necessary to achieve the final storage pressure.

These results illustrate the importance of the maximum storage pressure for an AA-CAES plant. While Figure 6.6a seems to suggest that higher pressure leads to higher efficiencies, this result should be carefully interpreted as losses have been assumed to be independent of the maximum storage pressure. This is unlikely to be true as higher pressures lead to higher temperatures, and as shown in Figure 6.6b the maximum thermal fluid and air temperatures increase very rapidly with the maximum storage pressure. This will create larger temperature gradients to drive thermal losses and will also place higher thermal stress on the system, which could affect its longevity. Higher compression ratios also increase the range of compression ratios encountered by the compressors and turbines. Figure 6.6c shows the how the storage volume required to store 2 MWh of work decreases with the maximum pressure.

The maximum temperature of the working fluid passing through the heat exchangers and the maximum temperature of the thermal fluid are also important parameters in the design of an AA-CAES system, as these will determine what thermal fluid can be used, impacting on system cost. The advantage of more stages is clear here as having more stages reduces system temperatures.

6.5.2 Effect of minimum storage pressure

There are two main effects of increasing the minimum storage pressure (i.e. the initial pressure in the store at the beginning of the charging process). Firstly, the store volume must be increased in order to hold the same amount of potential energy, and secondly, there is less variation between the compressors (and turbines) minimum and maximum compression ratio. This means that the system efficiency is marginally increased with a higher minimum pressure, as there is less variation in the exit temperatures of the compressors and thus less mixing of the thermal fluid at different temperatures. Figure 6.7 shows the store volume required when the maximum pressure is 80 bar and the minimum is varied from ambient (assumed 1 bar) to 40 bar.

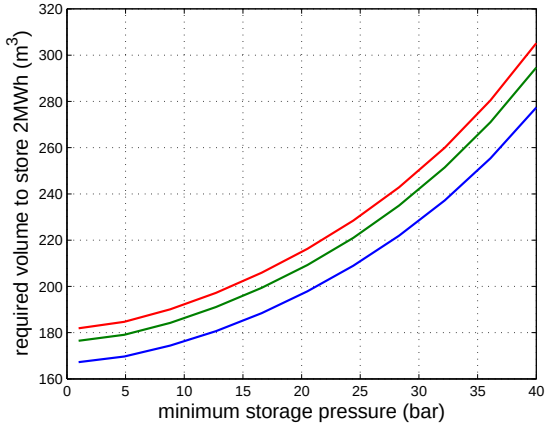

Figure 6.7: The storage volume required for 2 MWh against minimum storage pressure.

6.5.3 Sensitivity Analysis

Focussing now on a system with a maximum storage pressure of 80 bar, the sensitivity of the efficiency to each of the loss parameters discussed in the Losses section is displayed in Figure 6.8, for the 3-stage, 4-stage and 5-stage systems. As the maximum storage pressure at the McIntosh CAES facility is 79.3 bar (Nakhamkin *et al.*, 1992), it is anticipated that this storage pressure could not only be contained within a specially manufactured vessel but suitable underground caverns. The black dotted lines on Figure 6.8 mark the loss estimates as outlined in Table 6.4.

The overall efficiency is very sensitive to heat exchanger effectiveness, turbine efficiency and compressor efficiency, as can be seen in Figure 6.8. The efficiency of the 5-stage system is also very sensitive to pressure drop; the dependence being less for the 4-stage system and less again for the 3-stage. The 5-stage system is only the most efficient below a pressure drop of 0.03 bar, and above a pressure drop of 0.06 bar the 3-stage system is the most efficient. However, the 5-stage system is the least sensitive to heat exchanger effectiveness, and becomes the most efficient system below an exchanger effectiveness of $\sim$70%, with the 4-stage system being most efficient between $\sim$70-77%, and the 3-stage the most efficient above $\sim$77%.

The temperatures of the exhaust air are also important; if they are too low freezing may occur. These depend strongly on the exchanger effectiveness, although using more stages lessens this dependence. The effect of temperature drop in the TES's on both the system efficiency and exhaust temperatures is small in the range modelled here. Freezing isn't encountered until effectiveness is below 75% or the temperature drop from the TES's is more than about 45K.

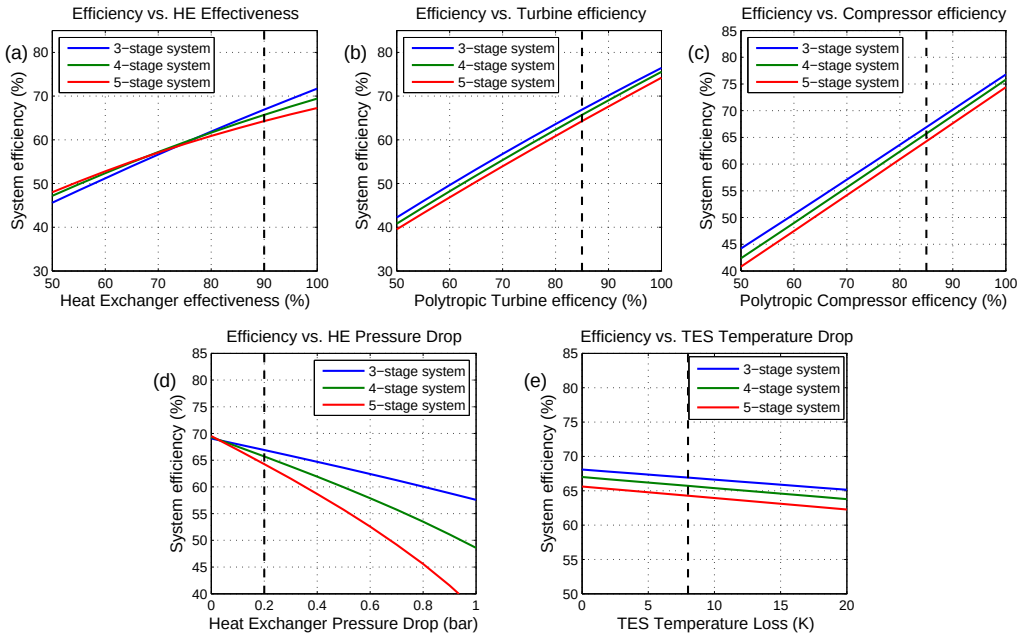

Figure 6.8: Results for the sensitivity of the overall system efficiency of the 3-stage, 4-stage and 5-stage AA-CAES systems to variation in the loss parameters. For all the results the loss parameters have the values shown in Table 6.4, except for the parameter on the x-axis. The dotted line shows the nominal values as shown in Table 6.4.

6.6 Estimating AA-CAES Costs

This section attempts to briefly develop some approximate costs for a 3-stage AA-CAES system. Costs for many of the components are difficult to estimate, and getting manufacturer quotes for purpose built equipment is too often difficult. However, the cost of the High Pressure (HP) air tank, the heat exchangers and the compressors and expanders are estimated. The HP air tank is cost by mass of steel required and the heat exchangers, the compressors and the expanders from tables of existing costs. Although these can only be regarded as "ballpark" estimates, they are useful to at least gain a preliminary cost estimate for the system.

The HP air tank

Assuming the HP air tank is cylindrical with hemispherical ends and the thickness of the walls, t_w, is constant and much smaller than the radius ($r \gg t_w$), then the volume of material required can be approximated as:

$$V_{mat} = 2\pi r t_w L + 4\pi r^2 t_w \tag{6.23}$$

where r is the internal radius and L is the length of the cylinder. Again assuming $r \gg t_w$, the thin-walled assumption, the hoop stress in the cylinder walls is:

$$\chi = \frac{pr}{t_w} \tag{6.24}$$

The ratio of the material volume to internal volume of the tank is:

$$\frac{V_{mat}}{V} = \frac{2t_w L + 4rt_w}{rL + \frac{4r^2}{3}} \tag{6.25}$$

If the length is 10 times the radius ($L = 10r$), then:

$$V_{mat} = \frac{36pV}{17\chi} \tag{6.26}$$

With an allowable steel stress of 100 MPa, a HP air store of 170m^3 at a pressure of 80 bar would require ∼225 tonnes of steel, assuming a density of 7800 kgm^{-3}. At a cost of steel of $800/tonne this would cost ∼$180000.

The Heat Exchangers

The largest heat exchanger has a transfer area of 156 m^2, and has an overall heat transfer coefficient of 94.6 Wm^{-2}. Costs estimates are taken from page 75 of IChemE. These suggest around £20000 ($31000) for the low pressure HE, £24000 ($37000) for the medium pressure HE and £46000 ($71000) for the high pressure HE.

Compressors

The compression train is required to produce air at 80 bar, at a power of around 500 kW. Referring to page 77 of IChemE, delivering air at 80 bar could just be achieved using a three stage horizontal compressor at a cost of 34.7 £/m^{3}h^{-1}. In terms of Free Air Delivery (FAD), the system would require about 4000 m^{3}h^{-1}. The total cost of the compression is then estimated at ∼ £140000 ($216000).

Turbines

Without manufacturer quotes it is simply assumed that the air turbines cost will be broadly similar to the cost of the compressors. A cost of £140000 for 500 kW equates to ∼440 $/kW. This is not dissimilar to costs per kW for large gas turbines (see NYE Thermodynamics Corporation). The air turbines should be considerably easier to manufacture, as they have only to withstand temperatures up to ∼500 K, as opposed to gas turbines which work at around 2200 K and the air turbines will not have to work simultaneously with a compressor (unlike a modern gas turbine).

Summing these costs comes to nearly $800000. This is anticipated to constitute the majority of the capital costs, but does not include costs for pipes, valves, thermal fluid, thermal fluid

containers, pumps and insulation. These considered it may not be unreasonable to expect total costs in excess of $1 million for the system.

6.7 Discussions

The simulations described in the present analysis are a simplified representation of how a real AA-CAES system may operate. The loss estimates have attempted to be conservative and it may also be possible to increase performance slightly by optimisation of the intermediate expansion pressures. However some losses have been omitted, i.e. leakages, pipe losses, and coolant pumping power. Heat exchanger fouling has also been ignored, and will have to be minimised. This may require additional filtration, which would introduce additional pressure losses. It has also been assumed that the compressor and turbine efficiency will remain constant as the pressure ratio over each device varies from unity to $(\frac{p_{s,max}}{p_0})^{1/N}$, where N is the number of stages. Hence the losses in the real system may also turn out to be more costly. On balance, these effects are likely to have some cancellation effect, though further experimental work is likely to be necessary in order better specify their combined effect.

The results illustrate that choosing the number of stages for an AA-CAES system is not straightforward. Any efficiency increase expected from adding more stages is likely to be negated if the pressure losses introduced by each stage are significant, however, by adding more stages system temperatures are reduced. This suggests a trade-off between efficiency and reducing the temperatures. In terms of specifying a minimum storage pressure, there is a trade-off between having a lower variation in compression ratio (and hence compressor exit temperatures) and having to oversize the store to account for the minimum pressure. Varying the minimum pressure has very little effect on the sensitivity analysis.

The polytropic compressor and turbine efficiencies are of paramount importance in an AA-CAES system in order to maximise the efficiency and the simulated systems are very sensitive to both of these parameters. Figure 6.5 shows that the compressor and turbine introduce the biggest losses and together these constitute nearly 21% of the total work input. We also suggest that heat exchanger effectiveness and pressure drop are two hugely important factors. With less effective heat exchangers efficiency can be increased by adding more stages, but with more stages the pressure drop very quickly becomes a limiting factor for the efficiency. Indeed, with the parameters in Table 6.4, there is no efficiency increase by adding more stages to the 3-stage system with a pressure drop above 0.06bar.

Thermal losses from the TES's are less problematic (unless the storage time or insulation level are sizably different from those assumed here) and exchanger effectiveness has a larger impact on both efficiency and exhaust air temperatures. Freezing problems seem unlikely due to the fact that any inefficiency in the turbine or the compressor will tend to increase the temperature of the air compared to the isentropic case.

With a maximum storage pressure of 80 bar the maximum air temperature reached in the 3-stage system is 512 K while the maximum thermal fluid temperature is 490 K. Therefore, a thermal fluid is required that is both liquid and stable at this temperature. A suitable fluid is likely to constitute significant expense, as identified by Pickard *et al.* (2009). With 5 compression stages, the maximum air temperature is 409 K, while the thermal fluid reaches a maximum temperature of 397 K. This raises the possibility of using pressurised water as coolant, as suggested in Grazzini and Milazzo (2008), eliminating the cost associated with a specialised thermal fluid. In order to further decrease the temperatures reached in all cases, the storage pressure could be decreased, but this will reduce the efficiency and increase the size of the air store required.

The heat transfer coefficients required to achieve a constant temperature in the air store are moderate, and should be easily achievable with a specially designed storage vessel, although this may not be the case if using a single large cavern.

To lessen the restrictions on temperatures, a direct-contact heat exchanging system could be used, i.e. rather than using a liquid thermal fluid packed beds of stones could be used as both the heat exchangers and the thermal stores. This would remove the need for a thermal fluid and potentially provide an inexpensive method of storing high temperature heat, and is thus worth further consideration.

The estimated costs ($\sim$\$1 million for a 500 kW 2 MWh plant) are significant, however there is potential for reductions. The costs of the HP air tank could be reduced by using natural caverns (which could reduce the incremental cost of storage capacity from $\sim$90 \$/kWh to $\sim$2 \$/kWh in salt caverns (Succar and Williams, 2008)). Mass produced costs for air turbines should fall significantly below gas turbine prices due to the lower heat tolerance required and the fact they don't require compressors and compressor costs may also reduce if constructed en mass.

The results presented here compliment the work of Grazzini and Milazzo (2012) and the value of efficiency calculated at their chosen heat exchanger effectiveness ($\varepsilon = 0.7$) is similar. However, while they suggest that more stages (up to 8) give a better efficiency, our results suggest that this is very sensitive to the pressure losses, and in practice even 5 stages in series may reduce efficiency.

As has been stated, a potentially problematic area is the need for the compressors and turbines to function efficiently over the range of compression ratios encountered. To avoid this would require isobaric storage, which is the approach taken by Pimm *et al.* (2011). Here, by locating the store deep underwater, static water pressure is used to maintain a constant storage pressure.

6.8 Conclusions

We estimate that an efficiency of 64-67% is achievable with AA-CAES systems. However, this is strongly dependent on the individual efficiencies of the constituent components. Regarding the design of an AA-CAES system it appears that the optimal number of stages will depend on the exchanger effectiveness and pressure losses, although physical limitations of the thermal fluid and other components may necessitate more stages to reduce the temperatures encountered.

While the fundamental problem facing AA-CAES is the generation of large quantities of heat with the compression of air, it is not the loss of this heat from the thermal stores but the technical difficulties associated with returning it that poses the biggest challenge.

A small scale AA-CAES system will have to compete with the other storage technologies; one notable technology in the capacity and power range modelled here (2 MWh 500 kW) being NaS (Sodium Sulphur) battery systems. These systems have efficiencies in excess of 80% over the time range modelled (Wen *et al.*, 2008). However with current cost estimates of about £2-3million (∼$3-5 million) for a 10 MWh 1 MW NaS system (Walawalkar *et al.*, 2007) it may not be unreasonable to expect that a similar size AA-CAES plant will be significantly cheaper.

AA-CAES has potential as an energy storage medium. Although the work here suggests that it may struggle to match emerging battery technologies in terms of efficiency, the current high costs for battery storage, its problems with cycle life and depth of discharge, and the fact that an AA-CAES system shouldn't contain on any exotic materials, suggest that further work and experiment is worthwhile. This should focus on maximising heat exchanger performance while minimising pressure losses and maximising compressor and turbine efficiency over the anticipated pressure range. Further analysis into a direct-contact heat exchanging system may also prove worthwhile.

Chapter 7

An AA-CAES system with packed bed heat exchangers

The previous chapter has considered AA-CAES as a mechanism for energy storage. It has been concluded that the process is indeed thermodynamically sound, but there are a number of outstanding engineering issues. One such issue is that the system must be able to withstand high pressures and temperatures, which may be an issue in the heat exchangers, and the cost of the heat exchanging units and a thermal fluid designed to withstand the high range of temperatures and pressures encountered may turn out in reality to be far too costly for a commercial system. Chapter 6 pointed out that increasing the number of compression stages (5 or more), would reduce the system temperatures enough to start to consider using water as a thermal fluid, but in order to keep the overall efficiency reasonable, any pressure drops in the exchangers (and other components) must be minimised, which may not turn out to be practical.

Chapter 6 also identified the possibility of using a direct contact type heat exchanger- i.e. using packed beds of granitic gravel as both the heat exchangers and the thermal stores. This would replace the six (or three flow symmetric) heat exchangers and three different thermal stores shown in Figure 6.2 with three packed bed exchangers, leading to an altogether simpler system. This Chapter considers just that; replacing the separate indirect-contact type heat exchangers and their respective thermal energy stores with packed bed heat exchangers.

7.1 Introduction

Packed bed heat exchangers are packed columns of a porous solid (or packed solid particulate matter with some space between the particles — this space is called void fraction, voidage or porosity) used for direct transfer heat processes. Packed columns are also extensively used for many processes in the chemical and food industries, i.e. adsorption, desorption, and rectification. In heat transfer applications, packed bed exchangers can offer very high rates of heat transfer (especially in gas to solid applications), have very good pressure and temperature tolerances and offer relatively inexpensive construction. There has been significant recent research analysing packed beds for high temperature thermal energy storage for solar applications (i.e.

Hänchen *et al.* (2011); Villatoro *et al.* (2009)). However they are less common than indirect-contact type exchangers, and this is perhaps why information concerning their application in AA-CAES thus far remains scarce in the available literature (discussing AA-CAES). Grazzini and Milazzo (2012), Jubeh and Najjar (2012), Grazzini and Milazzo (2008), Pickard *et al.* (2009) and Bullough *et al.* (2004) all discuss the design of an AA-CAES system considering indirect-contact type exchangers. Grazzini and Milazzo (2012) emphasizes the importance of heat exchanger optimisation (sizing a shell and tube exchanger as an example) and Pickard *et al.* (2009) questions the feasibility of AA-CAES for large scale energy storage due to the volume and cost of the thermal fluid required, and the complexity of the heat exchanging units. Crucially using indirect-contact heat exchangers forgoes the need for a thermal fluid, could provide simpler heat exchanger geometry and thus could be very suitable for use in an AA-CAES system.

This chapter does a brief re-analysis of the 3-stage AA-CAES system described in Chapter 6, but considers using direct-contact type heat exchangers, i.e. packed beds of granitic gravel. This is expected to be advantageous for a number of reasons:

1. There is no need for separate heat exchangers and thermal stores- the heat exchangers are the thermal stores.
2. The temperature limitations are likely to be much less than for an indirect-contact heat exchanger with a thermal fluid, as the thermal reservoir could just be a bed of stones and therefore the system temperatures wouldn't be restricted by the need to keep the coolant in the liquid phase.
3. The heat transfer rates achievable with direct-contact type heat exchangers are generally higher than with indirect-contact type exchangers.
4. Exchanger construction is generally inexpensive.

The choice of material for the packed bed is important, as its heat capacity will determine the thermal mass of the exchanger and this choice will also affect the heat transfer coefficient. The particle size and void fraction are also important in determining heat transfer coefficient and pressure drop, which will affect the size of the exchanger. The packing material should also be inexpensive. We suggest using granitic gravel may be appropriate, as it has a modest heat capacity, good packing properties and should be inexpensive. Table 7.1 shows the assumed gravel properties, as well the properties of some other possible materials.

Figure 7.1 shows the system arrangement considered herein, which is similar to that shown in Figure 6.2 except that the indirect-contact heat exchangers and thermal energy stores have been substituted for packed bed heat exchangers. C_{1-3} represent the compressor units and E_{1-3} are the expanders. PB_{1-3} are the Packed Bed heat exchangers. Valves to switch the flow through the packed beds to the expanders during the discharge process rather than the compressors (during the charging process) are not shown but will also be required.

Table 7.1: Properties of common packing materials in packed bed exchangers.

material	heat capacity ($Jkg^{-1}K^{-1}$)	void fraction	density (kgm^{-3})
Sand	840	0.37-0.4	2650
Crushed rock	920	0.42-0.47	2200
Granitic gravel	1068	∼0.38	2500
Acrylic pebbles	1185	∼0.4	1180
Iron balls	460	0.39-0.41	7870

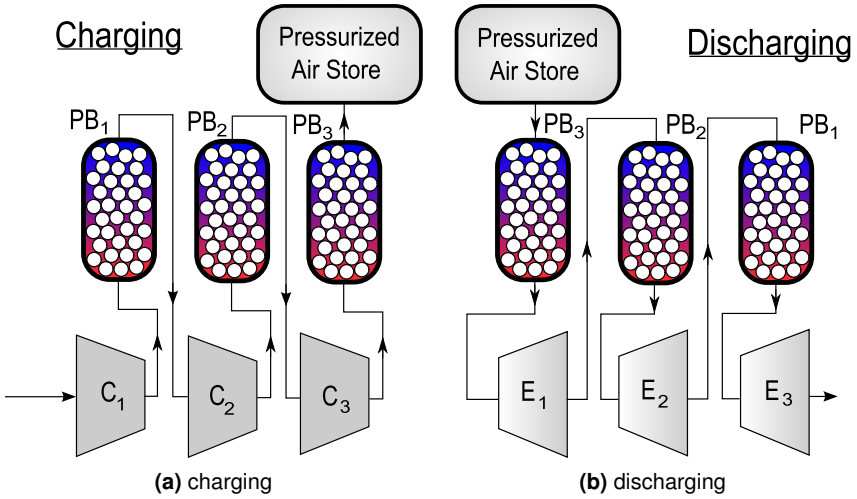

Figure 7.1: The AA-CAES system using packed bed heat exchangers rather than indirect contact exchangers (as shown in Figure 6.2).

7.2 Heat transfer in a packed bed heat exchanger

Again, as in Chapter 6 the heat exchanging phases are assumed isobaric — that is except for frictional and turbulent losses, the pressure of the air is assumed to be approximately constant as it passes through the packed bed- so a cooling stage will result in a reduction in volumetric flowrate and a heating stage will result in an increase. A schematic of a typical packed bed heat exchanger is shown in Figure 7.2.

Analytically the case of transfer heat transfer in a packed bed has been solved under a number of assumptions. This is generally first attributed to Schumann (1929), who solved for the temperature of the system under the assumptions that; any given solid particle has a uniform temperature at any given time; there is negligible heat conduction between the solid particles; there is negligible heat conduction among the fluid particles; the fluid motion is only in the axial direction of the bed; the solid has a constant void fraction (porosity) and negligible radial temperature gradient. Writing down the heat transfer rate balance (i.e. rate of heat accumulated = rate of heat in - rate of heat out + rate of heat generated) for the fluid and solid phases

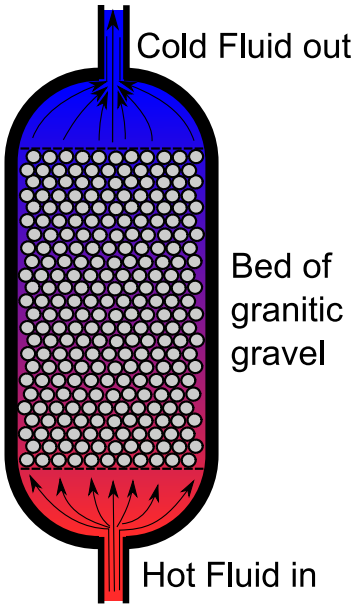

Figure 7.2: An illustration of a typical packed bed heat exchanger.

in an incremental slice of the packed bed we obtain the following coupled partial differential equations.

$$\phi \rho_f c_f \frac{\partial T_f}{\partial t} = -(1-\phi)\rho_s c_s \frac{\partial T_s}{\partial t} - u_0 c_f \rho_f \frac{\partial T_f}{\partial z} \tag{7.1}$$

$$(1-\phi)\rho_s c_s \frac{\partial T_s}{\partial t} = -\hat{h}_{vol}(T_s - T_f) \tag{7.2}$$

The term ϕ denotes the void fraction, c_s is the solid specific heat capacity, u_0 is the superficial velocity of the fluid moving through the bed (= flow rate/bed cross sectional area) and $\hat{h}_{vol}$ is the volumetric heat transfer coefficient ($\hat{h}_{vol}$ has units of $\mathrm{Wm^{-3}K^{-1}}$) and depends on the flow properties of the fluid (air), the surface area to volume ratio of the gravel and the packing geometry of the bed. $\frac{\partial T_f}{\partial z}$ is the temperature gradient of the fluid in the z-direction (along the length of the bed). Several empirical relationships to determine $\hat{h}_{vol}$ exist, as outlined in Adeyanju and Manohar (2009). The solution to Equations 7.1 and 7.2 yields the Schumann Curves for the temperature profile of the bed. A more sophisticated treatment of systems like this using perturbation methods can be found in Villatoro *et al.* (2011).

Here we adopt a numerical approach. The instantaneous heat transfer rate from the fluid to the solid particles in an incremental slice of the exchanger is given by:

$$\dot{Q}_{f\to s} = \hat{h}_{vol}(T_f - T_s) \tag{7.3}$$

There will also be a (parasitic) flow of heat through the gravel that depends on the thermal conductivity of the gravel. This can be expressed using Fourier's Law:

$$\dot{Q}_{cond} = \lambda_s A \frac{dT_s}{dz} \tag{7.4}$$

Here, λ_s is thermal conductivity of the gravel, A is the contact area, and $\frac{dT}{dz}$ is the temperature gradient in the relevant direction.

The packed beds also suffer from constant thermal losses, just like the Thermal Energy Stores described in Chapter 6. These are estimated in a similar fashion, i.e. we assume that each packed bed exchanger is at a uniform temperature and wholly contained within a cylinder of inner radius r_{bed} which has a layer insulation of thickness t_{ins} surrounding it. The power loss from the cylinder is given by:

$$\dot{Q}_{loss} = \frac{T_s - T_a}{R_{th}} \tag{7.5}$$

R_{th}, is the thermal resistance and is given by:

$$R_{th} = \frac{ln\left(\frac{r_{bed}+t_{ins}}{r_{bed}}\right)}{2\pi L \lambda_{ins}} \tag{7.6}$$

The derivation of R_{th} is outlined in Appendix C.

The thermal resistance of the cylinder ends is also approximated. In the numerical model the heat transfers ($\dot{Q}_{f\to s}$, $\dot{Q}_{cond}$ and $\dot{Q}_{loss}$, shown Equations 7.3, 7.4 and 7.5) are evaluated and the temperatures of the solid and fluid (assumed uniform in each slice) are calculated for each incremental slice of the exchanger at each time-step of the simulation.

The model assumes that; any given solid particle has a uniform temperature at any given time; there is negligible heat conduction among the fluid particles; the fluid motion is only in the axial direction; and the solid has a constant void fraction (porosity) and negligible radial temperature gradient. Conduction is present between the solid particles and there are constant losses from the packed bed to the surroundings.

7.2.1 Sources of Irreversibility in the Packed Beds

The inclusion of packed bed heat exchangers rather than indirect contact type exchangers (i.e. shell and tube, plate-fin etc...) and a thermal fluid to store the heat will introduce slightly different sources of irreversibility to those described in Chapter 6:

- As hot air passes through the packed bed exchangers, it will be cooled and the bed heated. However, there will also will also be conduction through the bed, which will cause a smoothing of thermal profile of the bed (during charging, storage and discharging), reducing the work available during discharge. This is illustrated by Figure 7.3.
- Any heat that isn't extracted in the heat exchangers will remain with the air and will have its own associated loss rate from the compressed air store.
- Each packed bed exchanger will suffer from constant thermal power losses to the external environment that will depend on the degree of insulation.
- Frictional and turbulent losses associated with fluid flow through the porous solid of the packed bed will result in pressure losses. These pressure drops through the packed beds are under the designers control to some extent and should be lower than the corresponding pressure losses in an indirect-contact exchanger of a similar effectiveness, but cannot be removed completely.
- After the storage system has been discharged, there will be some residual heat still left in the packed bed (due to the losses the compression phase is longer than the expansion phase). This will reduce the cooling efficiency of the bed during the charging in the next cycle and could lead to air entering the store above the desired temperature. In order to avoid this it may be necessary to periodically flush the beds with cold fluid, or have more than one set of packed bed exchangers to allow longer cooling time between the cycles.

7.3 The Model System

As in Chapter 6, a model of a 2000 kWh 500 kW AA-CAES system with a maximum storage pressure of 80 atm is constructed in MATLAB and adopts a numerical integration style approach. The model considers a finite increment of air, Δm, which is passed through the compression train and compressed from the ambient pressure to some final pressure $\bar{p}_f$. Again the work required to compress this amount of air, Δm, depends on how many compressions it must undergo, with the work through the last compressor given by Equation 6.8 and the work through any prior compressions by Equation 6.6. The ambient pressure is assumed to be 1 atm and the ambient temperature is assumed to be 290K.

During the expansion process an amount of air, Δm, is expanded from the store pressure to the ambient pressure. The work available depends on the number of expansions undergone; with the work available from the first expansion given by Equation 6.9 (and the work from any subsequent expansions given by Equation 6.7).

Each increment of air, Δm, must also pass through the relevant packed bed exchanger(s). To model this process each exchanger is split into incremental slices and the heat transfer solved (Equations 7.1 and 7.2) in each slice of the exchanger, in order to calculate the thermal profile of both the air and the bed along the entire length of the exchanger as a function of the amount of air that has been compressed. The time spent in each slice by each increment of air is found by calculating the flowrate using the total charging/discharging time and the mass of air added to the store.

Starting with some initial guess for the cross sectional dimensions of the exchanger and the exchanger length (a first estimate of the exchanger volume can be attained by considering the mass of gravel required to store the heat extracted in each compression at the maximum compression temperature), the thermal profile along the bed is solved for each increment of air passing through, and the output temperature of the air for the entire charging process is attained. The bed dimensions can then be adjusted until the output temperature (at all times) of the air and the exchanger pressure drops (as discussed in the next section) are acceptable. To calculate the volumetric heat transfer coefficient we use the relationship suggested by Lof and Hawley (1948) when investigating the heat transfer between granitic gravel and air, shown in Equation 7.7. G is the core mass velocity ($\mathrm{kgm^{-2}s^{-1}}$) of the fluid and d_p is the average particle size (m). The granitic gravel in the packed bed has a heat capacity of 1.05 $\mathrm{kJkg^{-1}}K^{-1}$ and a thermal conductivity of 1 $\mathrm{Wm^{-1}}K^{-1}$.

$$\hat{h}_{vol} = 652\left(\frac{G}{d_p}\right)^{0.7} \tag{7.7}$$

The assumptions made to model the packed bed are as follows:

- The PBHE is a cylinder and the fluid molar flow rate is uniform throughout the cylinder
- Conduction in plane perpendicular to the direction of fluid flow has been neglected; therefore the temperature of both the fluid and the bed in each incremental slice of the exchanger is uniform.
- There is no change in volume of the solid with temperature
- The rate of heat transfer between the fluid and the solid bed is proportional to the temperature difference between them (Equation 7.3)
- Each of the individual solid particulates have uniform temperature, i.e. $Bi << 1$.

Bi is the Biot number, defined as the ratio of resistance to heat transfer via conduction to the resistance of heat transfer via convection (see Equation 7.8). L_c is the characteristic length scale for heat transfer, d_p is the particle diameter, λ_p is the thermal conductivity and a_p is the ratio of surface are to volume. With a gravel diameter of 10 mm this leads to a Biot number $\sim$0.01.

$$Bi = \frac{\hat{h}L_c}{\lambda_p} = \frac{\hat{h}_{vol}d_p}{2\lambda_p a_p} \tag{7.8}$$

In this manner we find that two PBHE's of granitic gravel with void fraction 0.36, with radius 0.7 m and length 8 m and one with the same dimensions except length 6 m are sufficient to store all the heat of compression, and ensures that the air always enters the store at the ambient temperature.

7.3.1 Losses

As is the case in Chapter 6 the turbines and compressors are assumed to have a polytropic efficiencies of 85%.

The methods for estimating the pressure losses in the packed bed heat exchangers and their thermal losses to the environment are outlined as follows.

The Pressure Losses

The pressure drop through a PBHE depends on the exact exchanger geometry, the arrangement of the packed bed and the particulate size, and the fluid flow regime of the air. The Ergun equation (Ergun, 1929) provides one method of estimating the pressure drop through a packed column and is generally regarded as suitable for a first estimate, providing the porosity is in the range $0.35 < \phi < 0.55$, the bed is made up of similar sized particles and the flow rates are moderate (Nemec and Levec, 2005; Subramanian, 2001). It is an empirical relationship, although Plessis and Woudberg (2008) has provided some theoretical validation. Equation 7.9 shows the Ergun equation for determining the pressure drop for fluid flowing through packed media.

$$\frac{\Delta p}{L} = \frac{150\mu}{\psi^2 d_p^2}\frac{(1-\phi)^2}{\phi^3}u_0 + \frac{1.75\rho_f}{\psi d_p}\frac{(1-\phi)}{\phi^3}u_0^2 \tag{7.9}$$

d_p is the particle diameter, ρ_f is the fluid density, u_0 is the superficial bed velocity (the velocity that the fluid would have through an equivalent empty tube, given by volumetric flowrate divided by cross sectional area), μ is the dynamic viscosity of the fluid and ϕ is the void fraction of the packed bed. ψ is the shape factor to correct for the granitic gravel pieces not being spherical. The shape factor is defined as:

$$\psi = \frac{6V_p}{A_p d_p} \tag{7.10}$$

V_p is the volume of a single particle and A_p its surface area. The product (ψd_p) in Equation 7.9 is known as the equivalent spherical particle diameter.

In the models the pressure drop is calculated through each incremental slice of the exchanger and then these contributions are summed to get the total pressure drop across the whole exchanger.

The maximum pressure drop encountered in the simulation is around 1000 Pa. We assume a pressure drop of 0.1 bar (10000 Pa) per stage, to try and account for an under estimation due to entrance and exit effects and pressure losses in other components such as valves and pipes. From Equation 7.9 we see that the pressure losses could be decreased by increasing the particle size, however this reduces the heat transfer coefficient $\hat{h}_{vol}$, which increases irreversibility in the packed bed. It also increases the Biot number of the individual particulates, so that it may no longer be a good approximation to consider each individual particulate as having uniform temperature.

The Thermal Losses

A thermal conductivity of 0.3 $\mathrm{Wm^{-1}K^{-1}}$ is assumed for the insulation layer surrounding the packed bed and it is assigned a thickness of 0.3 m. Figure 7.3 illustrates how the temperature profile of a packed bed exchanger changes as the storage time is increased from 4 - 48 hours. It can be seen that there is a general trend for smoothing and cooling over time, and the cylinder ends cool much faster than the rest due to the larger surface to volume ratio at the ends. A more thorough modelling of the thermal losses could be formulated by considering the heat transfer in 3 dimensions and methods of heat transfer other than conduction, however this has been omitted here and rather the estimates made aim to err on the side of caution.

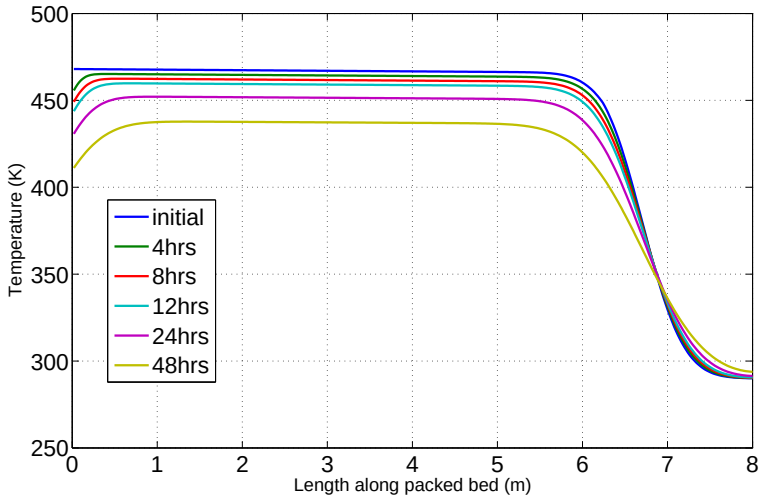

Figure 7.3: The temperature profile of the bed as the storage time is increased from 4-48 hours.

The numerical heat transfer model used here has the same result as Schumann's analytical solution (yielding the Schumann Curves (Furnas, C.C.)) when the length-step of the simulation

is small, and the conductivity through the gravel is negligible and there are no thermal losses from the bed (the Schumann Curves are obtained by solving the coupled partial differential equations for the Solid and Fluid phases at different times, shown in Equations 7.1 and 7.2).

7.4 Results

With polytopic turbine and compressor efficiencies of 85%, and assuming a total pressure loss of 0.1 bar for each of the compression stages, the efficiency for a 3-stage AA-CAES system is estimated at 72.8%. A total work of 2000 kWh is input during the compression phase and 1457 kWh of work is released after an idle storage time of 6 hours. This is a significant improvement on the system simulated in the previous chapter (the efficiency of the simulated 3-stage system was 66.9%). Figure 7.4 shows a Sankey diagram illustrating how the losses are made up when direct-transfer heat exchangers are used.

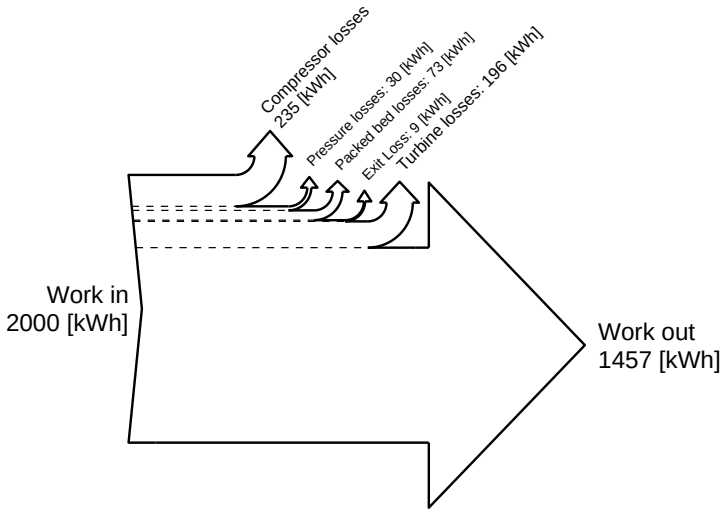

Figure 7.4: Availability diagram estimating how the losses are distributed for a 3-stage AA-CAES system using PBHE's. The packed bed losses heat include thermal losses to the ambient and losses due to conduction through the bed.

Losses in the compressors and expanders account for the biggest loss of extractable work, although heat losses to the surroundings are also significant. The pressure losses for the simulated packed beds are smaller than those for the simulated shell and tube exchangers in Chapter 6, and again they have the effect of shortening the expansion phase relative to the compression phase, resulting in significant left over heat in the packed beds at the end of the discharge phase.

The maximum air temperature encountered is 476 K and the packed beds reach this same maximum temperature, and the maximum pressure encountered is 80 atm. Using packed beds

of granitic gravel there should be no major issues in withstanding these pressures and temperatures. Observing the temperature profiles of the 3 packed bed heat exchangers (shown in Figure 7.5), it can be seen that the first exchanger needs to be the longest, as the first compression runs for the entire charging process, whereas the high pressure compressor (and expander) only operates when the pressure in the air store is above $p_{s,max}^{2/3}$. The slight cooling along each of the bed profiles is due to the constant thermal power losses driven by the temperature difference between the bed and the ambient environment. The ends of the packed beds cool faster, as they have a comparatively larger surface to volume ratio than the middle sections. There is also a smoothing effect due to the axial conduction of heat along the bed. The drastic difference between the profile of the third bed compared to the first and second beds is due to the pressure of the store constantly increasing; hence the temperature of the air leaving the last compressor is always increasing as it enters the third bed. This increasing temperature stage is much shorter in the previous compression stages. The length required for the third bed is also shorter, due to the fact that less air passes through the third compressor (it only functions when the pressure in the store is between $p_{s,max}^{2/3}$ and $p_{s,max}$).

The first two packed beds have a volume of 12.3m^3, of which 4.4m^3 is void space, the third has a volume of 9.2m^3 of which 3.3m^3 is void space and the compressed air store has a volume of 172m^3.

7.4.1 Costs

In section 6.6 of the previous chapter the costs for a 500 kW 2 MWh AA-CAES system based on indirect-contact heat exchangers were estimated. The system based on packed beds will not have the costs for the heat exchangers, but will essentially require 3 extra pressure vessels. The LP, MP and HP packed bed exchangers have volumes of 12.3 m^3, 12.3 m^3 and 9.2 m^3 respectively. The high pressure heat exchanger will require the same pressure tolerance as the HP air tank, while the Medium Pressure (MP) and Low Pressure (LP) exchangers will require lower tolerances. Using Equation 6.26, and assuming the LP exchanger and MP exchanger require tolerances of 5 and 20 bar respectively, the cost of the casing for the LP, MP and HP exchangers is \$1000 + \$3300 + \$10000 = \$14300.

Consequently, it is anticipated that an AA-CAES system using PBHE's will be cheaper than a system with indirect-contact heat exchangers, the reduction estimated at ∼\$125000 from the costs in section 6.6. A PBHE based system will also avoid the costs associated with a thermal fluid and pumps. Gravel (or some other porous solid) will be required to fill the packed beds, though this is unlikely to constitute a significant expense. The packed beds may also necessitate extra filtration which would add to total costs.

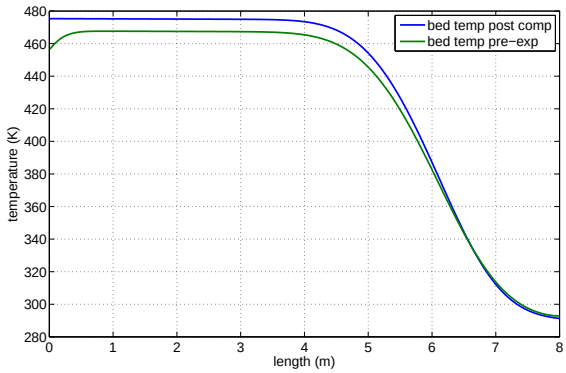

(a) Bed 1

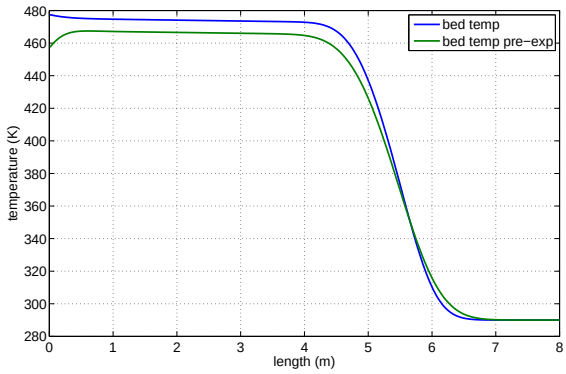

(b) Bed 2

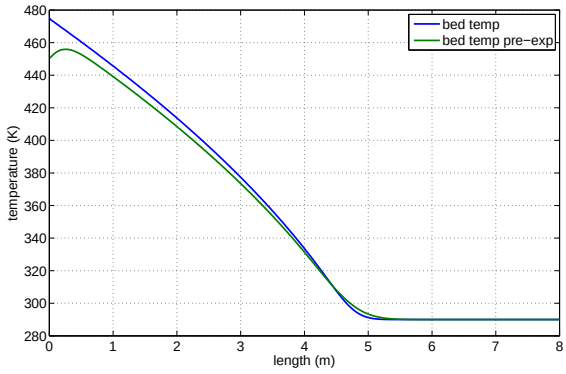

(c) Bed 3

Figure 7.5: The temperature profiles of the 3 Packed Bed Heat Exchangers immediately after the compression phase and immediately before the expansion phase.

7.5 Discussion

Using PBHE's seems to have a number of advantages over conventional indirect-contact heat exchangers in an AA-CAES system. Compared to the indirect-contact heat exchangers and TES's in the system described in Chapter 6, the PBHE based system has no thermal fluid requirements, doesn't suffer as much from stratification loss while in storage (it was assumed in Chapter 6 that the fluid in the TES's was well mixed) and has much higher estimated heat transfer coefficients. Consequently, the heat efficiency of the system is much higher- about 80% of the heat generated in the compression is returned during the expansion, rather than 68%. Accordingly the overall efficiency is also higher, estimated at 72.8% rather than 66.9% (for the simulated 3-stage system in Chapter 6). The preliminary pressure drop calculations performed here suggest that PBHE's also offer lower pressure drops than their indirect-contact heat exchanger counterparts. They should also have very high pressure tolerances, offer simple construction and be less expensive than the combination of indirect-contact exchangers, TES's and a suitable thermal fluid. Furthermore, as there is no liquid coolant required, there is no pumping power required to move the thermal fluid around the system (though this was assumed small and hence neglected in the simulations in Chapter 6).

There are also some aspects which have been omitted from this analysis, and which will require careful consideration during the design procedure. For example, ensuring that the flow is uniform through the packed beds is likely to be a challenge and will probably require specialised exchanger geometry (a suitably designed nozzle manifold for the injection of air or the inclusion of flow-guiding fins at the entrance and exits of the beds), which will have to be included while still aiming to minimise exchanger pressure losses.

7.6 Conclusions

This model is a simplification of what a real AA-CAES system incorporating direct-contact heat exchangers may be like. However the author regards it as a useful contribution, especially given that any analysis of an AA-CAES system using Packed Bed Heat Exchangers is lacking in current literature on the subject.

It is anticipated that an AA-CAES system based on direct-contact heat exchangers (packed beds) is a better preliminary design than a system based on indirect-contact heat exchangers which requires the inclusion of a high temperature thermal fluid. The calculated efficiency of 72.8% here is high enough to compete with pumped hydro (the best current form of utility scale energy storage) and begs the question of why this type of process has not successfully been implemented already. One potential reason is that the compressors and expanders required for AA-CAES are not readily available; one advantage of AA-CAES often cited in the literature is that an AA-CAES system should be constructible with "off-the-shelf" components. It seems

unlikely that this is the case, and more likely that an AA-CAES system will require the development of new compression and expansion machinery. This will need to be able to maintain high efficiency over the range of pressures encountered and all the inter-cooling (and inter-heating) must take place in the PBHE's. Consequently it is concluded that further research on AA-CAES needs to investigate the efficiency of compressors and turbines over the pressure and temperature ranges encountered, or must consider ways of keeping storage pressure constant. The development of specialised compression and expansion equipment seems a likely necessity for a system in which the storage pressure varies significantly. There is significant current research into constant storage pressure using underwater balloons (Pimm *et al.*, 2011; Hydrostor; Cheung *et al.*, 2012), which may turn out to be a viable approach, but the engineering complexities involved with locating the store deep enough underwater to achieve the desired storage pressure are still to be overcome.

Chapter 8

Preliminary experiments using a small scale air expander and variable pressure ratios

The previous two Chapters (6 and 7) have outlined theoretical analyses of two slightly different designs for AA-CAES systems. The concepts are thermodynamically sound; there seem to be no reasons in principle that forbid the construction of an efficient Advanced Adiabatic Compressed Air Energy Storage System. However its practicality depends on a number of key assumptions, such as the availability of air turbines/expanders that can maintain high efficiency between one variable and one fixed pressure and the ability to construct (direct-contact or indirect-contact) heat exchangers with high effectiveness, low pressure drops and low fouling tendencies at a reasonable cost (and in the case of indirect transfer exchangers the availability of a suitable thermal fluid). In this chapter, a set of experiments are described which measure the work obtained from a single stage expansion of air from a compressed air store and compare the results against the theoretical work available. Although the overall system efficiency is very low, the experiments serve to illustrate one of the main concerns postulated in the conclusions of the previous chapter (Chapter 7); that the efficiency of the expander may deteriorate significantly when the inlet pressure is rapidly varying. We test a single stage expansion using a small air motor (of reciprocating expander design), expanding the air from an 11.356 L (3 US Gallons) tank of compressed air at a pressure of 1 bar gauge down to the ambient pressure. By varying the pressure at which the air leaving the tank is regulated, the effect of regulating the pressure is demonstrated. Although the potential work available to the system is largest when the regulation pressure is 1 bar (i.e. the system is unregulated), the system develops the maximum work output when the regulation pressure is 0.5 bar. When accounting for the drop in the work available from the air tank due to the regulation, the system achieves maximum efficiency when the regulation pressure is 0.3 bar. This suggests that this simple motor works best between 2 constant pressures and the effect of a varying pressure ratio during the expansion process is to reduce the efficiency of the system.

8.1 Introduction

In order to gain some insight into the practical issues surrounding AA-CAES (AA-CAES was theoretically analysed in the previous two chapters), this chapter investigates the work obtained from the expansion of a tank of compressed air via a reciprocating expander, allowing the inlet pressure of the expander to vary by differing extents. Although there are air turbines available with high efficiencies working between two relatively static pressures, this work illustrates that this simple reciprocating expander struggles to achieve efficient operation when the inlet pressure is constantly reducing.

We test a reciprocating expander powered by compressed air from an 11.356 L storage tank filled with air at 1 bar gauge pressure. The maximum work available from the system is given by Equation 8.1 ($p_{i,max}$ is the maximum pressure in the air store, p_f is the final expansion pressure, V_s is the store volume, γ is the adiabatic index and $\eta_{pol,t}$ is the polytropic turbine efficiency), assuming that the pressure in the storage tank depends on the mass of air contained within the tank and that the temperature of the air in the tank remains constant. The derivation of this equation is outlined in Appendix B.

$$W = \frac{p_{i,max} V_s c_p}{R} \left[\frac{p_f}{p_{i,max}} - 1 + \frac{\gamma}{\eta_{pol,t}(\gamma-1) - \gamma} \left(\frac{p_f}{p_{i,max}} \right) - \frac{\gamma}{\eta_{pol,t}(\gamma-1) - \gamma} \left(\frac{p_f}{p_{i,max}} \right)^{\frac{\eta_{pol,t}(\gamma-1)}{\gamma}} \right] \tag{8.1}$$

Using Equation 8.1 we calculate that the largest possible work output (i.e. when $\eta_{pol,t}$=100%) from the compressed air tank is 417 J, when $p_{i,max}$ is an absolute pressure of 1.976 bar and p_f is an absolute pressure of 0.976 bar. Regulating the pressure of the air leaving the tank means that some of the expansion takes place outside of the expander (the regulator throttles the fluid leaving the store) and as work is only extractable from the expander the total extractable work available from the system is reduced. Regulating the pressure also results in two distinct periods of expansion; one in which the air motor operates between two constant pressures, and one during which the air entering (at the inlet of) the expander has an ever reducing (variable) pressure. For example, if the pressure of the air leaving the tank is regulated at 0.5 bar gauge, then while the pressure of the air in the storage tank is above 0.5 bar gauge, the air downstream of the regulator and entering the inlet of the expander should remain at a constant pressure of 0.5 bar. The work available during this constant pressure expansion phase can be calculated by using;

$$\frac{\dot{W}}{m} = c_p T_i \left[\left(\frac{p_f}{p_s} \right)^{\frac{\eta_{pol,t}(\gamma-1)}{\gamma}} - 1 \right] \tag{8.2}$$

and calculating the mass of air which will pass through the expander at constant pressure, which is given by the initial mass of air in the storage tank minus the mass of air when the pressure in the tank is 0.5 bar, i.e. $m(p_s = p_{s,max}) - m(p_s = 0.5 \text{ bar gauge})$. This can be calculated using the ideal gas law.

Table 8.1 shows the calculated values for the mass contained within the compressed air store at the regulated pressure value, the work available from the constant pressure expansion phase, the work available during the variable pressure expansion phase and the total work available (the sum of the work from the constant and variable pressure phases) as the regulation pressure is varied from 0.1 to 1.0 bar gauge (the pressure in the tank is 1 bar gauge so a regulation pressure of 1 bar means the flow is unregulated). The effect of changing the regulation pressure on the total work and the amount of work available during the constant pressure period of expansion is visible. The total work available is maximum when the regulation pressure is equal to (or greater than) $p_{s,max}$ (i.e. there is no regulation of the air leaving the storage tank). The maximum work developed between two constant pressures occurs with a regulation pressure of 0.4 bar. This is due to conflicting effects between how long the constant pressure expansion phase lasts and what the power output during this phase is, i.e. a higher regulation pressure will lead to more work output from each unit mass of air expanded, but the duration of the constant pressure expansion phase will be shorter and conversely a lower regulated pressure will have less power associated with it but last longer.

Regulation Pressure (bar gauge)	Mass contained at $p = p_{reg}$(kg)	Work (variable pressure phase) (J)	Work (constant pressure phase) (J)	Work (total) (J)
0.1	0.01444	-5.57	-98.32	-103.9
0.2	0.01578	-21.43	-164.93	-186.4
0.3	0.01712	-46.45	-205.11	-251.6
0.4	0.01847	-79.73	-222.92	-302.7
0.5	0.01981	-120.49	-221.52	-342.0
0.6	0.02115	-168.10	-203.43	-371.5
0.7	0.02249	-221.99	-170.69	-392.7
0.8	0.02383	-281.69	-124.98	-406.7
0.9	0.02517	-346.78	-67.69	-414.5
1	0.02651	-416.89	0	-416.9

Table 8.1: Theoretical predictions of the work available to the air expansion system from a 12L tank of compressed air at 1 bar gauge pressure (ambient pressure 0.976 bar and ambient temperature 295K).

The following section details the experiments measuring the work available at different regu-

lation pressures.

8.2 Experimental Setup

Figure 8.1a shows a schematic diagram of the experimental setup used to extract and measure the work from the tank of compressed air. A photograph of the arrangement is shown in Figure 8.1b. The air is discharged through the expander, which in turn drives a small DC electric motor, acting as a generator. The generator is connected to a resistor box with known resistance, and the voltage across the resistor box is logged using the software LoggerLite TM. The known resistance allows the voltage measurement across the resistor to be converted directly into power, using $P = \tilde{V}^2/R$. The resistor is confirmed to be Ohmic by comparing voltage, current and resistance measurements. Therefore this yields the power dissipated in the resistor box, and by integrating the power over the total running time the total work output is obtained.

The rotational speed of the generator during the discharge process is also recorded. The efficiency of the generator at different rotational speeds must be calibrated in order to account for the losses in the generator and thereby calculate the power output from the expander. In order to measure the speed of the motor, we use a laser and a photodiode, and use a blacked out patch on the clear Perspex flywheel which is part of the air expander (the flywheel is visible in Figure 8.1b; it is driven by the reciprocating piston and attached to the generator). The voltage produced by the photodiode is simultaneously recorded using the software LoggerLite along with the voltage in the resistor box. The frequency of the voltage spikes from the photodiode gives the speed of rotation. The pressure of the air leaving the store is also simultaneously recorded using a pressure transducer attached downstream of the regulator.

8.3 Calibrating generator efficiency

To account for the losses in the generator, the efficiency of the generator must be calibrated at different speeds (so that the power driving the generator can be obtained). In order to carry out the calibration, we use two identical DC motors with one acting as a motor and the other as a dynamo/generator. The method described in Ng *et al.* (2009) is then used to calculate the efficiency of both the motor and the generator as a function of rotational speed and load resistance. Figure 8.2 shows the results of dynamo/generator efficiency against rotational speed with a constant load resistance of 30 Ohms. A detailed description of the efficiency calibration can be found in Appendix Motor D.

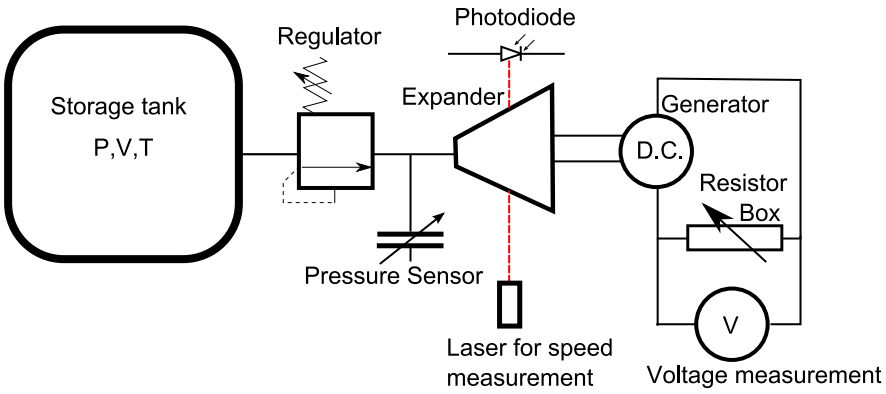

(a)

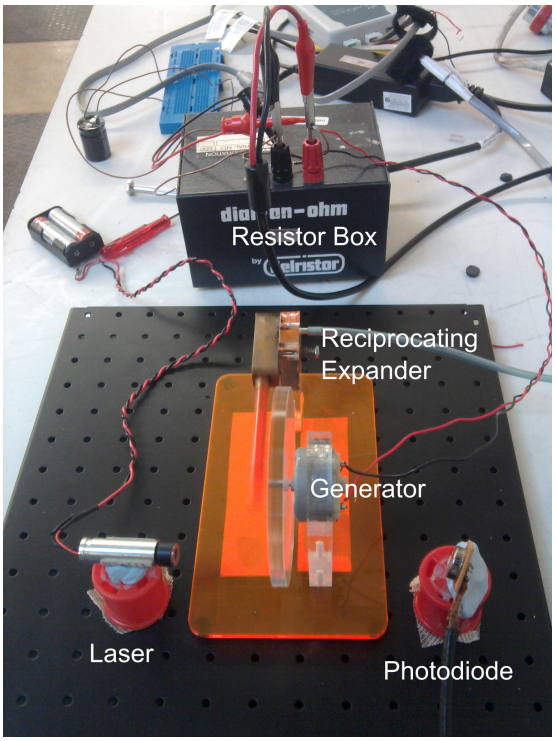

(b)

Figure 8.1: (a) Schematic diagram of experimental setup, (b) Photograph of experimental setup.

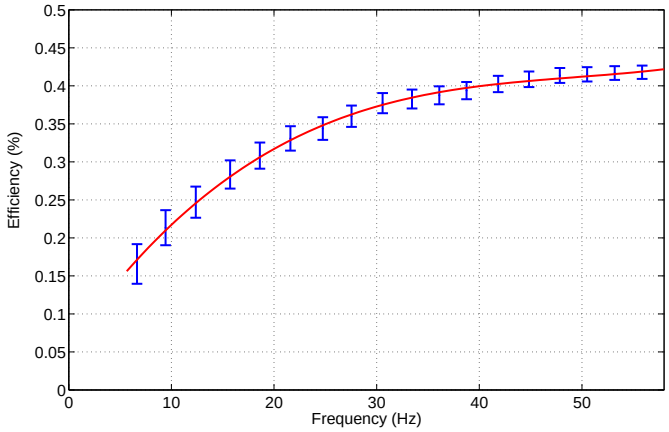

Figure 8.2: Generator efficiency against speed.

8.4 Methodology

- An 11.356 (3 US Gallons) litre air tank was charged to an initial pressure of 1 bar gauge pressure before each run.
- The regulator was set to the desired regulation level and the valve from the compressed air storage tank was opened.
- The voltage across the resistor, the voltage at the photodiode and the voltage at the pressure transducer were recorded for the entire duration of the discharge process (until the pressure in the air store was insufficient to drive the air motor).
- Using $P = \tilde{V}^2/R$ for the resistor, the power generated by the generator was calculated, and using the calibration curve for the generator efficiency with speed (shown in Figure 8.2), the power available from the air expander was estimated at each speed measurement (the measurement time-step was 0.001 s, i.e. a speed measurement, a pressure measurement and a circuit voltage measurement was taken every 0.001 s).
- This was then summed over the entire discharge process to obtain the total work obtained from the air expander.

Note: the air expander/motor was also lubricated periodically with a light machine oil to ensure smooth operation.

8.5 Results

When the tank of compressed air was discharged the two distinct periods of the expansion were clearly recognisable. With a moderate regulation pressure (i.e. 0.3-0.7 bar) there was a very clear period of the expansion when the pressure of the air exiting the regulator remained constant, and accordingly the speed of the generator was also constant. Hence the power output from the air motor must have remained at a constant level too. The variable pressure expansion phase was clearly observable after the constant pressure phase had elapsed, and at this point the power dissipated in the resistor box began to decay with time. These two phases are clearly visible in Figure 8.3a; in 8.3b there is no regulation so only the latter phase is present.

Figure 8.3a shows the results from the system run with the pressure regulated at 0.38 bar and Figure 8.3b shows the case when the regulation pressure is 1 bar. Each run starts with the compressed air storage tank initially at 1 bar gauge pressure allowing the air motor to run until there is not enough pressure difference to turn the motor. It can be seen that this point occurs at about 0.2bar. This was the case in all the runs, and it represented a loss of about 23 joules of work available to the system. There is also a loss of work due to the (flow) resistance of the regulator; when the tank is allowed to discharge without the regulator the work output is 21.2 J compared to 20.2 J when the regulator is included but the regulation pressure is set above the pressure contained in the tank. Upon inspection of Figure 8.3a we observe that the pressure of the air leaving the tank remains roughly constant at 0.38 bar for the first 260 seconds of the expansion. This is in stark comparison with Figure 8.3b, showing that when the pressure is unregulated it initially falls very rapidly from 1 bar, with the decline slope becoming more gentle as the discharge continues.

Figure 8.4a shows the results of the total work obtained from the system with different regulation pressures, and the estimated work available at the air motor shaft by accounting for the generator efficiency during the entire discharge process (using the calibration as shown in Figure 8.2). Figure 8.4b shows the theoretical work available to the system and Figure 8.4c shows the fraction of the theoretical work that is extracted by the air motor at each of the regulation pressure values used. Initially increasing the regulation pressure causes the actual work out of the system to increase, reaching a peak when the regulation pressure is around 0.5 bar, although it is still far below the value for the theoretical work available. Once the regulation pressure is increased above this, the work output from the system is reduced. This occurs despite the fact that increasing the regulation pressure increases the theoretical work available. Accounting for the increase in the theoretical work available due to the increase in the regulation pressure, the fraction of work extracted decreases with any increase in the regulation pressure above the initial value.

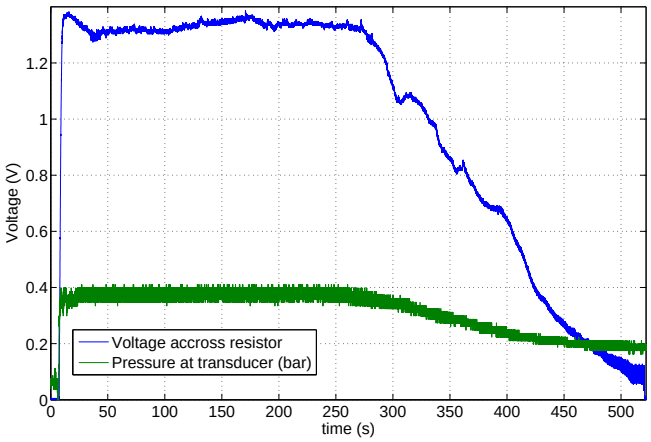

(a)

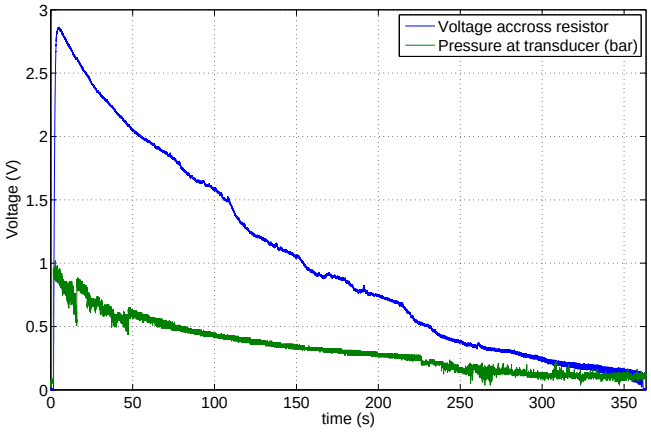

(b)

Figure 8.3: The discharge process when the pressure is (a) regulated at 0.38 bar and (b) unregulated.

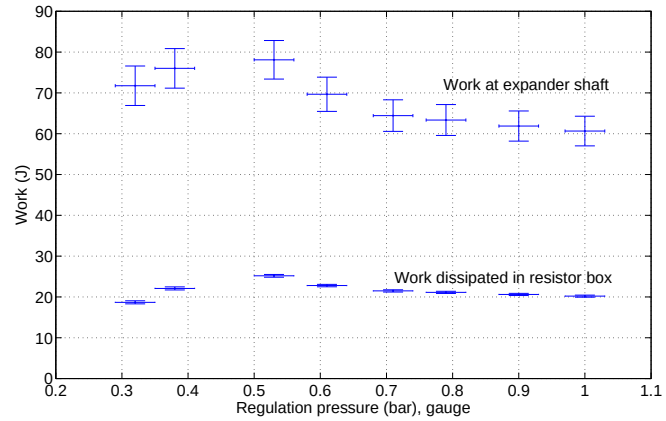

(a)

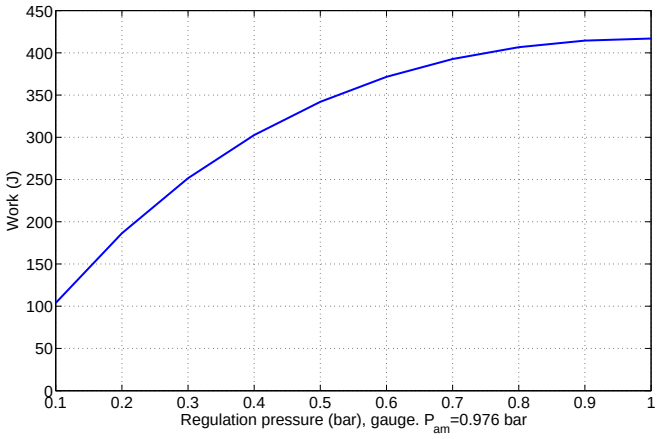

(b)

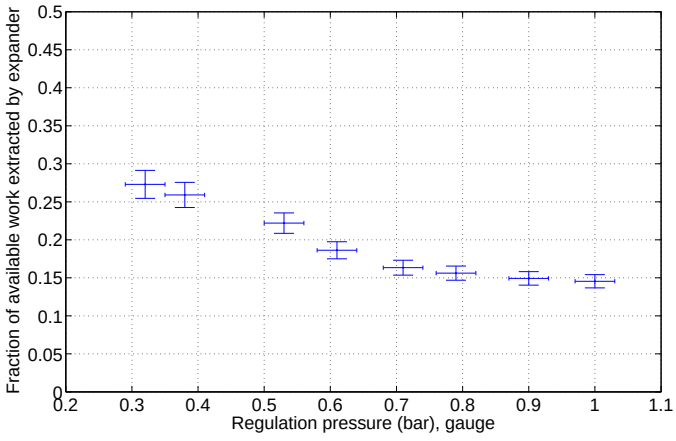

(c)

Figure 8.4: (a) The actual work dissipated in the resistor box and the inferred work at the expander shaft. (b) The theoretical work available from the 11.356 L tank with regulation pressure. (c) The fraction of the theoretical work obtained from the expander with regulation pressure.

8.6 Discussion

The results have two significant features. Firstly is the huge reduction between the actual work obtained from the discharge process compared to the theoretical work available. Secondly the fact that the actual work obtained reaches a peak with a regulation pressure around 0.5 bar, despite the fact that increasing the regulation pressure further increases the theoretical work available to the system.

The dramatic reduction between the work extracted by the expander and the theoretical work available from the expansion suggests that this expander is inappropriate for this process, and in order to make this type of process efficient the expander will need to be carefully sized, or, more likely designed specifically for this process. The reduction in the actual work extracted as the regulation pressure was increased above 0.5 bar (and the reduction in the fraction of work extracted as regulation pressure is increased) could be due to two possible explanations; the expander doesn't operate efficiently when the inlet pressure (and hence the pressure ratio across the expander) is allowed to vary, and/or when the flow rate exiting the store is high, the temperature of the remaining air in the air store falls, decreasing the storage pressure. Thus both the mass of air that can be extracted from the system and the power in the extracted air are reduced. In order to try and further deduce what is happening at this stage a temperature probe on the inside of the air store would be a necessary addition.

These preliminary experiments highlight some of the potential pitfalls and serve as an illustration (albeit a simple one) of how initial experimental tests into the practicality of an AA-CAES system may be constructed. They show how important the choice of the appropriate expansion hardware is and describe a basic method for testing the efficiency of the expanders. The method described here could also be improved by the addition of a torque transducer (to allow a direct measurement of the work at the expander shaft) and accurate flow-meters for testing expanders (both of which were above budget for this project). Further work will have to conclusively establish whether this type of system can indeed function efficiently, and it may be that the complications involved with designing a viable AA-CAES system in which a large range of pressure ratios are encountered are too severe. If this does turn out to the case, then research could switch focus to investigating the potential for creating an isobaric store for general use in an AA-CAES system. Further experimental work will also have to look at the heat exchanging parts of the system, investigating the acceptable level of pressure losses and examining the interaction with the expanders and compressors.

8.7 Conclusion

The small scale experiments described here are not sufficient to rigorously appraise the expansion stages of an AA-CAES system; however, they offer some useful insights into the process. The reduction in system efficiency with increasing the pressure ratio range encountered shows that it may be difficult to get an expander which works efficiently over the whole range of pressure ratios encountered in a real system (especially since they will be much larger than those encountered here). It also suggests that further experimental work should make a temperature recording inside the compressed air store, to try and establish if significant cooling is encountered during the expansion. If this is the case one potential solution may be to redesign the geometry of the air store in order to give a larger surface to volume area. Once this has been established, adding in a heat exchanger (or by heating the air leaving the store by via any means) before the expander (and measuring the temperature and pressure of the air flow after the heating stage) would allow the effect of the heat exchangers to be deduced, and the efficiency of the system as a function of the compression heat returned during expansion could be determined.

Chapter 9

Thesis conclusions

The question of how we will power the future in a sustainable manner remains one of the greatest challenges facing modern society. If renewable energy is to provide the answer then it seems likely that significant amounts of additional energy storage are also a necessity. This thesis has explored several aspects of energy storage working to combat the intermittency issues involved with renewable energy generation. It has looked at energy storage from both an economic and systems perspective, investigating the different manners in which energy storage can work and how it may be integrated within the current UK deregulated electricity market structure. Particular attention has been paid to tidal energy conversion as a renewable energy source that could benefit from a relatively modest amount of energy storage. It has also looked at the method of Advanced Adiabatic Compressed Air Energy Storage (AA-CAES) in significant detail.

This chapter provides a summary of the key conclusions and aims to give some direction to future work on the relevant subjects.

9.1 Thesis summary and key chapter conclusions

Chapter 2 provided an introduction to renewable energy and energy storage. Most types of renewable energy generation suffer from intermittency. In the UK especially, there is a vast wind resource (onshore and offshore), significant wave and tidal resources and a vast solar resource (although solar in the UK is less attractive than many other parts of the world due to the climate). All of these sources of renewable energy require large increases in energy storage capacity to transform them from a small complementary part of the generation mix to the reliable majority of electricity generation. While there are several methods of energy storage available, pumped hydroelectric storage is presently the only satisfactory method of large-scale grid energy storage. On a micro-grid scale, there are several options with potential, i.e. secondary batteries, however current costs need to be dramatically reduced if they are to become widespread, which in the case of batteries may be hindered by their reliance on exotic rare earth metals. Hydrogen storage, capacitors and SMES all show promise but are technologies in R&D rather than grid scale energy storage options.

Chapter 3 investigated tidal energy as a renewable energy resource which would benefit very significantly from the inclusion of a modest amount of energy storage, due to the cyclic nature of the tidal resource. The cyclic nature means that the storage requirements for specific base-load or demand-matching outputs can be accurately determined. The chapter concluded that the combination of a 1.2 MW tidal energy converter with a 1 MWh energy storage device (with modest self-discharge, charging efficiency and discharging efficiency) would offer very significant benefits in terms of output manipulation and could also offer significant gains in energy output, should transmission constraints be present. In order to provide a constant base-load energy supply with a 1.2 MW TCEC it is likely that a storage device with a capacity in the region of 30 MWh would be required, due to the presence of the spring/neap variation in energy output.

The economics of energy storage operating in the UK electricity market environment were investigated in Chapter 4. The electricity market structure was explained and areas where storage would be applicable were identified. Identifying the spot market as the market with the most potential for energy storage to exploit energy price differentials between different market time periods, an algorithm to determine the maximum possible revenue available to an energy storage device operating on such a market was derived. The model algorithm has the ability to simulate for different types of energy storage device through the inclusion of parameters for charging and discharging efficiency, self-discharge, minimum and maximum capacity and charging and discharging power limits. It was explained and validated, and then used to calculate the revenue available to some different types of energy storage device. We find that revenue generating ability is very strongly linked to charging and discharging efficiency, for devices with a relatively small daily self-discharge, but that the revenue available to any device is at present unlikely to be enough to justify investment, with the exception of the most easily exploitable pumped hydroelectric storage sites. It was also observed that storage operating in the spot market environment is likely to provide societal benefits in terms of smoothing market prices, displacing more expensive generation methods and allowing for an increase in base-load generation. The model algorithm described should therefore be a useful tool for policy makers interested in what extra incentives they would have to offer storage devices if they wish to have the inherent benefits of storage devices operating on the electricity spot market.

Chapter 5 built on the work in Chapter 4, investigating the value of energy storage in electricity systems with different levels of renewable energy generation. This was achieved by altering the model algorithm in Chapter 4, so that the optimisation determines the behaviour of the energy storage that minimises the overall fuel cost of the entire electricity system. In this manner we show that storage working to minimise the system-wide fuel cost acts to displace more expensive peaking plants, and allows for greater usage of base-load generation. Comparing the schedule of operation of the storage device that minimises the overall system fuel cost to that which maximises the revenue generated by an individual storage device, we see that there is a

significant extra fuel cost saving to the system (over the schedule that maximises the device's revenue). This is due to the higher volatility of market electricity prices compared to electricity demand. Hence while the spot market seems to be the most appropriate market for exploiting energy price differentials, it is not the case that the spot market provides the most appropriate environment to get the largest benefit from energy storage.

In Chapter 6, Advanced Adiabatic Compressed Air Energy Storage (AA-CAES) is identified as a storage mechanism with the potential for a small-medium scale grid energy storage device that doesn't depend on favourable geography, combustion or rare earth metals. We conclude that the AA-CAES concept is thermodynamically sound and calculate the theoretical efficiency at around 63-67%. However its feasibility depends on the availability of compressor and expander equipment that functions efficiently over a large range of pressure ratios. A sensitivity analysis is undertaken to gauge the effect of irreversibilities in the constituent components of the system. We also conclude that the optimum number of compression and expansion stages in an AA-CAES system depends strongly on the pressure drop introduced at each stage. With the preliminary pressure drop estimations made in Chapter 6 for a shell and tube exchanger, a 3-stage AA-CAES system is more efficient than the equivalent system with 4 or 5 stages. Unless the pressure drop can be minimised to a sufficient degree, there will be an efficiency penalty for adding more stages, although more stages does lead to a reduction in the temperatures achieved in compression and required in expansion.

Chapter 7 followed from the work in Chapter 6, where the possibility of using a direct-contact heat transfer system replacing both the indirect-contact heat exchangers and the stores of thermal fluid was identified. This chapter then did a re-analysis of the 3-stage AA-CAES system with packed bed heat exchangers. This design seems to offer a higher efficiency, calculated at 72.8%, and should also be able to endure higher temperatures than a system that requires a thermal fluid to act as the coolant during compression and in which the heat of compression is stored. It is speculated that one reason why this type of system has not been implemented already is that the required compressors and expanders (high efficiency over a range of pressure ratios, all the compression inter-cooling must be done through the packed bed) are not commonly available "off-the-shelf" components and may need to be purpose built.

Chapter 8 described experiments to gain insights into the effect of a variable pressure ratio during the expansion stages of an AA-CAES system. The work available from a reciprocating expander was compared to the theoretical work available from a tank of compressed air with the pressure regulated at different levels. The overall fraction of the theoretical work extracted was very low, however it was interesting to note that although the work available should have increased as the regulation pressure was increased, it only did this up to a certain point, illustrating that a rapidly varying pressure ratio across an expander can lead to a drop in the work output.

9.2 Suggested directions for future research

This thesis has contributed to the body of knowledge on energy storage by; highlighting areas in which energy storage devices are particularly applicable; exploring the economic drivers for energy storage and explaining how these incentivise particular ways of using storage; and examining how renewable energy generation in electricity systems gives energy storage economic, social and environmental value. In terms of future research, the model algorithm derived in Chapter 4 (and modified in Chapter 5) could be utilised to provide a comprehensive comparison of different storage technologies in different markets, to asses their respective attractiveness as investments. Using the methodology outlined in Chapter 5, a carbon cost could be added, so that the behaviour of storage could be optimised in terms of minimising emissions, or more usefully a combined fuel cost and emissions optimisation could be developed. This would allow estimation of the ability of energy storage to reduce emissions in a variety of settings and therefore would be another useful contribution to the body of knowledge on energy storage. The revenue optimisation described in Chapter 4 could also allow for quantification of the incentives required to encourage investment in energy storage devices to help shape the long-term interests of the nation and the global environment.

In addition, this thesis has extensively looked at the feasibility of a small-medium scale AA-CAES system. Theoretical analyses have estimated efficiencies around 67% for systems including shell and tube (indirect-contact) heat exchangers (and which require the storage of hot thermal fluid) and around 73% for systems including packed bed heat exchangers. It is felt that a system based on packed bed (direct-contact) heat exchangers is a better preliminary design, and should offer a better performance at a reduced cost. In order for this concept to be further scrutinised, significant experimental work is necessary. The focus of this work should be to identify the appropriate compression and expansion equipment for an AA-CAES system, as this is the first requirement of such a system, and if it proves unavailable future work should focus on designing purpose built equipment. Experiments which continue along the lines of Chapter 8, testing the work available from expanding a known volume of pressurised air and comparing it to the theoretical work available, should be carried out for different expanders. An improvement on the method used in Chapter 8 would be the addition of a Torque Transducer to measure the work at the motor shaft directly (this was above budget for this project). It would also be useful to test different expander designs at fixed pressures and known flow-rates, by including accurate flow-meters, which were unavailable during this work. Once suitable compressors and expanders have either been identified or constructed then work investigating the heat exchanging components could be undertaken. This should determine the best exchanger configuration and test packed bed exchangers against conventional indirect heat transfer systems. Should it be the case that variable pressure in the storage vessel renders the system unworkable in practice, focus should shift towards engineering a constant storage pressure solution.

9.3 Final remarks

This thesis has tested the hypothesis that *"with careful selection and sizing of an appropriate energy storage medium, energy storage is a useful tool for electricity systems which include a significant proportion of electricity generation from renewable energy conversion"*. The work in Chapters 3, 4, and 5 has verified this hypothesis, showing energy storage to not only be beneficial to electricity systems in general, but especially so to systems which utilise renewable energy conversion. Chapters 6, 7 and 8 have gone beyond this, realising that current methods have yet to provide a generally applicable, cost effective and easily constructible solution for energy storage. They provide a useful analysis of the hypothetical AA-CAES system, and while are not entirely conclusive, they give valuable insights into workings of such a system and provide direction for future research.

Appendix A

Monte Carlo maximisation algorithm

A.1 The operation of the algorithm

The following appendix provides details of the Monte Carlo optimisation algorithm used to find the optimum schedule of operation of a storage device of specified characteristics. The algorithm runs an iterative search of the space of feasible operations of the storage system. This space is defined by the characteristics of the storage system (efficiency, self-discharge, power limits, capacity) and by the physical constraint that the energy contained within the store cannot be negative. The inputs to the model are; a time-series for the price of electricity over the optimisation period (denoted *price*); values for the efficiency of transferring energy into and out of the store, η_{in} and η_{out}; a value for the maximum storage capacity, SOC_{max}; values for the storage charging and discharging limits, *PLI* and *PLO*; a value for the time constant of the store, τ_s (this can be directly converted into a self-discharge rate); and a value for the maximum number of iterations, n_{max}. The outputs are an array for the change in the state of charge (ΔSOC- the schedule of operation of the storage device), an array for Output "To the" or "Taken from" the Grid (OTG) and a single value for the total revenue yielded by the schedule of operation time-series ΔSOC, given by the scalar product of the time-series price and OTG. The round trip efficiency of the store between two time periods t_1 and t_2 is given by Equation A.1, where $\Delta t = t_1 - t_2$.

$$\eta_s(\Delta t) = \eta_{in} \times \eta_{out} \times exp(\frac{t_1 - t_2}{\tau_s}) \tag{A.1}$$

The following sequence describes the operation of the model:

Firstly two time periods are selected in the price time series (the UK spot market period has a length of 30 minutes with a single associated price). The first is selected at random, and the second is selected with regard to a certain normal distribution around the first. This distribution is chosen depending on the capacity of the device and the time dependent loss rate of the store; if there is a very high loss rate (with time) then it is unlikely that storing energy between two periods that are separated by a long time will be optimal. Similarly, if the capacity of the store is small, then storing for a long time is unlikely to be optimal as it will render parts of store

occupied for long periods. The earlier time period is assigned t_1 and the later time period is assigned t_2. The probability Ψ that a t_2 will be selected given t_1 is described by Equation A.2. The parameter NN_{bias} governs the width of the distribution.

$$\Psi(t_1|t_2) = exp\left(\frac{(t_1 - t_2)^2}{NN_{bias}}\right) \tag{A.2}$$

The model then increments a random change ΔE in the change in state of charge at t_1 (between the maximum charging limit (which is positive) and maximum discharging limit (which is negative)). A positive ΔE corresponds to an increase in the energy stored at t_1 (charging) and a negative amount of energy corresponds to a decrease in the energy stored at t_1 (discharging). The change in the state of charge at t_2 is then altered by $-\Delta E \times exp(\frac{\Delta t}{\tau_s})$.

The model then considers whether ΔE is positive or negative, and then whether the change in the state of charge ($\Delta SOC(t)$) is positive or negative or 0 (i.e. net-charge/net-discharge/no action) at the particular time periods chosen.

There are then 8 possible scenarios that will determine the action of the model. These are formed by considering the action of the store at each of the periods in question. These scenarios are described below:

For $\Delta E > 0$ ($\Delta E = 0$ implies no action)

$$\text{Scenario 1: } \Delta SOC(t_1) \geq 0 \text{ AND } \Delta SOC(t_2) > 0 \tag{A.3}$$
$$\text{Scenario 2: } \Delta SOC(t_1) \geq 0 \text{ AND } \Delta SOC(t_2) \leq 0 \tag{A.4}$$
$$\text{Scenario 3: } \Delta SOC(t_1) < 0 \text{ AND } \Delta SOC(t_2) > 0 \tag{A.5}$$
$$\text{Scenario 4: } \Delta SOC(t_1) < 0 \text{ AND } \Delta SOC(t_2) \leq 0 \tag{A.6}$$

For $\Delta E < 0$

$$\text{Scenario 5: } \Delta SOC(t_1) > 0 \text{ AND } \Delta SOC(t_2) \geq 0 \tag{A.7}$$
$$\text{Scenario 6: } \Delta SOC(t_1) > 0 \text{ AND } \Delta SOC(t_2) < 0 \tag{A.8}$$
$$\text{Scenario 7: } \Delta SOC(t_1) \leq 0 \text{ AND } \Delta SOC(t_2) \geq 0 \tag{A.9}$$
$$\text{Scenario 8: } \Delta SOC(t_1) \leq 0 \text{ AND } \Delta SOC(t_2) < 0 \tag{A.10}$$

Any move of energy ΔE will only be accepted if, the stored energy doesn't exceed the maximum storage capacity or fall below zero in the range $t_1 \leq t < t_2$, the energy into the store at t_1 doesn't exceed the charging power limit of the storage system, and the energy out of the store at

t_2 doesn't exceed the discharging power limit. These constraints are shown in Equations A.11, A.12 and A.13. The charging and discharging power limits (*PLI* and *PLO*) have been swapped for the charging and discharging energy limits (*ELI* and *ELO*), which are given by the charging or discharging power limit times the width of a time period.

$$\text{for } t_1 \leq t < t_2$$

$$0 < E_{stored}(t) + \Delta E exp\left(\frac{t_1 - t}{\tau_s}\right) \leq E_{max} \tag{A.11}$$

$$ELO \leq \Delta SOC(t_1) + \Delta E \leq ELI \tag{A.12}$$

$$ELO \leq \Delta SOC(t_2) - \Delta E exp\left(\frac{t_1 - t_2}{\tau_s}\right) \leq ELI \tag{A.13}$$

As initially there is no action of the store, the first move has to be made under scenario 2. This move will be accepted provided that there is a price increase of greater than $\frac{1}{\eta_s(\Delta t)}$ between periods t_1 and t_2 (as shown in Equation A.14).

$$price(t_2) \times \eta_s(\Delta t) > price(t_1) \tag{A.14}$$

A move of ΔE is accepted under scenario 1 with the extra constraints shown in Equations A.15 and A.16, a move will be accepted under scenario 3 with the extra constraints shown in Equations A.17 and A.18, and a move will be accepted in scenario 4 if it also satisfies Equations A.15 and A.18.

$$price(t_2) \times exp\left(\frac{t_1 - t_2}{\tau_s}\right) > price(t_1) \tag{A.15}$$

$$\Delta E \leq \Delta SOC(t_2) / exp\left(\frac{t_1 - t_2}{\tau_s}\right) \tag{A.16}$$

$$price(t_2) \times exp\left(\frac{t_1 - t_2}{\tau_s}\right) > \eta_{in} \times \eta_{out} \times price(t_1) \tag{A.17}$$

$$\Delta E \leq -\Delta SOC(t_1) \tag{A.18}$$

A move of ΔE is accepted under scenario 5 if it also satisfies (just to re-iterate, all moves must satisfy Equations A.11, A.12 and A.13) Equations A.19 and A.20, under scenario 6 if it also satisfies Equations A.20 and A.21, under scenario 7 if it also satisfies Equation A.22 and under scenario 8 if it also satisfies Equations A.19 and A.23.

$$price(t_1) > price(t_2) \times exp\left(\frac{t_1 - t_2}{\tau_s}\right) \tag{A.19}$$

$$\Delta E \geq \Delta SOC(t_1) \tag{A.20}$$

$$price(t_1) > \eta_s(\Delta t) \times price(t_2) \tag{A.21}$$

$$\eta_{in}\eta_{out} price(t_1) > price(t_2) \times exp\left(\frac{t_1 - t_2}{\tau_s}\right) \tag{A.22}$$

$$\Delta E \geq \Delta SOC(t_2)/exp\left(\frac{t_1 - t_2}{\tau_s}\right) \tag{A.23}$$

If the necessary price incentive between the two time periods is available, then action of the energy store will yield an increase in revenue. For example, if ΔE is positive, and the action of the store at periods t_1 and t_2 means the model is in scenario 2 and the price constraint in Equation A.14 is satisfied, then increasing the charging of the store at period t_1 and increasing the discharging at period t_2 will give an increased revenue. In order to speed the optimisation process the algorithm has the capability to revise ΔE to encourage moves. This forces the maximum allowable transfer of energy to occur between the two time periods in question. To illustrate, consider in scenario 2 that a move that would be rejected because it didn't satisfy all or any of the constraints in Equations A.11, A.12 and A.13 but did satisfy the price constraint, Equation A.14. Instead of rejecting the move the algorithm will change the value of ΔE so that all the constraints are satisfied. This allows the maximum possible value of ΔE. If the maximum ΔE is equal to zero, then it is not possible to increase the revenue any more via a move in scenario 2 between these two periods, and the move is rejected.

Scenarios 2 and 7 represent forward moves, while 1, 3, 4, 5, 6 and 8 can essentially be regarded as corrections for a sub-optimal moves (for example, a move under scenario 1 describes the situation in which charging at t_1 gives more revenue than charging at t_2, but this scenario can only arise after a move in scenario 2- see Figure A.1 for a simple example).

If a move satisfies all the relevant constraints, then the model accepts the move and updates the charging/discharging schedule accordingly (Equations A.24 and A.25):

$$\Delta SOC(t_1) = \Delta SOC(t_1) + \Delta E \tag{A.24}$$

$$\Delta SOC(t_2) = \Delta SOC(t_2) - \Delta E exp\left(\frac{t_1 - t_2}{\tau_s}\right) \tag{A.25}$$

In the case of an isolated storage system, the Output "To the" or "Taken from" the Grid ($OTG(t)$) is given by Equations A.26 and A.27:

$$\text{IF } \Delta SOC(t) \geq 0 \; OTG(t) = -\frac{\Delta SOC(t)}{\eta_{in}} \tag{A.26}$$

$$\text{IF } \Delta SOC(t) < 0 \; OTG(t) = -\Delta SOC(t) \times \eta_{out} \tag{A.27}$$

$$\tag{A.28}$$

Then the revenue generated at each period, t, is (Equation A.29):

$$Rev(t) = OTG(t) \times price(t) \tag{A.29}$$

The total revenue achieved over the time period in question is just the sum of the array $Rev(t)$, $\sum_{t_{end}}^{t_{start}} Rev(t)$.

Each iteration of the model repeats these steps. Once the solution reaches the point that the revenue doesn't increase with the number of iterations, the solution is considered to be optimal. In this case the model is unable to find any other movements of any amount of ΔE that will increase revenue, so further iterations cannot improve the solution. Every time the model increments a change ΔE in the change of state of charge (whether it is accepted or not) counts as an iteration and the counter, n, is incremented by 1. The optimisation procedure is ended once $n = n_{max}$.

Figure A.1 shows an illustrative example of how the model finds the optimum solution for a short time-series. The capacity is set at 3 units, the charging and discharging power limits in to and out of the store are 1 unit per period and to simplify matters there are no losses, i.e. $\tau_s = \infty$, and , $\eta_{in} = \eta_{out} = 100\%$. At the start there is no action of the storage system so the schedule of operation is initially flat (=0 at every period). The figure shows a possible path the algorithm could take to the optimum result, with the bars representing ΔSOC and the red line representing the price. It should be noted that the even though the price is described by a continuous line (as is the convention), it is really a stepped function where the price at the start of the integer time period describes the price until the beginning of the next integer time period.

1. The first move charges at period 2 and discharges at period 4. This move reduces the revenue at 2 by £8 and increases the revenue at 4 by £10, therefore increasing the total by £2.
2. The second move charges at period 1 instead of at 2, as charging at period 1 costs £1, rather than £8 at 2. The overall revenue is therefore increased by £7.
3. Move 3 charges at period 3 and discharges at period 5. It increases the total revenue by £3.
4. The fourth move increases the total revenue by £2, as discharging at period 6 generates more revenue than discharging at 5.

5. The last move (move 5) realises that there is energy stored at period 2, which could be discharged and recharged at a lower price at period 5. This move is only allowed as the energy discharged at period 2 is not required until after the store has been re-charged at period 5.

The schedule after move 5 is the optimum schedule of operation of the storage device with $PLI = PLO = 1$ unit/period over the price time-series given. There are no more moves of ΔE which can increase the revenue, and only that schedule of operation will generate a total revenue of £15. This is one of many paths to the optimum solution.

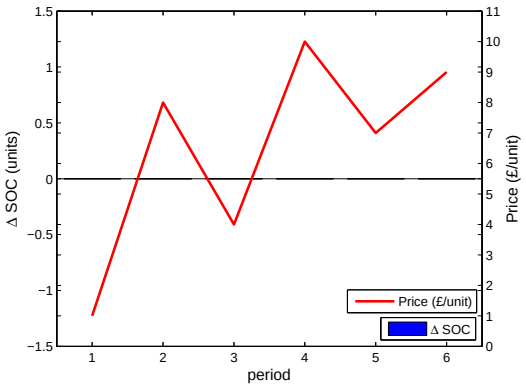

(a) Initially no action

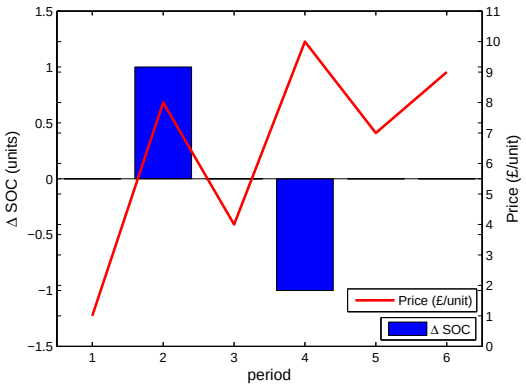

(b) Move 1 - scenario 2

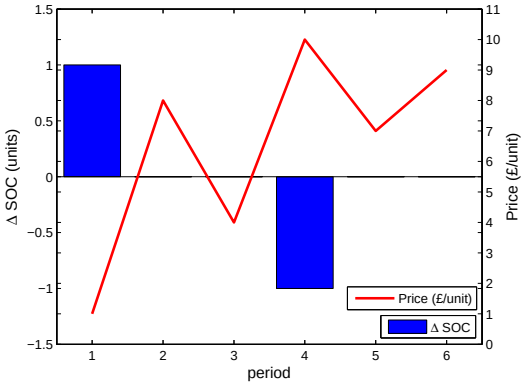

(c) Move 2 - scenario 1

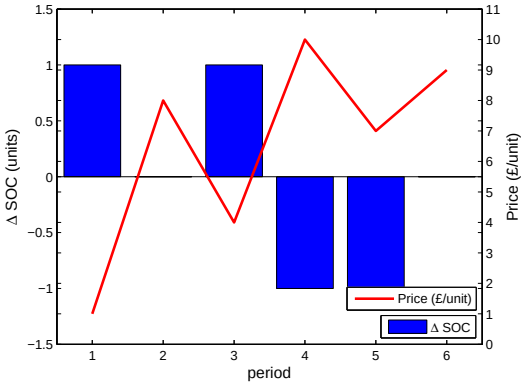

(d) Move 3 - scenario 2

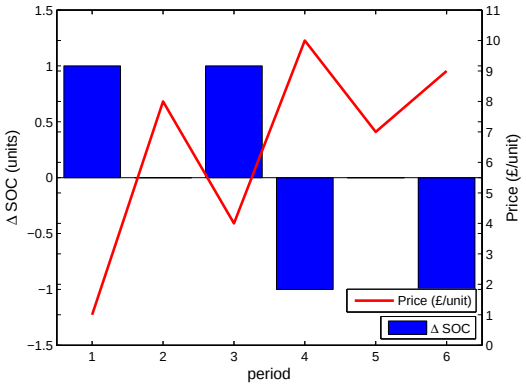

(e) Move 4 - scenario 3

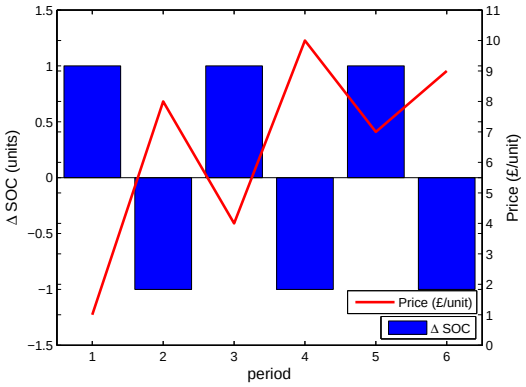

(f) Move 5 - scenario 7

Figure A.1: An illustrative of how the algorithm works. The figure depicts one possible path to the optimum solution for the algorithm on a 6 period time-series, for a storage device with capacity 3 units, power limits in and out (PLI and PLO) of 1 unit/period, and round trip efficiency of 100% over any time (τ_s=∞ and η_{in} = η_{out} = 100%).

A.2 Discussion: Does the algorithm always tend towards the optimum solution?

An important question to consider is whether or not the algorithm will always find the optimum schedule of operation of the storage device in order to maximise the revenue. As has been described, the algorithm runs an iterative search procedure, looking for changes to the schedule of operation of the storage system that increase the revenue. These changes can only be implemented if they are physically realisable- i.e. they do not breach the physical constraints on a real storage system. There are eight different scenarios (as described in Equations A.3 to A.10) under which the algorithm can find a move which tends towards the maximum achievable revenue. This discussion considers the making a perturbation to the optimum schedule of operation of the storage device, and shows that it has to be opposite to a move in one of the eight scenarios, and hence the model should always be able to find a move towards the optimum solution. These eight perturbations represent all possible changes in the operational schedule of the storage system, and are the opposite of the moves that occur under favourable price conditions for each of the eight scenarios. It is important to remember that a perturbation to the schedule of operation must involve a change at two time periods, as the storage level must be the same at the beginning and end of the time series. For example, if the schedule is changed so that the storage device is discharging at period 10, then it must charge in one of the periods leading up to this time (periods 1 - 9), and the amount by which it charges will be governed by the roundtrip efficiency between the two time periods, as well as the amount to be discharged. So if 1 unit is discharged at period 10 and charged at period 5, and the roundtrip efficiency between periods 5 and 10 is 20%, then the sore must be charged with 5 units at period 5. The perturbations that can be made to the optimal schedule of operation are as follows:

1. The optimum schedule is perturbed so that a period of charging is moved to a period closer to the discharge time. This is the opposite of a move under scenario 1, which moves the charging to an earlier period if the price at the earlier period is less than a factor of $exp(-\Delta t/\tau)$ (Δt is the time separation between the two periods) times the price at the later period (see Equation A.15).
2. The perturbation reduces charging at an earlier period and discharging is reduced at a later period. Opposite of a move in scenario 2.
3. The schedule is perturbed so that more energy is discharged at an earlier period and less is charged at a later period. Opposite move happens in scenario 3.
4. Discharging at an earlier period is increased and discharging at a later period is reduced. Opposite of a move in scenario 4.
5. Charging is increased at an earlier period and reduced at a later period. Opposite move occurs in scenario 5.
6. Charging is increased at an earlier period and discharging is increased at a later period. A move in scenario 6 is the opposite of this perturbation.

7. Discharging is reduced at an earlier period and charging reduced at a later period. Opposite to a move in scenario 7.
8. Discharging is reduced at an earlier period and increased at a later period. Opposite to a move in scenario 8.

Any change to the storage schedule can be made by using one or more of the above perturbations. For example, to change the schedule so that it charges rather than discharges at a particular period, perturbation 4 could be used to reduce the discharging at a particular period followed by perturbation 6 to increase the charging at that period. As any feasible schedule can be created by reversing any of the eight moves (perturbations 1 - 8), then provided that the initial schedule of operation is physically realisable, with enough iterations the algorithm should always tend towards the global optimum. There may be more than one optimal schedule of operation that leads to the same maximum revenue.

Appendix B

Deriving the work change between one fixed and one variable pressure at constant temperature

This brief appendix derives the expression for the work required to compress a gas from a fixed initial pressure to a variable final storage pressure which depends on the moles contained within the store (the store has a constant storage temperature T_s). The expression for the work available from expanding a gas from a variable initial pressure (in a state with a constant temperature) to final fixed pressure is also derived. The standard expression for adiabatic compressor work between two fixed pressures is given by Equation 6.6.

B.1 A fixed initial pressure and a variable final (storage) pressure

Equation B.1 shows the case when we consider compressing an infinitesimal amount of gas, δm, from the initial pressure p_i to the final pressure p_s. $\eta_{pol,c}$ is the polytropic compressor efficiency.

$$\delta W = \delta m \times c_p T_i \left[\left(\frac{p_s}{p_i} \right)^{\frac{\gamma-1}{\eta_{pol,c}\gamma}} - 1 \right] \tag{B.1}$$

Firstly we substitute $\delta m = M_g \delta \hat{n}$, where $\hat{n}$ is the number of moles contained and M_g is the molar mass of the gas. Letting $x = \frac{\gamma-1}{\eta_{pol,c}\gamma}$, then Equation B.1 can be written as:

$$\delta W = \delta \hat{n} \times M_g c_p T_i \left[\left(\frac{p_s}{p_i} \right)^{x} - 1 \right] \tag{B.2}$$

Using the ideal gas law ($pV = \hat{n}\bar{R}T$, where $\bar{R}$ is the universal gas constant) and substituting $\delta \hat{n} T_i = \frac{\delta p_i V_i}{\bar{R}}$ yields:

$$\delta W = \delta p_i \frac{M_g c_p V_i}{\bar{R}} \left[\left(\frac{p_s}{p_i} \right)^x - 1 \right] \tag{B.3}$$

Under the assumption that the store remains at a constant temperature T_s, which is equal to the ambient temperature T_a (that is to say that the gas is isobarically cooled back to ambient after it is compressed), then $p_i V_i = p_s V_s$ and hence $\delta p_i = \delta p_s (V_s / V_i)$. $\bar{R}$ is also replaced by the specific gas constant $R = \bar{R}/M_g$. Therefore it is possible to write:

$$\delta W = \delta p_s \frac{c_p V_s}{R} \left[\left(\frac{p_s}{p_i} \right)^x - 1 \right] \tag{B.4}$$

The total work required to change the storage pressure p_s from the initial pressure p_i to some maximum storage pressure $p_{f,max}$ can then be found by integrating Equation B.4. This is conveniently expressed in Equation B.4.

$$\begin{aligned} \int dW = & \quad \frac{c_p V_s}{R} \int_{p_i}^{p_{f,max}} \left(\frac{p_s}{p_i} \right)^x - 1 dp_s \\ = & \quad \frac{c_p V_s}{R} \left[\left(\frac{1}{p_i} \right)^x \frac{p_s^{x+1}}{x+1} - p_s \right]_{p_i}^{p_{f,max}} \end{aligned} \tag{B.5}$$

Putting in the limits of p_i and $p_{f,max}$, and re-substituting back in $x = \frac{\gamma - 1}{\eta_{pol,c} \gamma}$ leads to the expression for the work required to add gas initially at some ambient pressure and temperature to a gas store, which is also at the ambient temperature, in which the pressure is increased from p_i to $p_{f,max}$. This is shown in Equation B.6.

$$\begin{aligned} W = \frac{p_{f,max} V_s c_p}{R} \Bigg[& \frac{p_i}{p_{f,max}} - 1 + \frac{\eta_{pol,c} \gamma}{\gamma - 1 + \eta_{pol,c} \gamma} \left(\frac{p_{f,max}}{p_i} \right)^{\frac{\gamma - 1}{\eta_{pol,c} \gamma}} \\ & - \frac{\eta_{pol,c} \gamma}{\gamma - 1 + \eta_{pol,c} \gamma} \left(\frac{p_i}{p_{f,max}} \right) \Bigg] \end{aligned} \tag{B.6}$$

B.2 A fixed final pressure and a variable initial (storage) pressure

Now Equation B.7 shows the case when we consider expanding an infinitesimal amount of gas, δm, from the variable initial pressure p_s to the final pressure p_f. $\eta_{pol,t}$ denotes the polytropic turbine efficiency.

$$\delta W = \delta m \times c_p T_i \left[\left(\frac{p_f}{p_s} \right)^{\frac{\eta_{pol,t}(\gamma-1)}{\gamma}} - 1 \right] \tag{B.7}$$

Again by substituting $\delta m = \delta \hat{n} M_g$ and letting $y = \frac{\eta_{pol,t}(\gamma-1)}{\gamma}$, Equation B.7 can be rewritten as:

$$\delta W = \delta \hat{n} \times M_g c_p T_i \left[\left(\frac{p_f}{p_s} \right)^{y} - 1 \right] \tag{B.8}$$

Once more we use the ideal gas law to obtain:

$$\delta W = \delta p_s \frac{c_p V_s}{R} \left[\left(\frac{p_f}{p_s} \right)^{y} - 1 \right] \tag{B.9}$$

where R is the specific gas constant as before.

Integrating this between the limits $p_s = p_f$ and $p_s = p_{i,max}$ yields the work available when the pressure in the gas store drops from $p_{i,max}$ to p_f , as shown below.

$$\begin{aligned} \int dW = & \quad \frac{c_p V_s}{R} \int_{p_f}^{p_{i,max}} \left(\frac{p_f}{p_s} \right)^{y} - 1 dp_s \\ = & \quad \frac{c_p V_s}{R} \left[p_f^{y} \frac{p_s^{1-y}}{1-y} - p_s \right]_{p_f}^{p_{i,max}} \end{aligned} \tag{B.10}$$

Finally putting in the integration limits and substituting back in for y leads to the expression for the work available from expanding gas from a store with an inital pressure $p_{i,max}$ to a final pressure p_f, when the store temperature is constant.

$$\begin{aligned} W = \frac{p_{i,max} V_s c_p}{R} \Bigg[& \frac{p_f}{p_{i,max}} - 1 + \frac{\gamma}{\eta_{pol,t}(\gamma-1) - \gamma} \left(\frac{p_f}{p_{i,max}} \right) \\ & - \frac{\gamma}{\eta_{pol,t}(\gamma-1) - \gamma} \left(\frac{p_f}{p_{i,max}} \right)^{\frac{\eta_{pol,t}(\gamma-1)}{\gamma}} \Bigg] \end{aligned} \tag{B.11}$$

Appendix C

Estimating the thermal resistance of a cylinder

The Appendix develops an estimation of the thermal resistance of an insulated cylinder.

Consider a cylinder as shown in Figure C.1. The temperature inside the inner radius r_i is constant and at a Temperature T_1. The walls of the cylinder have an outer radius r_o, thickness $r_o - r_i$ and are contained within the region $r_i < r < r_o$. The temperature on the outside of the outer walls of the cylinder is also constant and at the Temperature T_2. The temperature in the walls of the cylinder then satisfies Laplace's Equation, shown in Equation C.1.

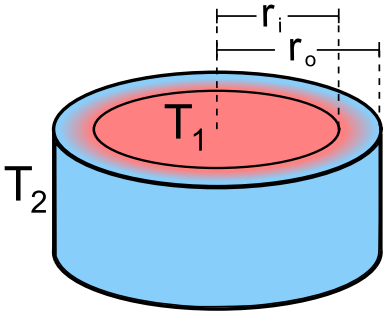

Figure C.1: An illustration of an insulated cylinder at a constant temperature T_1, with the ambient temperature outside the walls of the cylinder at T_2. The wall (insulation) thickness is $r_o - r_i$.

$$\nabla^2 T = 0 \tag{C.1}$$

Equation C.2 rewrites this in cylindrical polar coordinates.

$$\frac{1}{r}\frac{\partial}{\partial r}\left(r\frac{\partial T}{\partial r}\right) + \frac{1}{r^2}\frac{\partial^2 T}{\partial \theta^2} + \frac{\partial^2 T}{\partial z^2} = 0 \tag{C.2}$$

We then assume that the temperature only changes in the radial direction, i.e. $\frac{\partial^2 T}{\partial \theta^2} = \frac{\partial^2 T}{\partial z^2} = 0$. Therefore,

$$\frac{1}{r}\frac{\partial}{\partial r}\left(r\frac{\partial T}{\partial r}\right) = \frac{1}{r}\frac{\partial T}{\partial r} + \frac{\partial^2 T}{\partial r^2} = 0 \tag{C.3}$$

This can be solved by substitution; let $u = \frac{\partial T}{\partial r}$. Then Equation C.3 becomes Equation C.4.

$$\frac{1}{r}u\frac{\partial u}{\partial r} = 0 \tag{C.4}$$

Using an Integrating Factor, $I.F. = e^{\int \frac{1}{r}dr} = e^{ln(r)} = r$, we find that

$$\frac{\partial}{\partial r}(ur) = 0 \quad \text{and therefore} \quad ur = A \tag{C.5}$$

where A is a constant of the integration. Re-substituting back in for u, leads to the solution shown in Equation C.6. B is another constant of integration.

$$T = Aln(r) + B \tag{C.6}$$

Using the boundary conditions shown in Equation C.7 leads to the expression shown in Equation C.8 for the Temperature in the walls of the cylinder.

$$\text{At} \quad r = r_i, \quad T = T_1 \quad \text{and at} \quad r = r_o, \quad T = T_2 \tag{C.7}$$

$$T = \frac{T_1 - T_2}{ln(\frac{r_i}{r_o})} ln\left(\frac{r}{r_i}\right) + T_1 \tag{C.8}$$

Fourier's Law, expressed most conveniently in integral form (shown in Equation C.9), can then be used to work out the thermal Power Loss.

$$P = -\lambda \oint_S \nabla T.dA \tag{C.9}$$

where λ is the thermal conductivity of the cylinder walls. Integrating this over the surface of the cylinder leads to

$$P = -\lambda \int_0^{2\pi} \int_0^{L} \frac{T_1 - T_2}{ln(\frac{r_i}{r_o})} \frac{1}{r} r d\theta dz \tag{C.10}$$

$$= \frac{\lambda 2\pi L(T_1 - T_2)}{ln(\frac{r_i}{r_o})} \tag{C.11}$$

Using the definition of the thermal resistance, $P = \frac{\Delta T}{R_{th}}$ (where P is the thermal power loss), and comparing to Equation C.11 we find that the thermal resistance is given by Equation C.12.

$$R_{th} = \frac{ln\left(\frac{r_i}{r_o}\right)}{2\pi\lambda L} \tag{C.12}$$

Appendix D

Generator efficiency calibration

This appendix details a calibration of the efficiency of a DC motor acting as a both a motor and a generator as a function of the rotational speed of the motor/generator and load resistance. The method used is described in detail in Ng *et al.* (2009), but a brief outline is given here. The method requires two identical DC motors. The two identical motors are coupled (connected together so that one drives the other) and set up as shown in Figure D.1a. A photograph of the arrangement is shown in Figure D.1b. The rotational speed of the coupled motor generator is measured using the same laser/photodiode method as that used for recording the speed of the air motor in the experiments outlined in Chapter 8. Using conservation of energy arguments to obtain the power equations for each motor for each motor yields:

$$I_1\tilde{V}_1 = I_1^2\tilde{r} + \xi I_1 + P + \Delta P_f \tag{D.1}$$

$$P = I_2^2(\tilde{r} + \tilde{R}) + \xi I_2 + \Delta P_f \tag{D.2}$$

I_1 and I_2 and $\tilde{V}_1$ and $\tilde{V}_2$ are the currents and voltages in the motor circuit and the generator circuit respectively (shown in Figure D.1a), ξ is the back emf generated by each motor (which is the same for each motor as it is a function of speed), P is the power generated at the motor shaft and ΔP_f represents the frictional losses of each motor. $\tilde{r}$ is the internal resistance of the motor and $\tilde{R}$ is the load resistance.

Equations D.1 and D.2 can then be rearranged so that we have ξ and P in terms of measurable quantities, as shown:

$$\xi = \frac{(I_1\tilde{V}_1 - I_2\tilde{V}_2) - (I_1^2 + I_2^2)\tilde{r} - 2\Delta P_f}{I_1 + I_2} \tag{D.3}$$

$$P = \frac{(\tilde{V}_1 + \tilde{V}_2)I_1I_2 + (I_1 - I_2)(\Delta P_f - I_1I_2\tilde{r})}{I_1 + I_2} \tag{D.4}$$

In the same manner as described by Ng *et al.* (2009), the frictional losses at a particular rotational speed can be measured by running the motor at that speed and with the generator in an open circuit. From Equation D.2 it is clear that when $I_2 = 0$, the power of the dynamo is

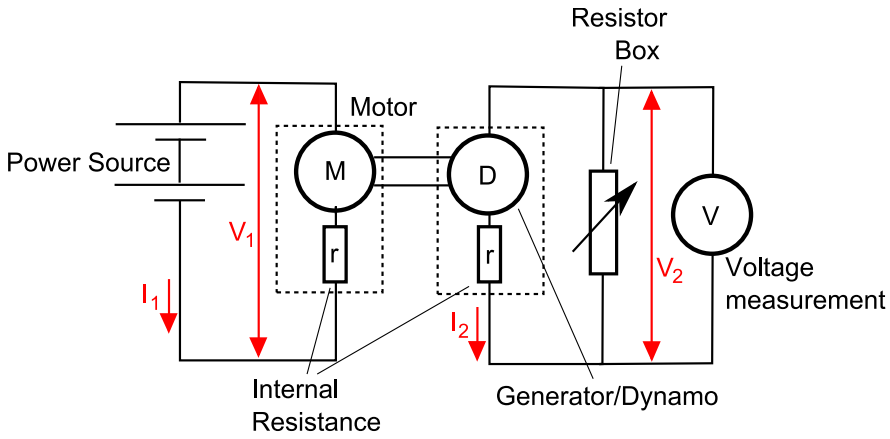

(a)

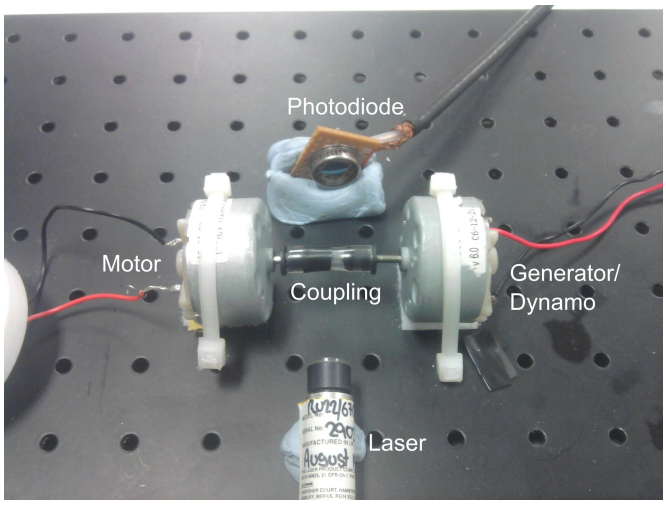

(b)

Figure D.1: (a) Schematic diagram of the coupled motor/generator setup for the efficiency calibration. (b) Photograph of the actual setup.

just equal to the frictional losses ΔP_f. Hence Equation D.1 for the first motor can be written as:

$$I_1\tilde{V}_1 = I_1^2\tilde{r} + \xi I_1 + 2\Delta P_f \tag{D.5}$$

Now the voltage generated by the dynamo is just the emf produced at that particular rotational speed. Measuring values for $\tilde{V}_1$, I_1 and $\tilde{V}_2$ the frictional power losses are calculated. It was found that the frictional power losses were in the range 0.5-1.5 mW for motor speeds between 8 and 50 Hz. This is much smaller than the magnitude of either $I_1\tilde{V}_1$ (0.1-0.6W) or $I_2\tilde{V}_2$ (0.7-2.8W).

Observing that the frictional losses are generally negligible compared to either $I_1\tilde{V}_1$ or $I_2\tilde{V}_2$, they are neglected in Equations D.3 and D.4. The definitions of the motor and generator efficiencies are then shown in Equations D.6 and D.7, and the overall efficiency is shown in Equation D.8.

$$\eta_{motor} = \frac{P}{I_1\tilde{V}_1} \times 100\% \tag{D.6}$$

$$\eta_{generator} = \frac{I_2\tilde{V}_2}{P} \times 100\% \tag{D.7}$$

$$\eta_{overall} = \frac{I_2\tilde{V}_2}{I_1\tilde{V}_1} \tag{D.8}$$

D.1 Results of the generator calibration

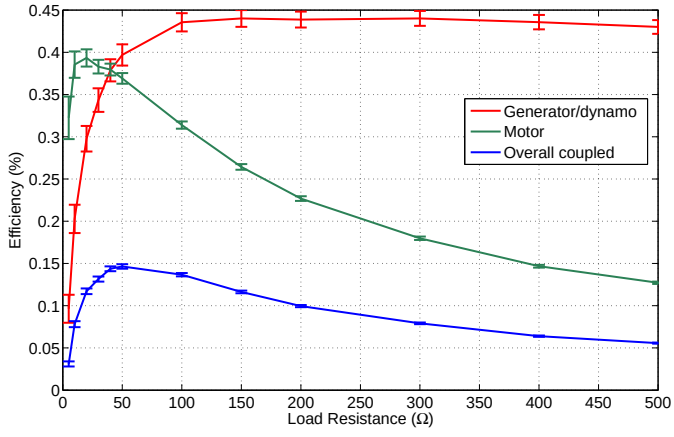

Figure D.2: Results for the motor, dynamo and overall efficiency with varying load resistance. The results are in agreement with those presented in Ng *et al.* (2009).

Figure D.3 shows the results from the motor and generator efficiencies with different load resistances, in order that the results can be compared with those of Ng *et al.* (2009). It shows the dependence of motor efficiency, dynamo efficiency and the overall efficiency of the coupled motor-dynamo arrangement. As is observed in Ng *et al.* (2009), we find that there is a definite peak in motor and overall system efficiencies, and that dynamo efficiency is more slowly varying over a reasonably wide range of resistances.

Figure D.3 shows the results when the load resistance is held constant at 30 ohms, and the speed of the motor-dynamo system is varied by changing the power supply voltage in the motor circuit. In the range of speeds that we expect to encounter when the generator is driven by the air motor, we find the results roughly yield one half of a quadratic, as shown in Figure D.3. This supports the results presented in Kraftmakher (2010), which serves to provide some validation for the results. The motor efficiency is also shown as well as the dynamo/generator efficiency although a fitted curve is only provided for the dynamo/generator efficiency.

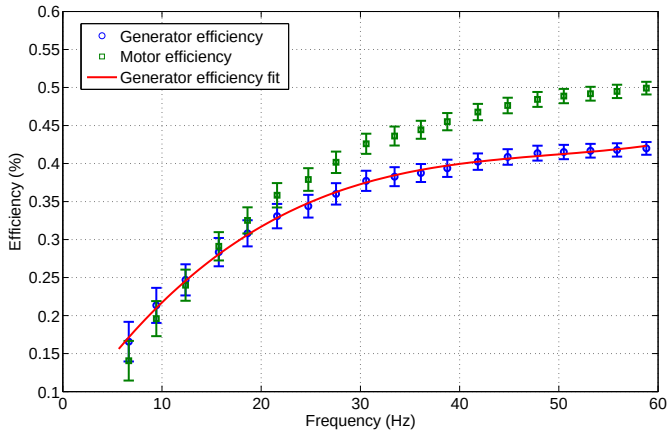

Figure D.3: Efficiency calibration with a constant load resistance of 30 Ohms and different motor/generator speeds.

The red line shown in Figure D.3 is used as a reference to find the generator efficiency at different speeds, so when the power output from the generator/dynamo is measured, the driving power can be inferred. The blue points are for the generator/dynamo efficiency (and the red line shows the fitted curve for calculating the generator/dynamo efficiency) and the green points are the motor efficiency.

Bibliography

RWE power. http://www.rwe.com/web/cms/mediablob/en/391748/data/364260/1/rwe-power-ag/innovations/adele/Brochure-ADELE.pdf. accessed Sept 2011.

A. A. Adeyanju and K. Manohar. Theoretical and Experimental investigation of Heat transfer in packed beds. *Research Journal of Applied Sciences*, 4(5):166–177, 2009.

AREVA Group and the University of Corsica. Corsican rplatform myrte: Coupling photovoltaic plant - hydrogen and fuel cells. URL http://www.docstoc.com/docs/10488571/Corsican-R-D-platform-MYRTE-Coupling-Photovoltaic-Plant-Hydrogen-and-Fuel-Cells. Accessed July 2012
.

Association of Electricity Producers. URL http://www.aepuk.com/about-electricity/electricity-market. accessed Oct 2011.

E. Barbour and I. G. Bryden. Energy storage in association with tidal current generation systems. *Proceedings of the Institution of Mechanical Engineers, Part A: Journal of Power and Energy*, 225(4):443–455, June 2011. ISSN 0957-6509. doi: 10.1177/0957650911399014.

E. Barbour, I. A. G. Wilson, I. G. Bryden, P. G. Mcgregor, A. Mulheran, and P. J. Hall. Towards an objective method to compare energy storage technologies : development and validation of a model to determine the upper boundary of revenue available from electrical price arbitrage. *Energy & Environemntal Science*, (5):5425–5436, 2012. doi: 10.1039/c2ee02419e.

M. Bartolozzi. DEVELOPMENT OF REDOX FLOW BATTERIES. A HISTORICAL BIBLIOGRAPHY. *Journal of Power Sources*, 27:219 – 234, 1989.

J. P. Barton and D. G. Infield. Intermittent Renewable Energy. *Energy*, 19(2):441–448, 2004.

G. N. Bathurst and G. Strbac. Value of combining energy storage and wind in short-term energy and balancing markets. *Electric Power Systems Research*, 67, 2003. doi: 10.1016/S0378-7796(03)00050-6.

Beacon Power. First 20mw flywheel plant. URL http://beaconpower.com/company/stephentown-archives.asp. Accessed January 2012.

L. E. Benitez, P. C. Benitez, and G. C. V. Kooten. The economics of wind power with energy storage. *Energy Economics*, 30:1973 – 1989, 2008. doi: 10.1016/j.eneco.2007.01.017.

B.I.N.E. Informationsdienst. Projekt info 05/07, 2007.

Black & Veatch. *Tidal stream phase 2: UK tidal stream energy resource assessment. Technical report no. 107799/D/2200/03.* Black & Veatch (for The Carbon Trust, London), July 2005. URL http://www.lunarenergy.co.uk/Userimages/PhaseIITidalStreamResourceReport.pdf.

Black & Veatch (2011). *UK Tidal Current Resource and Economics.* Black and Veatch, June 2011. Report prepared by Black & Veatch for the Carbon Trust.

BP statistical Review 2012. *BP Statistical Review of World Energy.* BP, June 2012. URL http://www.bp.com/sectionbodycopy.do?categoryId=7500&contentId=7068481.

I. Bryden and S. J. Couch. Me1âĂŤmarine energy extraction: tidal resource analysis. *Renewable Energy*, 31:133–139, 2006.

I. G. Bryden and D. M. Macfarlane. The utilisation of short term energy storage with tidal current generation systems. *Energy*, 25:893–907, 2000.

W. Buckles and W. V. Hassenzahl. Superconducting Magnetic Energy Storage. *IEEE Power Engineering review*, pages 16–20, 2000.

C. Bullough, C. Gatzen, C. Jakiel, M. Koller, A. Nowi, S. Zunft, M. A. N. T. Ag, and D. Oberhausen. Advanced Adiabatic Compressed Air Energy Storage for the Integration of Wind Energy. *Wind Energy*, (November):22–25, 2004.

BYD Battery Energy Storage. Chinas state grid and byd launch worlds largest battery energy storage station. URL http://www.businesswire.com/news/home/20111230005239/en/ChinaâĂŹs-State-Grid-BYD-Launch-WorldâĂŹs-Largest. Accessed January 2012.

J. M. Carrasco, L. G. Franquelo, J. T. Bialasiewicz, E. Galván, R. C. P. Guisado, M. Ángeles, M. Prats, J. I. León, and N. Moreno-alfonso. Power-Electronic Systems for the Grid Integration of Renewable Energy Sources : A Survey. *IEEE Transactions on Industrial Electronics*, 53(4):1002–1016, 2006.

D. E. Cartwright, A. C. Edden, R. Spencer, and J. M. Vassie. The tides of the northeast altantic ocean. *Philosophical Transactions of the Royal Society of London*, 298:1436–1487, 1980.

A. Cavallo. Controllable and affordable utility-scale electricity from intermittent wind resources and compressed air energy storage (CAES). *Energy*, 32:120–127, 2007. doi: 10.1016/j.energy.2006.03.018.

C. Chan, H. Peng, G. Liu, K. McIlwrath, X. Zhang, R. Huggins, and Y. Cui. High-performance lithium battery anodes using silicon nanowires. *Nature nanotechnology*, 3:31–35, 2008. doi: 10.1038/nnano.2007.411.

B. Cheung, N. Cao, R. Carriveau, and D. S. Ting. Distensible air accumulators as a means of adiabatic underwater compressed air energy storage. *International Journal of Environmental Studies*, 69(4):37–41, 2012.

D. Connolly, H. Lund, B. V. Mathiesen, and M. Leahy. The first step towards a 100 % renewable energy-system for Ireland. *Applied Energy*, 88(2):502–507, 2011.

J. Cox. Implications of intermittency, 2010. URL http://www.ilexenergy.com/pages/Documents/Other/Poyryarticle_New%20Power%208.pdf.

C. Crampes and M. Moreaux. Pumped storage and cost saving. *Energy Economics*, 32 (2):325–333, 2010. ISSN 01409883. doi: 10.1016/j.eneco.2009.10.004. URL http://linkinghub.elsevier.com/retrieve/pii/S014098830900187X.

F. Crotogino, K. B. B. Gmbh, K.-u. Mohmeyer, R. Scharf, and E. O. N. K. Bremen. Huntorf CAES : More than 20 Years of Successful Operation by. *North*, (April), 2001.

S. B. Darling, F. You, T. Veselka, and A. Velosa. Assumptions and the levelized cost of energy for photovoltaics. *Energy Environ. Sci.*, 4:3133–3139, 2011. doi: 10.1039/C0EE00698J. URL http://dx.doi.org/10.1039/C0EE00698J.

C. Defeuilley. Retail competition in electricity markets. *Energy Policy*, 37(2):377–386, February 2009. ISSN 03014215. doi: 10.1016/j.enpol.2008.07.025.

R. Dell. Energy storage âĂŤ a key technology for global energy sustainability. *Journal of Power Sources*, 100(1-2):2–17, November 2001. ISSN 03787753. doi: 10.1016/S0378-7753(01)00894-1.

DECC. *Annual Energy Statement Dept. of Energy and Climate Change*. Department of Energy and Climate Change, July 2010a. URL http://www.decc.gov.uk/en/content/cms/meeting_energy/aes/aes.aspx.

DECC. *Dept. of Energy and Climate Change: Wave Energy Technology*. Department of Energy and Climate Change, July 2010b. URL http://www.decc.gov.uk/en/content/cms/meeting_energy/wave_tidal/wave_tech/wave_tech.aspx.

Department of Energy and Climate Change. Fossil fuel prices, 2011. URL http://www.decc.gov.uk/en/content/cms/about/ec_social_res/analytic_projs/ff_prices/ff_prices.aspx. accessed Aug 2012.

DECC. *National Renewable Energy Action Plan for the United Kingdom*. Department of Energy and Climate Change, December 2009c. URL http://www.decc.gov.uk/assets/decc/what%20we%20do/uk%20energy%20supply/energy%20mix/renewable%20energy/ored/25-nat-ren-energy-action-plan.pdf.

DECC. *UK Renewable Energy Roadmap*. Department of Energy and Climate Change, July 2011d. URL http://www.decc.gov.uk/en/content/cms/meeting_energy/renewable_ener/re_roadmap/re_roadmap.aspx.

T. DeVries, J. McDowall, N. Umbricht, and G. Linhofer. Battery energy storage systems for golden valley electric assotiationsâĂŹ aab review, 2004. URL http://library.abb.com/global/scot/scot271.nsf/veritydisplay/627968be8161966fc1256e3f004e0366/$File/38-43%20M848.pdf. Accessed January 2012.

K. C. Divya and J. Ø stergaard. Battery energy storage technology for power systems âĂŤ An overview. *Electric Power Systems Research*, 79:511–520, 2009.

Dominiom Corporate. bath county pumped storage station. Accessed January 2012.

D. H. Doughty, P. C. Butler, A. A. Akhil, N. H. Clark, and J. D. Boyes. Batteries for lage-scale Stationary Electrical Energy Storage. *Electrochemical Society Interface*, pages 49–53, 2010.

Drake Landing Solar Community. URL http://www.dlsc.ca/. Accessed December 2012.

N. Duić and M. da Graça Carvalho. Increasing renewable energy sources in island energy supply: case study Porto Santo. *Renewable and Sustainable Energy Reviews*, 8(4):383–399, August 2004. ISSN 13640321. doi: 10.1016/j.rser.2003.11.004.

DUKES. Digest of united kingdom energy statistics: Electricity generated and supplied, 1970 to 2009 (dukes 5.1.3), 2010. URL http://www.decc.gov.uk/. Scottish and Southern Energy presentation.

Duratherm heat transfer fluids. http://www.heat-transfer-fluid.com/. Available online.

Elexon. Market index data (spot price) - elexon portal website. URL https://www.bsccentralservices.com/. accessed Oct 2011.

S. Ergun. Fluid flow through packed columns. *Chemical Engineering Progress*, 48:9–94, 1929.

K. Erkan, G. Holdmann, W. Benoit, and D. Blackwell. Understanding the Chena Hot Springs , Alaska , geothermal system using temperature and pressure data from exploration boreholes. *Geothermics*, 37:565–585, 2008. doi: 10.1016/j.geothermics.2008.09.001.

European Photovoltiac Industry Association. Global market report 2013 - 2017, 2013. URL http://www.epia.org/news/publications/.

J. Eyer. Energy Storage for the Electricity Grid : Benefits and Market Potential Assessment Guide A Study for the DOE Energy Storage Systems Program. *Contract*, (February), 2010.

F. Figueiredo and P. Flynn. Using Diurnal Power Price to Configure Pumped Storage. *IEEE Transactions on Energy Conversion*, 21(3):804–809, September 2006. ISSN 0885-8969. doi: 10.1109/TEC.2006.877373. URL http://ieeexplore.ieee.org/lpdocs/epic03/wrapper.htm?arnumber=1677672.

A. D. Fox, M. Desholm, J. Kahlert, T. K. Christensen, and I. K. Peterson. Information needs to support environmental impact assessment of the effects of European marine offshore wind farms on birds. *Ibis*, pages 129– 144, 2006.

Furnas, C.C. Heat transfer from a gas stream to a bed of broken solids. URL http://digital.library.unt.edu/ark:/67531/metadc12530/. Accessed October 2012.

J. B. Garrison and M. E. Webber. An integrated energy storage scheme for a dispatchable solar and wind powered energy system. *Journal of Renewable Sustainable Energy*, 3(1), 2011. doi: doi:10.1063/1.3599839.

S. Gill, E. Barbour, I. Wilson, and D. Infield. Maximising revenue for non-firm distributed wind generation with energy storage in an active management scheme. *IET Renewable Power Generation*, 2013.

L. Gouveia and A. Cristina. Microalgae as a raw material for biofuels production. *Journal Of Industrial Microbiology*, pages 269–274, 2009. doi: 10.1007/s10295-008-0495-6.

B. G. Grazzini and A. Milazzo. A Thermodynamic Analysis of Multistage Adiabatic CAES. *Proceedings of the IEEE*, 100(2):461–472, 2012.

G. Grazzini and A. Milazzo. Thermodynamic analysis of CAES/TES systems for renewable energy plants. *Renewable Energy*, 33(9):1998–2006, September 2008. ISSN 09601481. doi: 10.1016/j.renene.2007.12.003.

R. Green and N. Vasilakos. Market behaviour with large amounts of intermittent generation. *Energy Policy*, 38(7):3211–3220, 2010. ISSN 0301-4215. doi: 10.1016/j.enpol.2009.07.038. URL http://dx.doi.org/10.1016/j.enpol.2009.07.038.

R. Green, H. Hu, and N. Vasilakos. Turning the wind into hydrogen : The long-run impact on electricity prices and generating capacity. *Energy Policy*, 39(7):3992–3998, 2011. ISSN 0301-4215. doi: 10.1016/j.enpol.2010.11.007. URL http://dx.doi.org/10.1016/j.enpol.2010.11.007.

J. B. Greenblatt, S. Succar, D. C. Denkenberger, R. H. Williams, and R. H. Socolow. Baseload wind energy : modeling the competition between gas turbines and compressed air energy storage for supplemental generation. *Energy Policy*, 35:1474–1492, 2007. doi: 10.1016/j.enpol.2006.03.023.

R. Gross, J. Skea, T. Green, P. Heptonstall, M. Leach, and D. Anderson. Renewables and the grid: understanding intermittency. *Proceedings of the ICE - Energy*, 160(1):31–41, 2007.

R. Gross. *The Costs and Impacts of Intermittency: An assessment of the evidence on the costs and impacts of intermittent generation on the British electricity network*. UK Energy Research Centre, 2006.

R. Gross and P. Heptonstall. The costs and impacts of intermittency : An ongoing debate " East is East , and West is West , and never the twain shall meet .". *Energy Policy*, 36:4005– 4007, 2008. doi: 10.1016/j.enpol.2008.06.013.

M. Guerrero, E. Romero, F. Barrero, M. I. Milanés, and E. González. Overview of Medium Scale Energy Storage Systems. *COMPATIBILITY AND POWER ELECTRONICS 6TH INTERNATIONAL CONFERENCE*, pages 93–100, 2009.

I. Hadjipaschalis, A. Poullikkas, and V. Efthimiou. Overview of current and future energy storage technologies for electric power applications. *Renewable and Sustainable Energy Reviews*, 13:1513–1522, 2009.

M. Hänchen, S. Brückner, and A. Steinfeld. High-temperature thermal storage using a packed bed of rocks e Heat transfer analysis and experimental validation. *Applied Thermal Engineering*, 31(10):1798–1806, 2011. ISSN 1359-4311. doi: 10.1016/j.applthermaleng.2010.10.034.

S. Hawkins. *A High Resolution Reanalysis of Wind Speeds over the British Isles for Wind Energy Integration*. PhD thesis, 2012.

Heatric. Typical diffusion-bonded heat exchanger characteristics. http://www.heatric.com/typical_characteristics.html. accessed Sept 2011.

R. Hebner and J. Beno. Flywheel Batteries Come Around Again. *IEEE Spectrum*, 2002.

D. C. Holzman. The Vanadium advantage: flow batteries put wind energy in the bank. *Environmental Health Perspectives*, 115(7):A358–A361, 2007.

Honda. *The Honda FCX*. Honda Automobiles, 2012. URL http://automobiles.honda.com/fcx-clarity/refueling.aspx.

M. Hubbert. Nuclear energy and the fossil fuels. *Drilling and Production Practice, American Petroleum Institute*, 1956.

Hydrostor. http://hydrostor.ca/home/. Available online.

H. Ibrahim, a. Ilinca, and J. Perron. Energy storage systemsâĂŤCharacteristics and comparisons. *Renewable and Sustainable Energy Reviews*, 12(5):1221–1250, 2008.

IChemE. *A Guide to Capital Cost Estimating, 3rd Edition.* The Institution of Chemical Engineers, The Association of Cost Engineers.

INVESTIRE-NETWORK. *Investigation on Storage Technologies for Intermittent Renewable Energies: Evaluation and recommended R&D strategy. ST5: Electrolyser, hydrogen storage and Fuel Cell.* INVESTIRE-NETWORK, June 2003. URL http://www.itpower.co.uk/investire/pdfs/fuelcellrep.pdf.

Isentropic Ltd. Isentropic: A new era in energy storage. URL http://www.isentropic.co.uk/. Accessed June 2013.

Joseph B. Klemp. *A Description of the Advanced Research WRF Version 3*, 2008.

N. M. Jubeh and Y. S. H. Najjar. Green solution for power generation by adoption of adiabatic CAES system. *Applied Thermal Engineering*, 44:85–89, 2012. ISSN 1359-4311. doi: 10.1016/j.applthermaleng.2012.04.005. URL http://dx.doi.org/10.1016/j.applthermaleng.2012.04.005.

K. Kaldellis, J and D. Zafirakis. Optimum energy storage techniques for the improvement of renewable energy sources-based electricity generation economic efficiency. *Energy*, 32: 2295–2305, 2007.

B. Kirke. *Developments in ducted water current turbines.* Sustainable Energy Centre, University of South Australia, Mawson Lakes, SA 5095, Australia, 2006.

M. Korpaas, A. T. Holen, and R. Hildrum. Operation and sizing of energy storage for wind power plants in a market system. *Electrical Power and Energy Systems*, 25:599–606, 2003. doi: 10.1016/S0142-0615(03)00016-4.

Y. Kraftmakher. Experiments with a dc motor. *European Journal of Physics*, 31:863–870, 2010. doi: 10.1088/0143-0807/31/4/016.

J. Kwoka and K. Madjarov. Making Markets Work: The Special Case of Electricity. *The Electricity Journal*, 20(9):24–36, November 2007. ISSN 10406190. doi: 10.1016/j.tej.2007.10.008.

L S Blunden and A S Bahaj. Tidal energy resource assessment for tidal stream generators. *Proc. IMechE Part A: J. Power and Energy*, 221(Special issue paper):137–146, 2007.

N. Lannan. New pumped storage proposals, 2010. URL http://www.all-energy.co.uk/userfiles/file/neil-lannen-190510.pdf. Scottish and Southern Energy presentation.

J. D. Lewins. Optimising an intercooled compressor for an ideal gas model. *International Journal of Mechanical Engineering Education*, 31(3):189–200, 2003.

D. Lieurance, F. Kimball, and C. Rix. Design and Cost Studies for Small Scale Superconducting Magnetic Energy Storage (SMES) Systems. *IEEE Transactions on applied superconductivity*, 5(2):350–353, 1995.

Lightsail Energy. URL http://lightsailenergy.com/. Accessed November 2012.

S. Littlechild. Retail competition in electricity markets âĂŤ expectations, outcomes and economics. *Energy Policy*, 37(2):759–763, February 2009. ISSN 03014215. doi: 10.1016/j.enpol.2008.09.089.

G. Lof and R. Hawley. Unsteady state heat transfer between air and losse solids. *Journal of Industrial Engineering*, 40(6):1061–1070, 1948.

H. Lund. Renewable energy strategies for sustainable development. *Energy*, 32:912–919, 2007.

H. Lund. Towards 100 % renewable energy systems. *Applied Energy*, 88:419–421, 2011. doi: 10.1016/j.apenergy.2010.10.013.

H. Lund and G. Salgi. The role of compressed air energy storage (CAES) in future sustainable energy systems. *Energy Conversion and Management*, 50(5):1172–1179, 2009. ISSN 0196-8904. doi: 10.1016/j.enconman.2009.01.032. URL http://dx.doi.org/10.1016/j.enconman.2009.01.032.

C. A. Luongo, T. Baldwin, P. Ribeiro, and C. M. Weber. A 100 MJ SMES Demonstration at FSU-CAPS. *IEEE TRANSACTIONS ON APPLIED SUPERCONDUCTIVITY*, 13(2): 1800–1805, 2003.

M. Madaleno. Some stylized facts in electricity markets: a european comparison, 2008. URL http://www6.fe.uc.pt/pfn2008/UserFiles/pdf/724.pdf.

Maxwell Technologies. Ultracapacitor products. [Online] www.maxwell.com.

MCT. Marine current turbine: turning the tide. URL http://www.marinecurrentturbines.com.

Metzger & Willard. Moody diagram by tom davis. Adapted from code available online at MATLAB central - *http://www.mathworks.com/matlabcentral/fileexchange/7747-moody-diagram*.

P. Mokrian. A stochastic programming framework for the valuation of electricity storage. *26th USAEE/IAEE North American Conference, 2006*, 2006.

Mott MacDonald. Uk electricity generation costs update, 2010. URL http://www.decc.gov.uk/assets/decc/statistics/projections/71-uk-electricity-generationcosts-update-.pdf. accessed Aug 2012.

M. Mufti, S. A. Lone, S. J. Iqbal, M. Ahmad, and M. Ismail. Super-capacitor based energy storage system for improved load frequency control. *Electric Power Systems Research*, 79: 226–233, 2009.

M. Nakhamkin and M. Chiruvolu. Available Compressed Air Energy Storage (CAES) Plant Concepts, 2007. Available online.

M. Nakhamkin, L. Andersson, E. Swensen, J. Howard, R. Meyer, R. Schainker, R. Pollak, and B. Mehta. Aec 110 mw caes plant: Status of project. *Journal of Engineering for Gas Turbines and Power*, 114(4):695–700, 1992. doi: 10.1115/1.2906644.

National Grid. *NETS Seven Year Statement: Plant Margin*. National Grid, 2011. URL http://www.nationalgrid.com/uk/Electricity/SYS/current/.

National Grid. Operating the electricity transmission networks in 2020, 2011. URL http://www.nationalgrid.com/NR/rdonlyres/DF928C19-9210-4629-AB78-BBAA7AD8B89D/47178/Operatingin2020_finalversion0806_final.pdf. accessed Sept 2012.

National Grid. Metered half-hourly electricity demands, 2012. URL http://www.nationalgrid.com/uk/Electricity/Data/Demand+Data/. accessed Sept 2012.

National Grid. URL http://www.nationalgrid.com. accessed Oct 2011.

D. Nemec and J. Levec. Flow through packed bed reactors : 1 . Single-phase flow. *Chemical Engineering Science*, 60:6947 – 6957, 2005. doi: 10.1016/j.ces.2005.05.068.

P.-h. Ng, S.-l. Wong, and S.-y. Mak. Efficiency measurement using a motor ÃćâĆňâĂIJ dynamo module. *Physics Education*, 44(6):639–643, 2009.

Nord Pool Spot Market. accessed Oct 2011, url = http://www.nordpoolspot.com/.

P. Norgaard and H. Holttinen. A Multi-Turbine Power Curve Approach. *Nordic Wind Power Conference, March 2004*, 1, 2004.

NYE Thermodynamics Corporation. Gas turbine prices. URL http://www.gas-turbines.com/trader/prices.htm. Accessed June 2013.

J. Oswald, M. Raine, and H. Ashraf-ball. Will British weather provide reliable electricity ? *Energy Policy*, 36:3212– 3225, 2008. doi: 10.1016/j.enpol.2008.04.033.

Parsons Brinkerhoff. Electricity generation cost model, 2011 update revision 1, 2011. URL http://www.decc.gov.uk/assets/decc/11/about-us/economics-socialresearch/2127-electricity-generation-cost-model-2011.pdf. accessed Aug 2012.

Passive House. URL http://www.constructireland.ie/articles/0209passivehouse.php. Accessed December 2012.

W. F. Pickard, N. J. Hansing, and A. Q. Shen. Can large-scale advanced-adiabatic compressed air energy storage be justified economically in an age of sustainable energy? *Journal of Renewable and Sustainable Energy*, 1(3):033102, 2009. ISSN 19417012. doi: 10.1063/1.3139449.

A. J. Pimm, S. D. Garvey, and R. J. Drew. Shape and cost analysis of pressurized fabric structures for subsea compressed air energy storage. *Proceedings of the Institution of Mechanical Engineers, Part C: Journal of Mechanical Engineering Science*, 225(5):1027–1043, April 2011. ISSN 0954-4062. doi: 10.1177/0954406211399506.

J. P. Plessis and S. Woudberg. Pore-scale derivation of the Ergun equation to enhance its adaptability and generalization. *Chemical Engineering Science*, 63:2576 – 2586, 2008. doi: 10.1016/j.ces.2008.02.017.

C. Ponce De Leóna, A. Frías-Ferrerb, J. González-Garcíab, D. Szántoc, and F. Walsh. Redox flow cells for energy conversion. *Journal of Power Sources*, 160:716–732, 2006.

C. W. Price. The Effect of Liberalizing UK Retail Energy Markets on Consumers. *Oxford Review of Economic Policy*, 21(1):128–144, March 2005. ISSN 1460-2121. doi: 10.1093/oxrep/gri007.

Prudent Energy. Prudent energy announces megawatt-class energy storage project with major food processing company in california. URL http://www.pdenergy.com/press_121310_gillsonions.html. Accessed January 2012.

R. D. Ray and G. D. Egbert. Estimates of m2 tidal energy dissipation from topex/poseidon altimeter data. *JOURNAL OF GEOPHYSICAL RESEARCH*, 106(C.10):22,475–22,502, 2001.

E. Regnier. Oil and energy price volatility. *Energy Economics*, 29(3):405–427, May 2007. ISSN 01409883. doi: 10.1016/j.eneco.2005.11.003.

RenewableUK. *UK Offshore Wind: Building an Industry*, 2010. URL http://www.bwea.com/pdf/offshore/offshore-wind_building-an-industry.pdf.

D. M. Rosenberg, F. Berkes, R. A. Bodaly, R. E. Hecky, C. A. Kelly, and J. W. M. Rudd. Large-scale impacts of hydroelectric development. *Environmental Reviews*, 5:27–54, 1997.

J. Ruer, E. Sibaud, T. Desrues, and P. Muguerra. Pumped heat energy storage. URL http://www.keynergie.com/articles/paper%20PHS-paper.pdf. Accessed June 2013.

A. Ryddell.

S. Salter. Wave Power. *Nature*, pages 720—724, 1974.

Sandia National Laboratories. *Large Scale System Monitoring of Regenesys & NaS Battery Systems*.

R. Schainker. Executive overview: energy storage options for a sustainable energy future. *IEEE Power Engineering Society General Meeting*, 2:2310–2315, 2004a. doi: 10.1109/PES.2004.1373298.

R. Schainker. Executive overview: energy storage options for a sustainable energy future. In *Power Engineering Society General Meeting, 2004. IEEE*, pages 2309 –2314 Vol.2, june 2004b. doi: 10.1109/PES.2004.1373298.

S. M. Schoenung, J. M. Eyer, J. J. Iannucci, and S. a. Horgan. Energy Storage for a Competitive Power Market. *Annual Review of Energy and the Environment*, 21(1):347–370, 1996.

T. Schumann. A liquid flowing through a porous prism. *Journal of Heat Transfer*, 5:208–212, 1929.

R. K. Shah and D. P. Sekulic. *Fundamentals of Heat Exchanger Design*. John Wiley and Sons, Inc., 2007. ISBN 9780470172605. doi: 10.1002/9780470172605.fmatter.

S. E. Shaheen, D. S. Ginley, G. E. Jabbour, and G. Editors. O rganic-Based Photovoltaics : Toward Low-Cost Power Generation. *MRS Bulletin*, 30(January):10–19, 2005.

Siemens. URL http://www.zbbenergy.com/. Accessed January 2012.

G. Sinden. Characteristics of the UK wind resource : Long-term patterns and relationship to electricity demand. *Energy Policy*, 35:112–127, 2007. doi: 10.1016/j.enpol.2005.10.003.

R. S. Subramanian. Flow through Packed Beds and Fluidized Beds. 2001. URL http://web2.clarkson.edu/projects/subramanian/ch301/notes/packfluidbed.pdf.

S. Succar and R. H. Williams. Compressed air energy storage: Theory, resources, and applications for wind power. *Princeton Environmental Institute, Princeton University*, 2008.

SustainX smarter energy storage. URL http://www.sustainx.com/. Accessed November 2012.

B. Tamyurek, D. K. Nichols, and O. Demircri. The NaS battery: A Multi-Function Energy Storage System. *IEEE Power Engineering Society General Meeting*, pages 1991–1996, 2003.

A. Ter-Gazarian. *Energy Storage for Power Systems*. IET Power and Energy Series, 2nd ed. edition, 2011. ISBN 978-1-84919-219-4.

J. A. Turner. A Realizable Renewable Energy Future. *Science*, 285(687), 1999.

J. Twidell and A. D. Weir. *Renewable energy resources / John Twidell and Tony Weir*. Taylor & Francis, London ; New York :, 2nd ed. edition, 2006. ISBN 0419253300 0419253203. URL http://www.loc.gov/catdir/toc/ecip0513/2005015300.html.

N. Uddin, P. H. D, and M. Asce. Preliminary design of an underground reservoir for pumped storage. *Geotechnical and Geological Engineering*, 21:331–355, 2003.

F. R. Villatoro, J. Pérez, F. Domínguez-Muñoz, and J. M. Cejudo-López. APPROXIMATE ANALYTICAL SOLUTION FOR THE HEAT TRANSFER IN PACKED BEDS FOR SOLAR THERMAL STORAGE IN BUILDING SIMULATORS. *Eleventh International IBPSA Conference*, (July 2009):709–715, 2009.

F. R. Villatoro, J. Pérez, J. L. G. Santander, M. A. Borovsky, Y. L. Ratis, E. A. Izzheurov, and P. F. D. Córdoba. Journal of Mathematical Analysis and Perturbation analysis of the heat transfer in porous media with small thermal conductivity. *Journal of Mathematical Analysis and Applications*, 374(1):57–70, 2011. ISSN 0022-247X. doi: 10.1016/j.jmaa.2010.08.038. URL http://dx.doi.org/10.1016/j.jmaa.2010.08.038.

R. Walawalkar, J. Apt, and R. Mancini. Economics of electric energy storage for energy arbitrage and regulation in New York. *Energy Policy*, 35(4):2558–2568, April 2007. ISSN 03014215. doi: 10.1016/j.enpol.2006.09.005.

Y. Wang, Z. Shi, Y. Huang, Y. Ma, C. Wang, M. Chen, and Y. Chen. Supercapacitor Devices Based on Graphene Materials. *Journal of Physical Chemsitry*, 113:13103–13107, 2009.

Z. Wen, J. Cao, Z. Gu, X. Xu, F. Zhang, and Z. Lin. Research on sodium sulfur battery for energy storage. *Solid State Ionics*, 179(27-32):1697–1701, 2008.

R. Weron. *Modeling and Forecasting Electricity Loads and Prices: A Statistical Approach*. John Wiley and Sons; Chichester :, 2006. ISBN 978-0470057537.

R. Weron and A. Misiorek. Heavy tails and electricity prices: Do time series models with non-gaussian noise forecast better than their gaussian counterparts? *Prace Naukowe Akademii Ekonomicznej we Wroclawiu*, 1076:472 — 480, 2007.

I. A. G. Wilson, P. G. Mcgregor, D. G. Infield, and P. J. Hall. Grid-connected renewables , storage and the UK electricity market q. *Renewable Energy*, pages 1–5, 2011. ISSN 0960-1481. doi: 10.1016/j.renene.2011.01.007. URL http://dx.doi.org/10.1016/j.renene.2011.01.007.

I. A. G. Wilson, P. G. McGregor, and P. J. Hall. Energy storage in the UK electrical network: Estimation of the scale and review of technology options. *Energy Policy*, 38(8):4099–4106, 2010. ISSN 03014215. doi: 10.1016/j.enpol.2010.03.036.

ZBB Energy Corporation. URL http://www.zbbenergy.com/. Accessed January 2012.